Flood frequency analysis in a changing climate
Climate change impact on design flood

Philippe Crochet

Report number:	Date:	Number of pages:	Distribution:
2020-01	December 2020	160	Public

Report title:
Flood frequency analysis in a changing climate - Climate change impact on design flood

Author:
Philippe Crochet
philippec@simnet.is

Abstract:

The aim of this study was to evaluate the impact of climate change on flood characteristics in Icelandic rivers. Daily streamflow discharge series were simulated for three river catchments over the 1981-2100 period with the HYPE hydrological model forced with an ensemble of bias-corrected CORDEX climate projections under two emission scenarios. The catchments are located in the south-east, south-west and north of the country and their drainage area is ranging from 115 to 5700 km^2. The hydrological response of these catchments to projected climate change was analysed, considering moving 30-year time-windows and compared to the situation in the 1981-2010 reference period.

Prepared for:
Rannsóknarsjóður Vegagerðarinnar

Keywords:
Iceland - Design flood - Climate change - HYPE model - CORDEX

Executive summary

The aim of this study was to evaluate the impact of climate change on flood characteristics in Icelandic rivers. Daily streamflow discharge series were simulated for three river catchments over the 1981-2100 period with the HYPE hydrological model forced with an ensemble of bias-corrected CORDEX climate projections under two emission scenarios. The catchments are located in the south-east, south-west and north of the country and their drainage area is ranging from 115 to 5700 km^2. The hydrological response of these catchments was analysed, considering moving 30-year time-windows and compared to the situation in the 1981-2010 reference period.

A significant temperature warming was projected in all seasons and all studied catchments, along the projection horizon, more or less pronounced according to the emission scenario, the season and the catchment location (0.29 °C/decade on average for the lowest emission scenario and 0.45 °C/decade on average for the highest emission scenario). Precipitation did not exhibit any significant temporal linear trend in a large majority of cases. Instead, decadal to multi-decadal oscillations were observed in the precipitation time-series, especially in autumn-winter, corresponding to a succession of wet and dry periods. However, the wet and dry periods of the different projection scenarios were sometimes found not to be in phase with each other, complicating the interpretation of results in some cases.

The hydrological response of the studied river basins was found to depend on the physiographic characteristics of the catchments. The projected temperature warming was found to gradually alter snow conditions and lead to a shorter snow season combined with less snow accumulation and a shift toward an earlier and lower peak of snowmelt. A gradual change with increasing projection horizon toward an increase of streamflow discharge in autumn-winter, an earlier and lower spring streamflow peak and a reduction of summer streamflow discharge were also projected except for a glaciated catchment where summer streamflow was projected to remain mainly unchanged.

Projected climate change was observed to have an impact on flood characteristics and the results of this study suggest that if projected climate scenarios realise, the frequency of extreme floods is likely to change. However, the uncertainty of the projected changes is considerable. The changes were found to be specific to each catchment in relation to its physiographic properties and dominating flood-generating mechanisms (rain-fed, snowmelt-fed, interplay of rain and snowmelt). Under the lowest emission scenario, both an increase and decrease of extreme flood quantiles are projected in a recent future (until circa 2031-2060), depending on the catchment under consideration, while an increase of flood quantiles dominates in a more distant future (2041-2070 and thereafter). Under the highest emission scenario, a shift toward larger extreme flood quantiles dominates along most of the 21st century. The projected changes in flood quantiles are moderate (less than 20% increase, on average) but translate into larger changes in terms of return period (up to 50% reduction, on average). Concerning flood occurrence dates, a larger number of annual maximum flood events are projected to occur in autumn-winter and fewer in spring-summer, relative to 1981-2010, under both emission scenarios.

1 Introduction

Climate in Iceland is projected to change in the coming decades and lead to changes in temperature and precipitation which in turn will have an impact on the hydrological characteristics of river basins (Jóhannesson et al., 2007; Einarsson and Jónsson, 2010; Thorsteinsson and Björnsson Eds., 2011; Crochet 2013; Gosseling, 2017; Björnsson et al., 2018). Consequently, the statistical characteristics of river flow from the past decades may no longer adequately represent the situation of the coming decades.

Traditionally, flood frequency analysis (FFA) and the estimation of design floods are based on the implicit assumption of temporal stationarity or time-invariance of the flood frequency distribution (Crochet and Þórarinsdóttir 2014; Hróðmarsson and Þórarinsdóttir, 2018). This stationarity assumption may no longer be valid in the coming decades because of climate change. Assessing climate change impacts on flood characteristics is therefore very important in order to anticipate mitigating actions that may have to be taken to protect populations and infrastructures.

In this study, climate change impact on annual maximum flood characteristics of Icelandic rivers was assessed according to the following modelling chain (see for instance Arheimer and Lindström 2015): “emission scenario – global climate model – regional downscaling – bias correction – hydrological model – analysis”. The method was applied to three gauged river catchments located in different regions of the country. Section 2 presents the studied catchments and Section 3 presents the material and methods used in this study. Section 4 is dedicated to the hydrological modelling and Section 5 to the analysis of climate scenarios. The hydrological response to climate changes is analysed in Sections 6 and 7 and Section 8 concludes this report.

2 Study area

Three river basins with different characteristics and located in different regions were analysed (Table 1). These basins correspond to the drainage areas at three gauged sites monitored by Veðurstofa Íslands. Figure 1 presents the location of the studied catchments and Figures 2 to 8 their main characteristics. Fossá is located in south-east Iceland, east of the Vatnajökull ice-cap ; Hjaltadalsá is located in the Tröllaskagi mountain range in northern Iceland; Ölfusá is located in south-west Iceland and its drainage area includes a part of Langjökull and Hofsjökull ice-caps. The three catchments cover a large range of size and altitude, soil and land cover types. Icelandic rivers are usually classified in three main categories according to the origin of flow: direct runoff rivers (D), glacial fed rivers (J) and groundwater fed rivers (L). In practise, rivers are often a combination of several of these categories. The river at site vhm148 is classified as a direct runoff river. The river at site vhm51 is a combination of direct runoff and glacial fed river. The river at site vhm64 displays signs of all three categories.

Table 1: Discharge gauging stations and drainage areas of catchments

Name and location	ID	River type	Drainage area (km^2)
Fossá, Berufirði; Eyjólfsstaðir	vhm148	D	115
Hjaltadalsá, Skagafirði	vhm51	D+J	299
Ölfusá; Selfoss	vhm64	D+J+L	5693

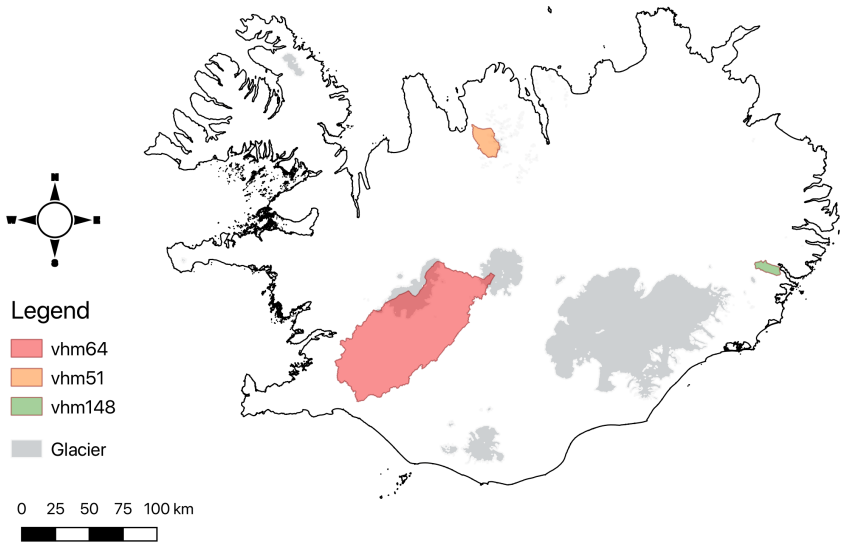

Figure 1: Overview of the studied catchments. Glaciers and coastline from National Land Survey of Iceland. Catchment delineation based on ArcticDEM (Porter et al., 2018).

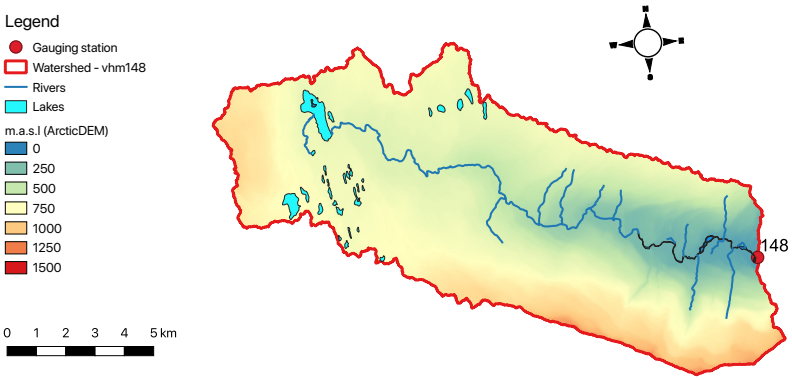

Fig. 2: Elevation map of the Fossá catchment (vhm148) based on ArcticDEM (Porter et al., 2018), including overlays for rivers and lakes (National Land Survey of Iceland).

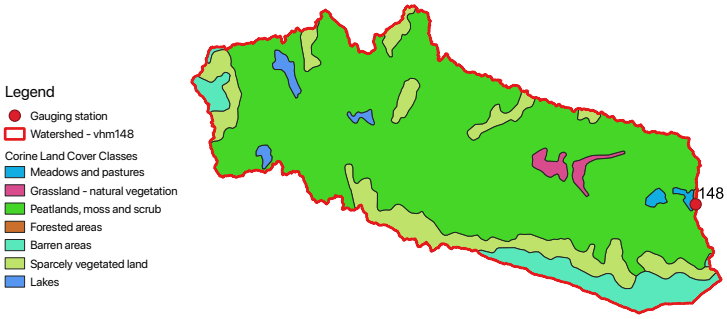

Fig. 3: CORINE (CLC 2012) land classification of the Fossá catchment (vhm148).

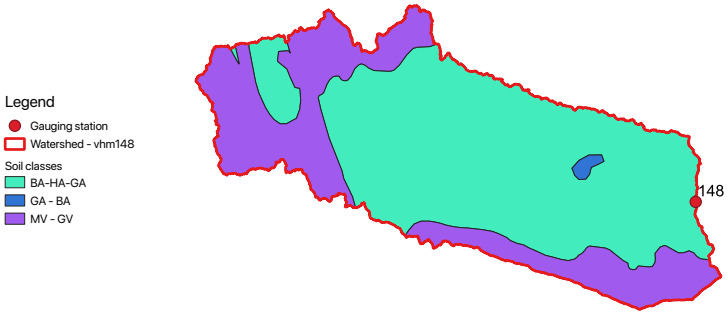

Fig. 4: Soil classification of the Fossá catchment (vhm148), based on the soil map of Iceland (Arnalds and Óskarsson, 2009; Arnalds, 2015)

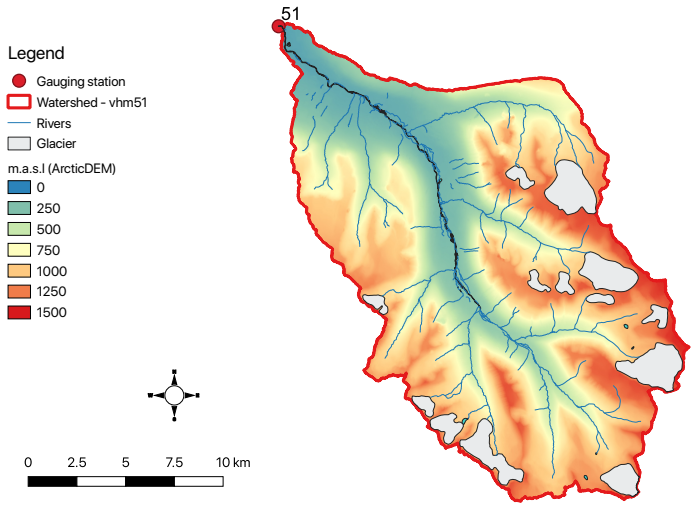

Fig. 5: Elevation map of the Hjaltadalsá catchment (vhm51) based on ArcticDEM (Porter et al., 2018), including overlays for rivers and glaciers (National Land Survey of Iceland).

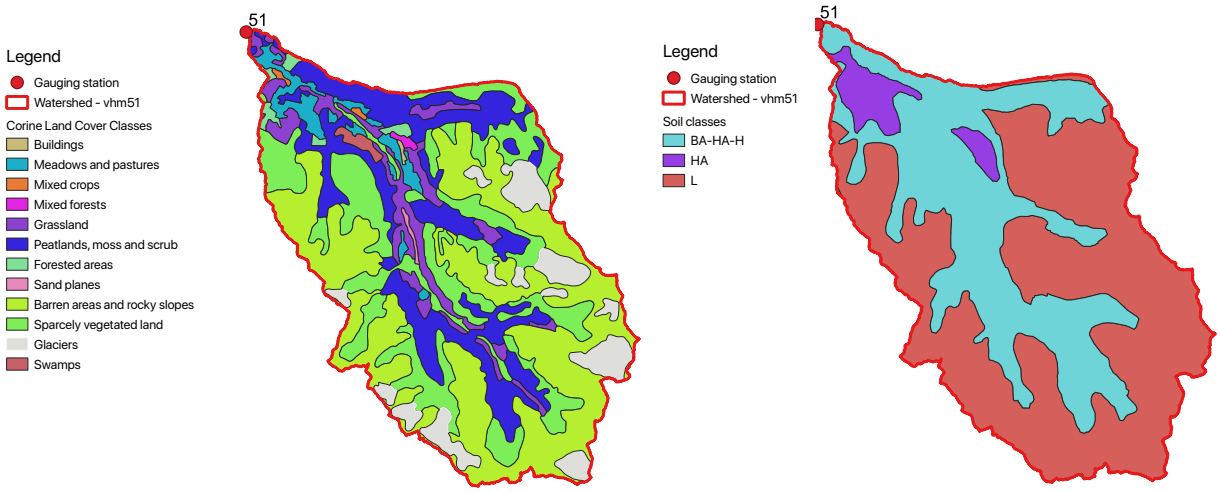

Fig. 6: Hjaltadalsá catchment (vhm51). Left: CORINE (CLC 2012) land classification. Right: Soil classification based on the soil map of Iceland (Arnalds and Óskarsson, 2009; Arnalds, 2015)

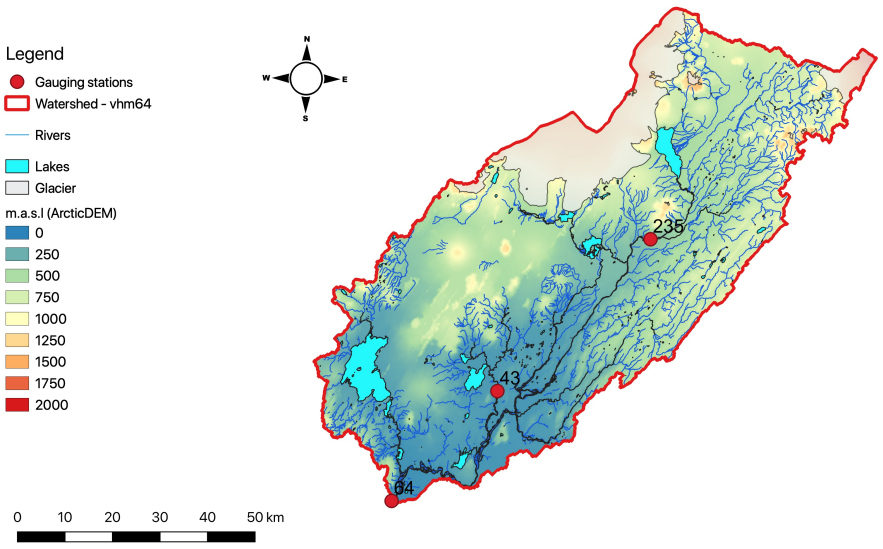

Fig. 7: Elevation map of the Ölfusá catchment (vhm64) based on ArcticDEM (Porter et al., 2018), including overlays for rivers, lakes and glaciers (National Land Survey of Iceland).

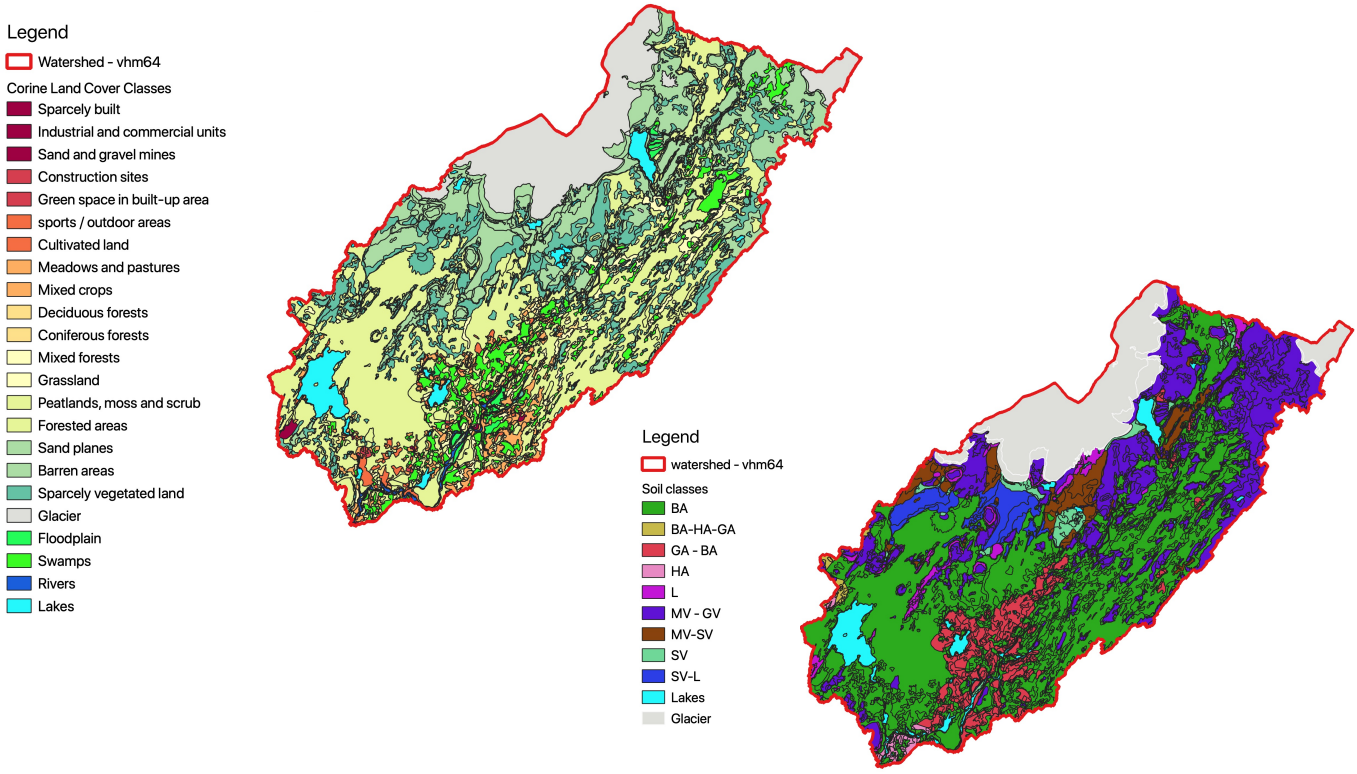

Fig. 8: Ölfusá catchment (vhm64). Left: CORINE (CLC 2012) land classification. Right: Soil classification based on the soil map of Iceland (Arnalds and Óskarsson, 2009; Arnalds, 2015)

3 Materials and methods

3-1 Method overview

Daily streamflow discharge series were simulated for the three river catchments over the 1981-2100 period with a hydrological model forced with an ensemble of bias-corrected regional climate scenarios. Various hydro-climatic variables were extracted from each simulated scenario considering moving 30-year time-windows (1981-2010; 1991-2020; 2001-2030; 2011-2040; 2021-2050; 2031-2060; 2041-2070; 2051-2080; 2061-2090; 2071-2100) and their evolution along these time-windows analysed. The 30-year moving-window technique has for instance been used in Thorsteinsson and Björnsson Eds. (2011). The use of an ensemble of climate scenarios allows a more robust estimation of projected changes and their uncertainty.

The following hydro-climatic variables were considered in the analysis:

- 30-year mean daily temperature, precipitation, snow accumulation, streamflow discharge
- 30-year mean seasonal temperature, precipitation, streamflow discharge
- 30-year mean annual temperature, precipitation, streamflow discharge

For seasonal and annual means, seasonal and annual values were first calculated each water-year by averaging all daily values from each season and water-year, respectively, and then the 30-year mean calculated. The water-year is defined from October of year *i* to September of year *i*+1 and the four seasons are October to December (OND), January to March (JFM), April to June (AMJ), and July to September (JAS).

For each scenario, a two-sided Mann-Whitney test with a 5% significance level was used to compare the hydro-climatic variables of each projected time-window to those in the 1981-2010 time-window taken as reference. The Mann-Whitney test is a non-parametric test estimating whether two samples can be considered drawn from populations having the same distribution or if they significantly differ. The null hypothesis H0 was that the two samples were drawn from populations having the same distribution against the alternative hypothesis that they were drawn from populations having different distributions.

- Annual maximum floods (AMF)

Annual maximum flood series and their occurrence dates were extracted from the observed daily streamflow discharge series in the 1981-2010 reference period and from the simulated daily streamflow discharge scenarios in the moving 30-year time-windows. A Gumbel distribution was fitted to the empirical AMF frequency distributions (Stephenson 2002; Delignette-Muller and Dutang 2015) and the evolution of the T-year floods Q(T) (T=2, 5, 10, 20, 50, 100 years) along these time-windows analysed and compared to the Q(T) values in the reference time-window (1981-2010). Then, the magnitude Q of floods was fixed and the return period T(Q) corresponding to Q in the projected time-windows estimated and compared to T(Q) in the reference time-window (1981-2010). The T(Q) analysis is complementary to the Q(T) analysis and presents the same

results from a different view point. Instead of fixing T and analysing the evolution of Q(T), the magnitude Q is fixed and the evolution of its return period T(Q) analysed. Finally, the number of AMF occurrences observed in each season was analysed along the different time-windows in order to examine possible changes in the dominating flood-generating processes.

3-2 Hydrological model

The hydrological simulations were performed with the HYPE open source model. HYPE (Hydrological Predictions for the Environment) is a semi-distributed conceptual hydrological model developed by the Swedish Meteorological and Hydrological Institute. HYPE uses lumped sub-catchments divided into soil type and land use combinations (SLCs). A detailed description of the model can be found in Lindström et al. 2010 and on the HYPE wiki page (http://www.smhi.net/hype/wiki/doku.php). This model has been used in various countries around the world, including in Iceland (Marschollek, 2017; de Niet et al. 2020). In the present study, only precipitation and temperature were used as weather input.

3-3 Climate scenarios

The CORDEX framework (Coordinated Regional Climate Downscaling Experiment) (www.cordex.org) has provided an ensemble of high-resolution (12.5 km) regional climate projections over several regions of the world for use in impact and adaptation studies (Giorgi et al., 2009). This framework was planned in support of the IPCC Fifth Assessment Report (referred to as CMIP5). The scenarios were obtained by dynamical downscaling of several General Circulation Models (GCMs) with a set of Regional Climate Models (RCMs) assuming various emission scenarios referred to as Representative Concentration Pathways (RCPs). The RCPs are a measure of the strength of the anthropogenic greenhouse effect. In this project, the climate scenarios were taken from the European branch of CORDEX, EURO-CORDEX (www.euro-cordex.net) (Jacob D., Petersen J., Eggert B. *et al.*, 2014), as this region includes Iceland. The EURO-CORDEX scenarios have for instance been used to assess the climate of Iceland in the 21st century (Gosseling, 2017).

The CORDEX scenario simulations consist of a historical period (1981-2005) and a projection period (2006-2100) under various RCPs. Note that the climate scenarios from the historical period (1981-2005) are not synchronised with observed climate which means that they do not correspond to the actual reality as it took place day by day but represent a possible realisation of what could have taken place. Only the long-term climate scenario statistics are expected to match the long-term statistics of observed climate during the historical period. CORDEX has also provided an ensemble of evaluation scenarios synchronised with observed climate in the period 1981-2010, obtained by dynamical downscaling of reanalysed weather (ERA-Interim) with the set of RCMs. ERA-Interim is a global atmospheric reanalysis made by the ECMWF (Dee et al., 2011). This dataset is useful for the RCMs evaluation within the historical period.
The present study makes use of an ensemble of CORDEX daily precipitation and near surface air temperature scenarios covering the 1981-2100 period.

Tables 2 and 3 present the GCMs and RCMs used in this study. The two selected GCMs are those suggested in Gossling (2017) as the best GCMs for the Icelandic domain, namely MOHC-HadGEM2-ES and MPI-ESM-LR. Two RCP emission scenarios were considered in this study. The first one (RCP4.5) assumes a stabilisation of radiative forcing by the end of the 21st century at 4.5 W/m² relative to pre-industrial conditions and the second one (RCP8.5), more pessimistic, assumes an increase in radiative forcing of 8.5 W/m² by the end of 21st century relative to pre-industrial conditions. RCMs driven by at least one of the selected GCMs and for which projections with both RCP emission scenarios were available, were selected. Evaluation scenarios driven by ERA-Interim reanalyses and downscaled with the selected RCMs were also used to investigate the intrinsic quality of these RCMs and the skills of the bias-correction methods.

Using an ensemble of climate scenarios rather than a single one gives a better representation of possible future states of the climate system and allows a more robust evaluation of the future temporal evolution of the hydrological systems under study.

Table 2: List of GCMs and RCMs

Model	Type	Institution	Reference
ERA-Interim	Reanalysis	ECMWF	Dee et al., 2011
MOHC-HadGEM2-ES	GCM	Met Office Hadley Centre	Jones et al., 2011
MPI-ESM-LR	GCM	ESM of the Max-Planck-Institut fur Meteorologie	Giorgetta et al. 2013
CCLM4-8-17	RCM	CLMcom	Rockel et al., 2008
RCA4	RCM	SMHI	Kupiainen et al. 2011 Samuelsson et al. 2011
RACMO22E	RCM	KNMI	Meijgaard van et al. 2012
REMO2009	RCM	MPI-CSC	Jacob et al., 2012

Table 3: List of GCM-RCM combinations and emission scenarios (RCP)

		RCP	RCMs			
			CCLM4-8-17	RCA4	RACMO22E	REMO2009
Forcing GCM	ERA-Interim (evaluation)		x	x	x	x
	MOHC-HadGEM2-ES	RCP4.5 & RCP8.5	x	x	x	
	MPI-ESM-LR	RCP4.5 & RCP8.5	x	x		x

3-4 Reference weather data

Daily precipitation and 2m-temperature from the high-resolution (2.5 km) ICRA weather reanalysis (Nawri et al., 2017) produced by Veðurstofa Íslands constitute the historical weather data of reference (1980-2017) used i) as input to calibrate the HYPE hydrological model ii) to verify the credibility of the CORDEX climate scenarios in the historical period and iii) to statistically bias-correct the CORDEX climate scenarios in the historical and projection periods prior to use them as input to HYPE.

3-5 Hydrological data

Daily streamflow discharge series from four gauging stations monitored by Veðurstofa Íslands were used to calibrate HYPE and verify the credibility of the simulated streamflow series in the historical period when HYPE was forced with the CORDEX scenarios (Table 1 and Figs. 2, 5, 7).

3-6 Other data

The river catchments and sub-catchments delineation was done with QGIS (v.3.6) using a digital elevation model (DEM) with resolution 10 m obtained from ArcticDEM (Porter et al., 2018). The hydrological modelling with HYPE requires the use of a landuse map and a soil map. The soil map of Iceland compiled by the Agricultural University of Iceland (Arnalds and Óskarsson, 2009; Arnalds, 2015) was used and downloaded from http://rangarvellir.ru.is. The Corine Land Cover data updated for the reference year 2012 (Árnason and Matthíasson, 2017) were used and obtained from the download page of the National Land Survey of Iceland (http://atlas.lmi.is/LmiData/). Additional information about coastline, lakes and water courses were also obtained from the download page of the National Land Survey of Iceland and used to verify the credibility of the extracted stream network made with QGIS, prior to perform the catchments delineation.

3-7 Bias-correction

In order to guaranty consistency between CORDEX climate scenarios and ICRA reference weather data used as input during the calibration of the HYPE hydrological model, a bias-correction was applied to each CORDEX temperature and precipitation scenario prior to be used as input to HYPE:

- The bias-correction of temperature was based on quantile mapping (QM) (Gudmundsson et al. 2012; Gudmundsson 2016). The goal of QM is to adjust the simulated climate variable such that its distribution matches the distribution of the observed variable. A specific correction was defined for each month. The correction coefficients were estimated by comparing ICRA data in the 1981-2010 period to the CORDEX scenarios in the historical period (1981-2005). The correction was then applied to the entire projection period (1981-2100).
- Two bias-correction methods were compared for precipitation: i) quantile mapping as for temperature and ii) an analog-based correction method (not documented yet) based on the analysis of spatial precipitation patterns using the S1 score (see Wilks, 1995), followed by

quantile mapping. Analog methods have for instance been used for post-processing coarse resolution Numerical Weather Prediction models and generate local ensemble precipitation forecasts (see for instance Obled et al., 2002).

4 HYPE model calibration

Daily discharge series from gauging station vhm148 were used to calibrate HYPE for the Fossá catchment; Daily discharge series from gauging station vhm51 were used to calibrate HYPE for the Hjaltadalsá catchment; Three gauging stations are located in the the Ölfusá catchment (Fig. 7) and two of them were used to calibrate HYPE: station vhm64 and station vhm235 (Hvítá, Árnessýslu). For the hydrological modelling, catchment vhm51 was divided into five sub-catchments, catchment vhm64 was divided into six sub-catchments and catchment vhm148 was not sub-divided into smaller sub-catchments.

ICRA daily precipitation and temperature fields were first area-averaged over each catchment and sub-catchment prior to be used as input to HYPE. A spin-up time of one year was used for vhm148 and vhm51 and two years for vhm64. The model calibration was made against observed daily discharge series considering a period of eleven water-years (01-Oct-1999 to 30-Sep-2010). Monte Carlo based optimisation methods were used for that purpose, considering a combination of criteria to judge the model performance (Kling-Gupta efficiency and relative bias). Note that default HYPE parameters were used for the glacier modelling part of the model except for the glacier melt coefficients that were optimised. Hydrological simulations were then made with the calibrated model over the water-years 1981-2016 and years which did not belong to the spin-up period nor to the calibration period and for which observed daily discharge was available were used to verify the quality of the simulations (validation). The ability of the simulated daily streamflow discharge series to correctly reproduce the observed AMF frequency distribution was also taken into consideration and a partial recalibration was made against observed daily high flow series for vhm51. The resulting improvement of the simulated AMF frequency distribution was usually obtained at the expense of a slight degradation of the overall model performance resulting from the sharpening of streamflow peaks in some cases. The ability for the simulated daily streamflow discharge series to correctly reproduce both AMF magnitude and occurrence date turned out to be difficult to systematically achieve but the number of AMF occurrences observed in each season was correctly simulated, on average, meaning that the proportion of different flood generating processes was well reproduced in the simulation period.

Table 4 and Fig. 9 summarise the results of the discharge simulations. For vhm148, the water-years 2010-2016 were better simulated than the water-years 1981-1998. For vhm51, model performances were poorest for water-year 2002 when streamflow discharges were much below an average year and water-year 2003 where many streamflow observations were missing. For vhm64, model performances were poorest for water-year 1994 resulting form an underestimation of winter streamflow discharge, water-year 2009 resulting from an underestimation of summer streamflow discharge and water-year 2014 where an overestimation was observed in relation to snowmelt.

The seasonality of mean daily streamflow discharge is presented in Fig. 10. Winter streamflow appears to be slightly underestimated on average for vhm64, in relation to the underestimation of winter streamflow in some individual years but winter streamflow was usually well simulated in most other years. The same situation was observed for summer streamflow in a few individual years. Simulations for one water-year are presented in Fig 11 for illustration.

The AMF magnitude and occurrence date were extracted for each water-year. The AMF empirical frequency distributions and Gumbel fits are shown in Fig. 12. The AMF magnitude versus occurrence date is shown in Fig. 13. The three catchments experienced extreme floods in different seasons, associated to different generating mechanisms (rain-fed floods, snowmelt floods, interplay of rain and snowmelt floods). Fossá (vhm148) in the south-east is dominated by rain-fed floods in late summer and autumn; Hjaltadalsá (vhm51) in the north is dominated by an interplay of rain and snowmelt floods in late spring and early summer; Ölfusá (vhm64) in the south-west is dominated by an interplay of rain and snowmelt floods from autumn to spring on frozen ground.

Table 4: Results of the HYPE discharge validation procedure. Kling-Gupta efficiency (KGE), Nash-Sutcliffe efficiency (NSE), mean relative error (MRE). All water-years (1981-2016) except vhm64 (1982-2016). Validation water-years (1981-1998; 2010-2016) except vhm64 (1982-1998; 2010-2016).

Catchment	**All water-years**			**Validation water-years**		
	NSE	KGE	MRE (%)	NSE	KGE	MRE (%)
vhm148	0.69	0.83	6.2	0.66	0.81	9
vhm51	0.73	0.86	-3	0.74	0.86	-3.8
vhm64	0.73	0.83	-3.6	0.685	0.77	-2.6

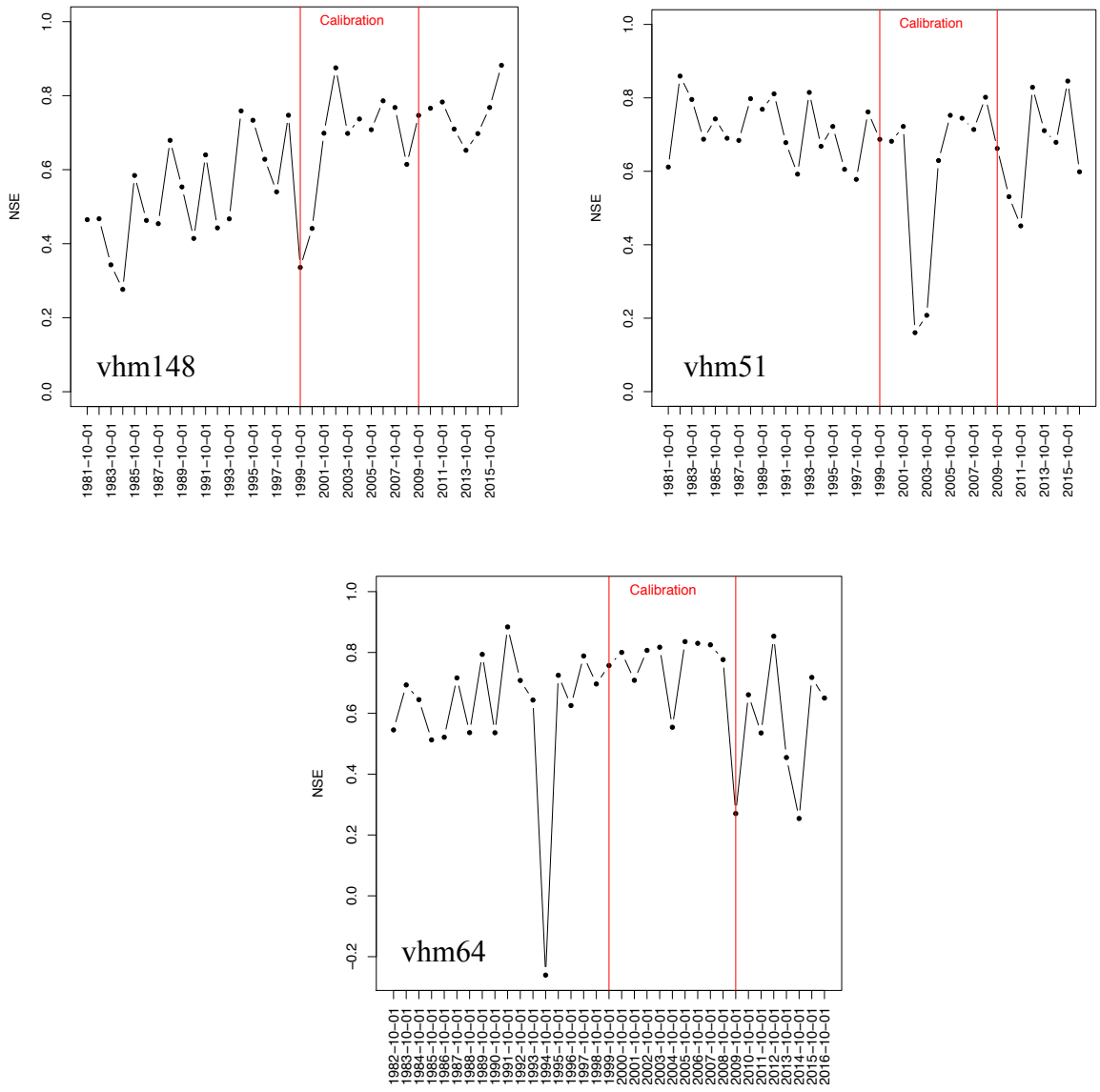

Fig.9: Annual NSE (water-years 1981-2016): vhm148 (top-left); vhm51 (top-right); vhm64 (bottom).

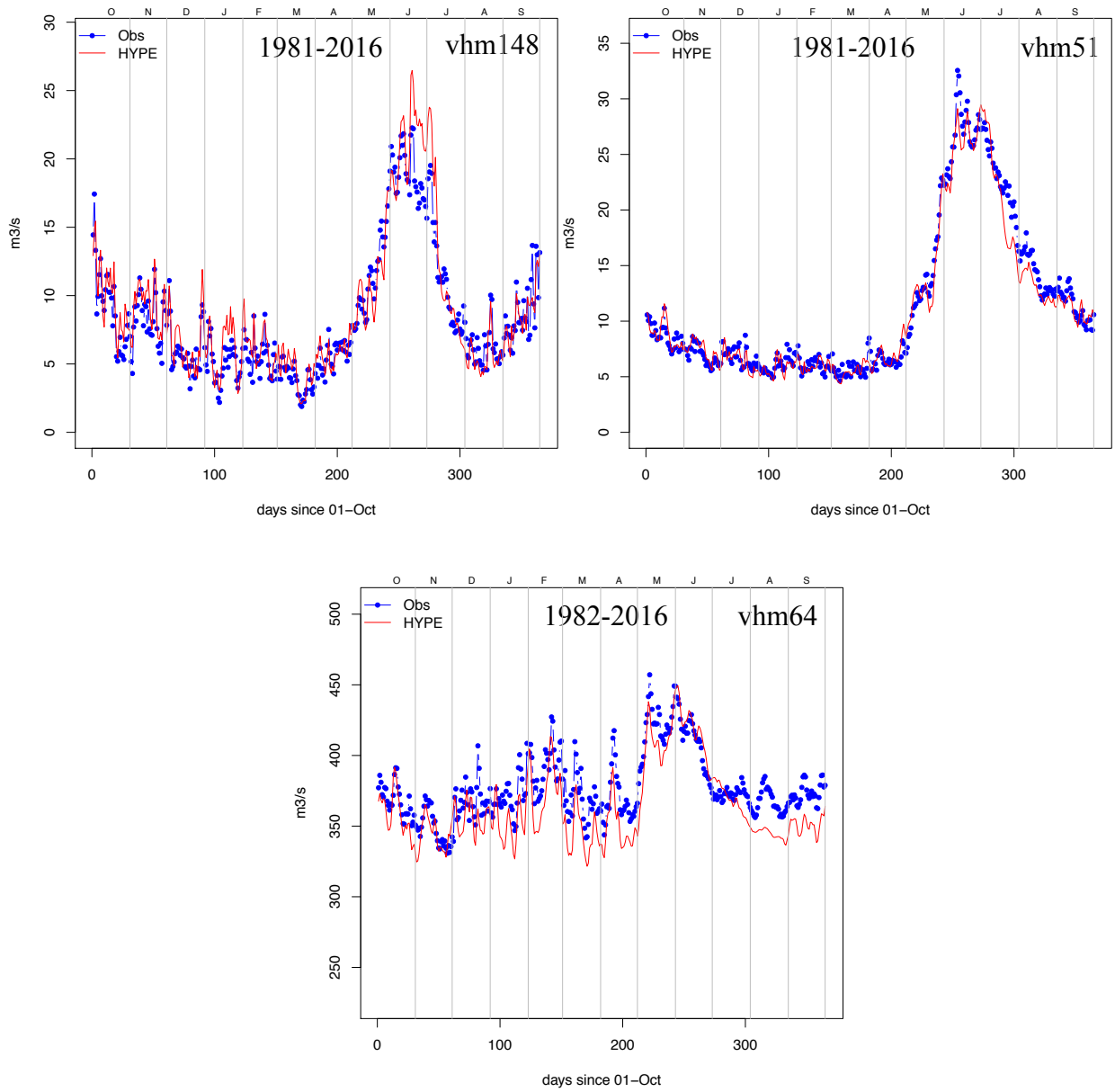

Fig.10: Seasonality of mean daily discharge in the water-years 1981-2016. Observed discharge (blue); HYPE discharge simulations (red); vhm148 (top-left); vhm51 (top-right); vhm64 (bottom).

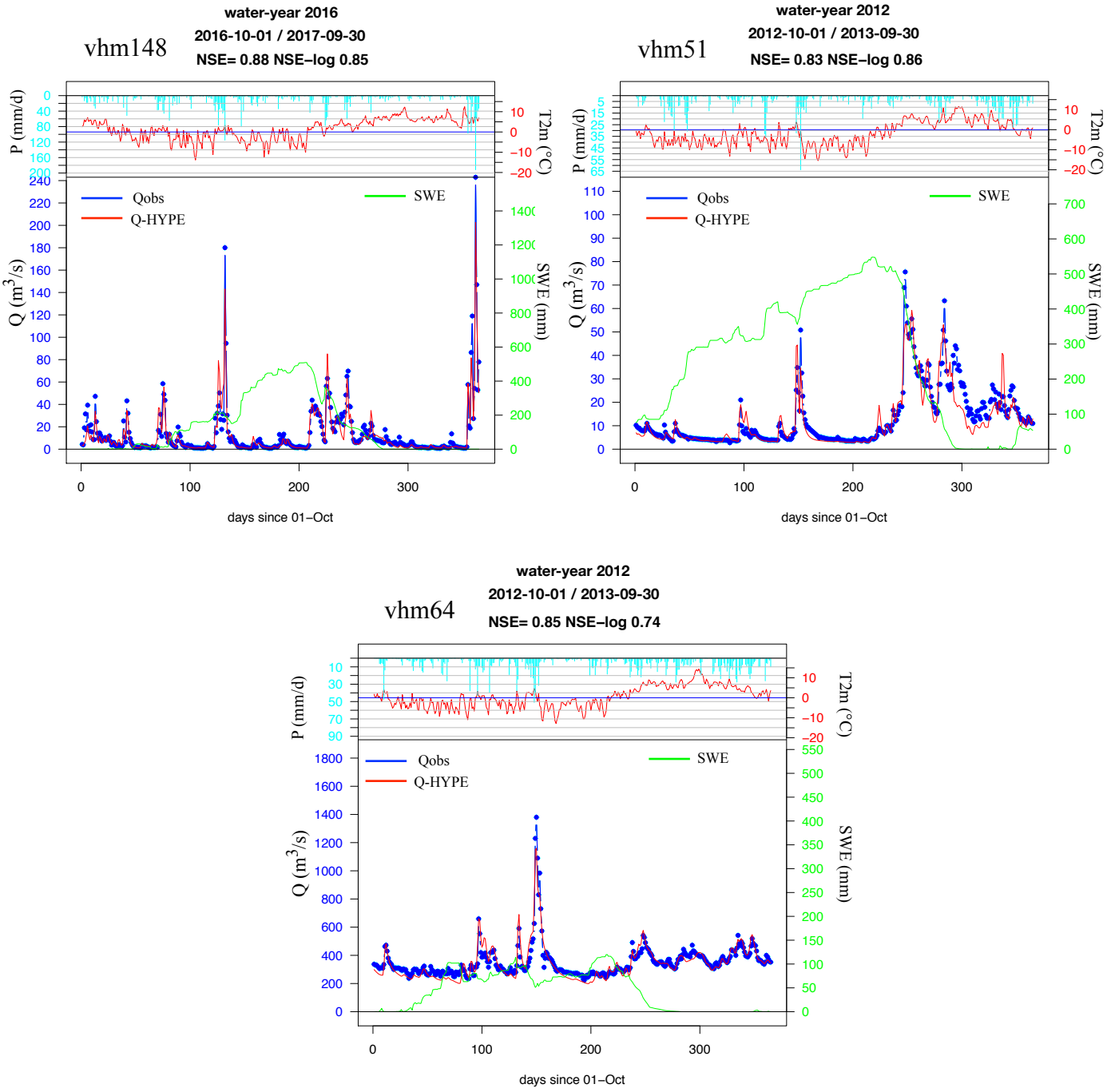

Fig.11: Observed precipitation (P) and temperature (T2m) from ICRA reanalysis, observed discharge (Qobs), simulated snow accumulation (SWE) and simulated discharge with HYPE (Q-HYPE), during a particular water-year in the validation period; vhm148 (top-left); vhm51 (top-right); vhm64 (bottom).

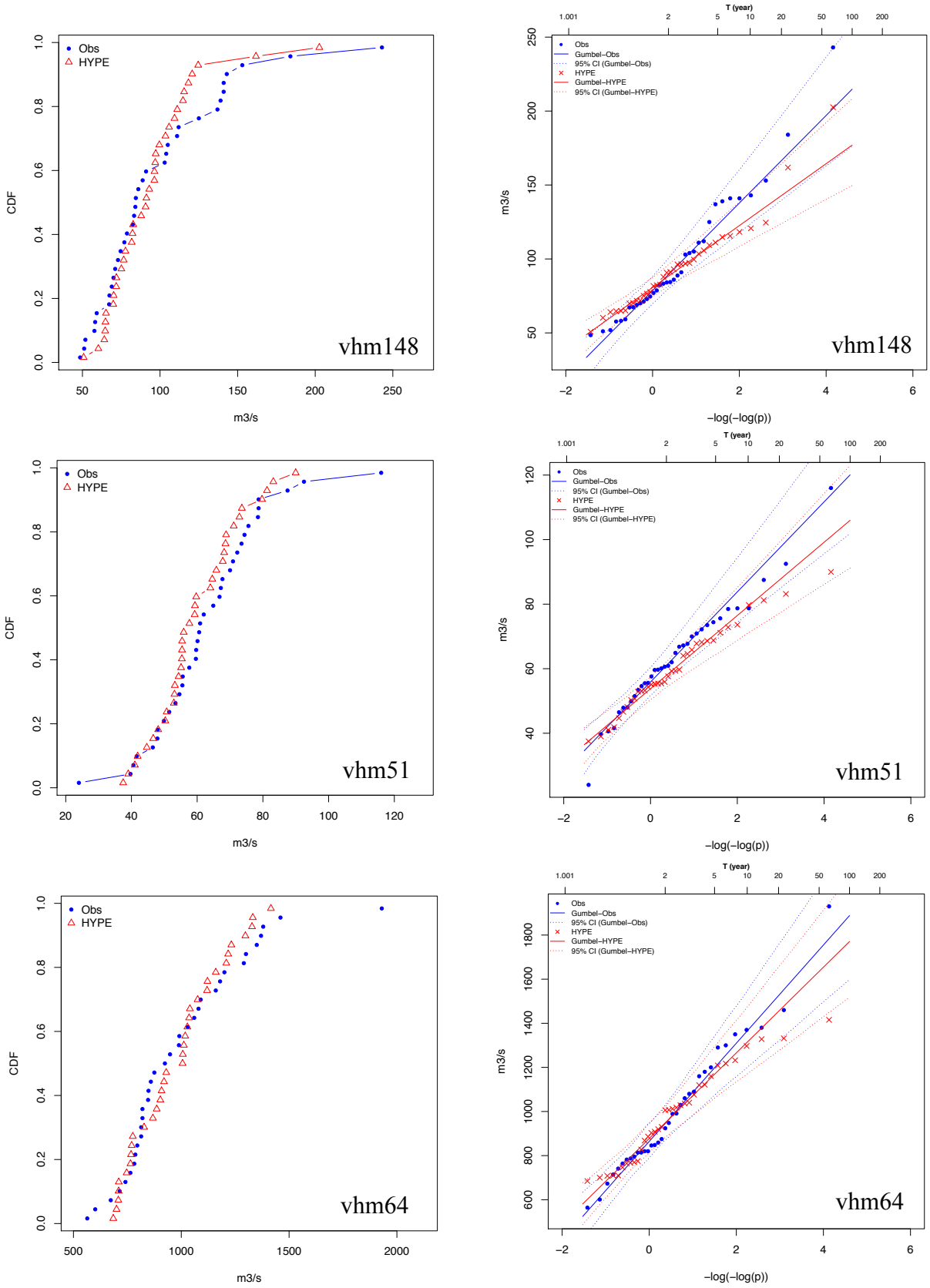

Fig.12: Annual maximum flood (water-years 1981-2016): Empirical cumulative distribution functions, F(q)=Prob(Q≤q)=p, (left panel) and Gumbel fits (right panel), where T=1/(1-p); vhm148 (top); vhm51 (middle); vhm64 (bottom).

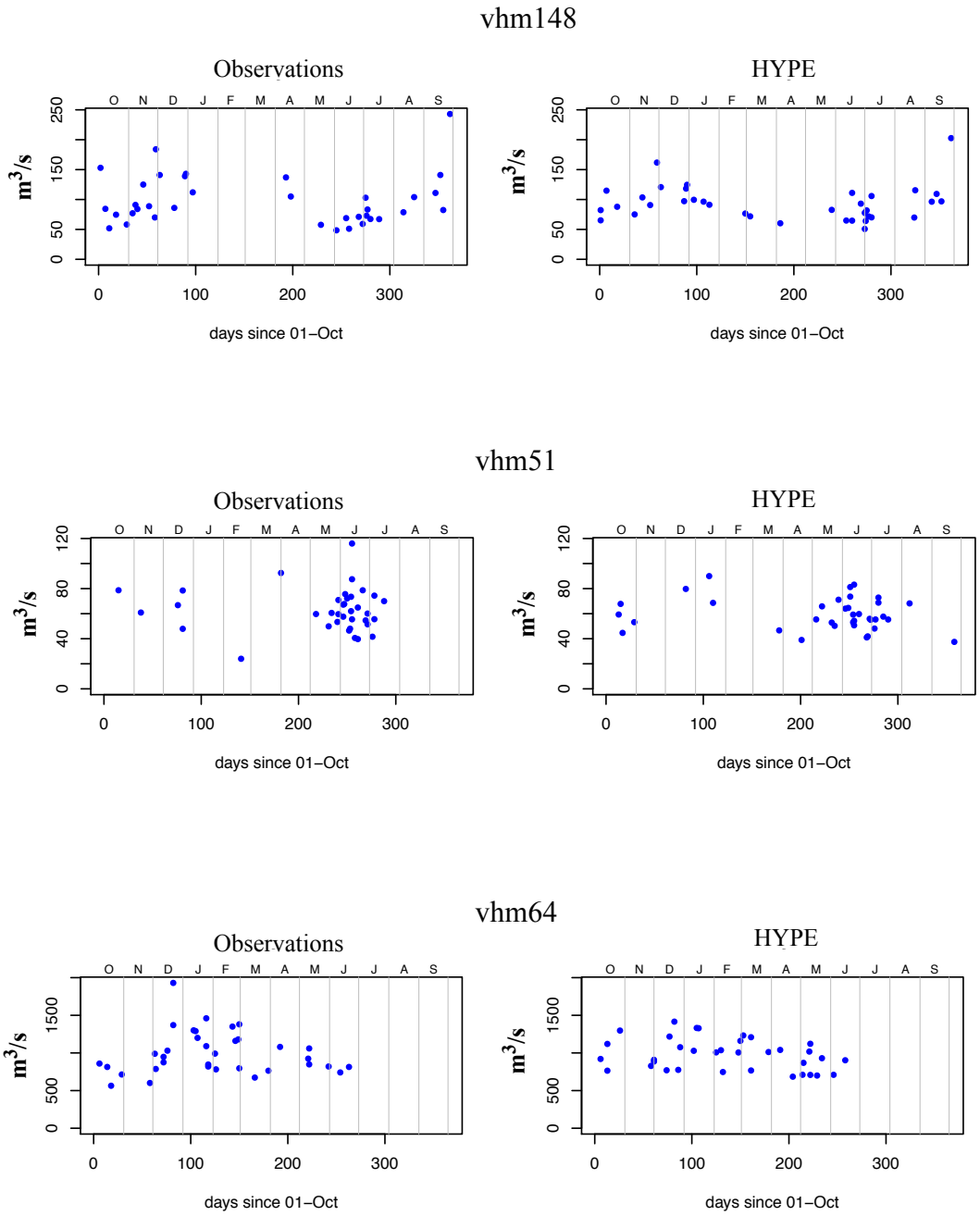

Fig.13: Annual maximum flood vs. day of occurrence (water-years 1981-2016). Observations: vhm148 (top-left); vhm51 (center-left); vhm64 (bottom-left). HYPE simulations: vhm148 (top-right); vhm51 (center-right); vhm64 (bottom-right).

5 EURO-CORDEX climate scenarios

CORDEX daily precipitation and temperature scenarios were area-averaged over the respective catchments and sub-catchments. In total, four climate evaluation scenarios were used and an ensemble of six climate projection scenarios under two RCP emission scenarios were used (See Table 3).

5-1 Evaluation of RCMs and bias-corrections skills using the evaluation scenarios

In order to evaluate the intrinsic quality of the different RCMs and the skill of the bias-correction methods, a comparison was made between ICRA weather reanalysis and CORDEX evaluation scenarios. The evaluation scenarios have been obtained by dynamical downscaling of weather reanalyses (ERA-interim) with the selected RCMs and are therefore synchronised with observed climate. For sake of simplicity, the results presented in this report are limited to the analysis of daily precipitation and temperature series area-averaged over the entire catchments only. Quantile mapping correction coefficients were defined by comparing ICRA data in the 1981-2010 period to the CORDEX evaluation scenarios in the available period (1981-2010 or 1989-2008, depending on the RCM). The following evaluation statistics were calculated in the period 1989-2008, common to all evaluation scenarios:

Mean error: ME=E[CORDEX-ICRA]

Root-mean-square error: RMSE=$\sqrt{E[(CORDEX\text{-}ICRA)^2]}$

5-1-1 Temperature evaluation scenarios

Appendix 1 presents ME and RMSE between ICRA and CORDEX evaluation scenarios before and after bias-correction. All scenarios display a systematic temperature bias in all three catchments, usually more pronounced in summer. The bias is essentially negative (underestimation) in most months and catchments, with RCA4 and RACMO22E scenarios and both positive and negative with CCLM-4-8-17 and REMO2009 scenarios. Quantile mapping eliminated the bias and reduced the RMSE in months where the bias was the strongest. After bias-correction, the different evaluation scenarios became relatively similar in terms of RMSE with a slight advantage for CCLM-4-8-17.

5-1-2 Precipitation evaluation scenarios

Appendix 2 presents ME and RMSE between ICRA and CORDEX evaluation scenarios before and after bias-correction. All scenarios displayed a systematic precipitation bias in all three catchments. For vhm148, precipitation was mainly underestimated on average by all scenarios in most months. For vhm51, precipitation was mainly overestimated on average in most months by all scenarios except with REMO2009 which underestimated precipitation. For vhm64, precipitation was mainly underestimated on average by all scenarios, except in winter with RCA4, REMO2009 and RACMO22E which overestimated precipitation. Direct quantile mapping (method 1) eliminated the bias and either reduced the RMSE in some occasions or kept it similar.

The analog-based correction method was efficient at reducing the systematic bias in months where it was substantial and at reducing the RMSE. Applying quantile mapping after the analog-based correction (method 2) reduced the bias further but either slightly increased the RMSE or kept it similar. After bias-correction, the different evaluation scenarios were relatively similar in terms of RMSE, with a slight advantage for CCLM-4-8-17 and RACMO22E with both methods. Method 2 led to very slightly better results than method 1 regarding RMSE but was similar to method 1 regarding ME. Both methods were selected to correct the CORDEX precipitation scenarios.

5-2 Projection scenarios

Comparisons between CORDEX climate projection scenarios and ICRA reference climate in the 1981-2010 period confirmed the presence of biases in the original CORDEX data. The analysis of monthly temperature and precipitation seasonality in the 1981-2010 reference period confirmed the efficiency of the correction methods at removing any systematic bias (cf. section 3-7 and Appendix 3 and 4). The analog-based correction method alone was found to be efficient at reducing existing precipitation bias, especially in the complex terrain of vhm51 (Appendix 4). Quantile mapping reduced it further.

After bias-correction, a temporal trend test based on simple linear regression was applied to monthly averaged daily temperature and precipitation scenarios in the 1981-2100 period, considering a 5% significance level. Changes in the seasonality of monthly temperature and precipitation series were also analysed, considering moving 30-year time-windows.

5-2-1 Bias-corrected temperature scenarios

A significant temperature warming (linear trend) was observed in all months and for all scenarios, in all three catchments, more or less pronounced according to the emission scenario and the month under consideration (see Table 5). On average over all catchments, an ensemble mean warming rate of 0.29°C/decade is projected under the RCP4.5 emission scenario and 0.45°C/decade under the RCP8.5 emission scenario. The warming rate is largest in the northern catchment (vmh51). The warming rate is usually larger with scenarios driven by HadGEM2ES GCM than by MPI−ESM−LR GCM (not shown). The projected temperature warming is also well reflected in the evolution of the seasonal temperature cycle in different 30-year time-windows. Appendix 5 presents the catchment-averaged temperature seasonal cycle for the different time-windows under the RCP4.5 and RCP8.5 emission scenarios, for one selected pair of GCM-RCM. Similar results were observed with the other GCMs-RCMs pairs.

5-2-2 Bias-corrected precipitation scenarios

Catchment-averaged precipitation did not exhibit any significant linear trend in a large majority of cases. When a significant trend was detected, it often concerned one scenario only or several scenarios driven by the same GCM, seldom by both GCMs. Significant trends were mainly observed under the RCP8.5 emission scenario, in different seasons, toward a precipitation increase in the northern catchment and both an increase and a decrease in the south-western and south-

eastern catchments. Results from the two bias-correction methods are usually similar. For illustration, Table 6 presents the slope of the linear regressions for the bias-corrected precipitation using quantile mapping (method 1).

The main features characterising precipitation scenarios are decadal to multi-decadal oscillations, especially in autumn-winter, corresponding to a succession of “wet” and “dry” periods. These oscillations are characteristics of the natural variability of precipitation in the Icelandic domain (see for instance Crochet, 2007). However, the wet and dry periods of the different precipitation scenarios were often found to depend on the driving GCM and not to be in phase with each other, complicating the interpretation of results. Superimposed long-term trends may also coexist with the oscillations but this aspect was not investigated in this study. As an illustration, Appendix 6 presents the time-series of bias-corrected monthly precipitation in January, April, and October along the entire 1981-2100 period for the RCP4.5 scenarios, using bias-correction method 1. A 5-year moving average was applied to the monthly series in order to make the oscillations appear more clearly. Similar results were observed for the RCP8.5 scenarios. The presence of decadal to multi-decadal oscillations in the precipitation scenarios may have an influence on the hydrological response of the studied catchments as precipitation constitutes the input to the hydrological cycle.

Table 5: Projected average warming rate in degree Celsius/decade, estimated from the bias-corrected catchment-averaged monthly temperature series. All scenarios displayed a statistically significant linear trend (slope of the linear regression statistically different from zero).

Month	vhm148		vhm51		vhm64	
	RCP4.5	RCP8.5	RCP4.5	RCP8.5	RCP4.5	RCP8.5
1	0.269	0.332	0.304	0.404	0.272	0.356
2	0.269	0.433	0.308	0.479	0.285	0.446
3	0.268	0.421	0.282	0.449	0.278	0.424
4	0.297	0.422	0.269	0.405	0.268	0.4
5	0.295	0.437	0.276	0.456	0.259	0.395
6	0.286	0.429	0.301	0.487	0.261	0.384
7	0.306	0.505	0.353	0.615	0.31	0.557
8	0.304	0.553	0.37	0.626	0.279	0.554
9	0.319	0.506	0.349	0.525	0.254	0.393
10	0.310	0.465	0.368	0.538	0.289	0.428
11	0.254	0.399	0.287	0.491	0.242	0.407
12	0.253	0.411	0.298	0.483	0.257	0.413
Mean	**0.285**	**0.443**	**0.314**	**0.496**	**0.27**	**0.43**

Table 6: Projected precipitation linear trend (mm/day / decade), estimated from scenarios with a statistically significant linear trend (slope of the linear regression statistically different from zero). Estimation from the bias-corrected catchment-averaged monthly precipitation series using correction method 1. Number of scenarios used in the estimation is given in brackets.

Month	vhm148		vhm51		vhm64	
	RCP4.5	RCP8.5	RCP4.5	RCP8.5	RCP4.5	RCP8.5
1	/	-0.29 (2)	/	0.14 (2)	/	-0.21 (1)
2	/	/	/	/	/	-0.23 (2)
3	/	-0.174 (1)	/	0.106 (1)	/	-0.213 (1)
4	/	/	/	0.10 (1)	/	/
5	/	-0.14 (1)	/	/	-0.151 (1)	/
6	/	-0.097 (3)	-0.0073 (2)	0.009 (2)	/	-0.094 (1)
7	/	/	0.1127 (2)	0.11 (2)	0.122 (2)	0.136 (3)
8	/	-0.14 (3)	0.12 (2)	0.146 (2)	0.132 (1)	0.17 (3)
9	/	/	0.13 (2)	0.19 (5)	0.206 (3)	0.237 (3)
10	/	0.27 (3)	0.12 (2)	0.22 (3)	/	0.295 (4)
11	0.388 (2)	0.33 (1)	0.1325 (1)	0.208 (2)	-0.16 (1)	0.39 (3)
12	/	0.3 (2)	0.17 (1)	0.21 (3)	/	0.243 (2)

6 Streamflow projection scenarios

Daily streamflow discharge scenarios were simulated for the three catchments over the 1981-2100 period by forcing HYPE with the ensemble of bias-corrected CORDEX precipitation and temperature scenarios. Two simulated streamflow discharge series were obtained for each climate scenario (Table 3): one by forcing HYPE with the precipitation scenario bias-corrected with method 1 and the other one by forcing HYPE with the precipitation scenario bias-corrected with method 2 (cf. Section 3-7), leading to an ensemble of twelve simulated streamflow discharge series for each RCP emission scenario.

6-1 Comparison with observed streamflow in the reference period

In order to evaluate the skill of the bias-correction methods applied to CORDEX precipitation and temperature series and their transmission into the hydrological modelling chain, the streamflow discharge scenarios simulated in the 1981-2010[1] reference period (water-years 1981 to 2010) were compared to observed discharge series and to streamflow discharge simulations made with HYPE forced with ICRA weather data. Figs 14 to 16 present the seasonality of mean daily streamflow discharge in the 1981-2010 period, together with temperature, precipitation and snow accumulation. The seasonality of these hydro-climatic variables was found to be usually well reproduced by the ensemble mean of all scenarios. Mean daily streamflow discharge was found to be partly underestimated in winter for vhm64, as was the reference streamflow discharge simulation made with HYPE forced with ICRA reanalysis (see also Fig. 10). So there is consistency between HYPE simulations forced with ICRA reanalysis and with the bias-corrected CORDEX scenarios.

Some variations can be observed between the different scenarios, as expected. The spread of the ensemble reflects the uncertainty associated to the climate scenarios, the evolution of climate projections, the bias-correction methods and their transmission into the hydrological modelling chain. In conclusion, the climatology of projected streamflow scenarios in the 1981-2010 period offers a reliable estimation of reference streamflow climatology in that period, giving credibility to the bias-correction methods applied to the CORDEX climate scenarios. It is assumed in the rest of the study that the validity of the bias-correction methods holds for the entire projection period.

[1] the reference period is 1982-2011 for vhm64 because a spin-up period of two years was used

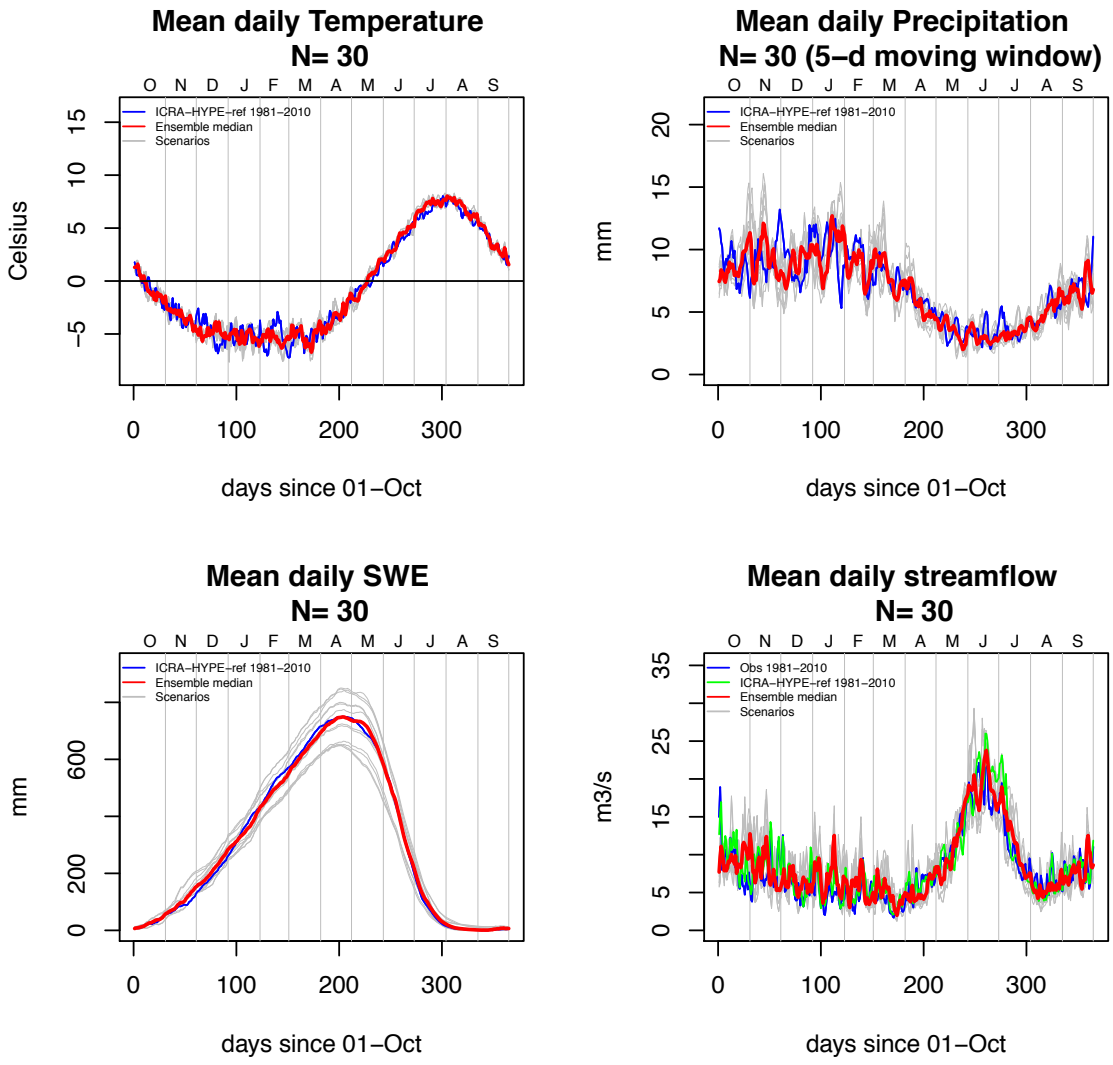

Fig.14: Catchment vhm148: Mean daily temperature (top-left); Mean daily precipitation (top-right); Mean daily snow accumulation (bottom-left); Mean daily discharge (bottom-right). Estimations derived from observations and HYPE simulations forced with CORDEX scenarios in the 1981-2010 period. Individual scenarios are coloured in grey and the ensemble median of all scenarios is coloured in red.

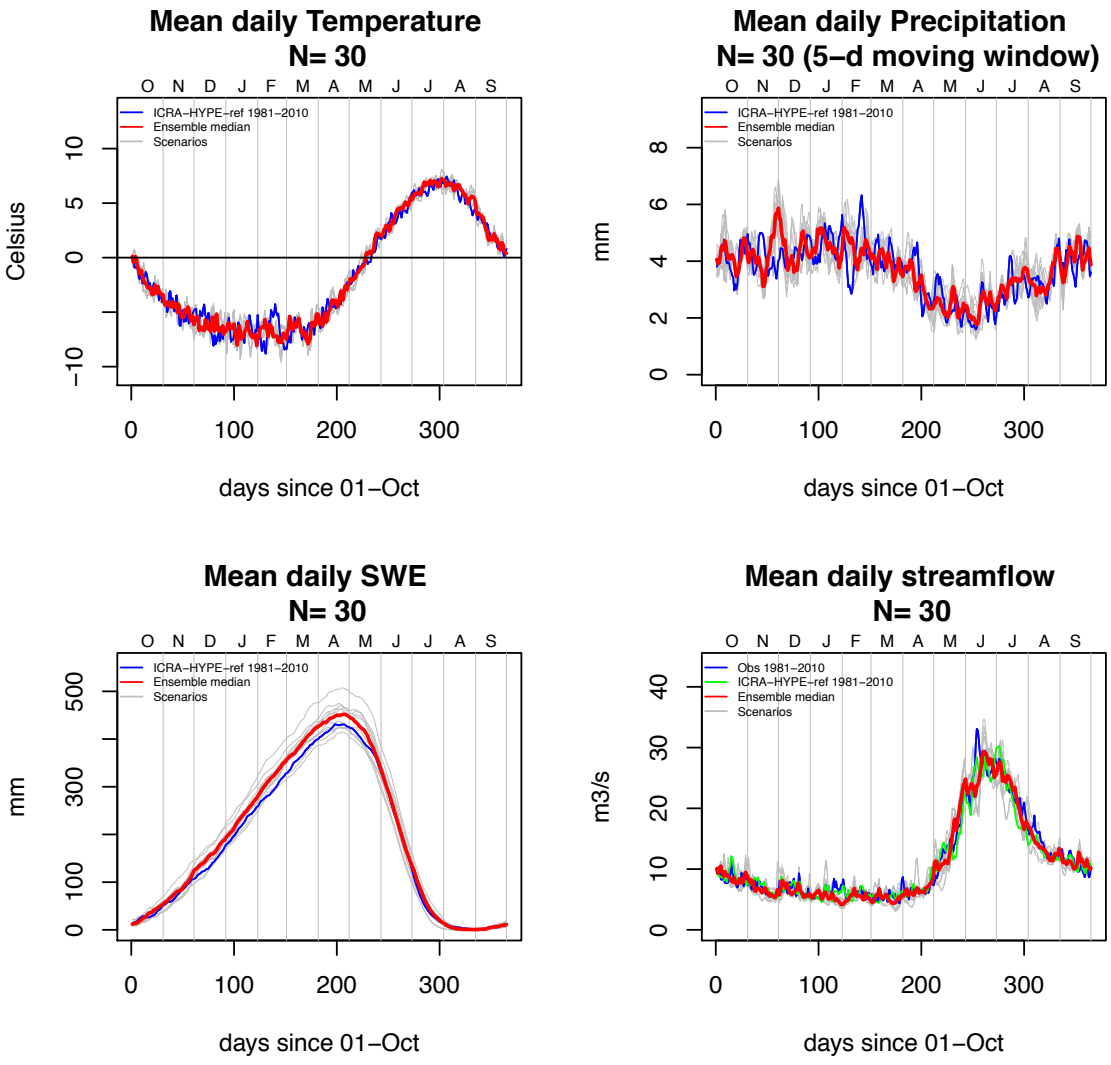

Fig.15: Catchment vhm51: Mean daily temperature (top-left); Mean daily precipitation (top-right); Mean daily snow accumulation (bottom-left); Mean daily discharge (bottom-right). Estimations derived from observations and HYPE simulations forced with CORDEX scenarios in the 1981-2010 period. Individual scenarios are coloured in grey and the ensemble median of all scenarios is coloured in red.

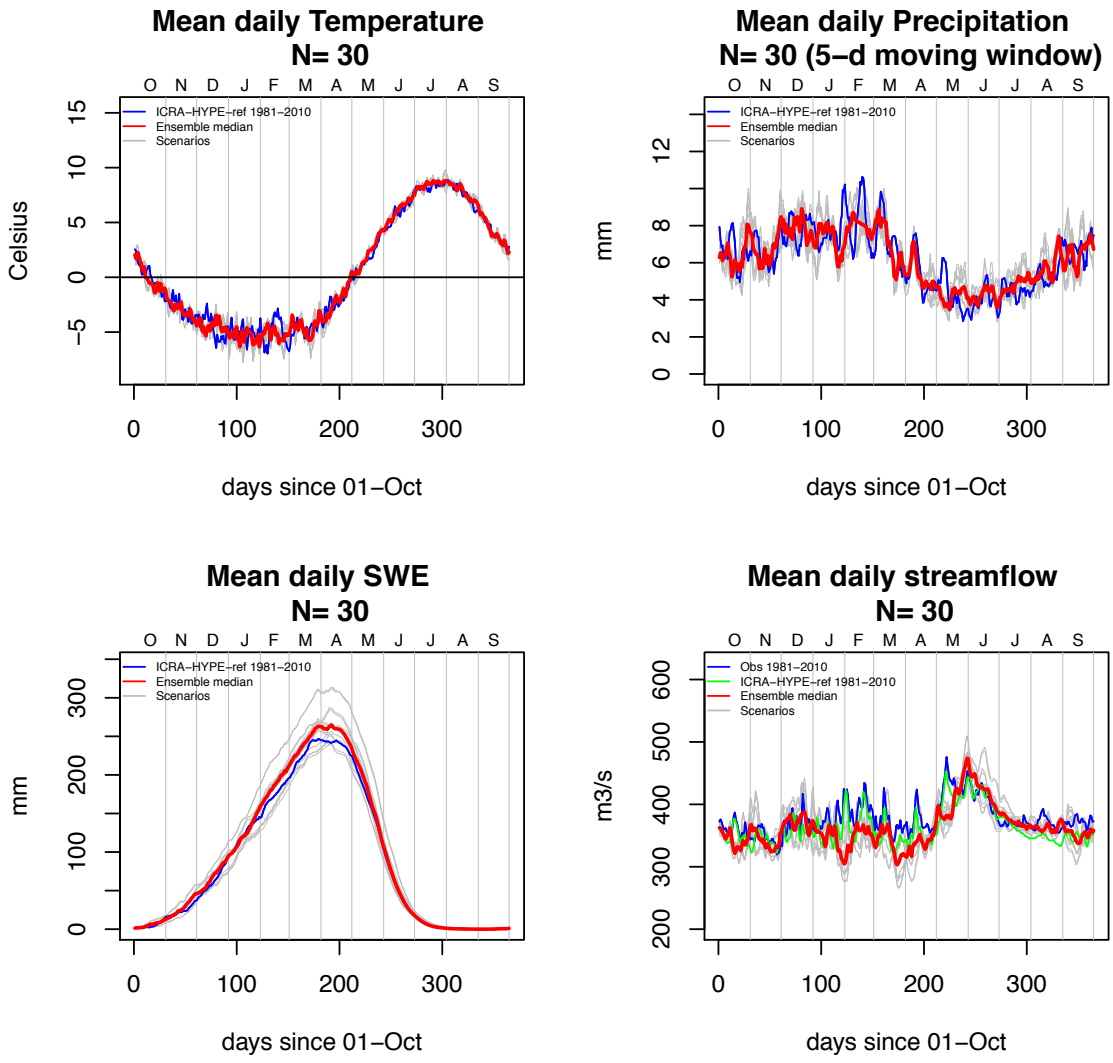

Fig.16: Catchment vhm64: Mean daily temperature (top-left); Mean daily precipitation (top-right); Mean daily snow accumulation (bottom-left); Mean daily discharge (bottom-right). Estimations derived from observations and HYPE simulations forced with CORDEX scenarios in the 1982-2011 period. Individual scenarios are coloured in grey and the ensemble median of all scenarios is coloured in red.

6-2 Hydrological response to projected climate changes

This section examines the impact of projected climate change on the seasonality of mean daily streamflow discharge. For illustration, the results of the 2021-2050, 2041-2070 and 2071-2100[2] time-windows are presented in Figures 17 to 22, together with the seasonality of mean daily snow accumulation. The ensemble median is coloured in red for days when the Mann-Whitney test detected a significant change relative to the 1981-2010[3] reference period and orange otherwise. The percentage of days in the water-year with a significant change is also indicated.

Overall, the studied rivers basins were found to respond to projected climate change, in particular to temperature warming. As expected, results displayed variations between scenarios, mainly related to the driving GCM. As the projection horizon increases, increasing temperature warming is projected to gradually lead to a shorter snow season combined with less snow accumulation and a shift toward an earlier peak of snow accumulation. The hydrological simulations projected i) a change toward an increased streamflow in autumn-winter related to an increased fraction of rain over snow and an increased number of snowmelt events, ii) an earlier and lower spring peak and iii) a decrease of summer streamflow, except for glaciated catchment vhm64 where summer streamflow is maintained to a level comparable to the reference period around August and September thanks to the glacier melt contribution that will be maintained or even increased along the 21st century (not shown). As expected, the larger temperature warming projected by the RCP8.5 emission scenario was found to lead to more dramatic changes in the streamflow seasonality of all catchments than the RCP4.5 emission scenario. A glacier retreat was also projected along the 21st century for both glaciated catchments (not shown).

Towards the end of the 21st century (2071-2100), snow accumulation in catchment vhm148 is projected to drastically shrink, a rain-fed flow regime is projected to dominate, especially under the RCP8.5 emission scenario. The streamflow seasonality pattern will be more like the precipitation seasonality pattern. Catchment vhm64 is also projected to experience a large reduction of snow accumulation and the influence of spring snowmelt in the flow seasonality will diminish but glacier melt will partly compensate snowmelt reduction (not shown), especially under the RCP8.5 emission scenario. The streamflow seasonality pattern will also be a bit more like the precipitation seasonality pattern. Catchment vhm51 in the north is projected to be less vulnerable to temperature warming with respect to snow accumulation, thanks to the very negative winter temperature and the elevated altitude of a large part of its catchment. Consequently, spring is projected to remain the season with the highest streamflow in vhm51 thanks to a considerable snowmelt, but glacier melt will be considerably reduced compared to the reference period (not shown).

[2] The period 2071-2100 is in fact made of 28 water-years : water-years 2071 to 2098

[3] for vhm64, the reference time-window is 1982-2011 because a spin-up period of two years was used

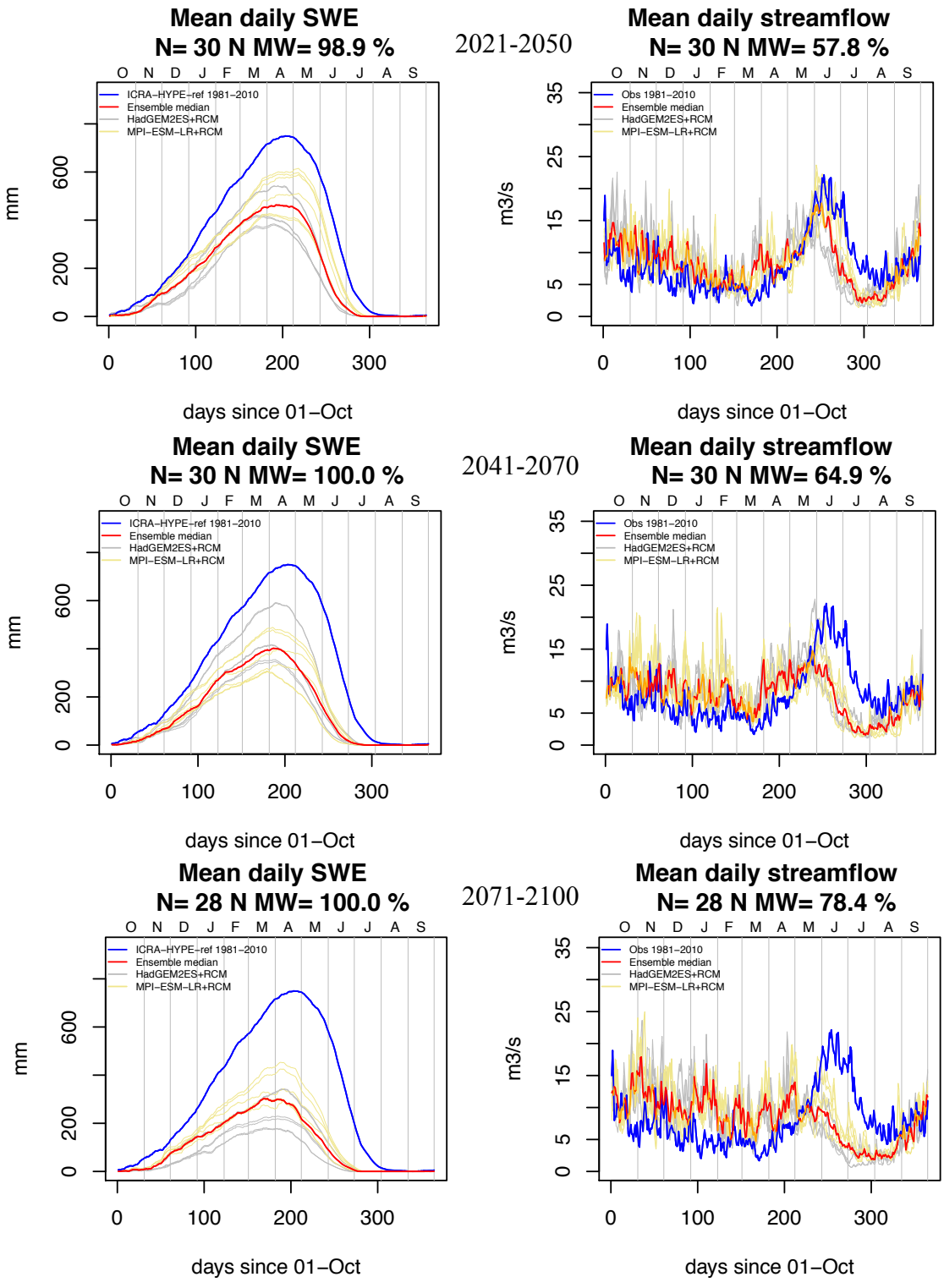

Fig. 17: Catchment vhm148: Projected mean daily snow accumulation (left-panel) and mean daily streamflow discharge (right-panel) under the RCP4.5 emission scenarios. Projection horizon: 2021-2050 (top), 2041-2070 (middle) and 2071-2100 (bottom). Individual scenarios are coloured in grey and khaki. The ensemble median is coloured in red for days when the Mann-Whitney test detected a significant shift compared to the 1981-2010 time-window and orange otherwise. Number of years in the time-window (N). Percentage of days in the water-year with a significant shift relative to 1981-2010 is also given (N MW). Observed situation in 1981-2010 (blue).

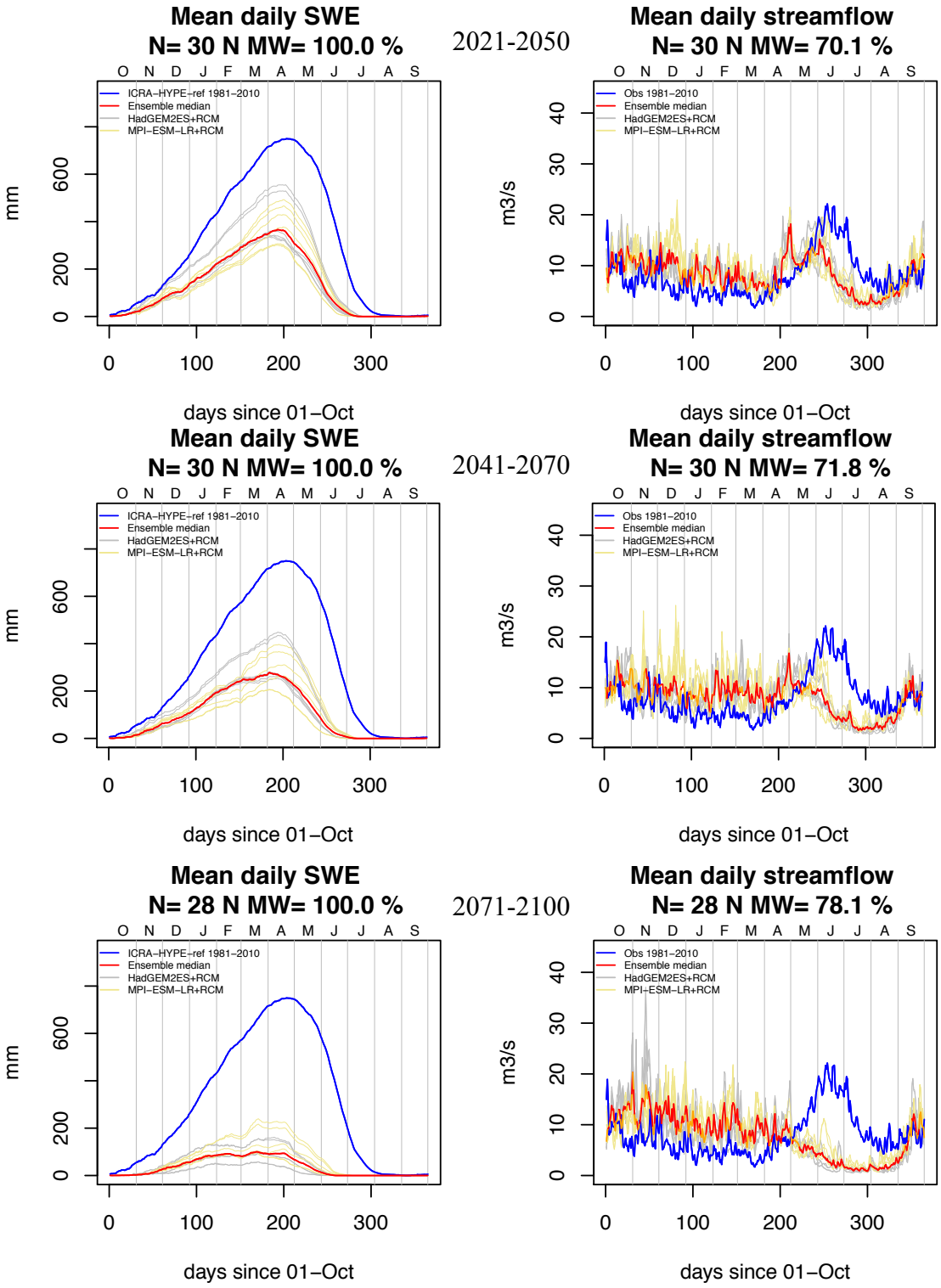

Fig. 18: Catchment vhm148: Projected mean daily snow accumulation (left-panel) and mean daily streamflow discharge (right-panel) under the RCP8.5 emission scenarios. Projection horizon: 2021-2050 (top), 2041-2070 (middle) and 2071-2100 (bottom). Individual scenarios are coloured in grey and khaki. The ensemble median is coloured in red for days when the Mann-Whitney test detected a significant shift compared to the 1981-2010 time-window and orange otherwise. Number of years in the time-window (N). Percentage of days in the water-year with a significant shift relative to 1981-2010 is also given (N MW). Observed situation in 1981-2010 (blue).

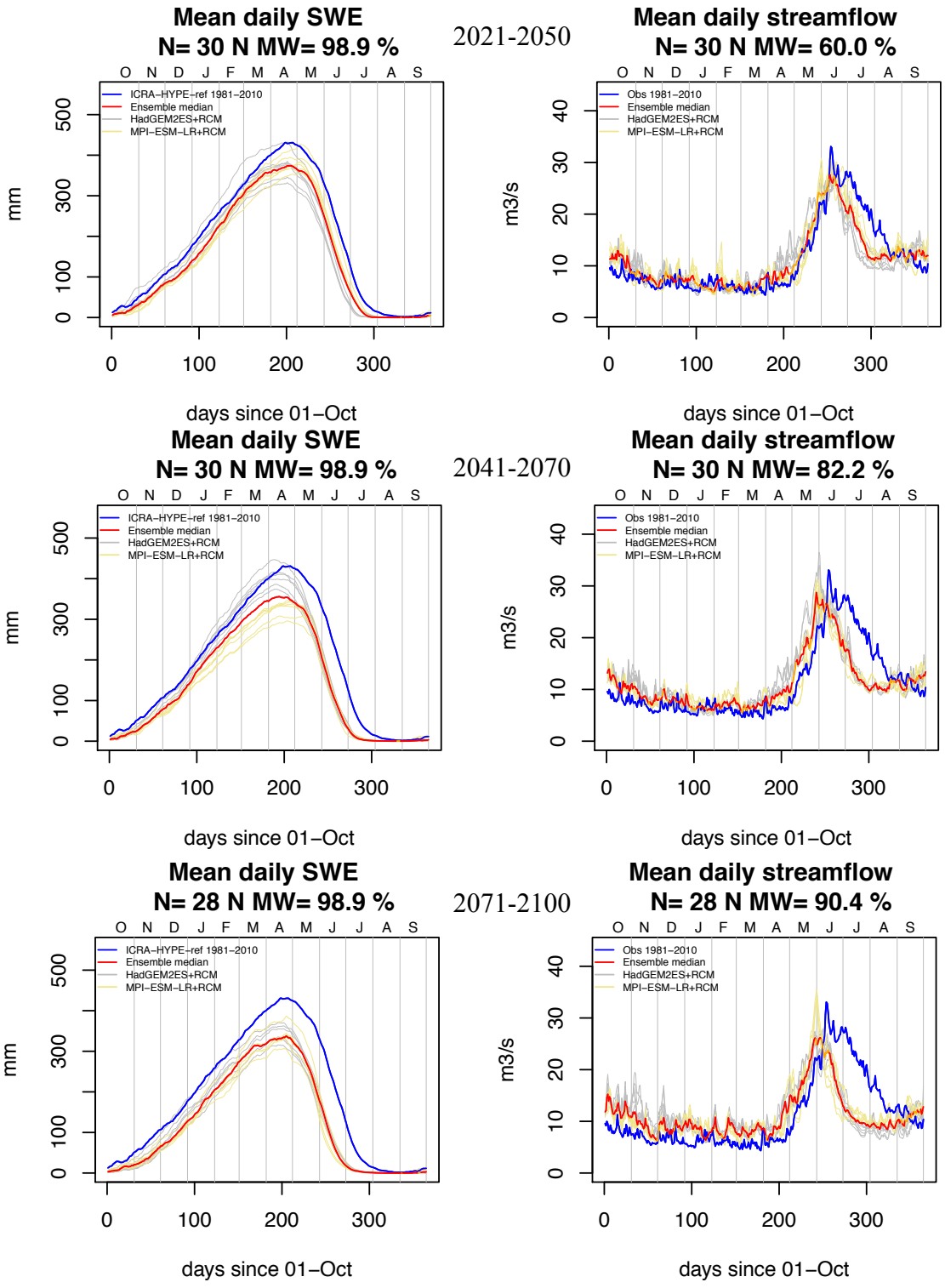

Fig. 19: Catchment vhm51: Projected mean daily snow accumulation (left-panel) and mean daily streamflow discharge (right-panel) under the RCP4.5 emission scenarios. Projection horizon: 2021-2050 (top), 2041-2070 (middle) and 2071-2100 (bottom). Individual scenarios are coloured in grey and khaki. The ensemble median is coloured in red for days when the Mann-Whitney test detected a significant shift compared to the 1981-2010 time-window and orange otherwise. Number of years in the time-window (N). Percentage of days in the water-year with a significant shift relative to 1981-2010 is also given (N MW). Observed situation in 1981-2010 (blue).

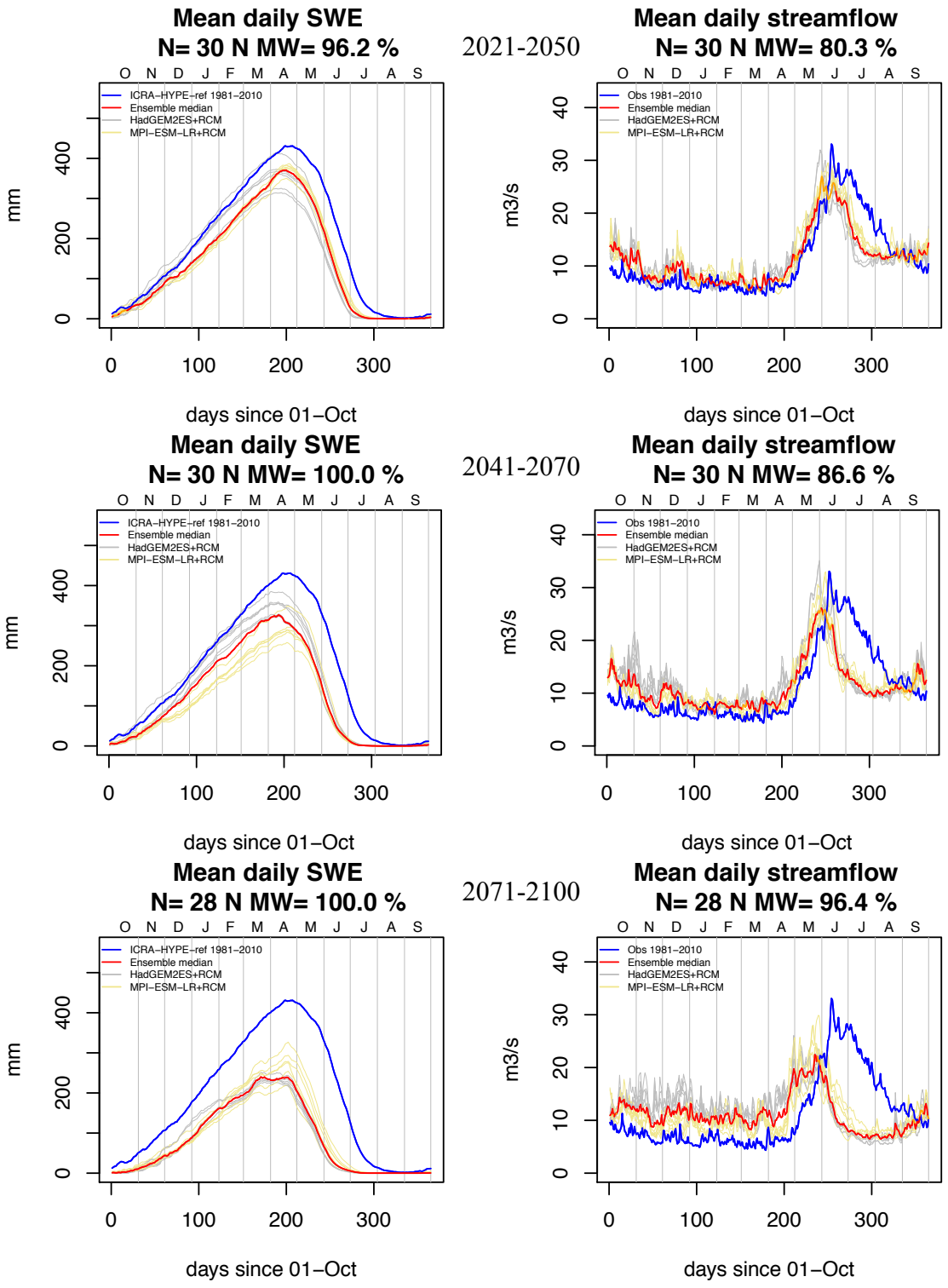

Fig. 20: Catchment vhm51: Projected mean daily snow accumulation (left-panel) and mean daily streamflow discharge (right-panel) under the RCP8.5 emission scenarios. Projection horizon: 2021-2050 (top), 2041-2070 (middle) and 2071-2100 (bottom). Individual scenarios are coloured in grey and khaki. The ensemble median is coloured in red for days when the Mann-Whitney test detected a significant shift compared to the 1981-2010 time-window and orange otherwise. Number of years in the time-window (N). Percentage of days in the water-year with a significant shift relative to 1981-2010 is also given (N MW). Observed situation in 1981-2010 (blue).

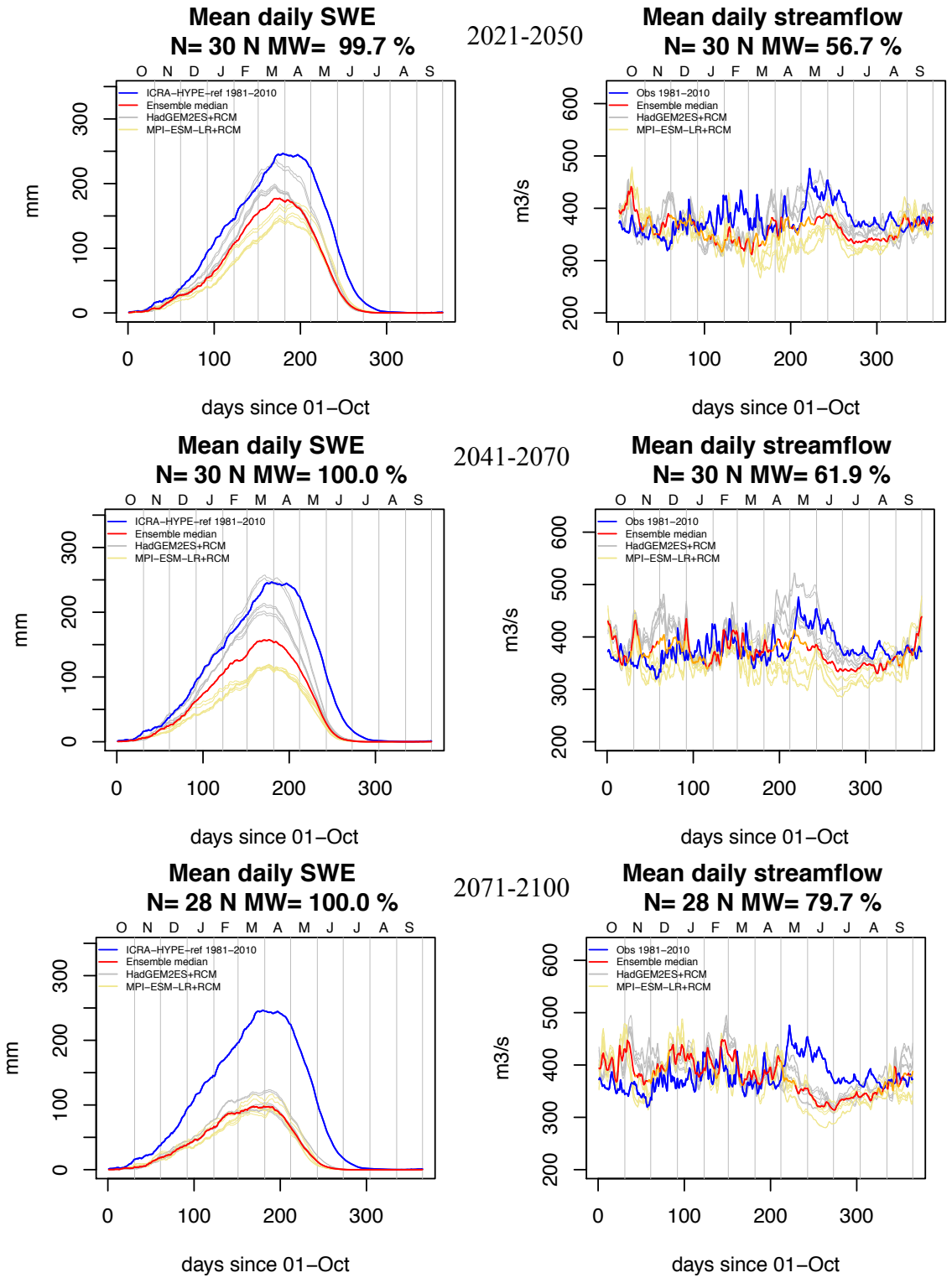

Fig. 21: Catchment vhm64: Projected mean daily snow accumulation (left-panel) and mean daily streamflow discharge (right-panel) under the RCP4.5 emission scenarios. Projection horizon: 2021-2050 (top), 2041-2070 (middle) and 2071-2100 (bottom). Individual scenarios are coloured in grey and khaki. The ensemble median is coloured in red for days when the Mann-Whitney test detected a significant shift compared to the 1982-2011 time-window and orange otherwise. Number of years in the time-window (N). Percentage of days in the water-year with a significant shift relative to 1982-2011 is also given (N MW). Observed situation in 1982-2011 (blue).

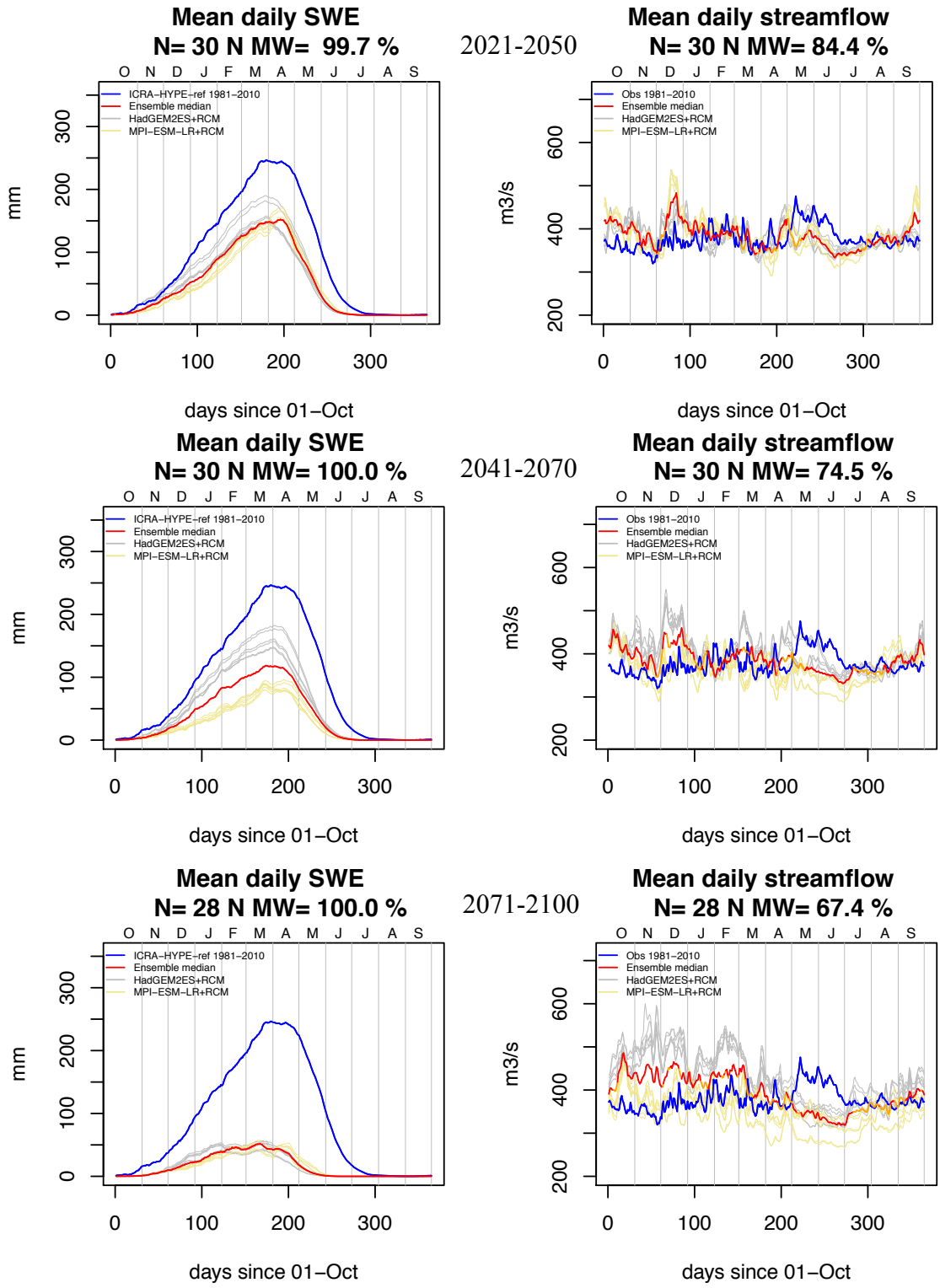

Fig. 22: Catchment vhm64: Projected mean daily snow accumulation (left-panel) and mean daily streamflow discharge (right-panel) under the RCP8.5 emission scenarios. Projection horizon: 2021-2050 (top), 2041-2070 (middle) and 2071-2100 (bottom). Individual scenarios are coloured in grey and khaki. The ensemble median is coloured in red for days when the Mann-Whitney test detected a significant shift compared to the 1982-2011 time-window and orange otherwise. Number of years in the time-window (N). Percentage of days in the water-year with a significant shift relative to 1982-2011 is also given (N MW). Observed situation in 1982-2011 (blue).

In order to get a further insight into the temporal evolution of the hydrological response, annual and seasonal streamflow discharge projections were analysed along the different 30-year time-windows, together with catchment-averaged temperature and precipitation. A Mann-Whitney test was first applied to each individual scenario to compare the sample of thirty seasonal and annual values of each time-window to the sample of thirty seasonal and annual values in the 1981-2010[4] reference time-window. Then a Mann-Whitney test was applied to compare the ensemble of twelve 30-year mean seasonal and mean annual values of each time-window to those of the 1981-2010 reference time-window. The results are presented in Appendix 7 and the analysis below summarised the projected variations of the ensemble of twelve mean annual and seasonal values.

- Catchment vhm148
  - RCP4.5 emission scenarios
    - Annual (water-year)
      Mean annual temperature is projected to remain negative until 1991-2020, then to become positive. Mean annual precipitation is essentially projected to fluctuate around the reference level. Mean annual streamflow follows the precipitation oscillations and stays close to the reference level of 1981-2010.
    - OND
      Mean seasonal temperature is projected to continuously increase but to remain negative. Mean seasonal precipitation is projected to oscillate around the 1981-2010 reference level and a significant increase is observed in time-windows corresponding to wetter periods. A significant increase of mean seasonal streamflow is projected along the 21st century, relative to the 1981-2010 reference period. Mean seasonal streamflow variations are driven by the combined effect of temperature warming, increasing the fraction of rain over snow, and precipitation fluctuations controlling the amount of water entering the catchment.
    - JFM
      Mean seasonal temperature is projected to rise continuously but to remain negative. Mean seasonal precipitation projections fluctuate close to the 1981-2010 level and a decrease is observed between 2011-2030 and 2051-2080. Mean seasonal streamflow is projected to continuously increase along most of the 21st century. Streamflow increase is mainly driven by temperature warming, increasing the fraction of rain over snow and the number of snowmelt events, and modulated by precipitation variations.
    - AMJ
      Mean seasonal temperature is projected to rise while mean seasonal precipitation is essentially projected to oscillate around the reference level. Mean seasonal streamflow is projected to remain close to the reference level until 2011-2040 and to decrease from 2021-2050 until the end of the 21st century, following a reduction of snow accumulation and snowmelt caused by temperature warming.

[4] for vhm64, the reference time-window is 1982-2011

- JAS

  Mean seasonal temperature is projected to continuously rise while mean seasonal precipitation is projected to oscillate around the reference level and to significantly increase during the wetter phases of the oscillations, between 1991-2020 and 2021-2050. Mean seasonal streamflow is projected to decrease as the result of decreased snowmelt caused by a depleted snowpack resulting from temperature warming.

- RCP8.5 emission scenarios
  - Annual (water-year)

    Mean annual temperature was negative in 1981-2010 and is projected to be positive from 1991-2020 until the end of the 21st century. Mean annual precipitation remains close to the reference level. Mean annual streamflow displays a pattern similar to precipitation and remains close to the reference level but a decrease is projected from 2051-2080 until the end of the century.
  - OND

    Mean seasonal temperature is projected to remain negative until 2041-2070, then to be positive until the end of the 21st century. Mean seasonal precipitation fluctuates around the reference level and significantly increases in some time-windows corresponding to wetter phases. Mean seasonal streamflow is essentially projected to increase along the 21st century as the result of continuous temperature warming increasing the fraction of rain over snow. Streamflow variations are also modulated by precipitation fluctuations.
  - JFM

    Mean seasonal temperature is projected to continuously increase but to remain negative. Mean seasonal precipitation is projected to oscillate around the 1981-2010 level and to decrease towards the end of the 21st century. A large spread between individual scenarios increasing with the projection horizon is observed. Mean seasonal streamflow is projected to continuously increase as the result of continuous temperature warming, leading to an increase of rain and snowmelt events.
  - AMJ

    Mean seasonal temperature is projected to continuously increase. Mean seasonal precipitation is projected to remain close to the 1981-2010 reference level and to significantly decrease in 2071-2100. Mean seasonal streamflow is projected to remain close to the reference level and to decrease after 2011-2040. This decrease is mainly driven by a continuous temperature warming leading to a snowpack depletion in winter and a reduction of snowmelt in spring.
  - JAS

    Mean seasonal temperature is projected to continuously increase. Mean seasonal precipitation oscillates around the 1981-2010 reference level and a significant change is projected in some time-windows corresponding to wet phases. Mean seasonal streamflow is projected to continuously decrease as the result of decreased snowmelt caused by a depleted snowpack resulting from temperature warming.

- Catchment vhm51
  - RCP4.5 emission scenarios
    - Annual (water-year)

      Mean annual temperature is projected to remain negative until 2021-2050, then to be positive until the end of the 21st century. Mean annual precipitation is projected to remain close to the reference level until 2031-2060 and then to increase. Precipitation projections from the two groups of scenarios driven by the two GCMs do not always vary in phase, leading to a large spread with increasing horizon. Mean annual streamflow follows variations similar to precipitation but remains essentially close to the reference level.
    - OND

      Mean seasonal temperature is projected to continuously increase but to remain negative. Mean seasonal precipitation is projected to remain close to the reference level but a large spread is observed between scenarios and their trajectories depend on the driving GCM. Mean seasonal streamflow is projected to continuously increase during the 21st century. Streamflow increase will be caused by temperature warming leading to an increase of rain and snowmelt events.
    - JFM

      Mean seasonal temperature is projected to continuously increase but to remain negative. Mean seasonal precipitation is projected to remain close to the reference level until 2051-2080 and then to increase. The two groups of precipitation scenarios driven by the two GCMs display oscillations which are out of phase with each other, making mean seasonal precipitation projections uncertain. Mean seasonal streamflow is projected to significantly increase from 2011-2040 until the end of the 21st century. This increase is driven by temperature warming, increasing the rain fraction over snow and the number of snowmelt events.
    - AMJ

      Mean seasonal temperature is projected to continuously increase. Mean seasonal precipitation is projected to remain close to the reference level but a large spread between scenarios is observed. Mean seasonal streamflow is projected to remain close to the reference level and to increase slightly after 2001-2030 but a large spread is observed between scenarios. This streamflow increase results from an earlier and larger snowmelt from a still large snowpack and from an increase of rain caused by increased temperature.
    - JAS

      Mean seasonal temperature is projected to continuously increase. Mean seasonal precipitation is projected to continuously increase while mean seasonal streamflow is projected to continuously decrease. This trend is driven by temperature warming that will deplete the snowpack earlier in spring and lead to lower snowmelt in summer. Glacier melt which is projected to remain at a similar level until circa 2001-2030 and then decrease until the end of the 21st century (not shown) further contributes to the streamflow decrease.

- RCP8.5 emission scenarios
  - Annual (water-year)

    Mean annual temperature is projected to remain negative until 2011-2040 and then to be positive until the end of the 21st century. Mean annual precipitation is projected to increase but the spread between scenarios increases with the projection horizon. Mean annual streamflow is also projected to increase and a large spread between scenarios is also observed with increasing horizon.
  - OND

    Mean seasonal temperature is projected to increase and become positive in 2071-2100. Mean seasonal precipitation is essentially projected to increase from 2001-2030 to 2071-2100, but the change is not significant between 2041-2070 to 2061-2090. A large spread is observed between the different precipitation scenarios and their trajectories depend on the driving GCM. Mean seasonal streamflow is projected to continuously increase during the 21st century but a large spread is also observed between scenarios. This increase is driven by the projected precipitation increase combined with temperature warming causing more rain and snowmelt events.
  - JFM

    Mean seasonal temperature is projected to increase continuously during the entire period but to remain negative. Mean seasonal precipitation is projected to fluctuate around the reference level and to increase from 2051-2080 until the end of the 21st century but some spread is observed between scenarios. Mean seasonal streamflow is projected to continuously increase. This increase is mainly driven by temperature warming, causing more rain and snowmelt events, and further enhanced by a precipitation increase from 2051-2080 until the end of the century.
  - AMJ

    Mean seasonal temperature is projected to continuously increase. Mean seasonal precipitation is projected to oscillate around the reference level without significant change before 2061-2090 when an increase is projected. Individual precipitation scenarios follow three distinct trajectories, leading to a large spread and a large uncertainty regarding the ensemble mean. Mean seasonal streamflow remains close to the reference level along the projection horizon but some significant increase is detected in some time-windows from 2001-2030 to 2031-2060 caused by an earlier and larger snowmelt and an increase of rain caused by temperature warming. A decrease is then projected in 2071-2100 most likely because snowmelt reduction is not compensated by rain increase.
  - JAS

    Mean seasonal temperature is projected to continuously increase. Mean seasonal precipitation is essentially projected to increase but streamflow is projected to continuously decrease because of a reduction of snowmelt caused by a snowpack reduction driven by continuous temperature warming. Glacier melt which is projected to remain at a similar level until circa 2011-2040 and then continuously decrease until the end of the 21st century (not shown) further contributes to the streamflow decrease.

- Catchment vhm64
  - RCP4.5 emission scenarios
    - Annual (water-year)

      Mean annual temperature, already positive in 1982-2011, is projected to increase until the end of the 21st century. Mean annual precipitation is projected to remain close to the 1982-2011 reference level until 2051-2080 and then to increase slightly but a large spread is observed between scenarios. Precipitation projections from individual scenarios strongly depend on the driving GCM. Streamflow projections follow the same trajectory than precipitation projections with a similar spread between scenarios. Mean annual streamflow is essentially projected to remain close to the reference level until 2051-2080 and then to increase slightly.
    - OND

      Mean seasonal temperature is projected to increase but to remain negative. Mean seasonal precipitation remains close to the reference level until 2051-2080 and then an increase is projected. However, a large spread is observed between scenarios after 2021-2050 and projections strongly differ according to the driving GCM. Mean seasonal streamflow is essentially projected to increase along the 21st century but a large spread is observed between scenarios. This increase is driven by projected temperature warming causing an increase of rain and snowmelt events and is also modulated by precipitation variations.
    - JFM

      Mean seasonal temperature is projected to continuously increase but to remain negative. Mean seasonal precipitation is projected to oscillate around the 1982-2011 level and some significant change is detected in some time-windows. The oscillations of individual scenarios depend on the driving GCM. Mean streamflow is projected to fluctuate around the 1982-2011 reference level until 2031-2060, as precipitation, and then an increase is projected until the end of the 21st century. This streamflow increase is mainly driven by temperature warming leading to an increase of rain and snowmelt events.
    - AMJ

      Mean seasonal temperature is projected to continuously increase. Mean seasonal precipitation is projected to remain close to the reference level but a large spread is observed between scenarios. Mean seasonal streamflow is projected to remain close to the reference level, as mean seasonal precipitation, and then to decrease in 2071-2100. A large spread is also observed between scenarios. Streamflow variations in spring are related to precipitation variations and to snowmelt variations which in turn depend on variations of snow accumulation in winter. Some glacier melt increase is also projected in spring and contributes to compensate the projected decrease of snowmelt caused by a depleted snowpack (not shown).
    - JAS

      Mean seasonal temperature is projected to continuously increase. Mean seasonal precipitation is projected to increase while mean seasonal streamflow is projected to remain close to the 1982-2011 level but a large spread between scenarios is observed after

2031-2060. Glacier melt is projected to remain close to the 1982-2010 reference period (not shown). Infiltration may also play some role at filtering out precipitation, snow and glacier melt and delaying their contribution to streamflow.

- RCP8.5 emission scenarios
  - Annual (water-year)
    Mean annual temperature, already positive in 1982-2011, is projected to increase until the end of the 21st century. Mean annual precipitation is projected to increase slightly along the 21st century but a large spread is observed between the scenarios that follow different paths depending on the driving GCM. Mean annual streamflow is projected to follow a pattern similar to precipitation and to increase slightly along the 21st century but a large spread is observed between scenarios.
  - OND
    Mean seasonal temperature is projected to continuously rise and to become positive after 2041-2070. Mean seasonal precipitation is essentially projected to increase slightly but a large spread between scenarios, increasing with the projection horizon, is observed. The precipitation scenarios follow different paths depending on the driving GCM. A significant increase of mean seasonal streamflow is projected in all time-windows but the spread between scenarios increases with the projection horizon. Mean seasonal streamflow variations are mainly driven by projected variations of mean seasonal precipitation and by temperature warming causing an increase of rain and snowmelt events.
  - JFM
    Mean seasonal temperature is projected to continuously increase but to remain negative. Mean seasonal precipitation remains close to the reference level until 2011-2040 and then a slight decrease is essentially projected until the end of the century but a large spread between scenarios, increasing with the projection horizon, is observed. Mean seasonal streamflow is projected to increase along the 21st century, mainly driven by temperature warming causing the number of rain and snowmelt events to increase. The spread between scenarios increases after 2031-2060, mainly because of the large spread observed in the precipitation scenarios.
  - AMJ
    Mean seasonal temperature is projected to continuously increase. Mean seasonal precipitation is projected to remain close to the reference level but a large spread between scenarios is observed. Mean seasonal streamflow is projected to remain close to the reference level, as precipitation, but to decrease after 2051-2080. Temperature warming leads to a snowmelt reduction resulting from a snowpack depletion. The decrease of snowmelt in spring is partly compensated by an increase of glacier melt (not shown).
  - JAS
    Mean seasonal temperature is projected to continuously increase. Mean seasonal precipitation is projected to increase during most of the 21st century. Mean seasonal streamflow is projected to fluctuate close to the reference level, in phase with precipitation

variations and some increase is projected from 2001-2030 to 2041-2070. An increasing spread is also observed between scenarios after 2041-2070. Glacier melt is projected to increase more than under the RCP4.5 scenario and to add its contribution to the projected streamflow increase (not shown). Infiltration may also play some role at filtering out precipitation, snow and glacier melt and delaying their contribution to streamflow.

In summary, variations of projected mean annual streamflow discharge along the different 30-year time-windows are mainly driven by variations of mean annual precipitation. Variations of mean seasonal streamflow discharge are driven by both precipitation and temperature variations, in relation to variations of rain, snowmelt and glacier melt. The projected temperature warming is quite linear and usually consistent between the different scenarios, for all catchments. Projected precipitation variations depend on the catchment and season and do not always vary in phase between the different scenarios.

Based on the analysis above, mean seasonal streamflow discharge is projected to i) essentially keep increasing along the 21st century in OND and JFM in all watersheds, ii) keep decreasing in AMJ for vhm148 and remain essentially unchanged for vhm51 and vhm64, iii) keep decreasing in JAS for vhm148 and vhm51 and remain essentially unchanged for vhm64.

The analysis of catchments vhm51 and vhm64 revealed some lack of consensus in the projected evolution of precipitation scenarios in some seasons, making the direction and magnitude of seasonal streamflow projections uncertain in some cases. The use of an additional group of scenarios driven by a third reliable GCM could be useful to help identifying the most probable direction of streamflow changes in these catchments.

7 Climate change impact on annual maximum flood characteristics

This section examines the impact of climate change on extreme flood characteristics. Annual maximum flood (AMF) and the corresponding occurrence date were extracted each water-year from the observed daily streamflow discharge series in the 1981-2010 reference period and from the daily streamflow discharge projection scenarios in the 1981-2100[5] period considering moving 30-year time-windows. A Gumbel extreme-value distribution was fitted to the empirical AMF frequency distributions and the T-year floods Q(T) extracted for return periods T=2, 5, 10, 20, 50, and 100 years. The evolution in the number of AMF occurrences taking place in each season along the time-windows was analysed and changes relative to the 1981-2010 period estimated. Then, the evolution of the magnitude of the T-year floods, Q(T), along these time-windows was analysed and changes relative to the 1981-2010 period estimated. Finally, the flood magnitude Q was fixed and the evolution of the corresponding return period T(Q) estimated along the moving time-windows.

7-1 AMF occurrence dates

Figs. 23 to 28 present the temporal evolution of the median number of AMF occurrences in each season along the different time-windows. Detailed results from all scenarios are given in Appendix 8.

- Catchment vhm148 (Fossá)

In the 1981-2010 reference period, this catchment was dominated by rain-fed floods and OND was by far the season with the largest number of AMF occurrences, followed by JFM, JAS and AMJ.

- RCP4.5 emission scenarios

The number of AMF occurrences taking place in JFM is projected to slowly increase along the projection horizon at the expense of a decrease in AMJ and JAS while no change is projected in OND which remains the season with the highest number of AMF occurrences. Note however that by the end of the 21st century, the number of AMF occurrences projected in OND and JFM becomes similar. These results are driven by temperature warming that leads to an increase in the number of rain and snowmelt flood events in winter, while reduced snow cover will lead to fewer snowmelt floods in spring. These changes are not linear and oscillations in the projected number of AMF occurrences along the projection horizon caused by variations of mean seasonal precipitation can be observed.

- RCP8.5 emission scenarios

Results are similar to those observed under the RCP4.5 emission scenarios except that the number of AMF occurrences taking place in JFM is projected to decrease after 2051-2080, most likely because of a larger reduction of snowmelt contribution to floods due to a larger snow cover reduction.

[5] for vhm64, the projection period is 1982-2100 and the reference time-window is 1982-2011

- Catchment vhm51 (Hjaltadalsá)

In the 1981-2010 reference period, this catchment was dominated by rain and snowmelt floods and AMJ was by far the season with the largest number of AMF occurrences followed by JAS and then OND and JFM.

- RCP4.5 emission scenarios

The number of AMF occurrences taking place in AMJ is projected to increase until 2041-2070 and then decrease and reach a level below the 1981-2010 level by the end of the 21st century. The number of AMF occurrences taking place in JAS is projected to decrease until 2021-2050 and then remain unchanged until the end of the 21st century. These results are driven by temperature warming causing a reduction of snow cover and a shift of snowmelt floods earlier in the year. The number of AMF occurrences taking place in OND is projected to increase and become larger than in JAS after 2011-2040 because larger precipitation amounts are projected in that season and temperature warming will lead more frequently to days with positive temperature causing more frequent rain events mixed with snowmelt. A moderate increase in the number of AMF occurrences is also projected in JFM toward the end of the 21st century.

- RCP8.5 emission scenarios

The number of AMF occurrences taking place in AMJ is projected to remain similar to the 1981-2010 level during the entire projection period while a decrease is projected in JAS. The number of AMF occurrences taking place in OND is projected to increase and become larger than in JAS after 1991-2020 because temperature warming will lead to more frequent rain events mixed with snowmelt in that season. A moderate increase is also projected in the number of AMF occurrences in JFM along the 21st century, caused by temperature warming. Note that a large spread between scenarios is observed in OND and AMJ and is probably related to the large spread of seasonal precipitation between scenarios.

- Catchment vhm64 (Ölfusá)

In the 1982-2011 reference period, this catchment was dominated by rain and by mixed rain and snowmelt floods on frozen ground. OND and JFM were the seasons with the largest (and similar) number of AMF occurrences, followed by AMJ and JAS.

- RCP4.5 emission scenarios

The number of AMF occurrences taking place in OND and JFM is projected to remain unchanged, while reduced snow cover will lead to fewer snowmelt floods in AMJ. The number of AMF occurrences taking place in JAS is projected to slowly increase until 2031-2060 and then slowly decrease but to remain above the 1982-2011 level. This increase in JAS is probably driven by floods taking place in September and caused by increased precipitation.

- RCP8.5 emission scenarios

The number of AMF occurrences taking place in OND is projected to increase until the end of the 21st century and oscillate after 2031-2060. This increase is related to the projected increase in precipitation in that season combined with temperature warming, leading more frequently to days with positive temperature and therefore rain and snowmelt events. The number of AMF occurrences taking place in JFM is projected to oscillate around a level close to 1982-2011 and JFM is projected to have fewer AMF occurrences than OND in most of the 21st century. Reduced snow cover and possibly increased infiltration caused by reduced frozen ground will lead to fewer snowmelt floods in AMJ while the number of AMF occurrences taking place in JAS is projected to remain similar to the 1982-2011 level.

In summary, a shift is projected to take place in the seasonal distribution of AMF occurrence dates along the 21st century, conditioned by the physiographic properties of each catchment and their dominating flood-generating mechanisms (rain-fed, snowmelt-fed, interplay of rain and snowmelt). Projected temperature warming will cause changes in snow accumulation and melt and affect their dominating influence on flood generation in AMJ and JAS. Temperature warming will lead to more instability in the snow cover in autumn-winter and to an increase in the frequency of rainy days in OND and JFM and the likelihood of rain floods. The evolution in the number of AMF occurrences taking place in seasons dominated by rain-fed floods will be conditioned by the projected evolution of precipitation which varies differently with the season and often displays decadal to multi-decadal oscillations rather than a linear trend. Disagreements in the projected evolution of seasonal precipitation between individual scenarios driven by the two GCMs contribute to increase the uncertainty in the projected evolution of seasonal distribution of AMF occurrences in some time-windows.

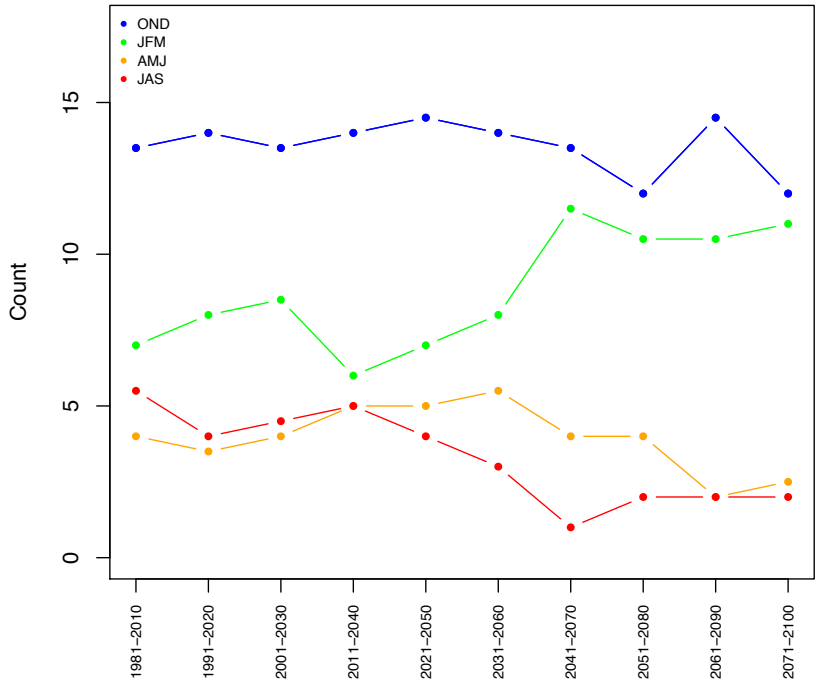

Fig. 23: Catchment vhm148: Projected median number of AMF occurrences in each season, in the 21st century, under the RCP4.5 emission scenario.

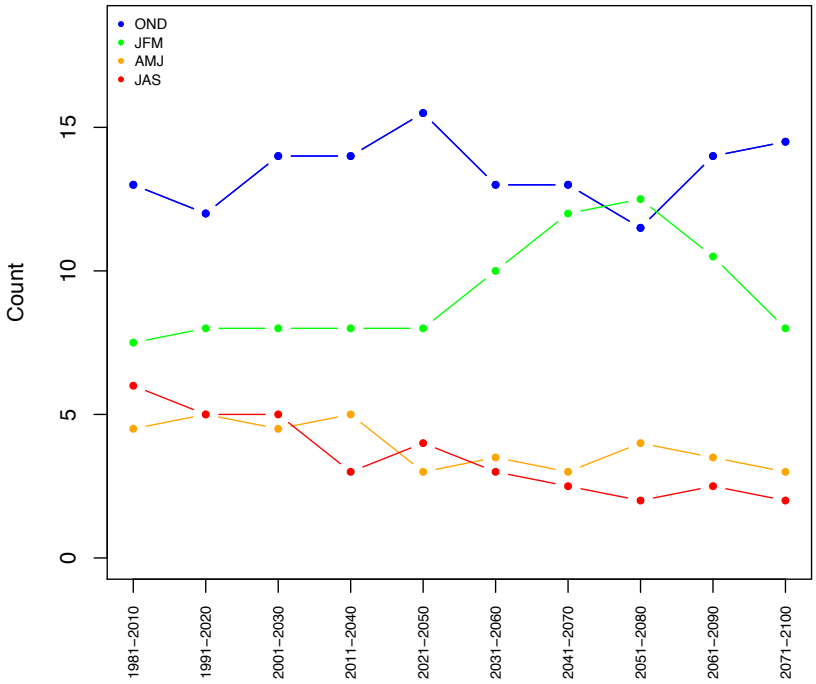

Fig. 24: Catchment vhm148: Projected median number of AMF occurrences in each season, in the 21st century, under the RCP8.5 emission scenario.

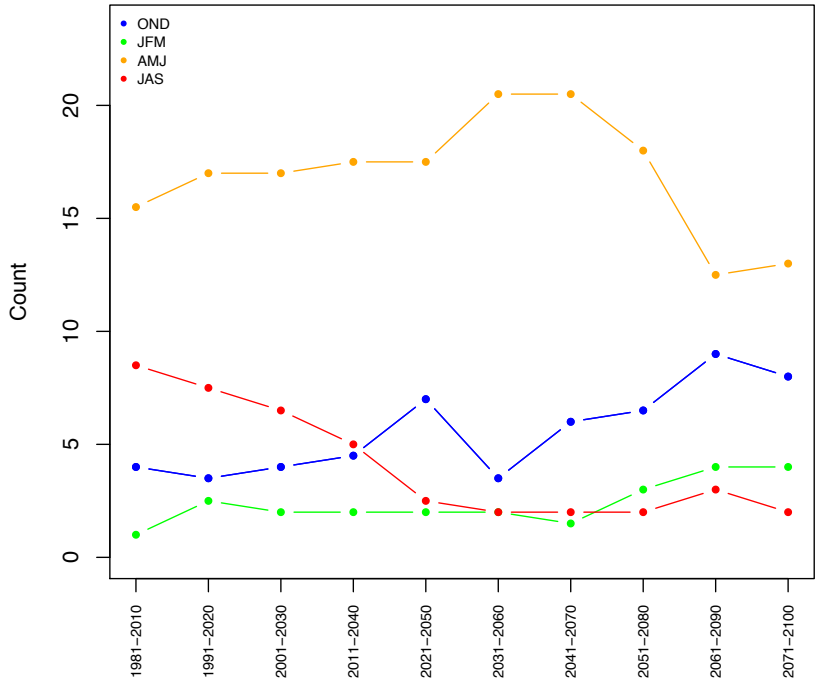

Fig. 25: Catchment vhm51: Projected median number of AMF occurrences in each season, in the 21st century, under the RCP4.5 emission scenario.

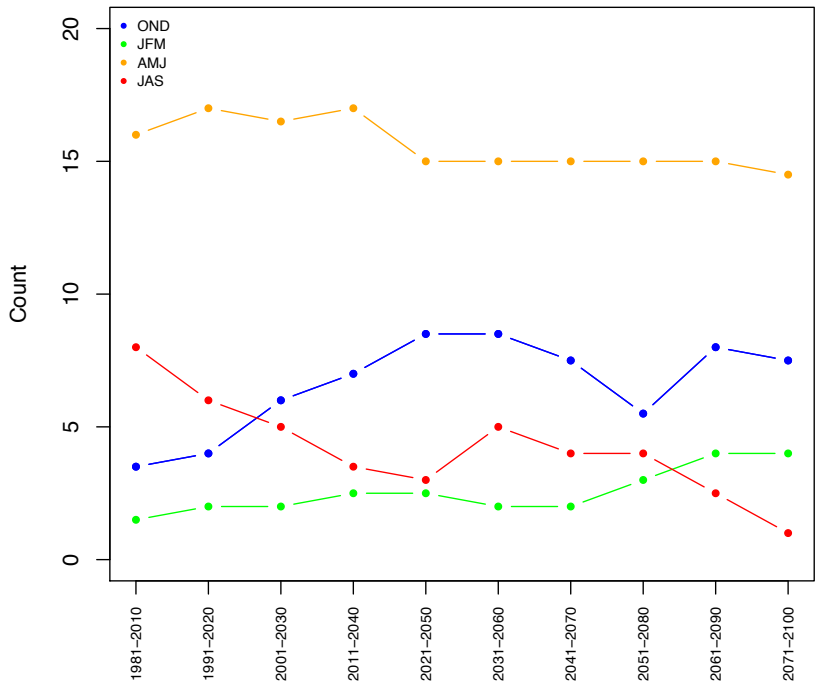

Fig. 26: Catchment vhm51: Projected median number of AMF occurrences in each season, in the 21st century, under the RCP8.5 emission scenario.

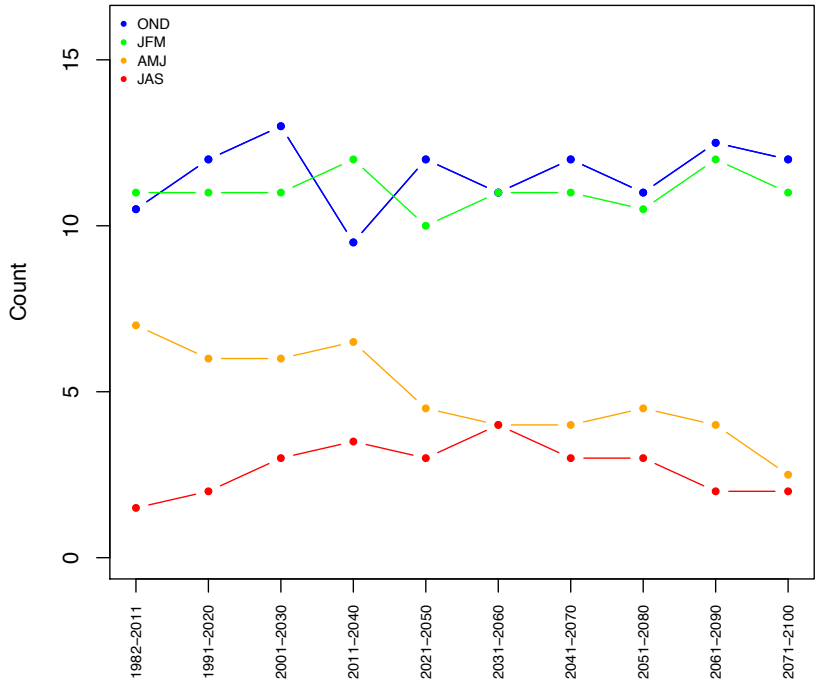

Fig. 27: Catchment vhm64: Projected median number of AMF occurrences in each season, in the 21st century, under the RCP4.5 emission scenario.

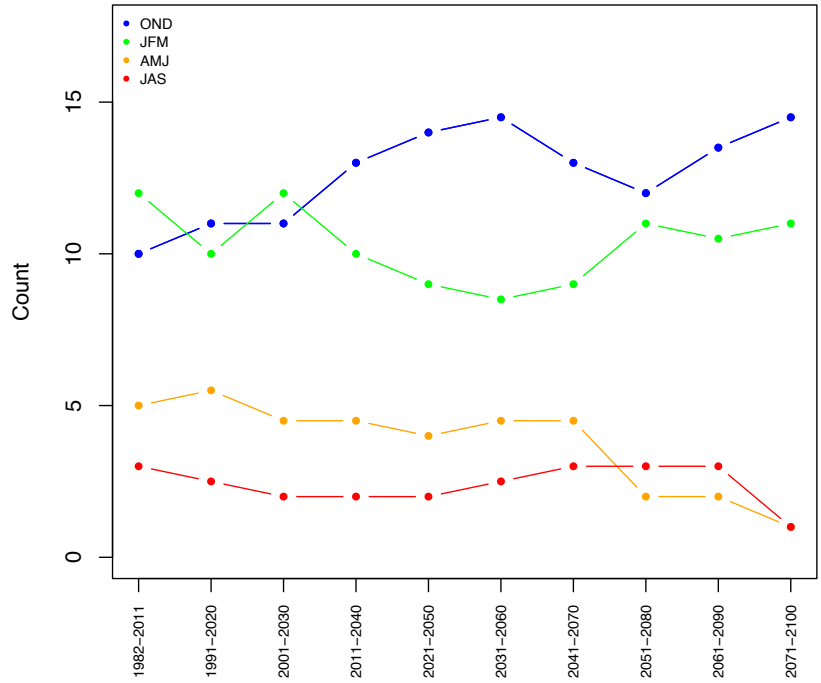

Fig. 28: Catchment vhm64: Projected median number of AMF occurrences in each season, in the 21st century, under the RCP8.5 emission scenario.

7-2 Projected flood frequency distributions

The projected empirical AMF frequency distributions are presented in Appendix 9 for selected time-windows. The spread between scenarios tends to increase as the projection horizon and return period T increase. As mentioned before, the projected evolution of precipitation sometimes differ between scenarios in relation to the driving GCM which in turn has an impact on streamflow projections and subsequently on AMF frequency distributions, especially when rain-fed floods are dominating.

A Gumbel distribution was fitted to each empirical AMF distribution (not shown) and the T-year flood extracted for return periods T=2, 5, 10, 20, 50 and 100 years. The uncertainty associated to the estimation of T-year flood quantiles increases with return period T. In other words, the overall level of uncertainty associated to the estimation of T-year floods from the ensemble of AMF scenarios is large and increases with T and the projection horizon.

7-2-1 Change in the magnitude of T-year floods

The temporal evolution of the different T-year floods of each scenario is similar for the different return periods and only detailed results for the 100-year floods are presented below. Results for each return period are presented in Appendix 10 for the RCP4.5 emission scenarios and in Appendix 11 for the RCP8.5 emission scenarios in form of box-plot statistics. The analysis below makes also use of the seasonal precipitation projections presented in Appendix 7.

- Catchment vhm148 (Fossá)

Figs. 29 and 30 present the evolution of the 100-year floods for all scenarios and Figs. 31 and 32 summarise the results of the percentage change in T-year floods relative to 1981-2010, for all Ts.

- RCP4.5 emission scenarios

According to the ensemble median, the T-year floods are projected to increase along the 21st century with a peak around 2021-2050. The longer the return period, the larger the projected change relative to 1981-2010, until 2051-2080 and then it inverts. The projected median change varies approximately between +5% and +20%. The direction of change is usually consistent between scenarios but the projected changes vary greatly between scenarios.

The projected increase of T-year floods until 2031–2060 is most likely related to an increase in the magnitude of floods in OND caused by a projected precipitation increase combined with temperature warming leading to an increase of rain occurrences, possibly combined with snow melt occurrences. Beyond 2031-2060, the increase of T-year floods relative to 1981-2010 becomes smaller, possibly because temperature warming is projected to deplete snow cover in such a way that snowmelt contribution to OND and JFM floods will be reduced and floods in these seasons will be mainly caused by rain.

- RCP8.5 emission scenarios

According to the ensemble median, the T-year floods are projected to increase along the 21st century. This increase is not gradual but is projected to oscillate. The longer the return period, the larger the projected change relative to 1981-2010, until 2051-2080 and then it inverts. The projected median change varies approximately between +5% and +10%. The direction of change is usually consistent between scenarios but the projected changes vary greatly between scenarios.

The projected increase of T-year floods is most likely related to i) the projected increase of precipitation in OND combined with temperature warming leading to more rain occurrences and ii) an increase in the magnitude of floods in JFM caused by an increase of rain and snowmelt resulting from temperature warming, until little snow is available to melt, making then rain the main driver of winter floods. The median relative change is lower than for RCP4.5 possibly because individual scenarios do not all project changes in the same direction and cancel each other out. Another explanation could be the larger temperature warming that is projected to deplete snow cover faster and to further reduce snowmelt contribution to floods in winter than under RCP4.5.

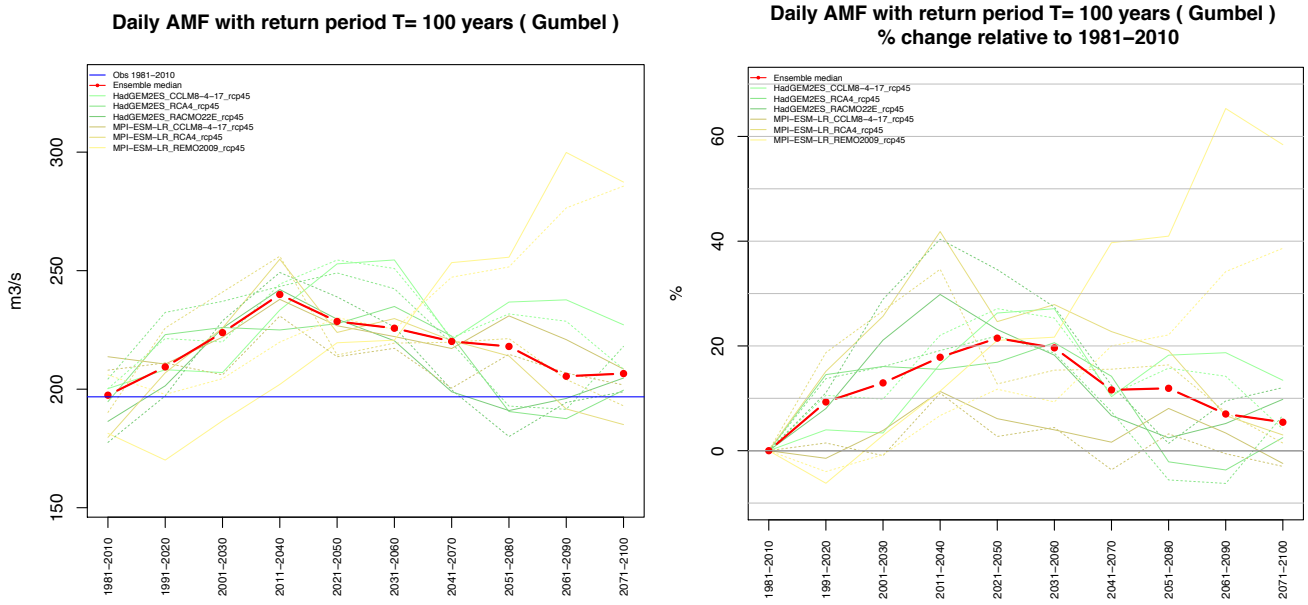

Fig. 29: Catchment vhm148: Evolution of the 100-year flood in the 21st century under the RCP4.5 emission scenarios (left) and percentage change relative to the 1981-2010 reference period (right). HYPE simulations forced with CORDEX precipitation scenarios corrected with method 1 (solid green and yellow lines) and with method 2 (dashed green and yellow lines). Ensemble median (red line) and 100-year flood from observations in 1981-2010 (blue line).

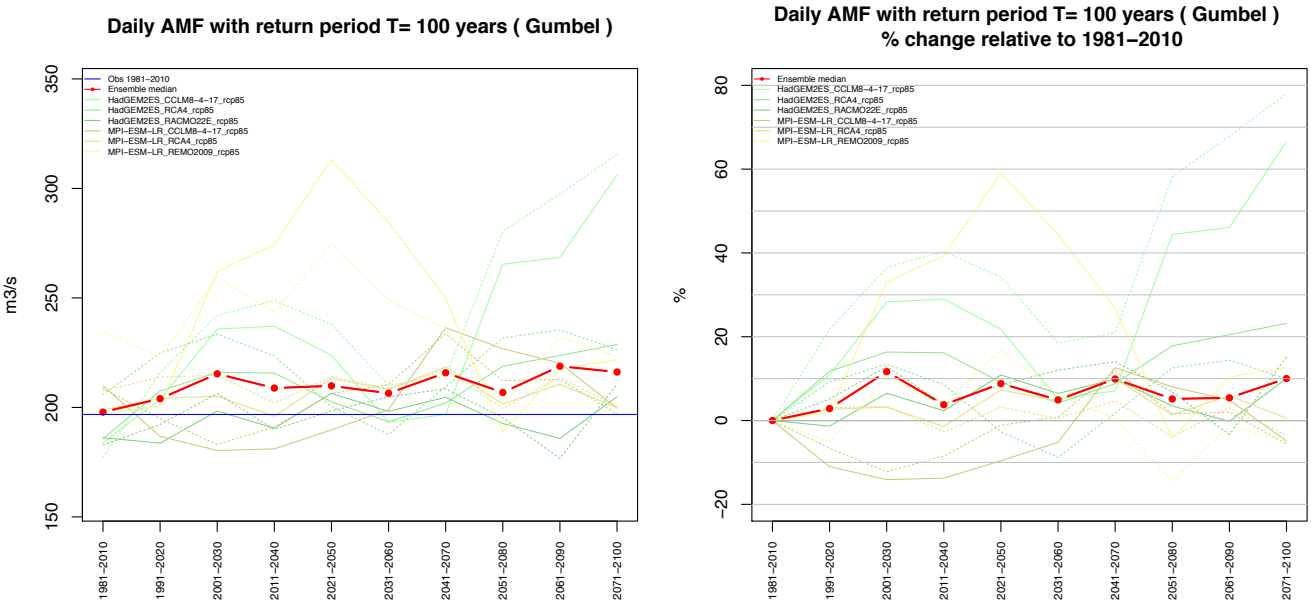

Fig. 30: As Fig. 29 but under the RCP8.5 emission scenarios.

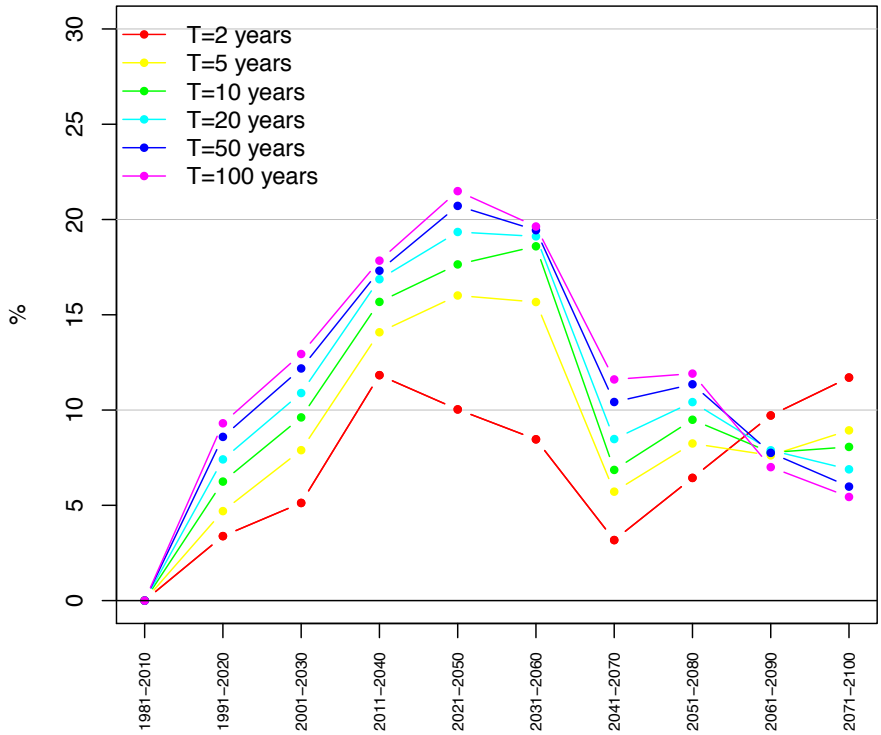

Fig. 31: Catchment vhm148. Projected median change (in percent) in the magnitude of T-year floods in the 21st century under the RCP4.5 emission scenario relative to the 1981-2010 reference period.

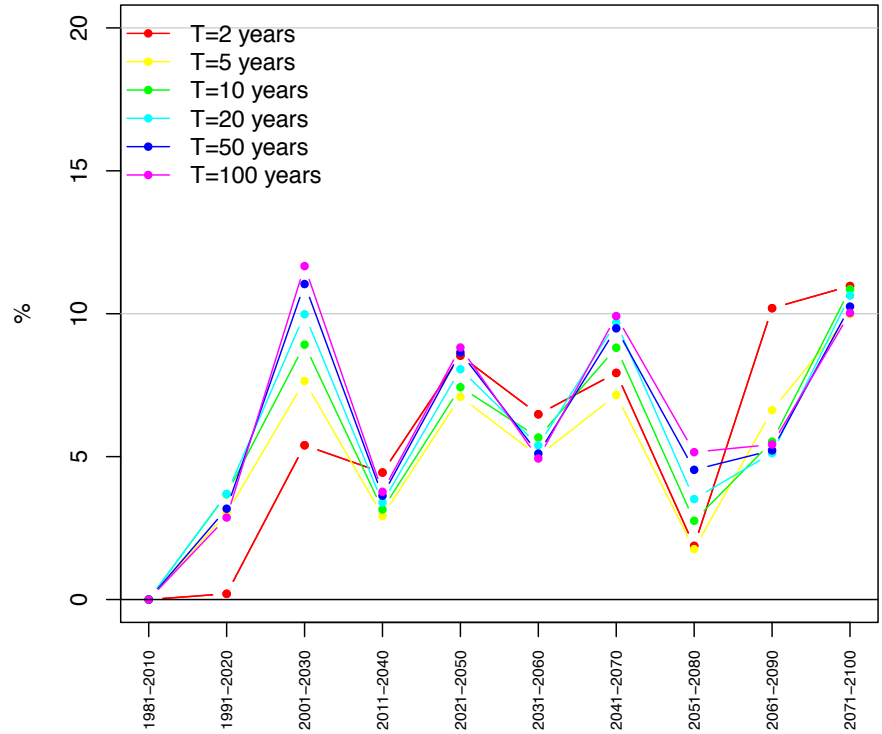

Fig. 32: as Fig.31 but under the RCP8.5 emission scenario.

- Catchment vhm51 (Hjaltadalsá)

Figs. 33 and 34 present the evolution of the 100-year floods for all scenarios and Figs. 35 and 36 summarise the results of the percentage change in T-year floods relative to 1981-2010, for all Ts.

- RCP4.5 emission scenarios

According to the ensemble median, variations of T-year floods are projected to oscillate around the 1981-2010 reference level until 2051-2080 and then a consistent increase is projected until the end of the 21st century. The longer the return period, the larger the projected median change relative to 1981-2010. The projected median change varies approximately between -3% and +5% until 2041-2070 and then reaches up to +11%. A large spread is observed between individual scenarios that do not project changes in the same direction depending on the driving GCM. This is caused by the uncertainty related to the precipitation projections that differ according to the driving GCM.

One group of scenarios driven by one GCM projects an increase of T-year floods with a peak around 2031-2060 and then the projected increase will diminish until the end of the 21st century. The other group of scenarios driven by the other GCM projects a decrease of T-year floods reaching its lowest value around 2021-2050 and then an increase is projected after around 2051-2080 until the end of the 21st century. As a result, the relative changes from these two groups cancel each other out until around 2051-2080 making the median relative change oscillate around to the 1981-2010 reference level before increasing until the end of the century.

For the group of scenarios driven by the MPI-ESM-LR GCM, the large increase of T-year floods is most likely driven by a projected increase of precipitation in AMJ combined with temperature warming causing an increase of rain and snowmelt from the still large snowpack. Later in the 21st century, temperature warming will deplete the snowpack in such a way that less snowmelt will contribute to flood events, reducing the projected increase relative to 1981-2010.

For the group of scenarios driven by the HadGEM2ES GCM, precipitation in AMJ is not projected to change and the relative decrease of T-year flood is most likely driven by temperature warming that will deplete the snowpack and reduce the magnitude of spring floods. The projected increase of precipitation in OND from around 2051-2080 until the end of the century is most likely the driver contributing to increase flood magnitude in that season and time-windows.

- RCP8.5 emission scenarios

According to the ensemble median, the T-year floods are projected to remain close to the 1981-2010 reference level until 2011-2040 and then increase until the end of the 21st century. The longer the return period, the larger the projected change relative to 1981-2010. From 2021-2050 to the end of the century, the projected median change varies approximately between +5% and +12% for $T > 2$ years and the direction of change is consistent in a majority of scenarios but the projected changes vary greatly between scenarios.

For the group of scenarios driven by the HadGEM2ES GCM, the projected decrease of T-year floods until around 2011-2030 is most likely related to a decrease of precipitation in AMJ combined with temperature warming leading to the depletion of snow cover and a reduction of snowmelt floods while the projected increase of T-year floods from around 2021-2050 until the end of the 21st century is most likely related to an increase of rain floods in OND resulting from a projected precipitation increase combined with temperature warming.

For the group of scenarios driven by the MPI-ESM-LR GCM, the projected increase of T-year floods during most of the 21st century is most likely related to the projected increase of precipitation in AMJ combined with temperature warming that may cause an increase in the magnitude of rain contribution to spring floods.

Both groups of scenarios most likely experience an increase of winter floods after 2041-2070 caused by the combined effects of increased precipitation and temperature warming in JFM leading to an increase of rain.

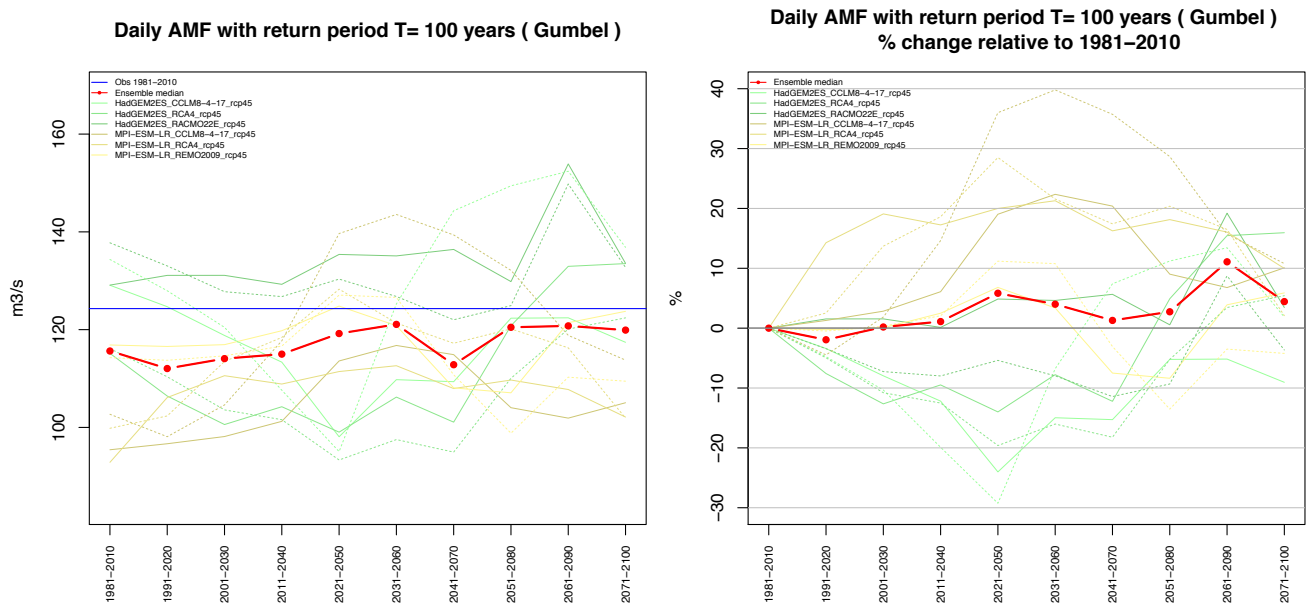

Fig. 33: Catchment vhm51: Evolution of the 100-year flood in the 21st century under the RCP4.5 emission scenarios (left) and percentage change relative to the 1981-2010 reference period (right).HYPE simulations forced with CORDEX precipitation scenarios corrected with method 1 (solid green and yellow lines) and with method 2 (dashed green and yellow lines). Ensemble median (red line) and 100-year flood from observations in 1981-2010 (blue line).

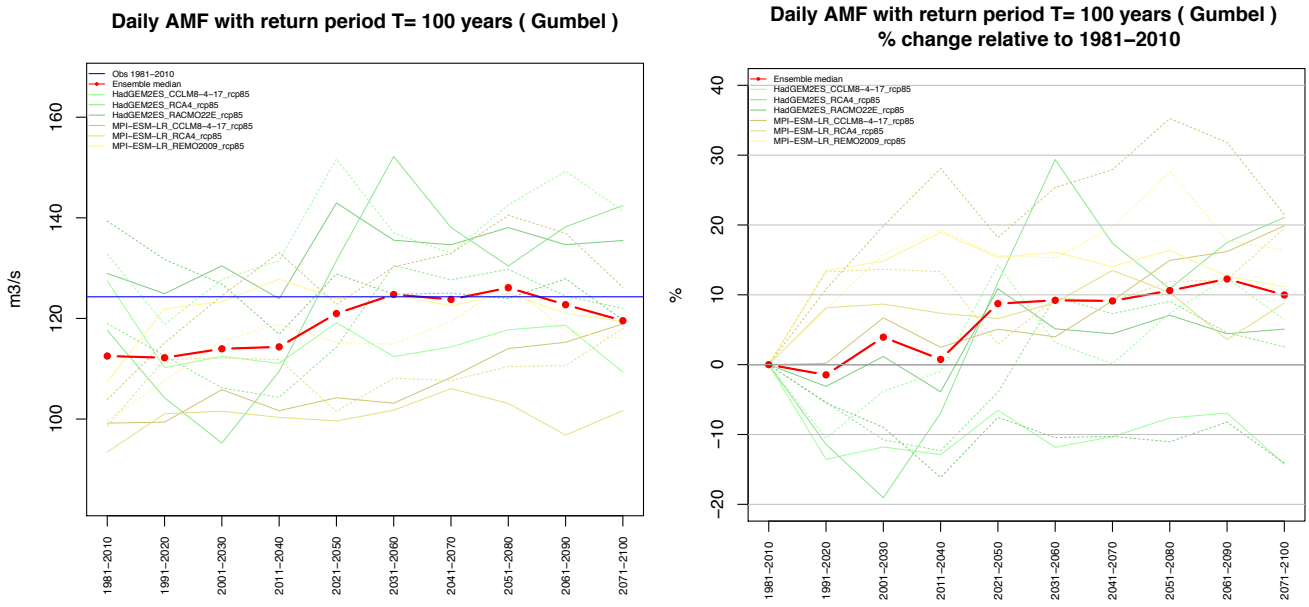

Fig. 34: As Fig. 33 but under the RCP8.5 emission scenarios.

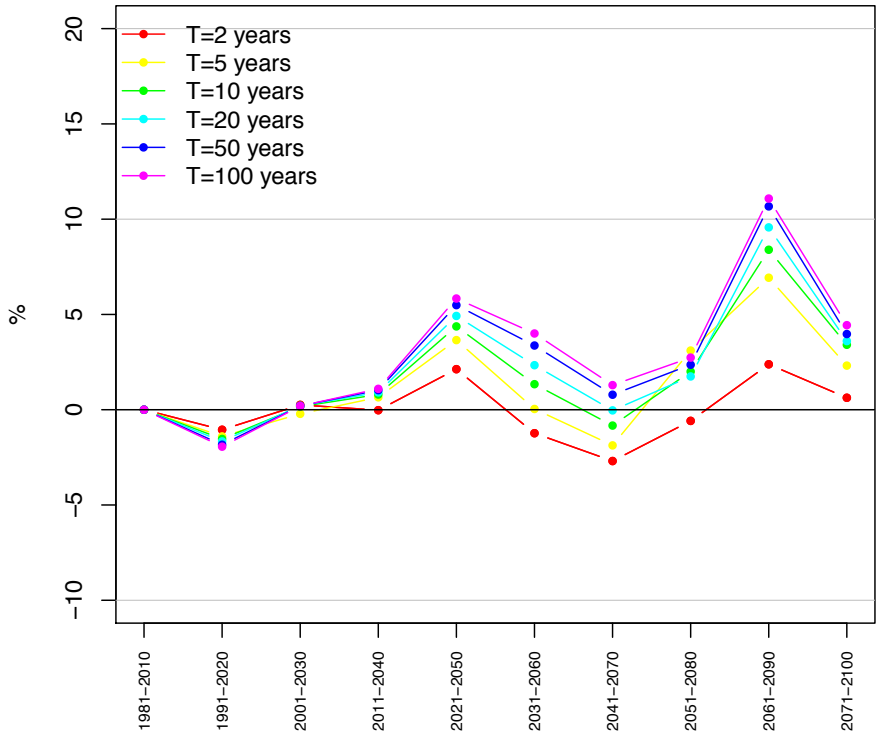

Fig. 35: Catchment vhm51. Projected median change (in percent) in the magnitude of T-year floods in the 21st century under the RCP4.5 emission scenario relative to the 1981-2010 reference period.

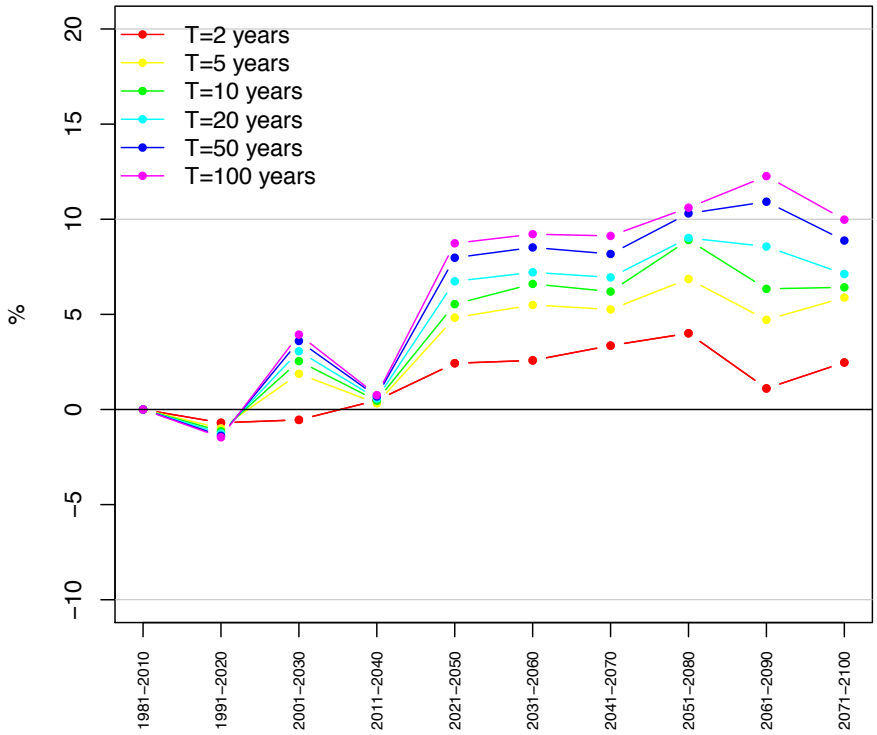

Fig. 36: as Fig.35 but under the RCP8.5 emission scenario.

- Catchment vhm64 (Ölfusá)

Figs. 37 and 38 present the evolution of the 100-year floods for all scenarios and Figs. 39 and 40 summarise the results of the percentage change in T-year floods relative to 1982-2011, for all Ts.

- RCP4.5 emission scenarios

According to the ensemble median, variations of T-year floods are projected to oscillate around the 1982-2011 reference level until 2031-2060 and then an increase is projected until the end of the 21st century. The projected median change varies approximately between -10% and +3% until 2031-2060 and then becomes positive and varies between +7 and +22%. From 2041-2070 until the end of the 21st century, the longer the return period, the larger the projected change relative to 1982-2011. In that period, the direction of change is consistent between scenarios but the projected changes vary greatly between scenarios.

The projected variations of T-year floods during the 21st century are related to the projected variations of precipitation in OND and JFM, combined with projected temperature warming that increases the rain fraction and leads to larger rain floods combined with snowmelt.

For the group of scenarios driven by the HadGEM2ES GCM, little change is projected until 2011-2040 as for precipitation in OND and JFM while the increase in the magnitude of T-year floods from 2021-2050 until the end of the century is driven by the projected temperature warming combined with an increase of OND precipitation causing more intense rain. Winter precipitation is not projected to increase but more rain events are expected because of temperature warming.

For the group of scenarios driven by the MPI-ESM-LR GCM, changes in T-year floods oscillate between +/- 10% and seem to match well precipitation variations in JFM and OND.

- RCP8.5 emission scenarios

According to the ensemble median, the T-year floods are projected to increase relative to 1982-2011. This increase is not gradual but is projected to oscillate. From 2011-2040 until the end of the century, the longer the return period, the lower the projected change relative to 1982-2011. The projected median change varies approximately between 0% and +17%. The longer the return period, the less consistent the direction of change between scenarios and the spread of the change greatly increases with the projection horizon.

The main driver causing the projected changes of T-year floods in both groups of scenarios appears to be the projected variations of precipitation in OND, followed by projected precipitation variations in JFM, combined with temperature warming which drives the variations of rain in these seasons, mixed with snowmelt.

As an example, from 2031-2060 to the end of the century, the group of scenarios driven by the HadGEM2ES GCMs projects an increase of 100-year flood while the other group of scenarios driven by the MPI-ESM-LR GCM projects a decrease relative to 1982-2011 (Fig. 38). These results can be compared to the projected evolution of OND and JFM precipitation from Appendix 7 (Figs. VII-12 and VII-13).

Smaller changes are projected under the RCP8.5 emission scenarios than under the RCP4.5 emission scenarios. One possible explanation could be that the larger warming projected under RCP8.5 will have more impact on snow cover and frozen ground in winter and lead to less snowmelt and more infiltration in winter causing a reduction of surface runoff during winter flood events.

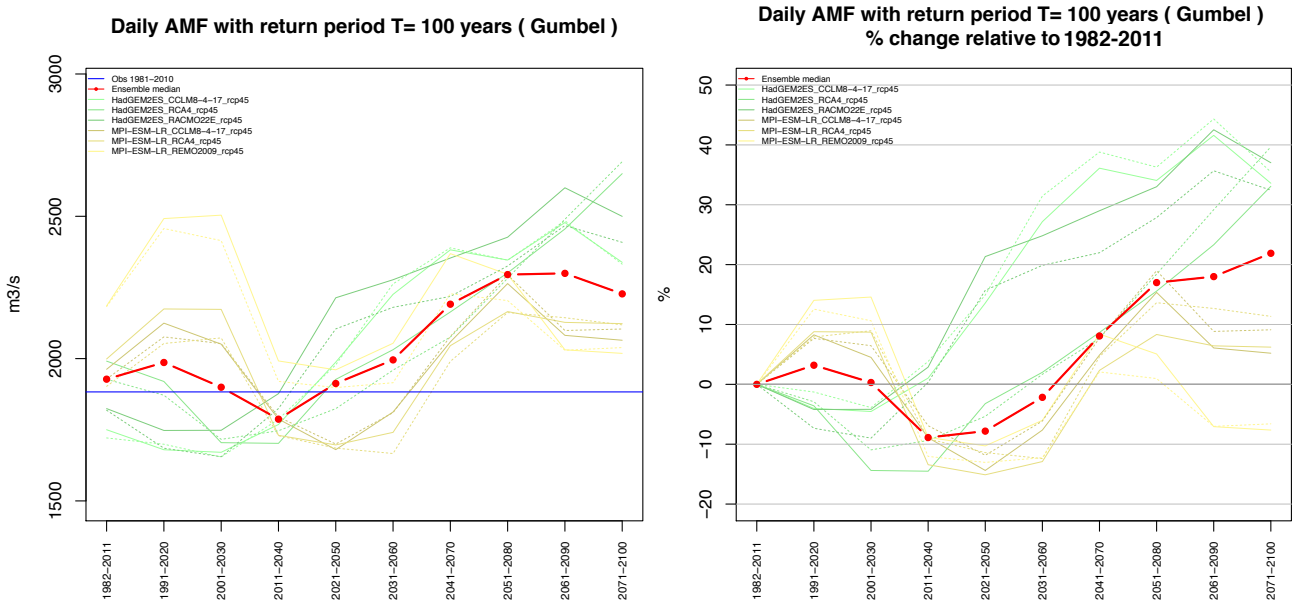

Fig. 37: Catchment vhm64: Evolution of the 100-year flood in the 21st century under the RCP4.5 emission scenarios (left) and percentage change relative to the 1982-2011 reference period (right). HYPE simulations forced with CORDEX precipitation scenarios corrected with method 1 (solid green and yellow lines) and with method 2 (dashed green and yellow lines). Ensemble median (red line) and 100-year flood from observations in 1982-2011 (blue line).

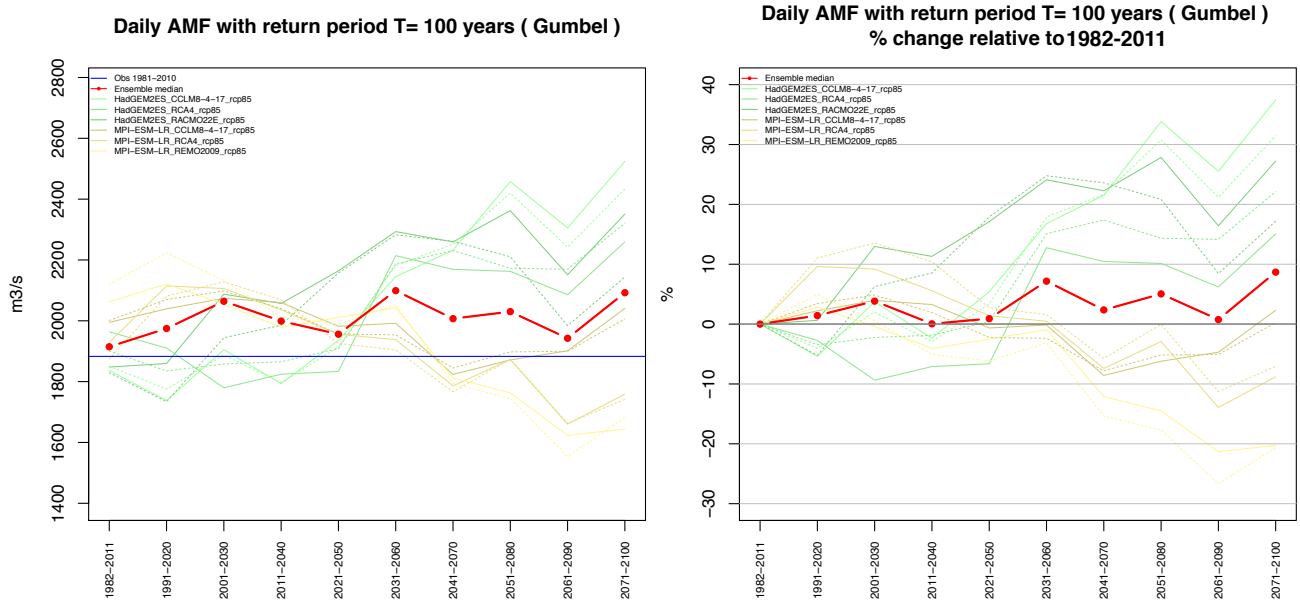

Fig. 38: As Fig. 37 but under the RCP8.5 emission scenarios.

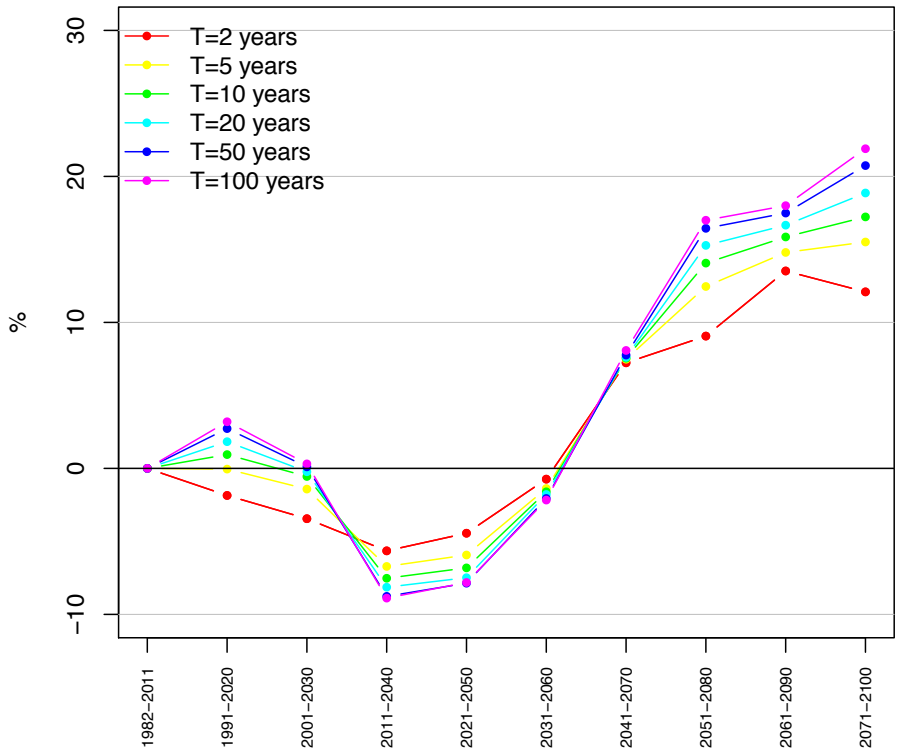

Fig. 39: Catchment vhm64. Projected median change (in percent) in the magnitude of T-year floods in the 21st century under the RCP4.5 emission scenario relative to the 1982-2011 reference period.

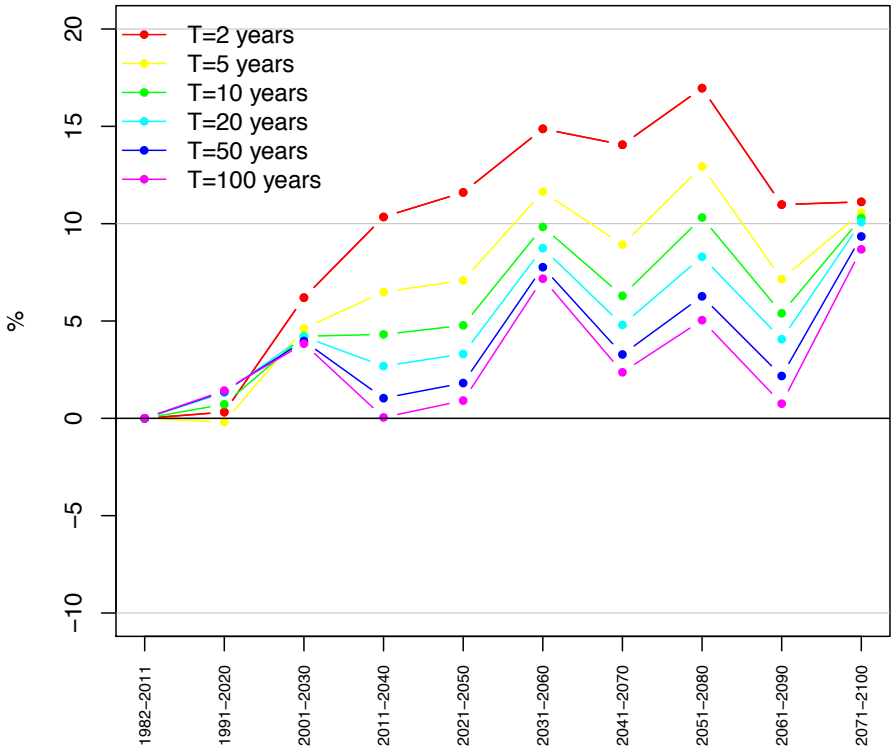

Fig. 40: as Fig. 39 but under the RCP8.5 emission scenario.

In summary, the projected climate change in the 21st century, if it realises, is expected to have an impact on flood characteristics. The changes were found to be specific to each catchment in relation to its physiographic characteristics and dominating flood-generating mechanisms (rain-fed, snowmelt-fed, interplay of rain and snowmelt). Under the RCP4.5 emission scenarios, T-year floods are projected to increase along the 21st century for Fossá, to oscillate around the 1981-2010 reference level until circa 2031-2060, for Ölfusá and Hjaltadalsá, before increasing in a more distant future (2041-2070 and thereafter). Under the RCP8.5 emission scenarios, a shift toward larger T-year floods dominates along most of the 21st century for the three catchments. The magnitude of changes remains modest (5 to 20%), according to the ensemble median. The direction of change is not always consistent between the scenarios driven by the two GCMs and the magnitude of change varies also greatly between scenarios, causing large uncertainties. This inconsistency between scenarios is most likely related to the multi-decadal oscillations of projected precipitation scenarios which do not always oscillate in phase with each other.

7-2-2 Change in the return period of extreme floods

The evolution of the return period T(Q), associated to a flood of given magnitude Q was estimated along the moving 30-year time-windows and analysed. The reference values Q were taken as the 1981-2010[6] Q(T) values for T=2, 5, 10, 20, 50 and 100 years. Detailed results are presented in Appendix 12 for RCP4.5 emission scenarios and in Appendix 13 for RCP8.5 emission scenarios.

If a flood of magnitude Q is exceeded more frequently in the future than in the 1981-2010 period, its return period T(Q) will decrease, while if it is exceeded less frequently, its return period T(Q) will increase. In other words, if Q(T) is projected to increase, then T(Q) will decrease and vice-versa. The results were found to mirror well the projected evolution of T-year floods above, with similar uncertainties and inconsistencies in some time-windows, between groups of scenarios driven by the two GCMs. A decrease of return period is projected when the T-year flood is projected to increase and vice-versa:

- Catchment vhm148 (Fossá)

The temporal evolution of the ensemble median T(Q) along the 30-year time-windows is presented in Figs 41 and 42 and Fig. 47 presents detailed results for T=100 years in 1981-2010.

- RCP4.5 emission scenarios

The 1981-2010 T-year floods are projected to be exceeded more frequently in the future but the evolution is not linear. The direction of change is usually consistent between scenarios. As an example, the median 100-year flood estimated in 1981-2010 is projected to become a 27-year flood in 2021-2050, a 45-year flood in 2041-2070 and a 65-year flood in 2071-2100.

[6] for vhm64, the reference time-window is 1982-2011

- RCP8.5 emission scenarios

The 1981-2010 T-year floods are projected to gradually be exceeded more frequently in the future and the evolution of the projected T oscillates. The direction of change is usually consistent between scenarios. As an example, the median 100-year flood estimated in 1981-2010 is projected to become a 52-year flood in 2021-2050, a 50-year flood in 2041-2070 and a 47-year flood in 2071-2100.

- Catchment vhm51 (Hjaltadalsá)

The temporal evolution of the ensemble median T(Q) along the 30-year time-windows is presented in Figs 43 and 44 and Fig. 47 presents detailed results for T=100 years in 1981-2010.

- RCP4.5 emission scenarios

The median T(Q) is projected to remain unchanged for short Ts and to decrease as the reference T increases but with increasing oscillations. The direction of change from individual scenarios depends on the driving GCM until 2051-2080 and then becomes consistent between most scenarios. As an example, the median 100-year flood estimated in 1981-2010 is projected to become a 62-year flood in 2021-2050, a 100-year flood in 2041-2070 and a 70-year flood in 2071-2100.

- RCP8.5 emission scenarios

The 1981-2010 T-year floods are projected to gradually be exceeded more frequently in the future and the median T(Q) is projected to stabilise after 2021-2050 to about half the value of the 1981-2010 reference period. The direction of change is consistent between most scenarios after 2021-2050. As an example, the median 100-year flood estimated in 1981-2010 is projected to become a 46-year flood in 2041-2070.

- Catchment vhm64 (Ölfusá)

The temporal evolution of the ensemble median T(Q) along the 30-year time-windows is summarised in Figs 45 and 46 and Fig. 47 presents detailed results for T=100 years in 1982-2011.

- RCP4.5 emission scenarios

The median T(Q) is projected to increase until 2031-2060 and then progressively decrease and stabilise to around half of the 1982-2011 value until the end of the 21st century. The direction of changes from individual scenarios depends on the driving GCM until 2031-2060 and then becomes consistent between scenarios. As an example, the median 100-year flood estimated in 1982-2011 is projected to become a 54-year flood in 2041-2070 and a 30-year flood in 2071-2100.

- RCP8.5 emission scenarios

The median T(Q) is projected to progressively decrease and oscillate. T(Q) will reach around half of the 1982-2011 value by the end of the 21st century. The direction of changes from individual scenarios depends on the driving GCM. As an example, the median 100-year flood estimated in

1982-2011 is projected to become a 110-year flood in 2041-2070 and a 56-year flood in 2071-2100.

In summary, while a moderate increase of T-year flood, Q(T), was projected, the corresponding changes in terms of return period, T(Q), look more dramatic. An average reduction of up to 50% or more for T(Q) was projected, in all catchments at some point along the 21st century, meaning that floods of a given magnitude observed in the 1981-2010 period could be exceeded up to twice more frequently, on average, in the future, if the scenarios realise.

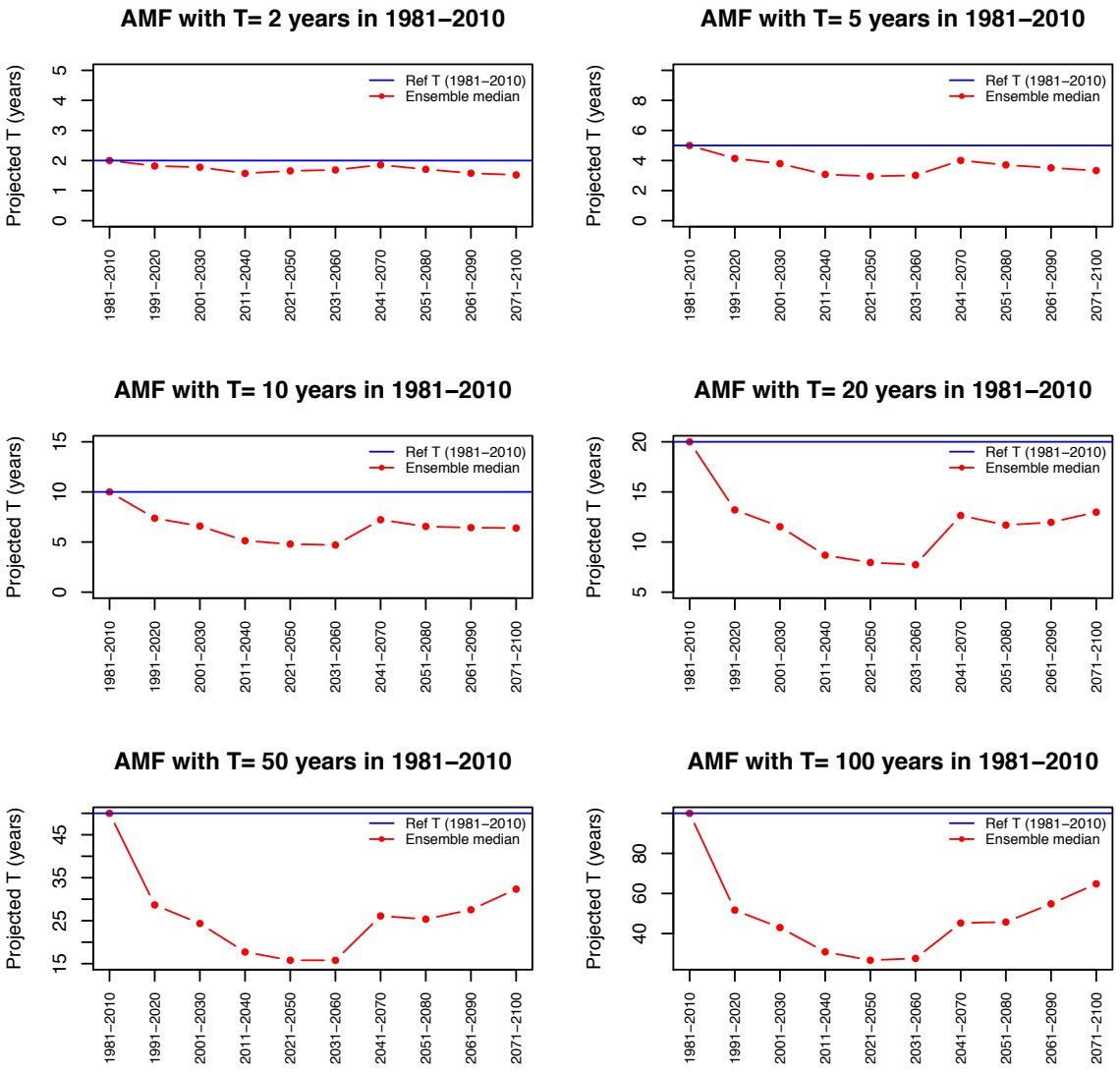

Fig. 41: Catchment vhm148: Projected evolution of the return period T(Q) associated to a flood of a given magnitude Q, along the 21st century. Projected median T under the RCP4.5 emission scenario. The magnitude Q is defined as the 1981-2010 Q(T) for T=2, 5, 10, 20, 50 and100 years.

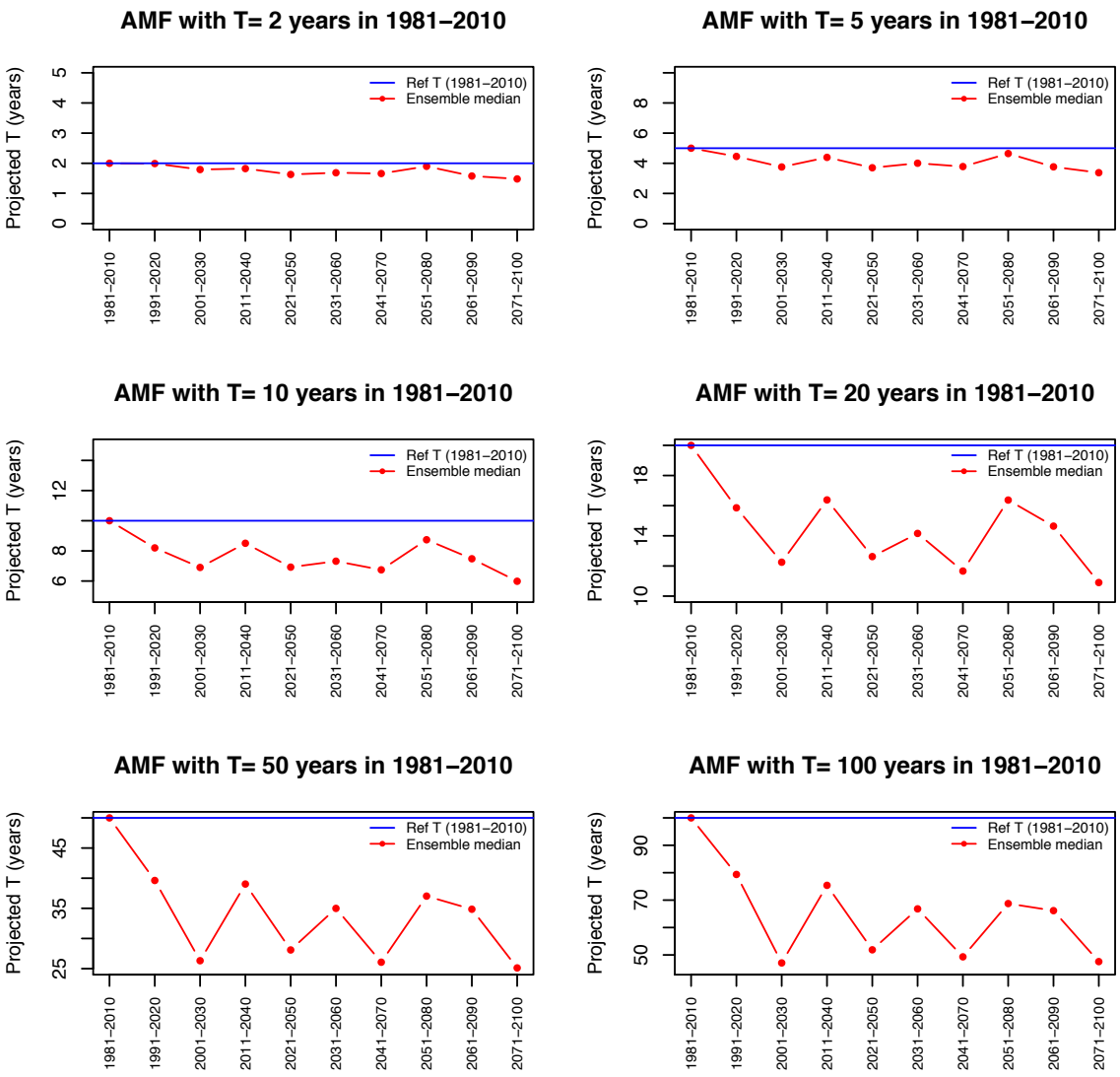

Fig. 42: Catchment vhm148: Projected evolution of the return period T(Q) associated to a flood of a given magnitude Q, along the 21st century. Projected median T under the RCP8.5 emission scenario. The magnitude Q is defined as the 1981-2010 Q(T) for T=2, 5, 10, 20, 50 and100 years.

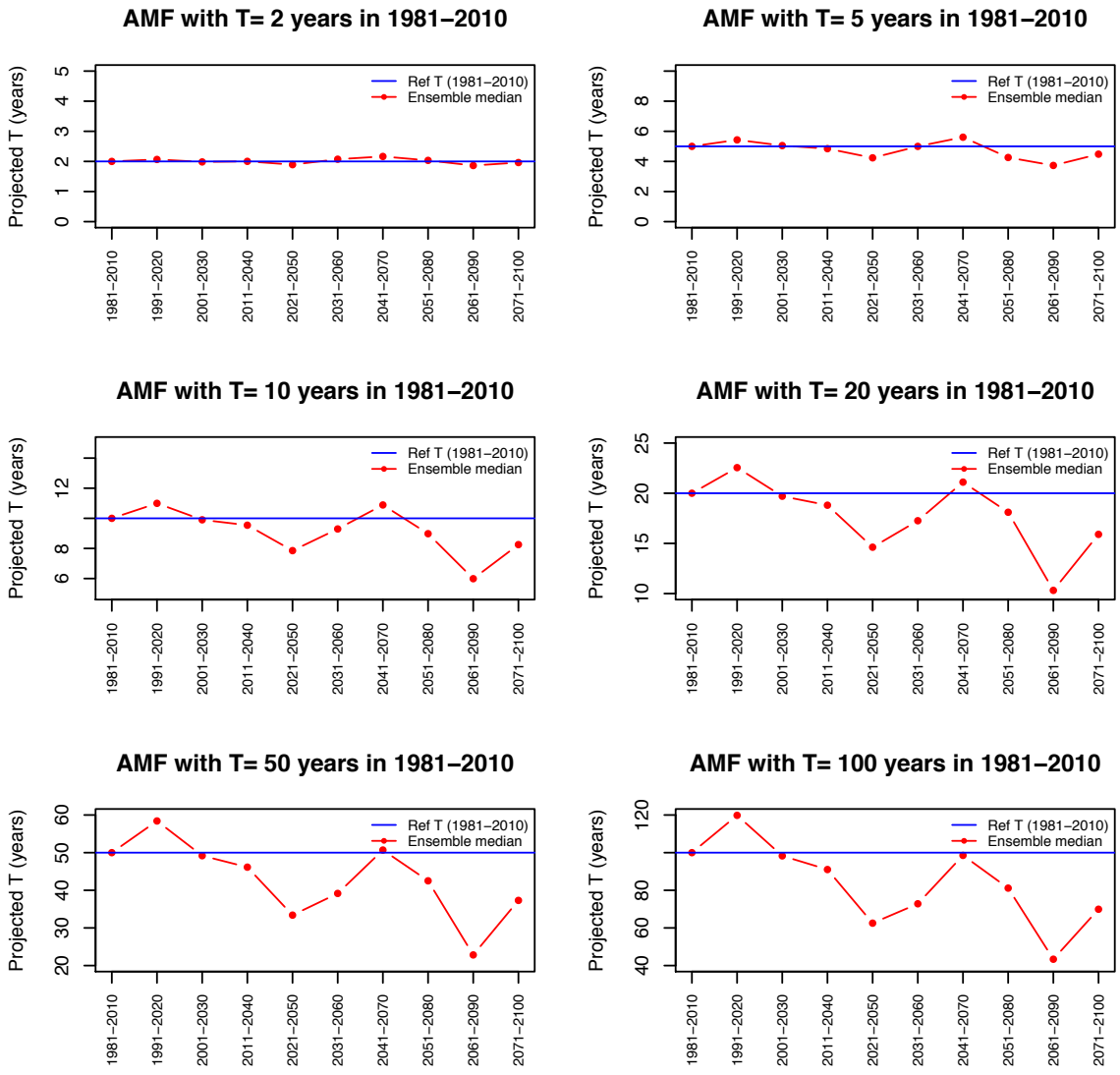

Fig. 43: Catchment vhm51: Projected evolution of the return period T(Q) associated to a flood of a given magnitude Q, along the 21st century. Projected median T under the RCP4.5 emission scenario. The magnitude Q is defined as the 1981-2010 Q(T) for T=2, 5, 10, 20, 50 and100 years.

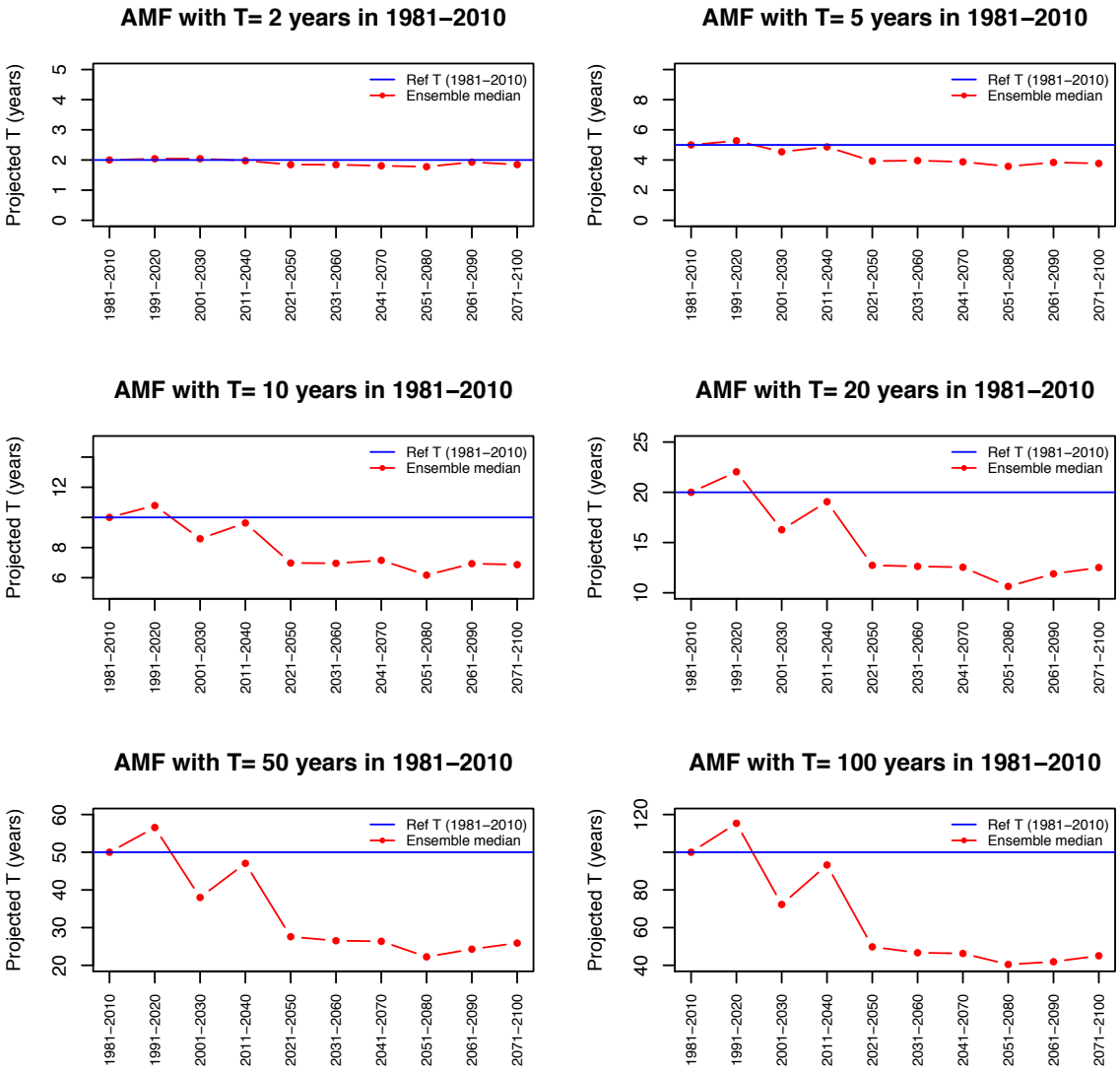

Fig. 44: Catchment vhm51: Projected evolution of the return period T(Q) associated to a flood of a given magnitude Q, along the 21st century. Projected median T under the RCP8.5 emission scenario. The magnitude Q is defined as the 1981-2010 Q(T) for T=2, 5, 10, 20, 50 and100 years.

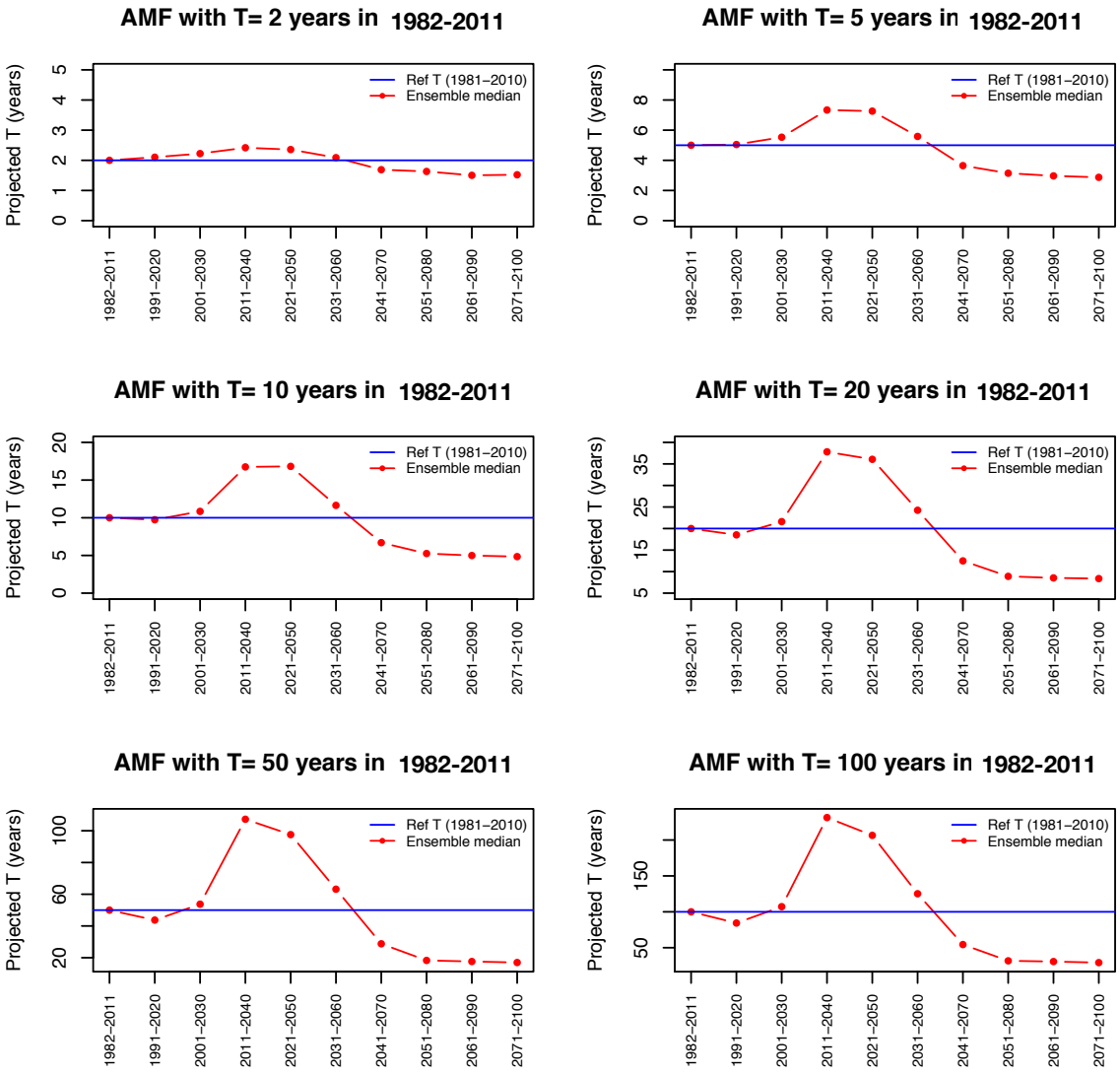

Fig. 45: Catchment vhm64: Projected evolution of the return period T(Q) associated to a flood of a given magnitude Q, along the 21st century. Projected median T under the RCP4.5 emission scenario. The magnitude Q is defined as the 1982-2011 Q(T) for T=2, 5, 10, 20, 50 and100 years.

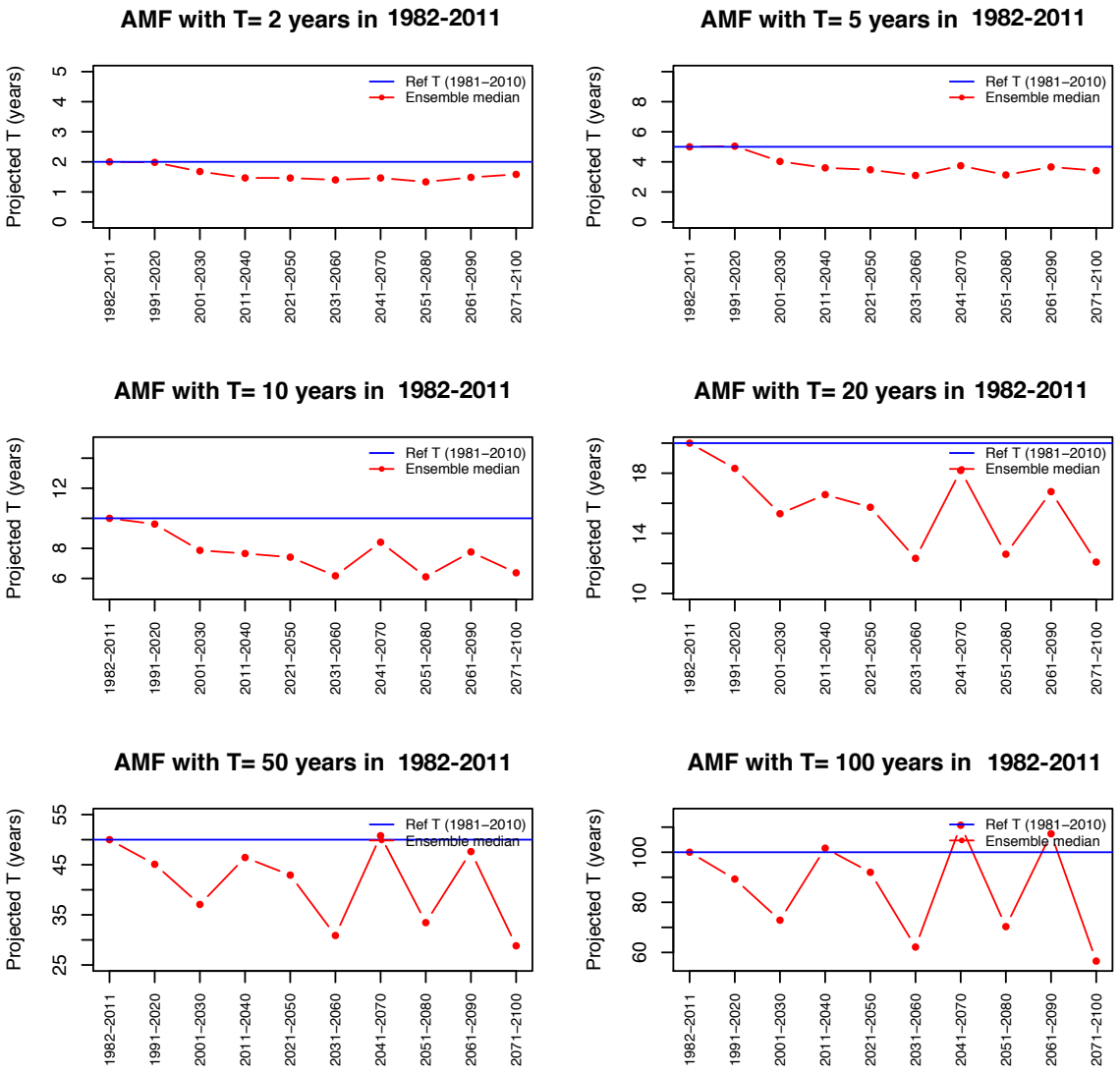

Fig. 46: Catchment vhm64: Projected evolution of the return period T(Q) associated to a flood of a given magnitude Q, along the 21st century. Projected median T under the RCP8.5 emission scenario. The magnitude Q is defined as the 1982-2011 Q(T) for T=2, 5, 10, 20, 50 and100 years.

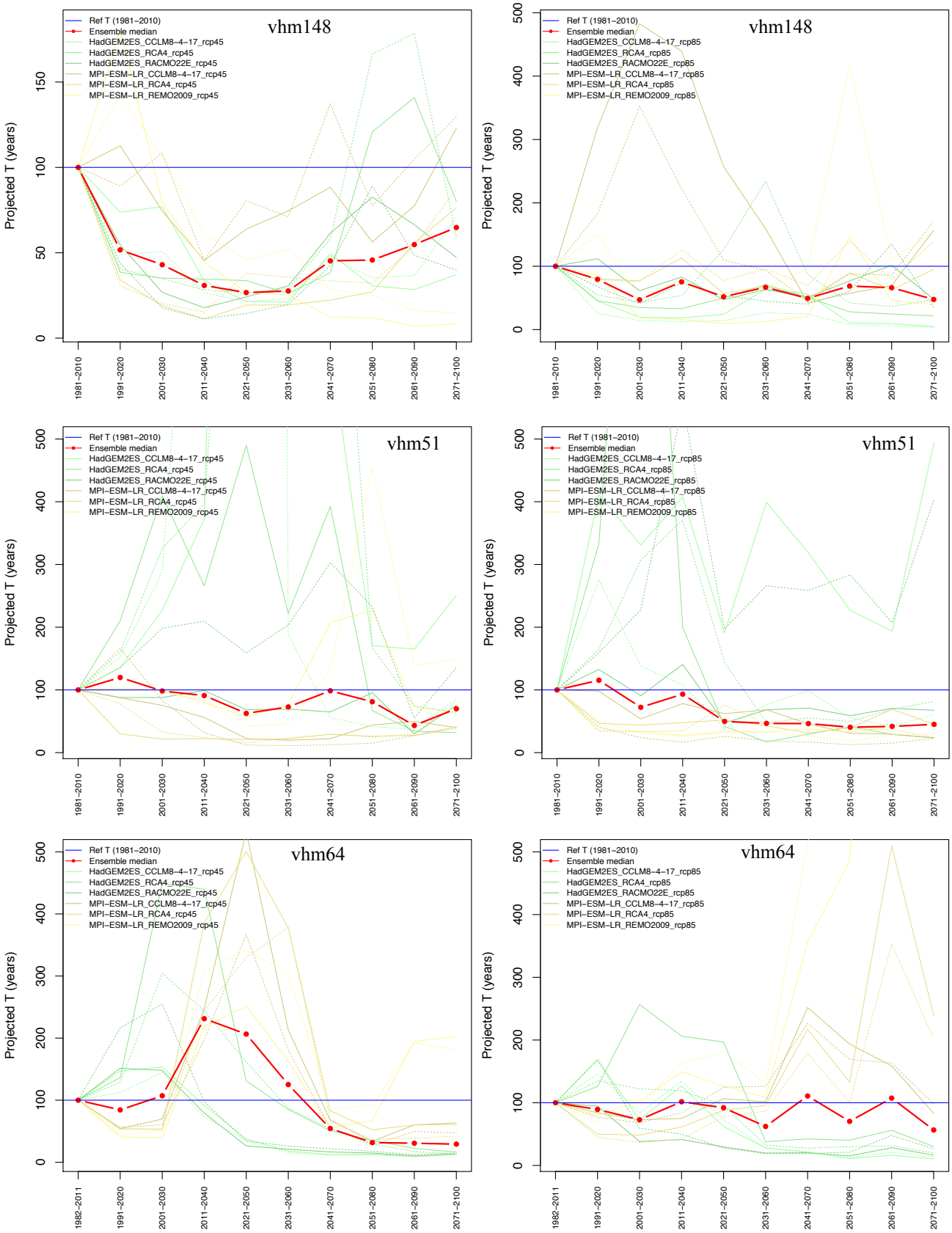

Fig. 47: Projected evolution of the return period T associated to a flood with return period T=100 years in 1981-2010. Ensemble median (red line). Individual scenarios (green and yellow lines). RCP4.5 emission scenarios (left panel), and RCP8.5 emission scenarios (right panel). Catchment ID indicated in each Figure.

8 Summary and conclusions

A rigorous methodology was applied to study the impact of climate change on flood characteristics in the 21st century for three Icelandic river catchments. The studied river basins are located in different regions, vary considerably in size and their physiographic and hydrologic characteristics are of different nature and representative of conditions found in Iceland.

A significant temperature warming was projected by the two emission scenarios considered in the study, in all seasons and all studied catchments. The RCP4.5 emission scenarios projected an average temperature warming of 0.29°C/decade and the RCP8.5 emission scenarios projected an average temperature warming of 0.45°C/decade. Precipitation did not exhibit any significant long-term temporal linear trend in a large majority of scenarios, catchments and months. Instead, decadal to multi-decadal oscillations were often observed in the projected precipitation time-series, especially in autumn-winter, corresponding to a succession of wet and dry periods. The precipitation oscillations of the different scenarios were sometimes found not to be in phase with each other and to depend on the driving GCM, leading sometimes to large uncertainties regarding the outcome in some time-windows and seasons. Note however that a significant increase of 30-year average summer precipitation was projected along the 21st century under both emission scenarios in the catchments located in the southwest and north.

The studied river basins were found to respond to projected climate change but the nature and magnitude of the changes were found to depend on the physiographic and hydrologic characteristics of the catchments. The projected temperature warming was found to gradually alter snow conditions and lead to a shorter snow season combined with less snow accumulation and a shift toward an earlier and lower peak of snowmelt. Results indicated a gradual change with increasing projection horizon, toward an increase of streamflow discharge in autumn-winter, an earlier and lower spring streamflow peak and a reduction of summer streamflow discharge except for a partly glaciated catchment where summer streamflow discharge was projected to remain essentially unchanged thanks to glacier melt. The changes are not linear but modulated by precipitation fluctuations along the projection horizon. Uncertainties related to hydrological modelling can be expected to add some uncertainties to streamflow projections. Glacier melt modelling could probably be improved by using additional information e.g. mass balance data to better constrain the model and a more sophisticated glacier melting model available in HYPE.

Concerning extreme flood characteristics, the changes were found to be specific to each catchment in relation to its physiographic characteristics and dominating flood-generating mechanisms (rain-fed, snowmelt-fed, interplay of rain and snowmelt):

- Overall, a shift was projected in the seasonal distribution of annual maximum flood occurrence dates with an increase in the number of extreme floods taking place in autumn and winter and a decrease in the number of extreme floods taking place in spring and summer, under both RCPs emission scenarios. This shift implies a change in the dominating flood-generating mechanisms,

with fewer snowmelt dominated floods and more rain-fed floods and mixed rain-fed and snowmelt floods. Reduced snow cover caused by temperature warming is expected to lead to smaller snowmelt dominated floods and reduce the likelihood of making them the AMF, while increased precipitation combined with temperature warming is expected to lead to more frequent rain-fed floods, including in winter, and increase the likelihood of making them the AMF.

- Both an increase and a decrease in the magnitude of the T-year floods were projected in a recent future (until circa 2031-2060) under the RCP4.5 emission scenarios, depending on the catchment under consideration, while an increase was projected to dominate in all catchments in a more distant future (2041-2070 and thereafter). Under the RCP8.5 emission scenarios, a shift toward an increase in the magnitude of T-year floods was projected to dominate along most of the 21st century. The uncertainties regarding both direction and magnitude of changes are considerable and a large spread was observed between individual scenarios, both because of large uncertainties regarding precipitation projections from the two driving GCMs used in the study and because of the expected sampling uncertainty related to the use of a limited data sample (30-year time-windows). The use of 30-year time-windows was the result of a compromise between having large enough samples to derive robust climate statistics while limiting the risk of non-stationarity within the time-windows.

- The projected median change in the magnitude of T-year floods, Q(T), was usually moderate (less than 20%) but this translated into a larger change in terms of return period, T(Q). A reduction of up to 50% in T(Q), on average, was projected in all catchments, at some point along the 21st century. In other words, a given T-year flood from the 1981-2010 period could be exceeded up to twice more frequently, in the future, if the climate projections realise.

In conclusion, if either one of the climate projections realises (RCP4.5 or RCP8.5), it will have an impact on the hydrological response of Icelandic river basins across all catchment scales. Traditionally, flood frequency analysis and the estimation of design floods are based on the implicit assumption of temporal stationarity of the flood frequency distribution. The results of this study suggest that if either one of the climate projections realises, the stationarity assumption will no longer be valid in the coming decades and both the seasonal distribution of flood occurrence dates and frequency of extreme floods will be likely to change. Assessing climate change impacts on extreme floods is therefore important and necessary in order to assist authorities to develop adaptation strategies and anticipate mitigating actions that may have to be taken to protect populations and infrastructures and insure public safety. This study should be extended to more river basins in order to get a more comprehensive overview of the hydrological response to climate change in Iceland.

Acknowledgements

This project was funded by the Icelandic Road and Coastal Administration Research Fund (Rannsóknarsjóður Vegagerðarinnar).

DEMs were created from DigitalGlobe, Inc., imagery and funded under National Science Foundation awards 1043681, 1559691, and 1542736.

The author acknowledges the World Climate Research Programme's Working Group on Regional Climate, and the Working Group on Coupled Modelling, former coordinating body of CORDEX and responsible panel for CMIP5. The author also thanks the climate modelling groups (listed in Table 2 of this report) for producing and making available their model output. The author also acknowledges the Earth System Grid Federation infrastructure an international effort led by the U.S. Department of Energy's Program for Climate Model Diagnosis and Intercomparison, the European Network for Earth System Modelling and other partners in the Global Organisation for Earth System Science Portals (GO-ESSP).

The author acknowledges Veðurstofa Íslands for providing the ICRA reanalysis weather data.

Discharge observations were provided by Veðurstofa Íslands (IMO database, service no. 2019-11-01 / 01).

The author acknowledges the Swedish Meteorological and Hydrological Institute for making HYPE freely available.

Data analysis was performed with the R software (R Core Team, 2016).

9 References

Arheimer B. and Lindström G. (2015). Climate impact on floods: changes in high flows in Sweden in the past and the future (1911–2100). Hydrol. Earth Syst. Sci., 19, 771–784, 2015. doi: 10.5194/hess-19-771-2015

Arnalds O. (2015). The Soils of Iceland. World Soils Book Series. Springer Netherlands.

Árnason K. and Matthíasson I. (2017). CORINE - landflokkun 2012. Landgerðabreytingar á Íslandi 2006-2012. Landmælingar Íslands.

Ólafur Arnalds, Hlynur Óskarsson (2009). Íslenskt jarðvegskort (Soil map of Iceland). Nátturufræðingurinn 78:107-121.

Björnsson H., Sigurðsson B. D., Davíðsdóttir B., Ólafsson J., Ástþórssson Ó. S., Ólafsdóttir S., Baldursson T., Jónsson T. (2018). Loftslagsbreytingar og áhrif þeirra á Íslandi – Skýrsla vísindanefndar um loftslagsbreytingar 2018. Veðurstofa Íslands.

Climate Change and Energy Systems. Impacts, risks and adaptation in the Nordic and Baltic countries. Th. Thorsteinsson and H. Björnsson Eds. TemaNord 2011:502, 226 pp.

Crochet P. (2007). A study of regional precipitation trends in Iceland using a high quality gauge network and ERA-40. J. Climate, 20(18), 4659-4677.

Crochet P. (2013). Sensitivity of Icelandic river basins to recent climate variations. Jökull, 63, 71-90.

Crochet P. and Þórarinsdóttir T. (2014). Flood frequency estimation for ungauged catchments in Iceland by combined hydrological modelling and regional frequency analysis. VÍ-2014-001 report, 50 pp.

Dee D. P., Uppala S. M., Simmons A. J., Berrisford P., Poli P., Kobayashi S., Andrae U., Balmaseda M. A., Balsamo G., Bauer P., Bechtold P., Beljaars A. C. M., van de Berg L., Bidlot J., Bormann N., Delsol C., Dragani R., Fuentes M., Geer A. J., Haimberger L., Healy S. B., Hersbach H., Hólm E. V., Isaksen L., Kållberg P., Köhler M., Matricardi M., McNally A. P., Monge-Sanz B. M., Morcrette J.-J., Park B.-K., Peubey C., de Rosnay P., Tavolato C., Thépaut J.-N. and Vitart, F. (2011). The ERA-Interim reanalysis: configuration and performance of the data assimilation system, Q.J.R. Meteorol. Soc., 137(656), 553–597, doi:10.1002/qj.828.

Delignette-Muller M.L., Dutang C. (2015). "fitdistrplus: An R Package for Fitting Distributions." *Journal of Statistical Software*, **64**(4), 1–34.

de Niet J., Finger D.C., Bring A., Egilson D., Gustafson D. and Kalantari Z. (2020): Benefits of combining satellite-derived snow cover data and discharge data to calibrate a glaciated catchment in sub-arctic Iceland. *Water* 2020, *12*, 975; doi:10.3390/w12040975

Einarsson B. and Jónsson S. (2010). The effect of climate change on runoff from two watersheds in Iceland. VÍ-2010-016 report, 34 pp.

Giorgetta M.A., Jungclaus J., Reick C., Legutke S., Bader J., Böttinger M., Brovkin V., Crueger T., Esch M., Fieg K., Glushak K., Gayler V., Haak H., Hollweg H., Ilyina T., Kinne S., Kornblueh L., Matei D., Mauritsen T., Mikolajewicz U., Mueller W., Notz D., Pithan F., Raddatz T., Rast S., Redler R., Roeckner E., Schmid H., Schnur R., Segschneider J., Six K.D., Stockhause M., Timmreck C., Wegner J., Widmann H., Weiners K., Claussen M., Marotzke J. and Stevens B. (2013). Climate and carbon cycle changes from 1850 to 2100 in MPI-ESM simulations for the coupled model intercomparison project phase 5. Journal of Advances in Modeling Earth Systems 5:572–597. https://doi.org/10.1002/jame.20038.

Giorgi F., Jones C. and Asrar G. R. (2009). Addressing climate information needs at the regional level: the CORDEX framework, World Meteorological Organization (WMO) Bulletin, 58(3), 175-183.

Gosseling M. (2017). CORDEX climate trends for Iceland in the 21st century. VI-report 2017-009.

Gudmundsson L., Bremnes J. B., Haugen J. E. and Engen-Skaugen T. (2012). Technical Note: Downscaling RCM precipitation to the station scale using statistical transformations – a comparison of methods, Hydrol. Earth Syst. Sci., 16, 3383–3390, https://doi.org/10.5194/hess-16-3383-2012.

Gudmundsson, L. (2016). qmap: Statistical transformations for post-processing climate model output. R package version 1.0-4.

Hróðmarsson H.B. and Þórarinsdóttir T. (2018). Flóð íslanskra vatnsfalla, Flóðagreining rennslisraða. VÍ-2018-003 skýrsla, 144 pp.

Jacob D., Elizalde A., Haensler A., Hagemann S., Kumar P., Podzun R., Rechid D., Remedio A.R., Saeed F., Sieck K., Teichmann C. and Wilhelm C. (2012). Assessing the transferability of the regional climate model REMO to different coordinated regional climate downscaling experiment (CORDEX) regions. Atmosphere 3(1): 181-199. https://doi.org/10.3390/atmos3010181.

Jacob D., Petersen J., Eggert B., Alias A., Christensen O.B., Bouwer L.M., Braun A., Colette A., Déqué M., Georgievski G., Georgopoulou E., Gobiet A., Menut L., Nikulin G., Haensler A., Hempelmann N., Jones C., Keuler K., Kovats S., Kröner N., Kotlarski S., Kriegsmann A., Martin E., van Meijgaard E., Moseley C., Pfeifer S., Preuschmann S., Radermacher C., Radtke K., Rechid D., Rounsevell M., Samuelsson P., Somot S., Soussana J.-F., Teichmann C., Valentini R., Vautard R., Weber B. and Yiou P. (2014). EURO-CORDEX: new high-resolution climate change projections for European impact research. Reg Environ Change 14:563–578. https://doi.org/10.1007/s10113-013-0499-2.

Jones C. D., Hughes J. K., Bellouin N., Hardiman S. C., Jones G. S., Knight J., Liddicoat S., O'Connor F. M., Andres R. J., Bell C., Boo K.-O., Bozzo A., Butchart N., Cadule P., Corbin K. D., Doutriaux-Boucher M., Friedlingstein P., Gornall J., Gray L., Halloran P. R., Hurtt G., Ingram W. J., Lamarque J.-F., Law R. M., Meinshausen M., Osprey S., Palin E. J., Parsons Chini L., Raddatz T., Sanderson M. G., Sellar A. A., Schurer A., Valdes P., Wood N., Woodward S., Yoshioka M. and Zerroukat M. (2011). The HadGEM2-ES implementation of CMIP5 centennial simulations. Geosci. Model Dev., 4, 543-570. doi:10.5194/gmd-4-543-2011.

Jóhannesson T. and co-authors (2007). Effect of climate change on hydrology and hydro-resources in Iceland. OS-2007/011, 91 pp.

Kupiainen M., Samuelsson P., Jones C., Jansson C., Willén U., Hansson U., Ullerstig A., Wang S., and Döscher R. (2011). Rossby Centre regional atmospheric model, RCA4. Rossby Centre Newsletter.

Lindström G., Pers C., Rosberg J., Strömqvist J. and Arheimer B. (2010). Development and testing of the HYPE (Hydrological Predictions for the Environment) water quality model for different spatial scales.Hydrology Research, 41, 3-4, 295-319.

Marschollek S. (2017). Discharge Modelling of the Tungnaá River in Iceland using the HYPE Model. Faculty of Civil and Environmental Engineering School of Engineering and Natural Sciences University of Iceland, Reykjavik.

Meijgaard E. van, Van Ulft L.H., Lenderink G., de Roode S.R., Wipfler L., Boers R. and Timmermans R.M.A. (2012). Refinement and application of a regional atmospheric model for climate scenario calculations of Western Europe. Climate changes Spatial Planning publication: KvR 054/12, ISBN/EAN 978-90-8815-046-3, pp 44.

Nawri N., Pálmason B., Petersen G.N., Björnsson H. and Þorsteinsson S. (2017). The ICRA atmospheric reanalysis project for Iceland. VÍ Report, 2017-005, Veðurstofa Íslands.

Obled, C. Bontron, G., and Garçon, R. (2002). Quantitative precipitation forecasts: A statistical adaptation of model outputs through an analogue sorting approach. Atmos. Res., 63 (3-4), 303-324.

Porter C., Morin P., Howat I., Noh M.-J., Bates B., Peterman K, Keesey S., Schlenk M., Gardiner J., Tomko K., Willis M., Kelleher C., Cloutier M., Husby E., Foga S., Nakamura H., Platson M., Wethington M. Jr., Williamson C., Bauer G., Enos J., Arnold G., Kramer W., Becker P., Doshi A., D'Souza C., Cummens P., Laurier F. and Bojesen M. (2018). "ArcticDEM", https://doi.org/10.7910/DVN/OHHUKH, Harvard Dataverse, V1, [Accessed Nov. 2019].

R Core Team (2016). R: A language and environment for statistical computing. R Foundation for Statistical Computing, Vienna, Austria. URL https://www.R-project.org/.

Rockel B., Will A. and Hense A. (2008). Special issue regional climate modelling with COSMO-CLM (CCLM). Meteorol Z 17:347–348. doi:10.1127/0941-2948/2008/0309.

Samuelsson P., Jones C., Willén U., Ullerstig A., Gollvik S., Hansson U., Jansson C., Kjellström E., Nikulin G. and Wyser K. (2011). The Rossby Centre Regional Climate Model RCA3: model description and performance. Tellus 63A. doi:10.1111/j.1600-0870.2010.00478.x.

Stephenson, A.G (2002). evd: Extreme Value Distributions. R News, 2(2):31-32, June 2002. URL: http://CRAN.R-project.org/doc/Rnews/.

Wilks, D.S. (1995). Statistical methods in the atmospheric sciences: an introduction. Academic Press. International geophysics series v. 59.

Appendix 1

CORDEX daily temperature evaluation scenarios : RCMs and bias-correction skills

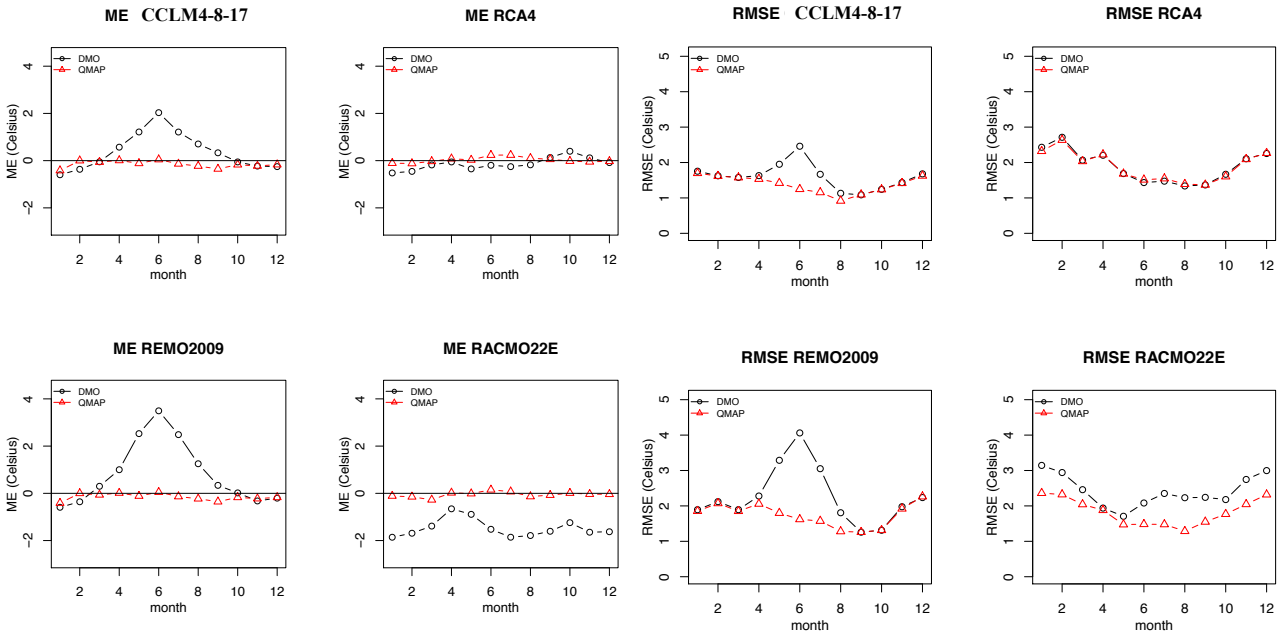

Fig. I-1: Catchment vhm148: Mean error (ME) and root-mean-square error (RMSE) between CORDEX temperature evaluation scenarios and ICRA reference temperature. DMO=original CORDEX; QMAP=bias-corrected CORDEX. Period 1989-2008.

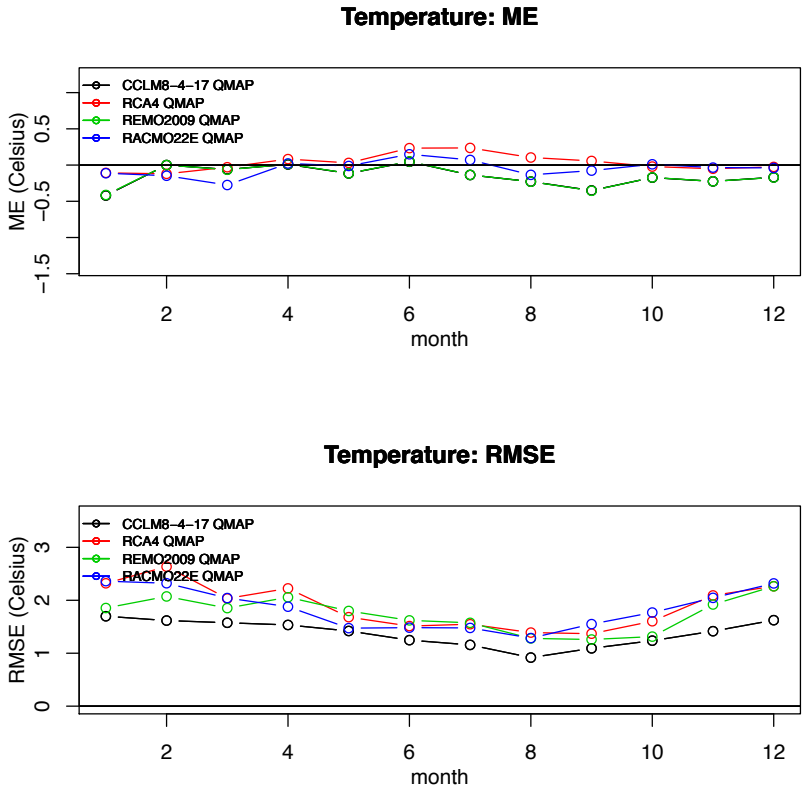

Fig. I-2: Catchment vhm148: Mean error (ME) and root-mean-square error (RMSE) between bias-corrected CORDEX temperature evaluation scenarios and ICRA reference temperature.

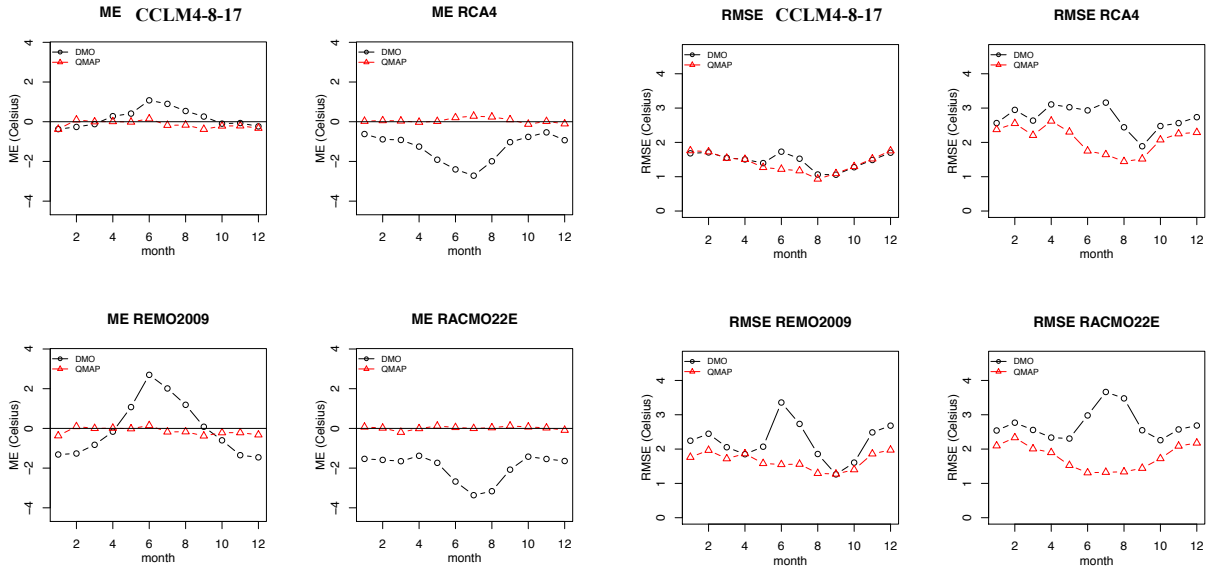

Fig. I-3: Catchment vhm51: Mean error (ME) and root-mean-square error (RMSE) between CORDEX temperature evaluation scenarios and ICRA reference temperature. DMO=original CORDEX; QMAP=bias-corrected CORDEX. Period 1989-2008.

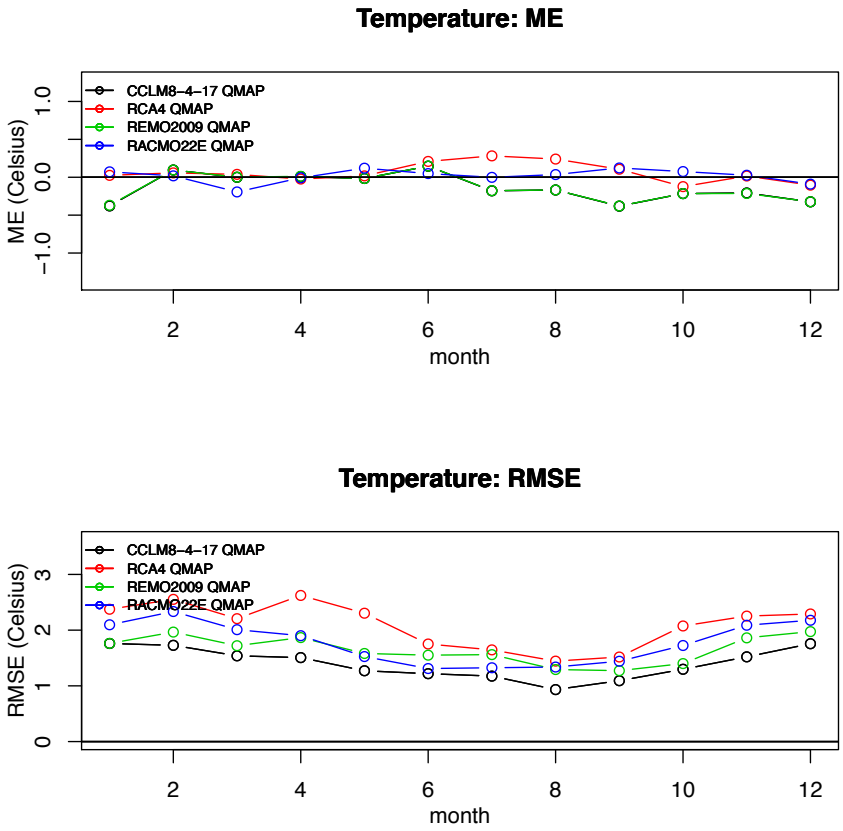

Fig. I-4: Catchment vhm51: Mean error (ME) and root-mean-square error (RMSE) between bias-corrected CORDEX temperature evaluation scenarios and ICRA reference temperature.

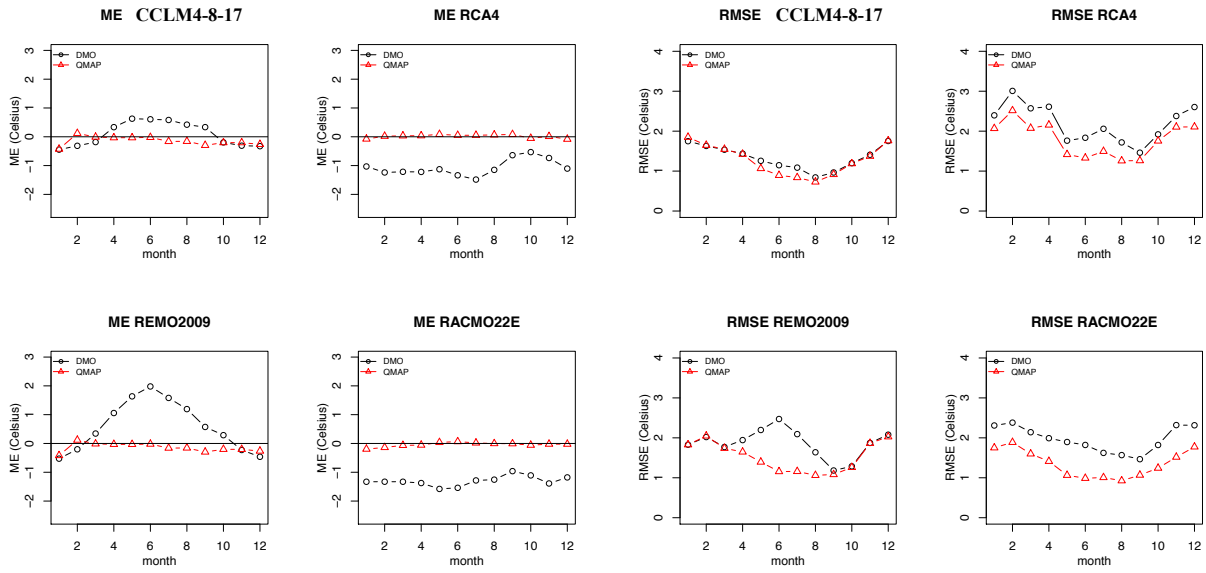

Fig. I-5: Catchment vhm64: Mean error (ME) and root-mean-square error (RMSE) between CORDEX temperature evaluation scenarios and ICRA reference temperature. DMO=original CORDEX; QMAP=bias-corrected CORDEX. Period 1989-2008.

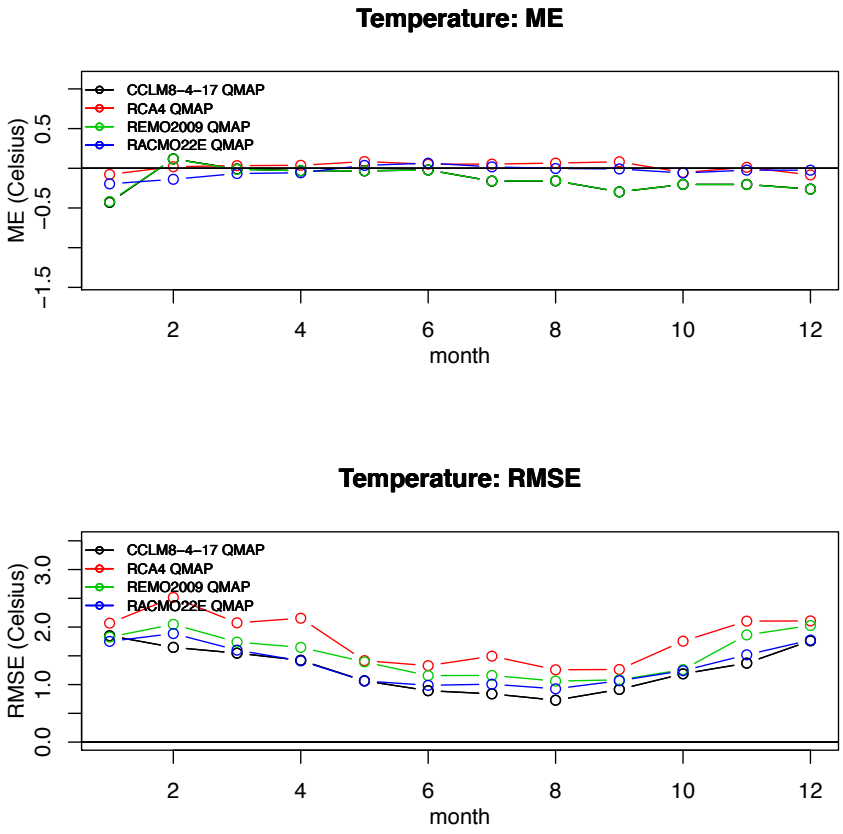

Fig. I-6: Catchment vhm64: Mean error (ME) and root-mean-square error (RMSE) between bias-corrected CORDEX temperature evaluation scenarios and ICRA reference temperature.

Appendix 2

CORDEX daily precipitation evaluation scenarios : RCMs and bias-correction skills

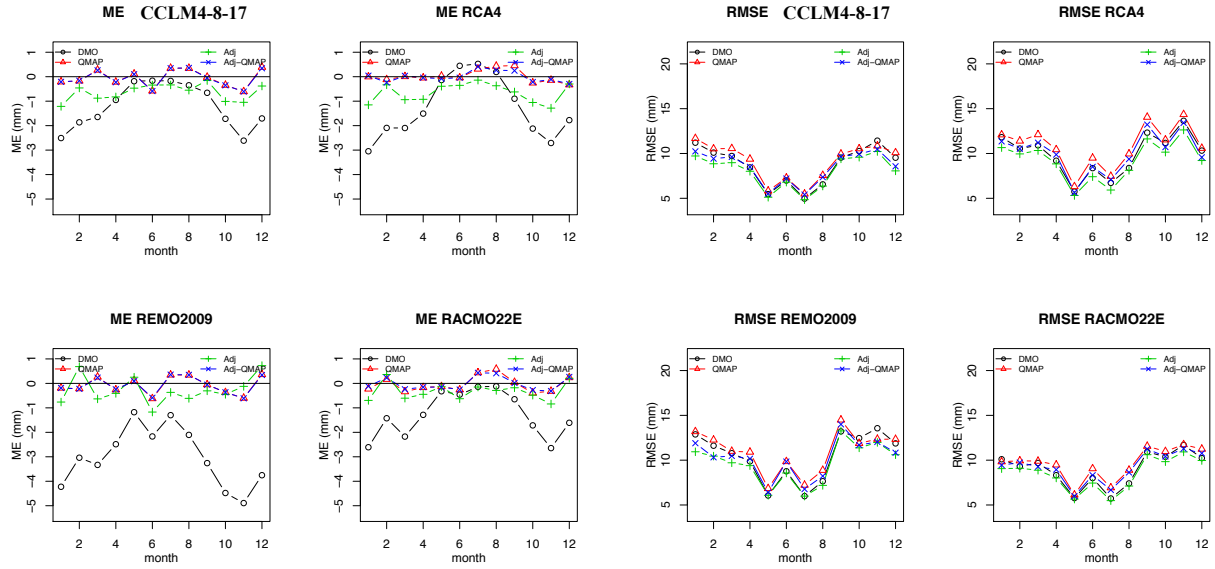

Fig. II-1: Catchment vhm148: Mean error (ME) and root-mean-square error (RMSE) between CORDEX precipitation evaluation scenarios and ICRA reference precipitation. DMO=original CORDEX; QMAP=quantile mapping (method 1); Adj=analog-based correction; Adj-QMAP= analog-based correction + quantile mapping (method 2). Period 1989-2008.

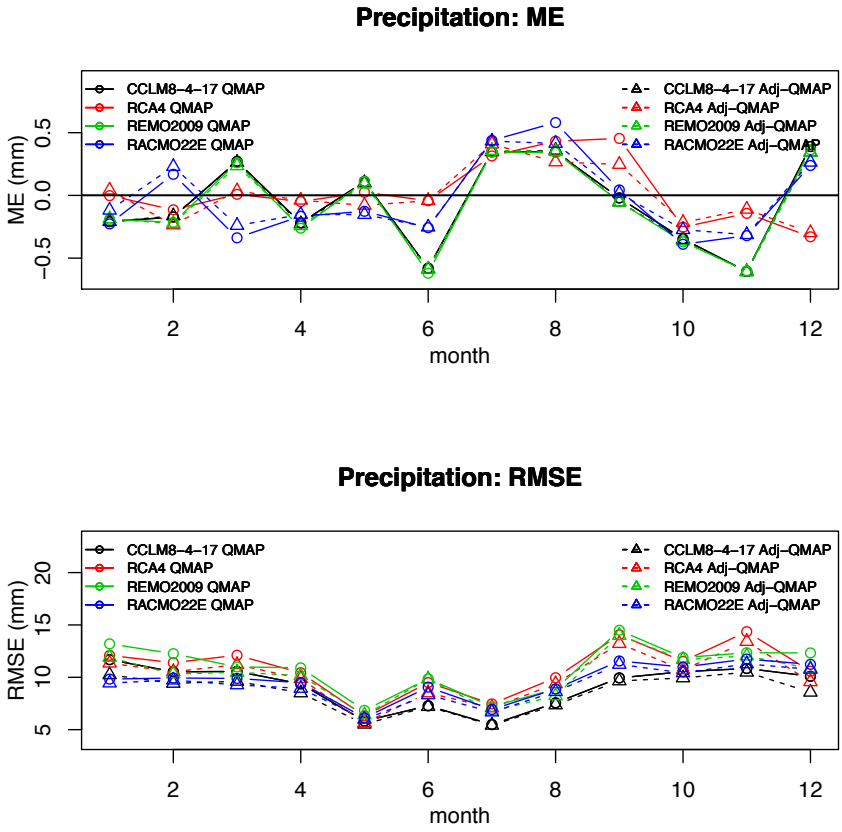

Fig. II-2: Catchment vhm148: Mean error (ME) and root-mean-square error (RMSE) between bias-corrected CORDEX precipitation evaluation scenarios and ICRA reference precipitation. QMAP=bias-correction method 1; Adj-QMAP=bias-correction method 2.

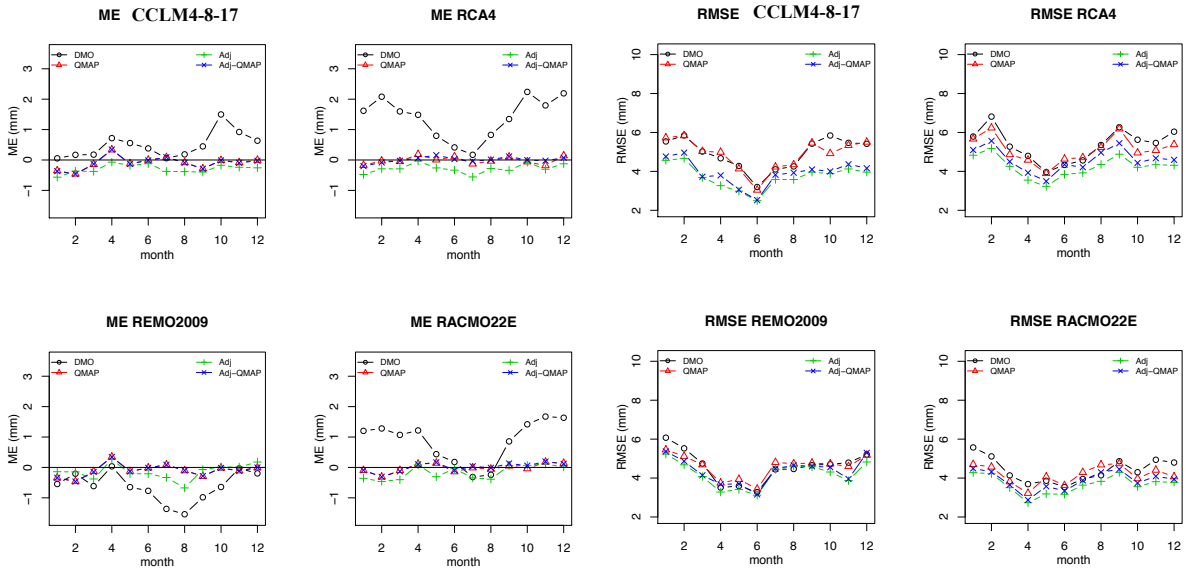

Fig. II-3: Catchment vhm51: Mean error (ME) and root-mean-square error (RMSE) between CORDEX precipitation evaluation scenarios and ICRA reference precipitation. DMO=original CORDEX; QMAP=quantile mapping (method 1); Adj=analog-based correction; Adj-QMAP= analog-based correction + quantile mapping (method 2). Period 1989-2008.

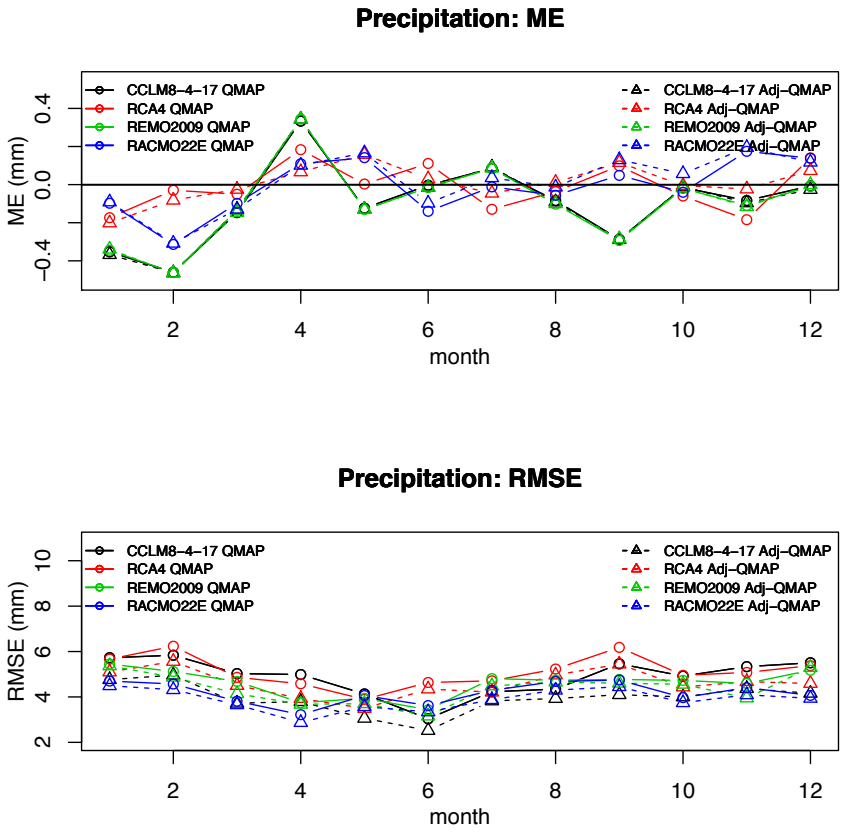

Fig. II-4: Catchment vhm51: Mean error (ME) and root-mean-square error (RMSE) between bias-corrected CORDEX precipitation evaluation scenarios and ICRA reference precipitation. QMAP=bias-correction method 1; Adj-QMAP=bias-correction method 2.

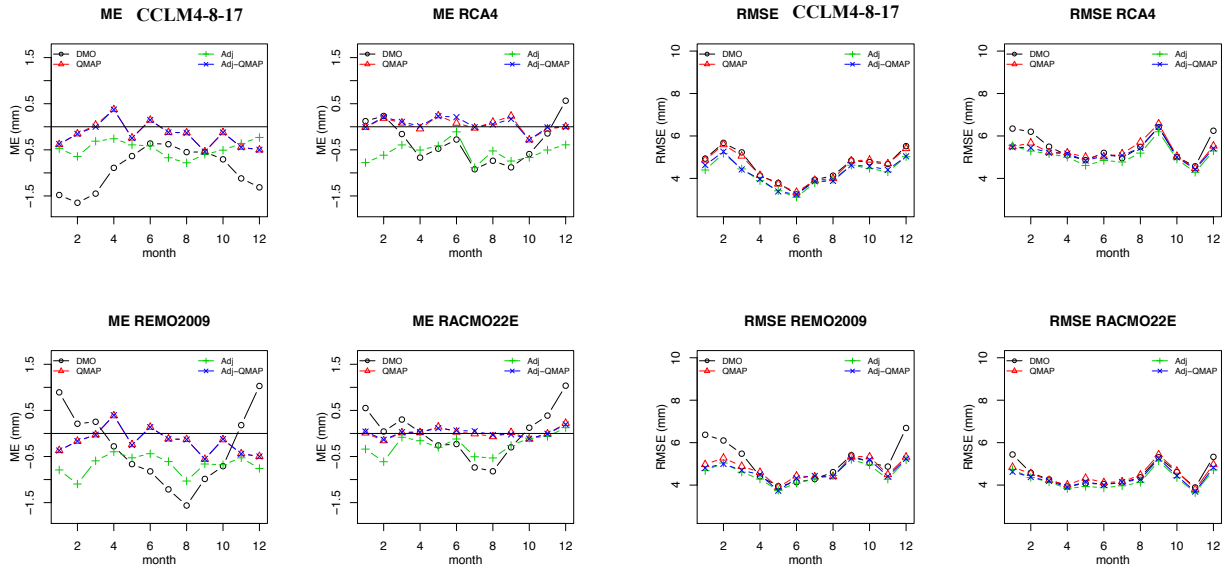

Fig. II-5: Catchment vhm64: Mean error (ME) and root-mean-square error (RMSE) between CORDEX precipitation evaluation scenarios and ICRA reference precipitation. DMO=original CORDEX; QMAP=quantile mapping (method 1); Adj=analog-based correction; Adj-QMAP= analog-based correction + quantile mapping (method 2). Period 1989-2008.

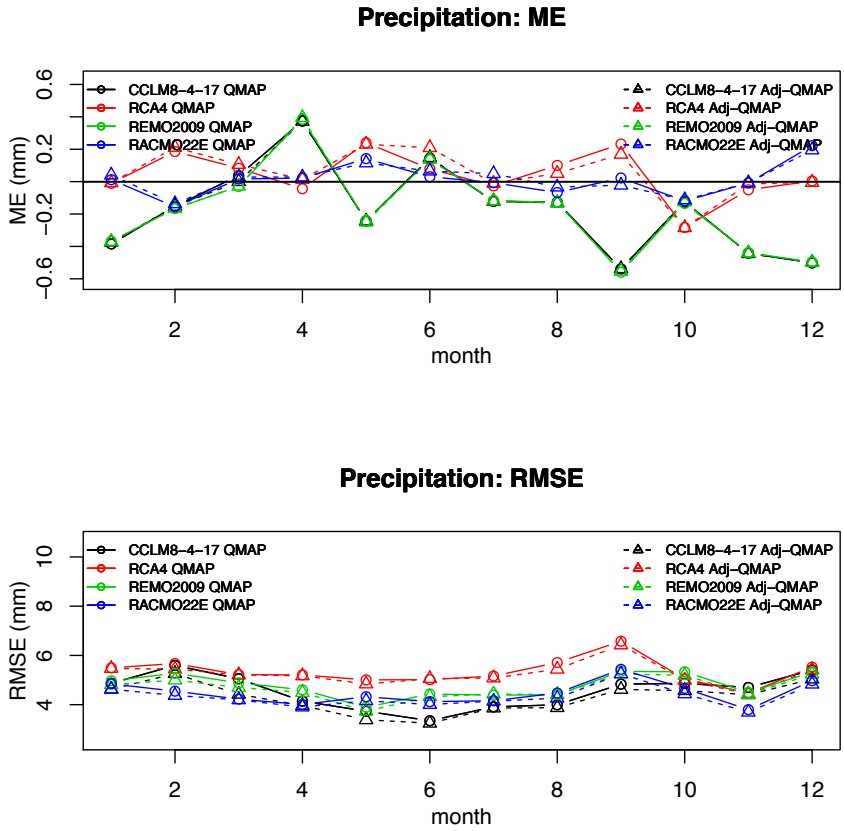

Fig. II-6: Catchment vhm64: Mean error (ME) and root-mean-square error (RMSE) between bias-corrected CORDEX precipitation evaluation scenarios and ICRA reference precipitation. QMAP=bias-correction method 1; Adj-QMAP=bias-correction method 2.

Appendix 3

30-year mean monthly temperature seasonality in the 1981-2010 reference period before and after bias-correction of the CORDEX scenarios

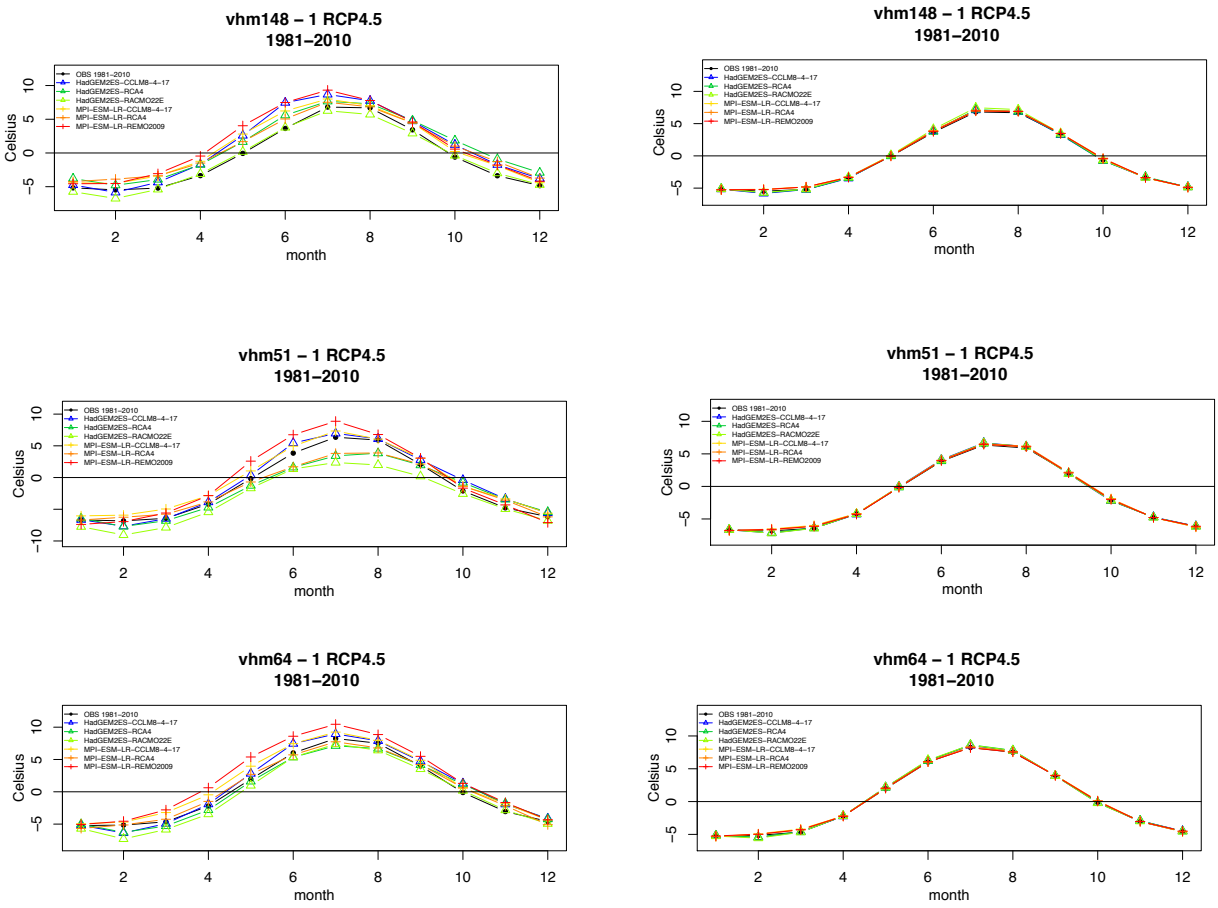

Fig. III-1: 30-year mean monthly temperature seasonality in the 1981-2010 reference period. Left-panel: CORDEX original; Right-panel: after bias-correction by quantile mapping.

Appendix 4

30-year mean monthly precipitation seasonality in the 1981-2010 reference period before and after bias-correction of the CORDEX scenarios

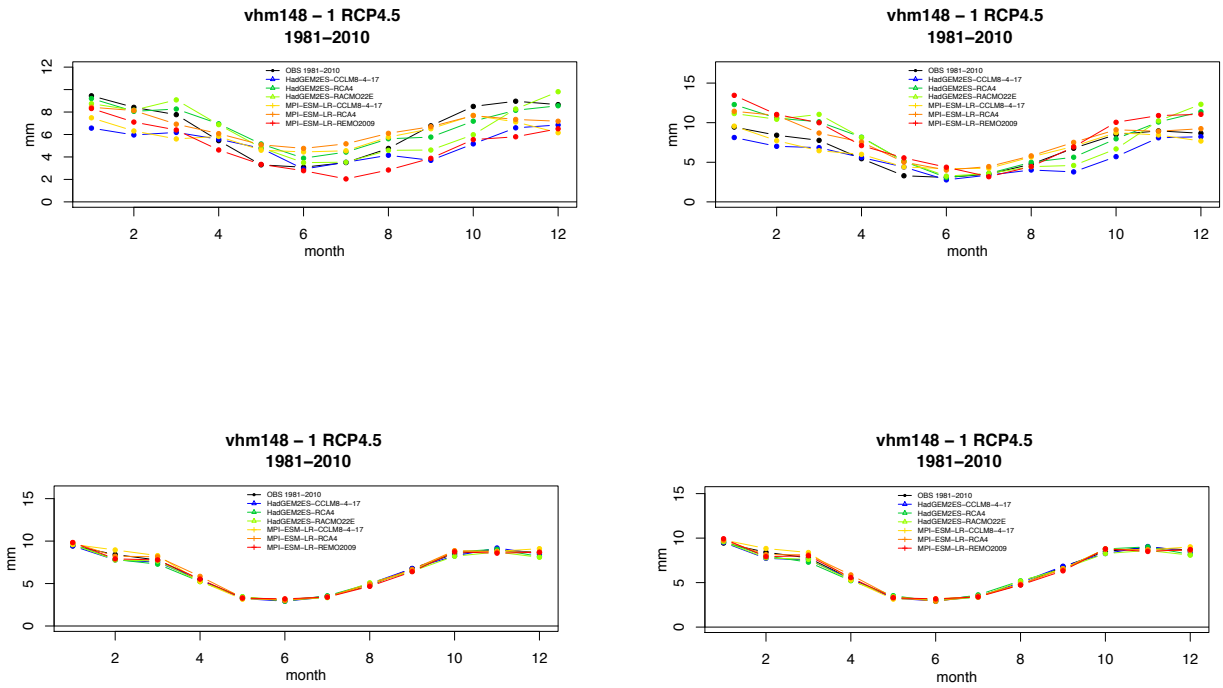

Fig. IV-1: Catchment vhm148: 30-year mean monthly precipitation seasonality in the 1981-2010 reference period. Top-left: CORDEX original; Bottom-left: bias-corrected with quantile mapping (method 1); Top-right: analog-based correction; Bottom-right: analog-based correction + quantile mapping (method 2).

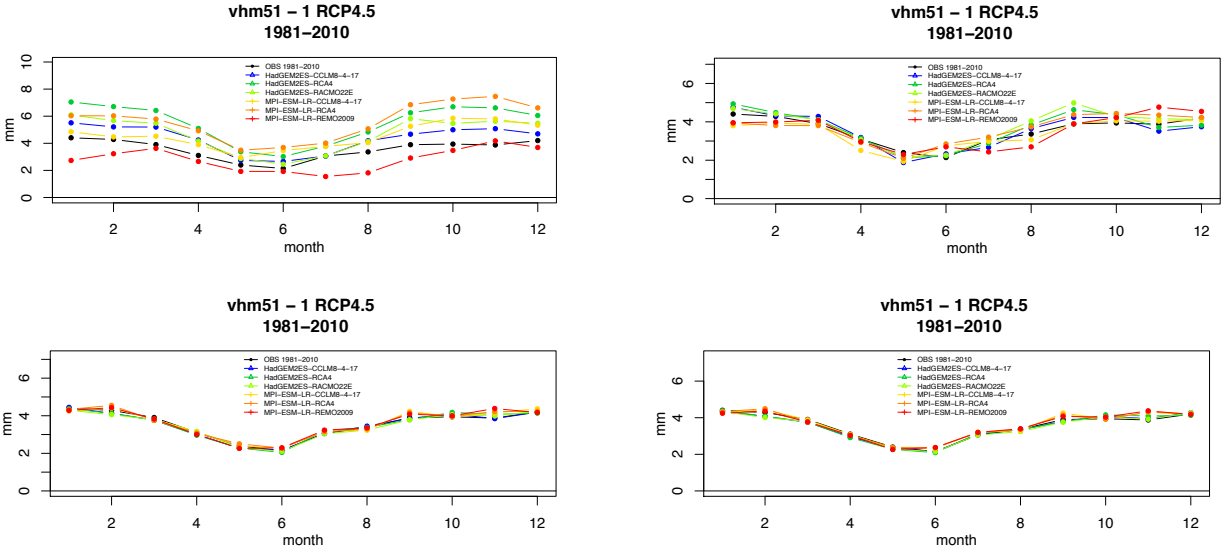

Fig. IV-2: As Fig. IV-1 but for catchment vhm51.

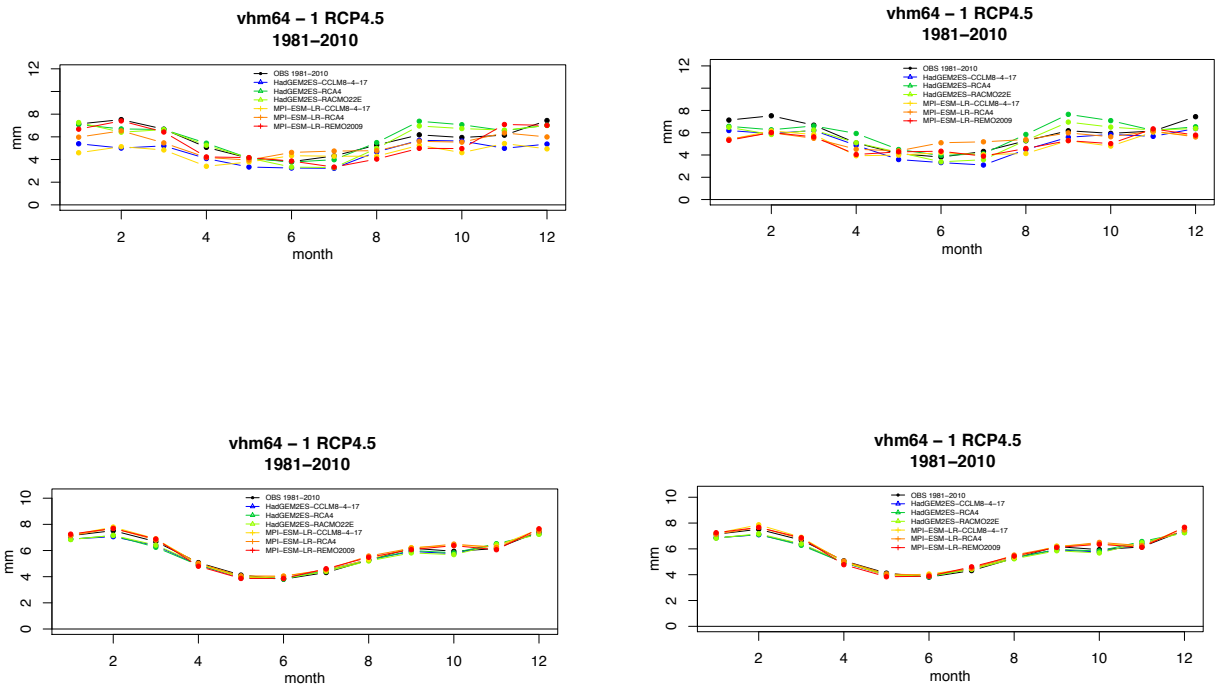

Fig. IV-3: As Fig. IV-1 but for catchment vhm64.

Appendix 5

Evolution of the bias-corrected mean monthly temperature seasonality along the 21st century under the RCP4.5 and RCP8.5 emission scenarios for a selected pair of GCM-RCM

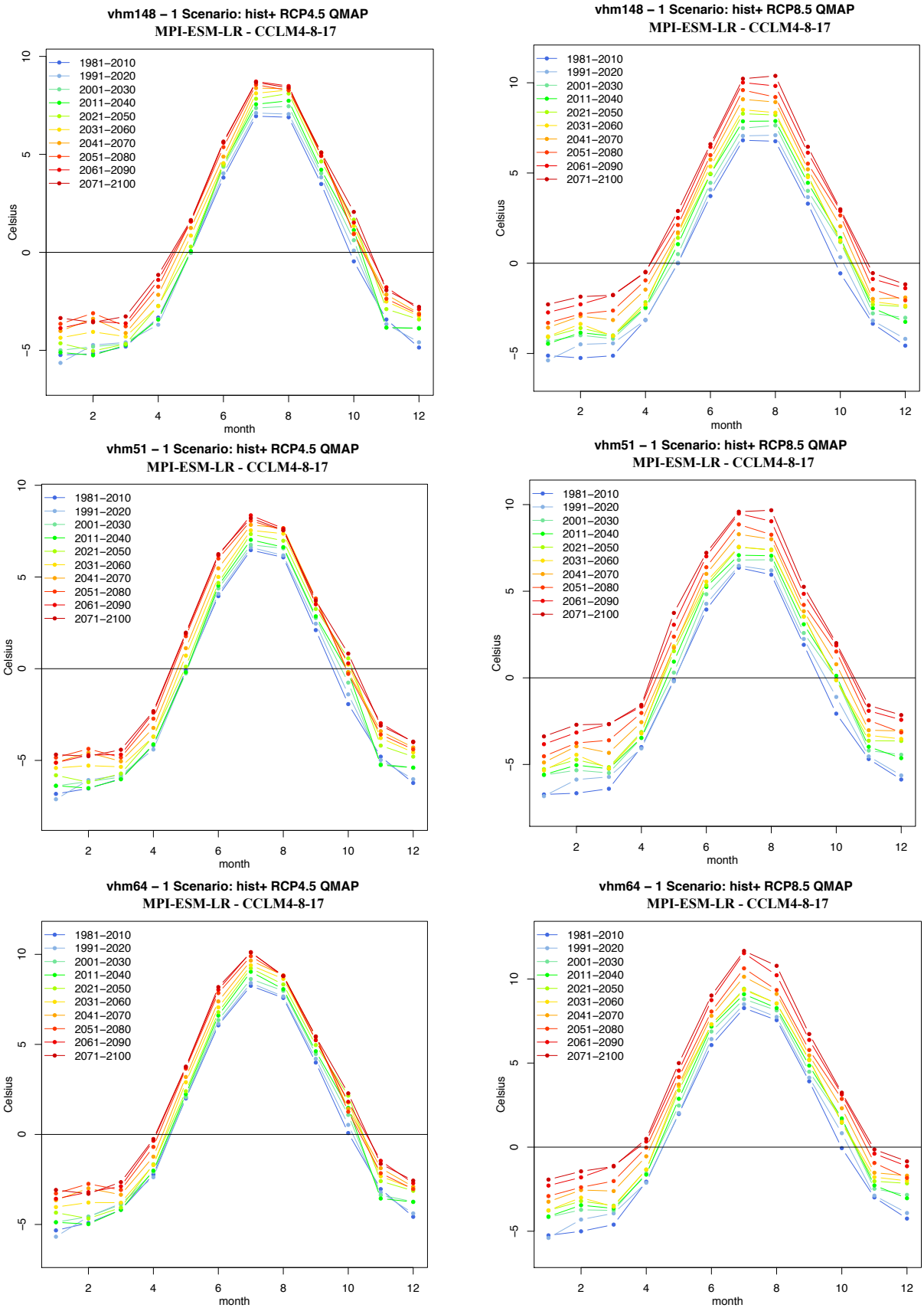

Fig. V-1: Projected mean monthly temperature seasonality under the RCP4.5 emission scenario (left panel) and RCP8.5 emission scenario (right panel). GCM:MPI-ESM-LR; RCM:CCLM4-8-17. Catchment vhm148 (top panel), vhm51 (middle panel), vhm64 (bottom panel).

Appendix 6

Projected bias-corrected (method 1) monthly precipitation time-series along the 21st century under the RCP4.5 emission scenario

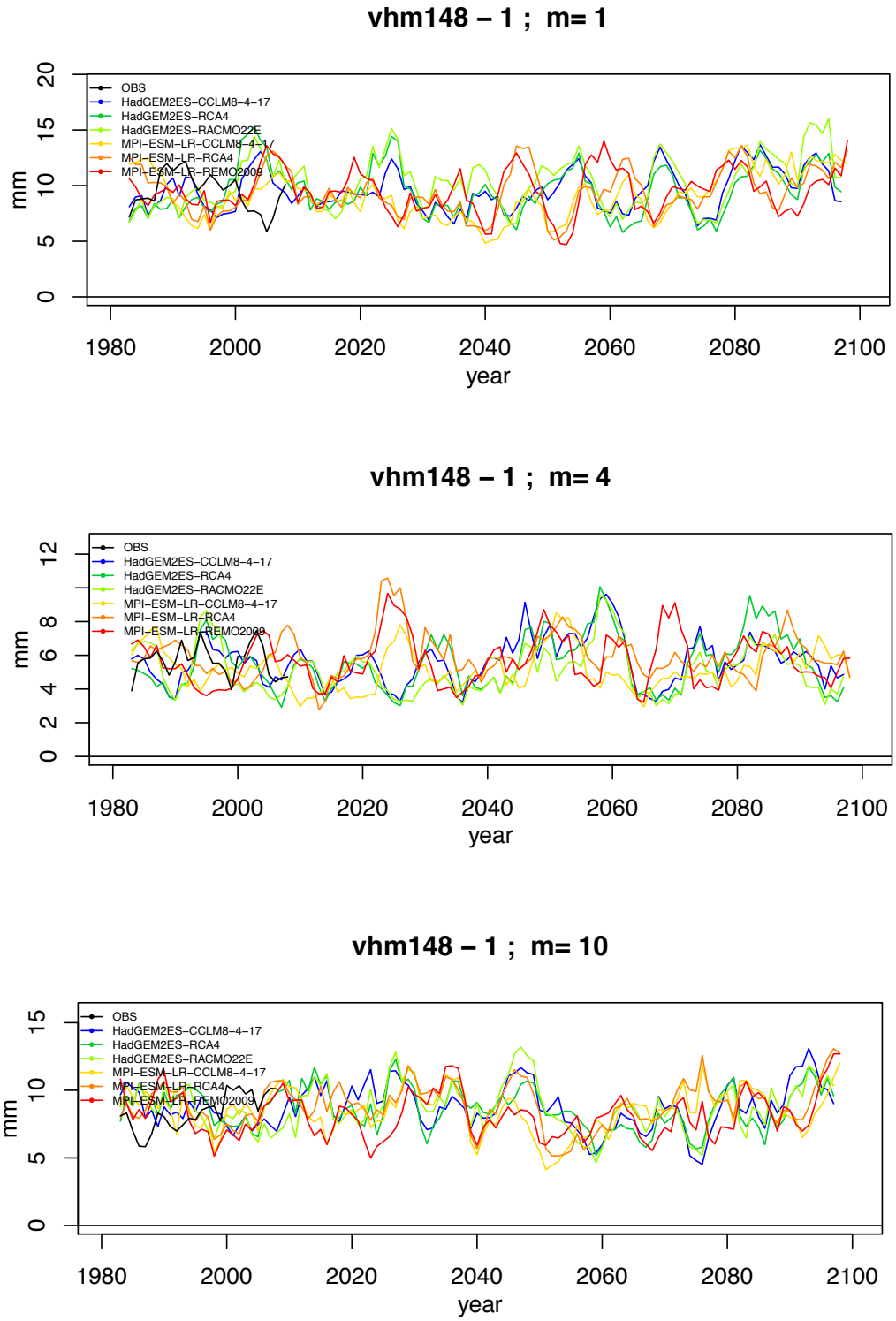

Fig. VI-1: Projected monthly precipitation scenarios (mm/d) for catchment vhm148 under RCP4.5. Top (January); Middle (April); Bottom (October). A 5-year running mean was applied.

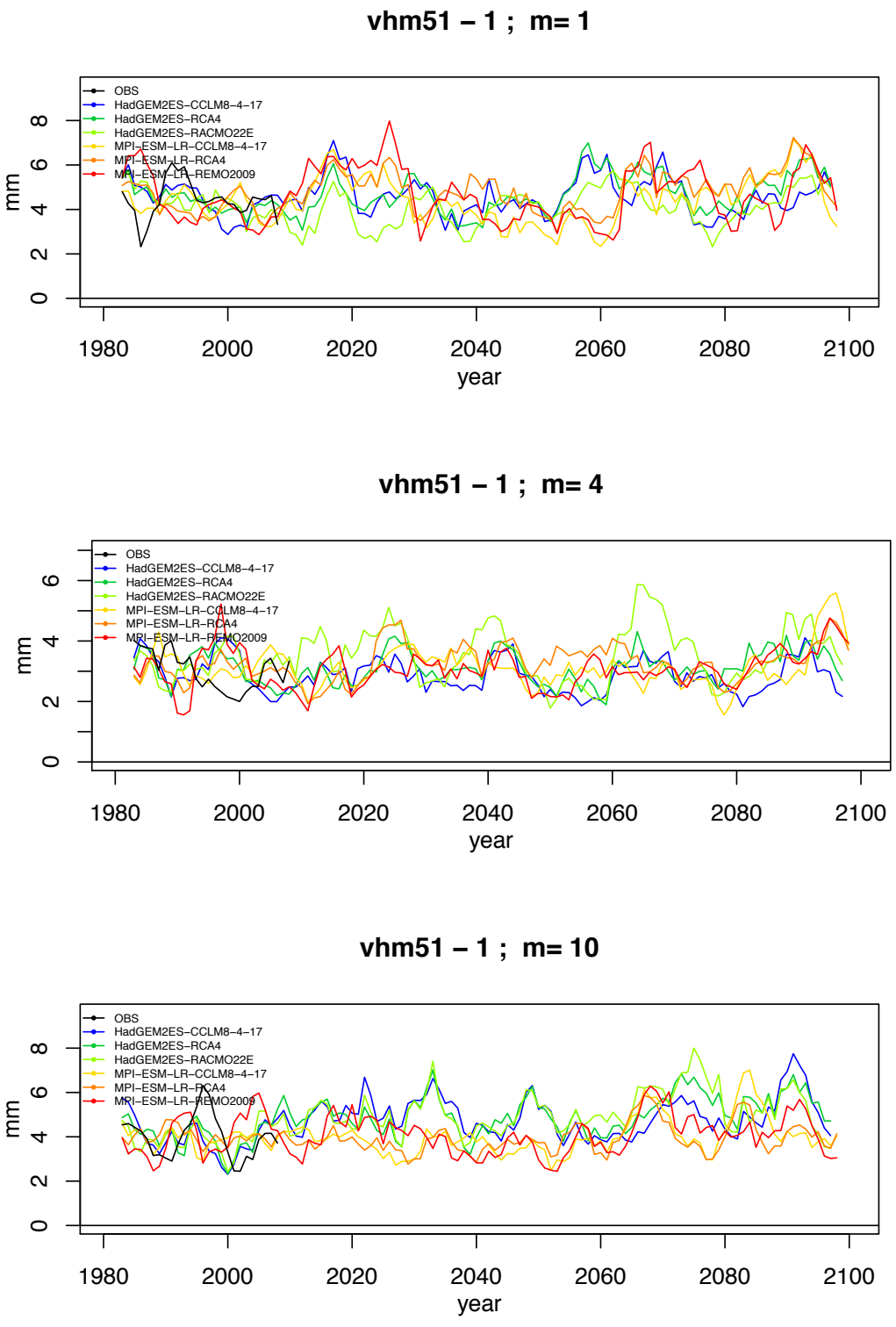

Fig. VI-2: Projected monthly precipitation scenarios (mm/d) for catchment vhm51 under RCP4.5. Top (January); Middle (April); Bottom (October). A 5-year running mean was applied.

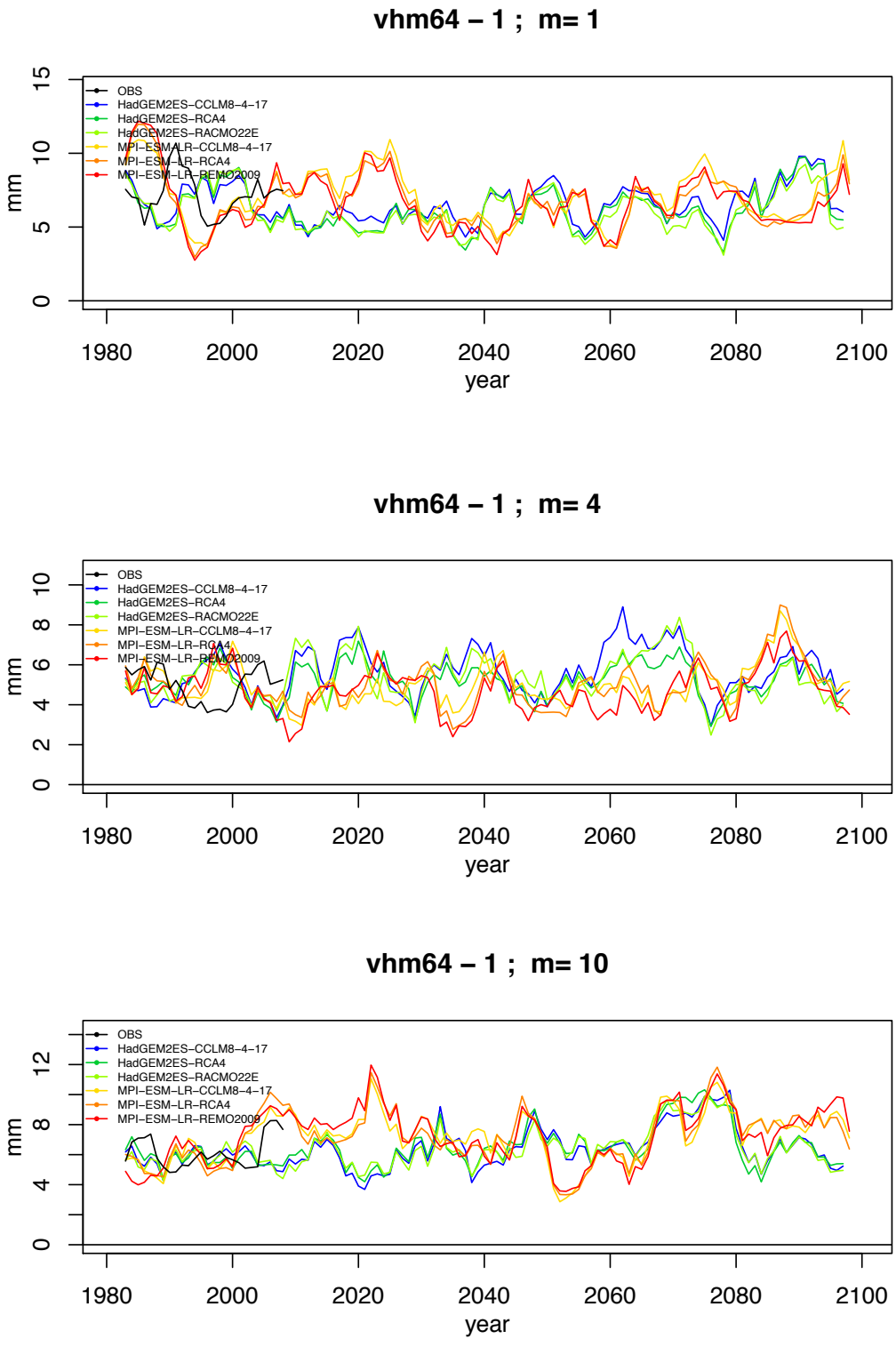

Fig. VI-3: Projected monthly precipitation scenarios (mm/d) for catchment vhm64 under RCP4.5. Top (January); Middle (April); Bottom (October). A 5-year running mean was applied.

Appendix 7

Projected 30-year averaged annual and seasonal temperature, precipitation and streamflow discharge along the 21st century under the RCP4.5 and RCP8.5 emission scenarios

vhm148

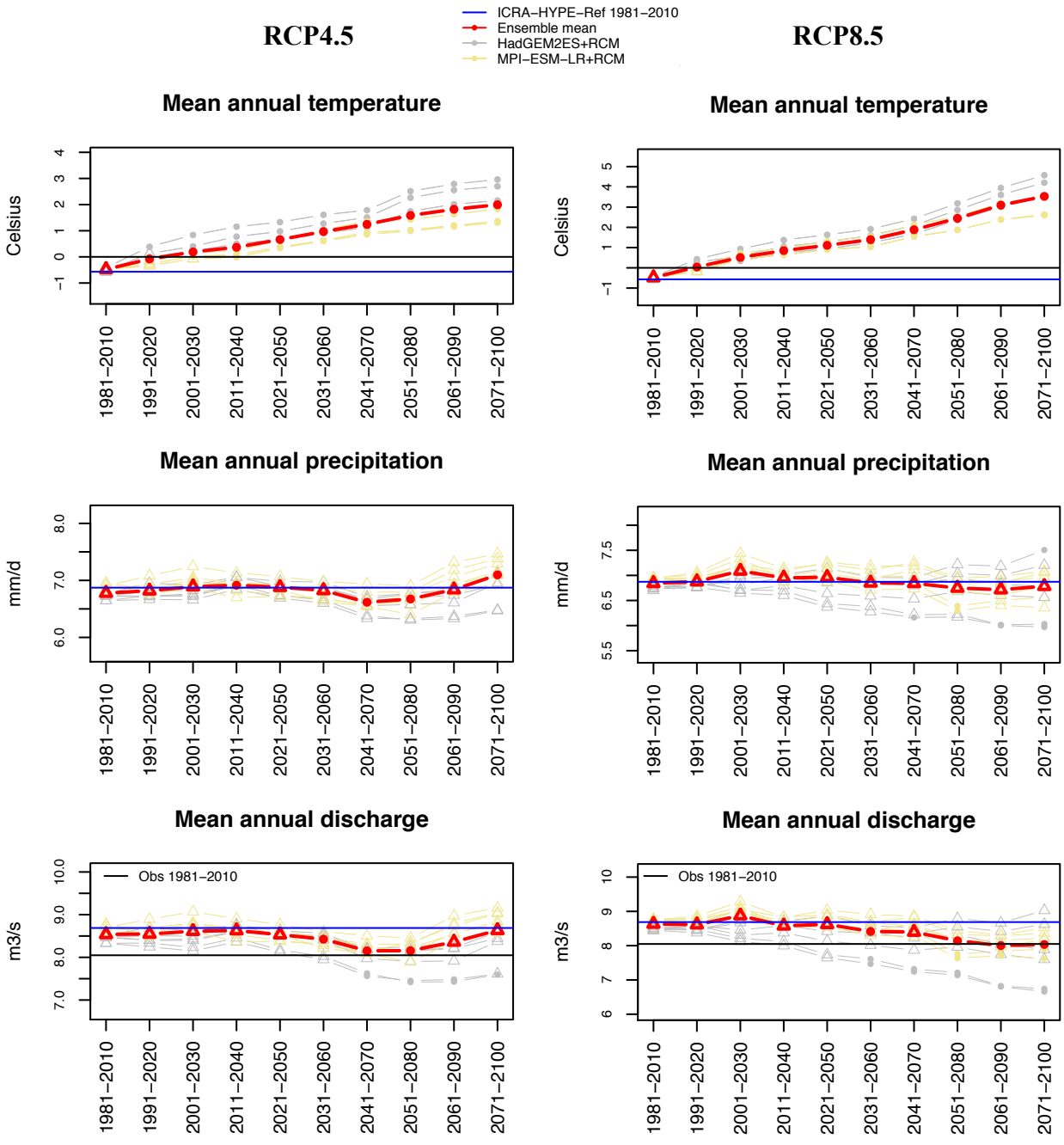

Fig. VII-1: Projected 30-year mean annual temperature, precipitation and streamflow discharge for catchment vhm148 under RCP4.5 emission scenarios (left panel) and RCP8.5 emission scenarios (right panel). Time-windows where a statistically significant shift relative to the 1981-2010 reference period was detected by the Mann-Whitney test are marked with a solid circle and those where no shift was detected are marked with a triangle. Ensemble median of all scenarios (red).

vhm148

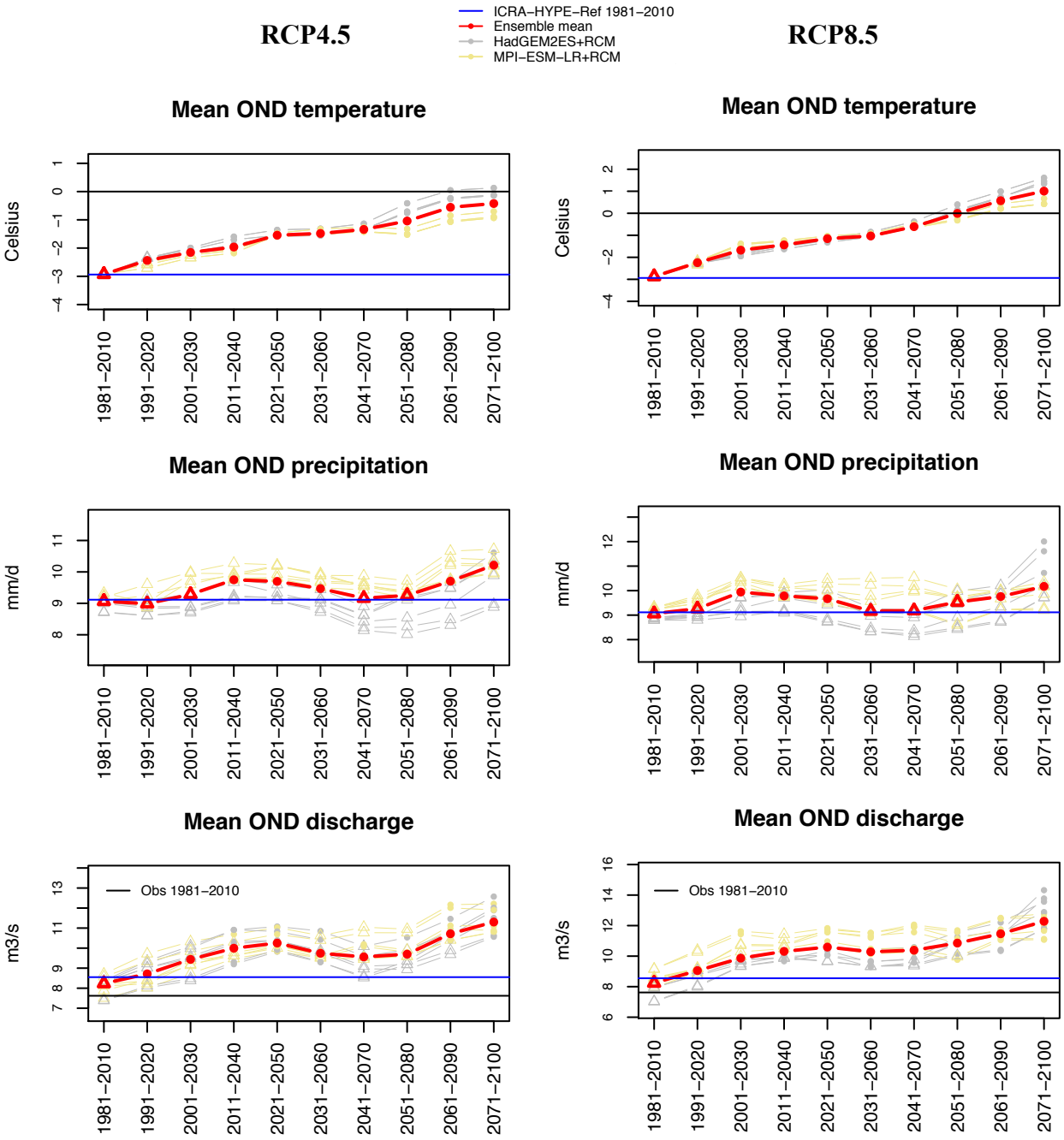

Fig. VII-2: Projected 30-year mean seasonal (OND) temperature, precipitation and streamflow discharge for catchment vhm148 under RCP4.5 emission scenarios (left panel) and RCP8.5 emission scenarios (right panel). Time-windows where a statistically significant shift relative to the 1981-2010 reference period was detected by the Mann-Whitney test are marked with a solid circle and those where no shift was detected are marked with a triangle. Ensemble median of all scenarios (red).

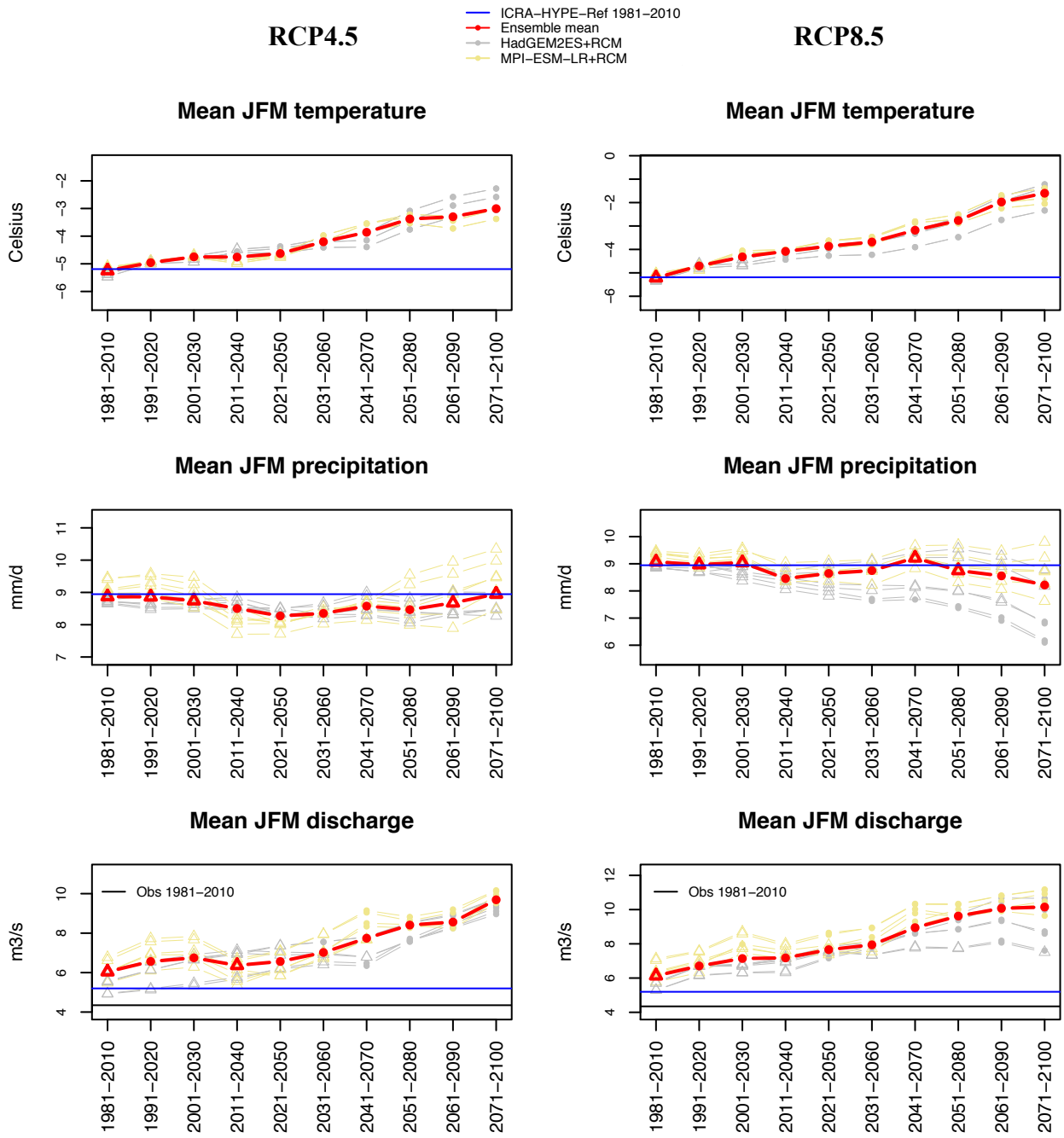

Fig. VII-3: Projected 30-year mean seasonal (JFM) temperature, precipitation and streamflow discharge for catchment vhm148 under RCP4.5 emission scenarios (left panel) and RCP8.5 emission scenarios (right panel). Time-windows where a statistically significant shift relative to the reference period 1981-2010 was detected by the Mann-Whitney test are marked with a solid circle and those where no shift was detected are marked with a triangle. Ensemble median of all scenarios (red).

vhm148

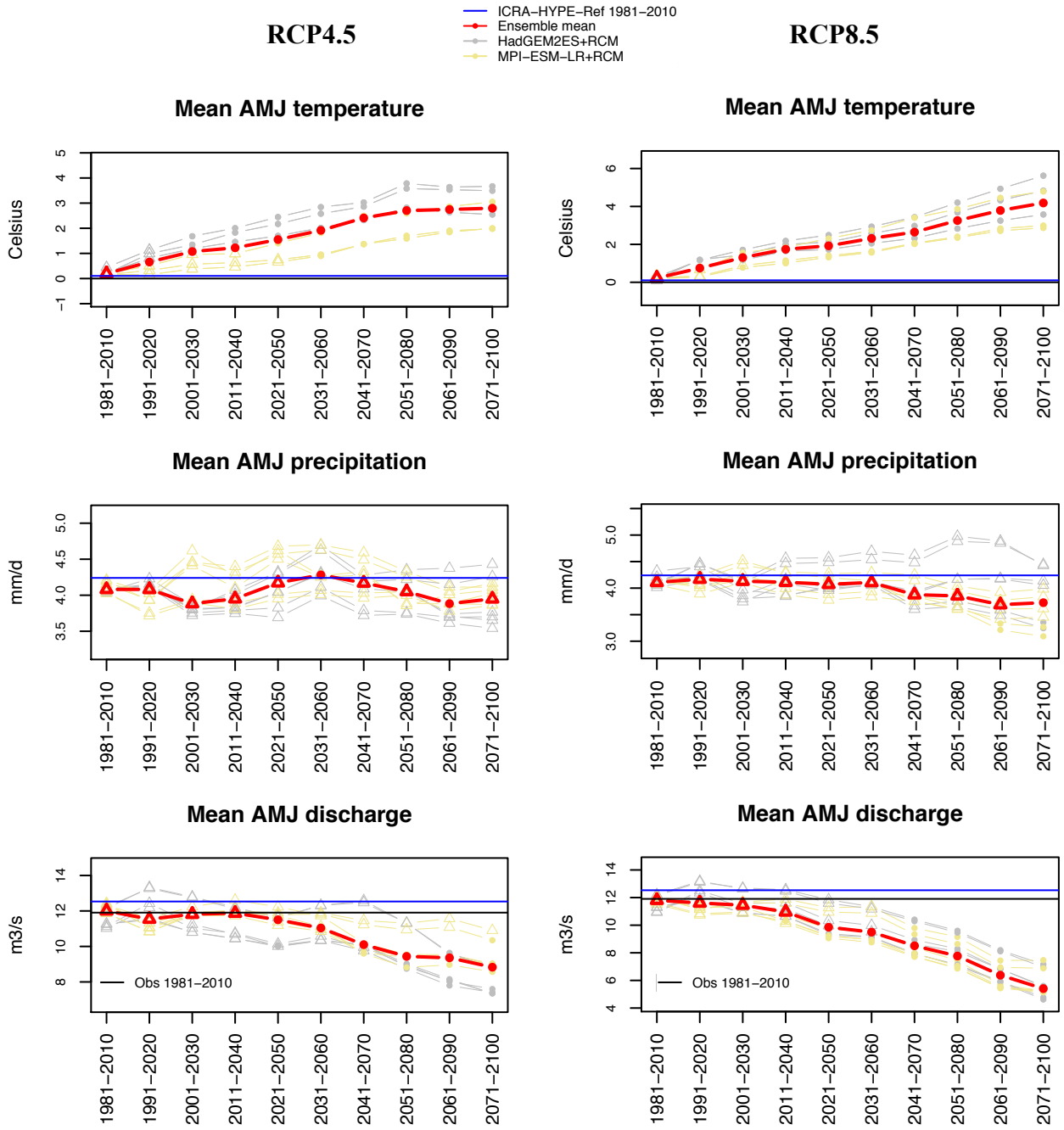

Fig. VII-4: Projected 30-year mean seasonal (AMJ) temperature, precipitation and streamflow discharge for catchment vhm148 under RCP4.5 emission scenarios (left panel) and RCP8.5 emission scenarios (right panel). Time-windows where a statistically significant shift relative to the 1981-2010 reference period was detected by the Mann-Whitney test are marked with a solid circle and those where no shift was detected are marked with a triangle. Ensemble median of all scenarios (red).

vhm148

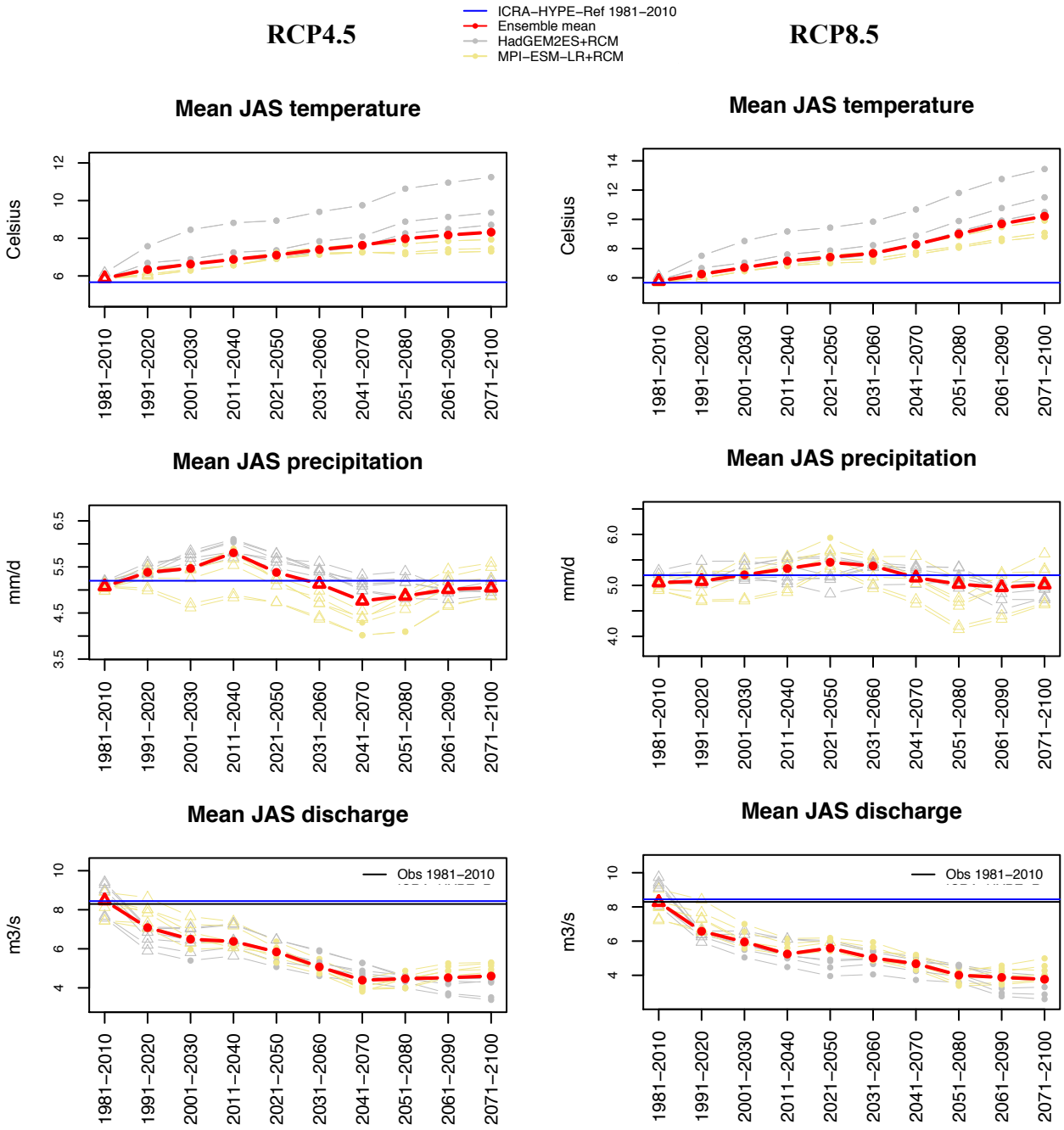

Fig. VII-5: Projected 30-year mean seasonal (JAS) temperature, precipitation and streamflow discharge for catchment vhm148 under RCP4.5 emission scenarios (left panel) and RCP8.5 emission scenarios (right panel). Time-windows where a statistically significant shift relative to the 1981-2010 reference period was detected by the Mann-Whitney test are marked with a solid circle and those where no shift was detected are marked with a triangle. Ensemble median of all scenarios (red).

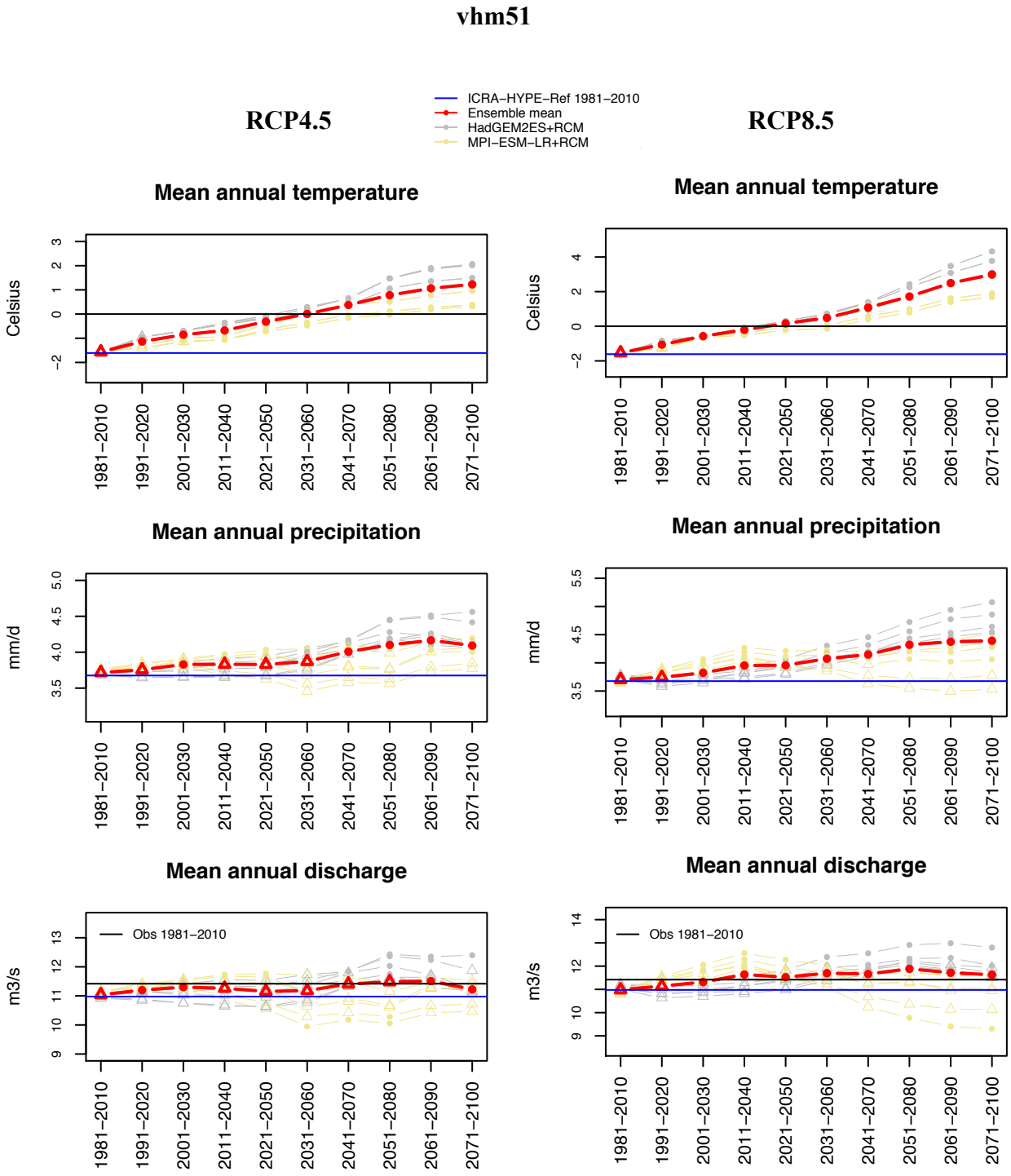

Fig. VII-6: Projected 30-year mean annual temperature, precipitation and streamflow discharge for catchment vhm51 under RCP4.5 emission scenarios (left panel) and RCP8.5 emission scenarios (right panel). Time-windows where a statistically significant shift relative to the 1981-2010 reference period was detected by the Mann-Whitney test are marked with a solid circle and those where no shift was detected are marked with a triangle. Ensemble median of all scenarios (red).

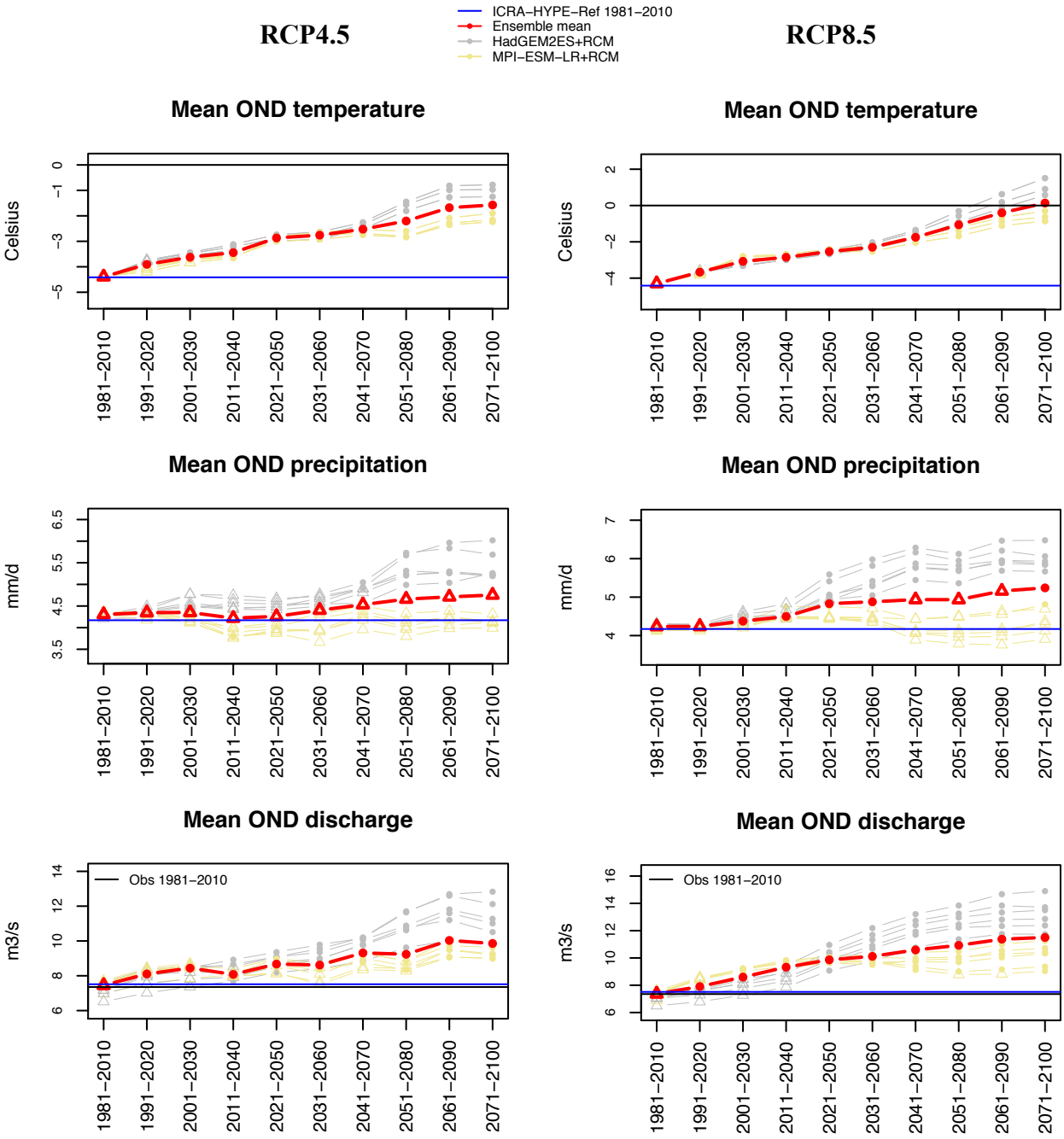

Fig. VII-7: Projected 30-year mean seasonal (OND) temperature, precipitation and streamflow discharge for catchment vhm51 under RCP4.5 emission scenarios (left panel) and RCP8.5 emission scenarios (right panel). Time-windows where a statistically significant shift relative to the 1981-2010 reference period was detected by the Mann-Whitney test are marked with a solid circle and those where no shift was detected are marked with a triangle. Ensemble median of all scenarios (red).

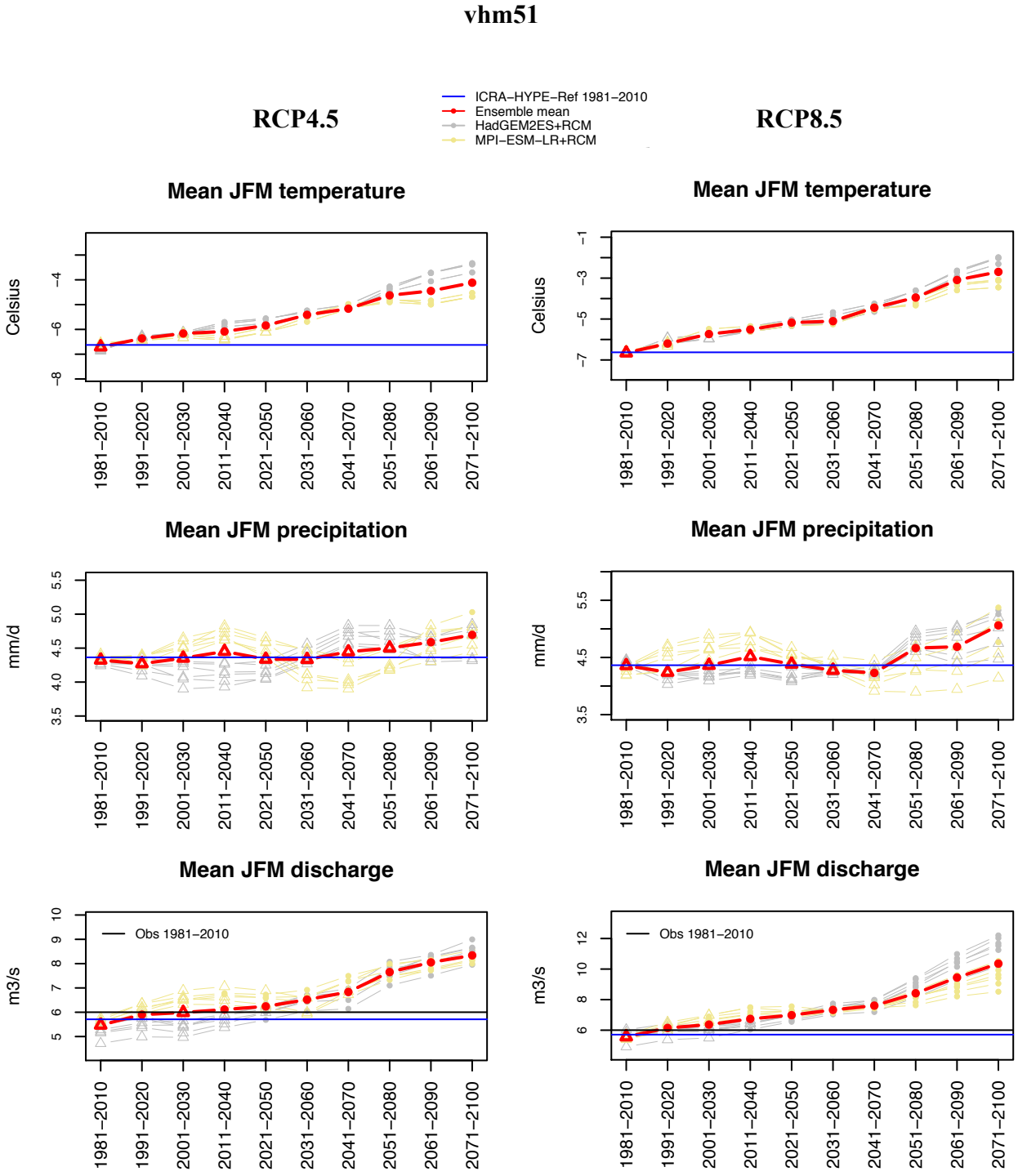

Fig. VII-8: Projected 30-year mean seasonal (JFM) temperature, precipitation and streamflow discharge for catchment vhm51 under RCP4.5 emission scenarios (left panel) and RCP8.5 emission scenarios (right panel). Time-windows where a statistically significant shift relative to the 1981-2010 reference period was detected by the Mann-Whitney test are marked with a solid circle and those where no shift was detected are marked with a triangle. Ensemble median of all scenarios (red).

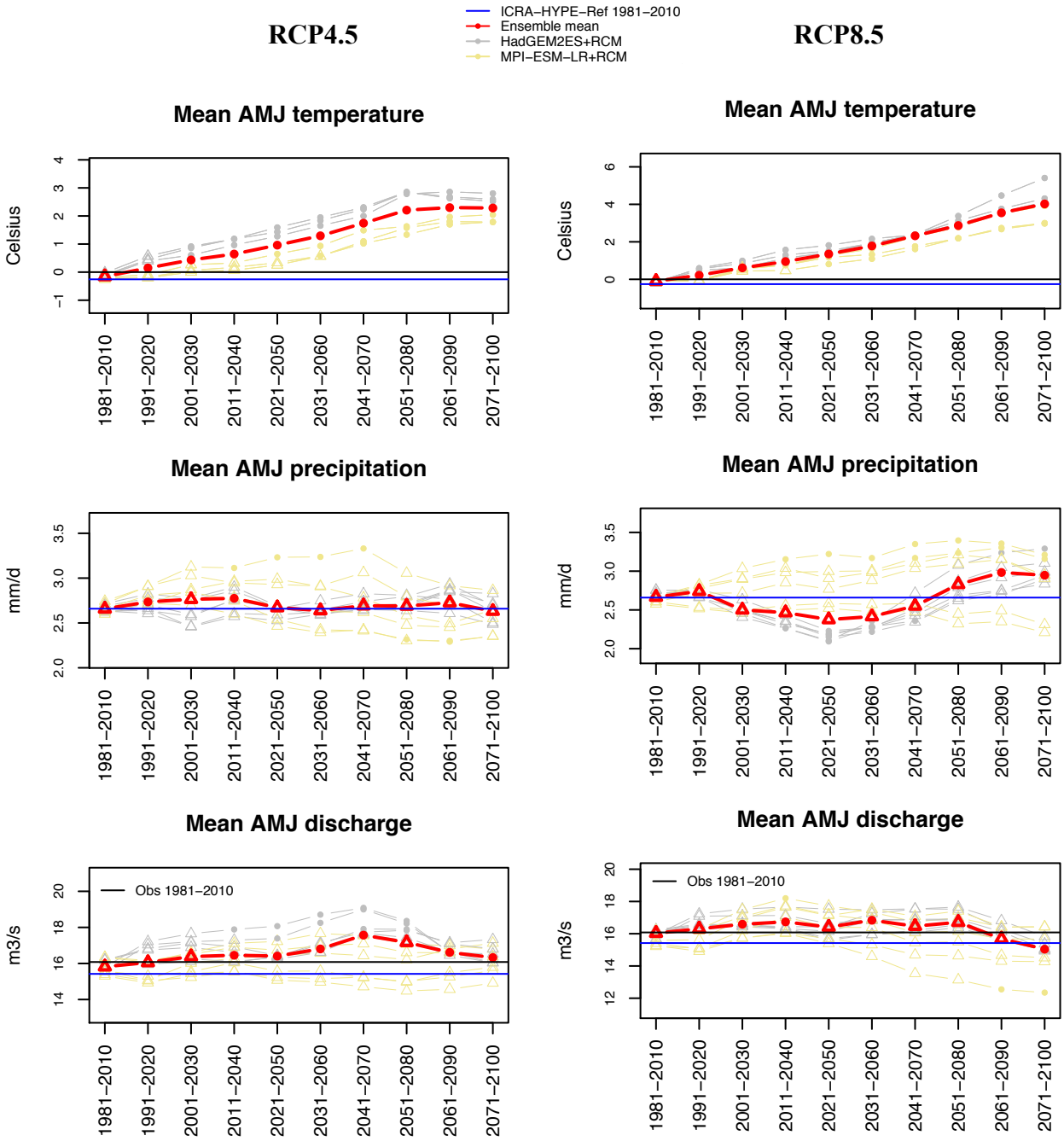

Fig. VII-9: Projected 30-year mean seasonal (AMJ) temperature, precipitation and streamflow discharge for catchment vhm51 under RCP4.5 emission scenarios (left panel) and RCP8.5 emission scenarios (right panel). Time-windows where a statistically significant shift relative to the 1981-2010 reference period was detected by the Mann-Whitney test are marked with a solid circle and those where no shift was detected are marked with a triangle. Ensemble median of all scenarios (red).

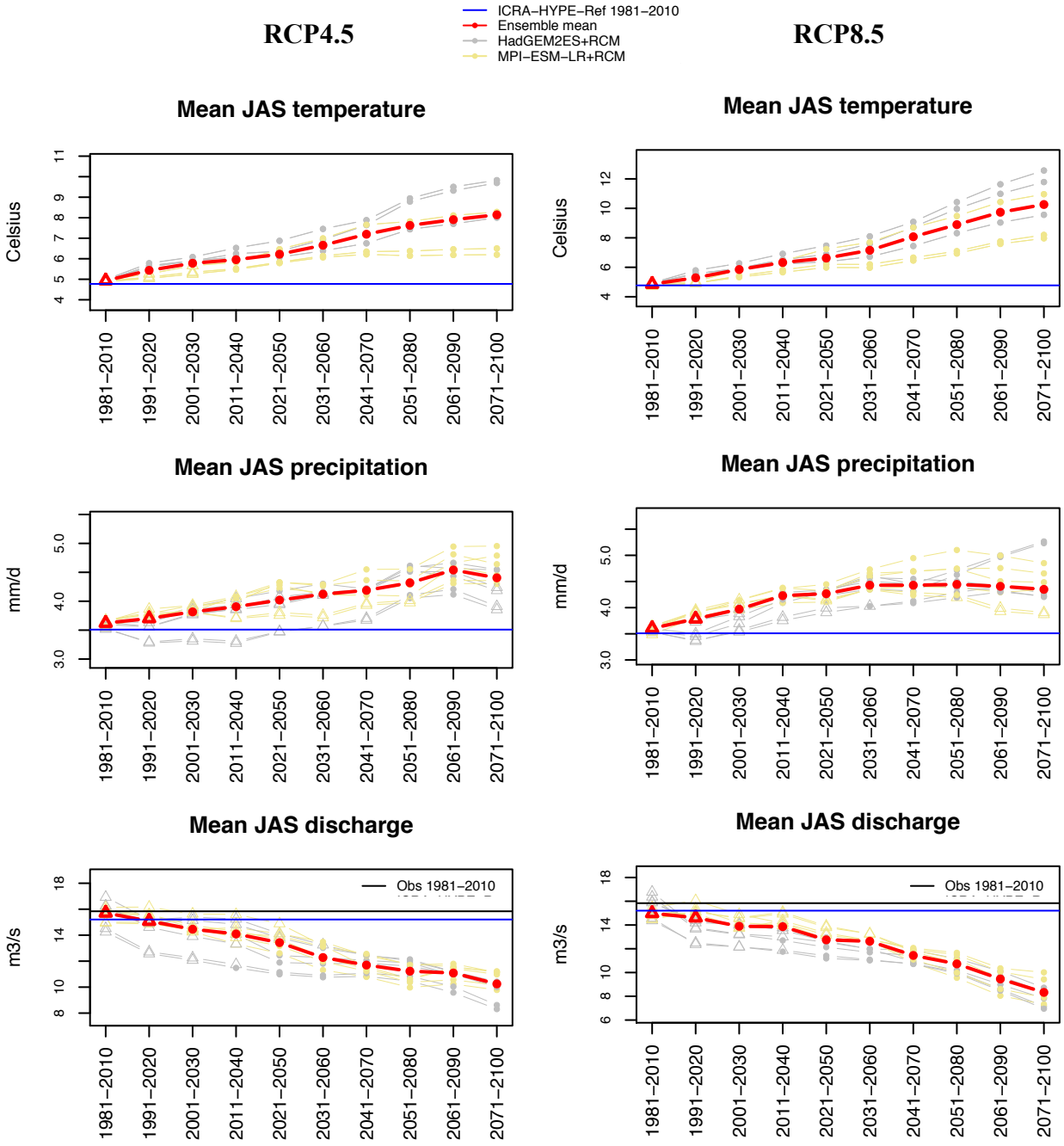

Fig. VII-10: Projected 30-year mean seasonal (JAS) temperature, precipitation and streamflow discharge for catchment vhm51 under RCP4.5 emission scenarios (left panel) and RCP8.5 emission scenarios (right panel). Time-windows where a statistically significant shift relative to the 1981-2010 reference period was detected by the Mann-Whitney test are marked with a solid circle and those where no shift was detected are marked with a triangle. Ensemble median of all scenarios (red).

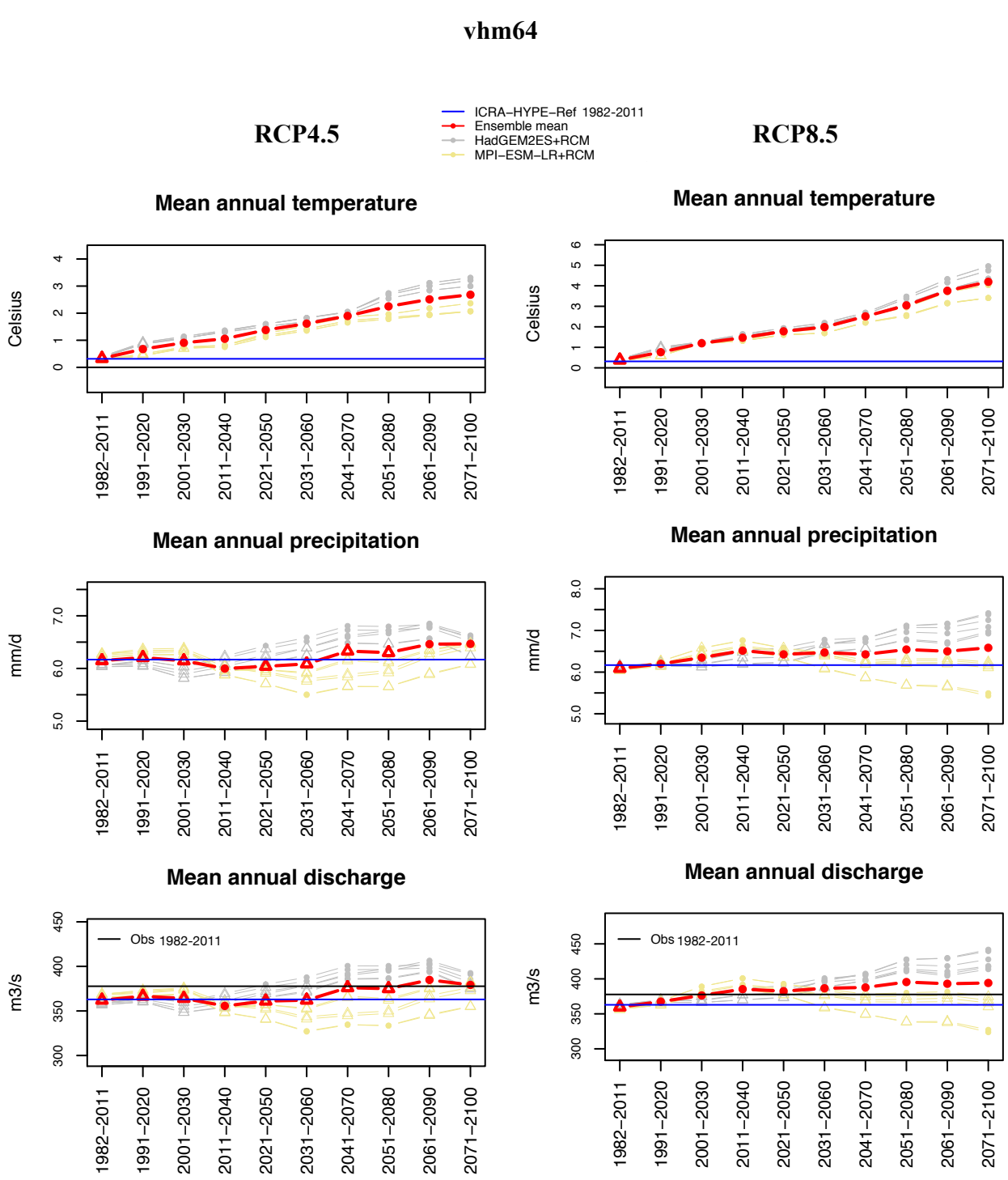

Fig. VII-11: Projected 30-year mean annual temperature, precipitation and streamflow discharge for catchment vhm64 under RCP4.5 emission scenarios (left panel) and RCP8.5 emission scenarios (right panel). Time-windows where a statistically significant shift relative to the 1982-2011 reference period was detected by the Mann-Whitney test are marked with a solid circle and those where no shift was detected are marked with a triangle. Ensemble median of all scenarios (red).

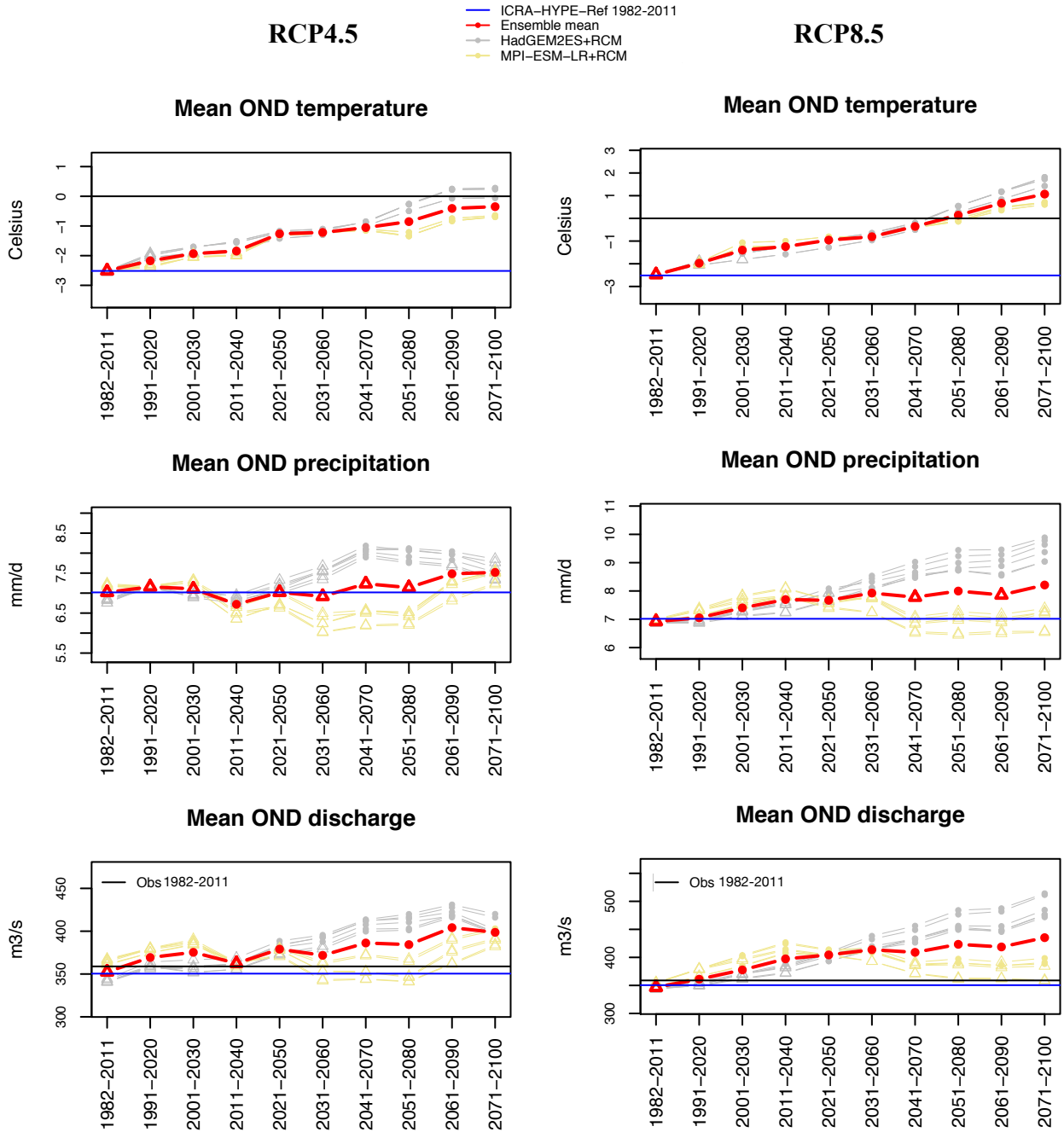

Fig. VII-12: Projected 30-year mean seasonal (OND) temperature, precipitation and streamflow discharge for catchment vhm64 under RCP4.5 emission scenarios (left panel) and RCP8.5 emission scenarios (right panel). Time-windows where a statistically significant shift relative to the 1982-2011 reference period was detected by the Mann-Whitney test are marked with a solid circle and those where no shift was detected are marked with a triangle. Ensemble median of all scenarios (red).

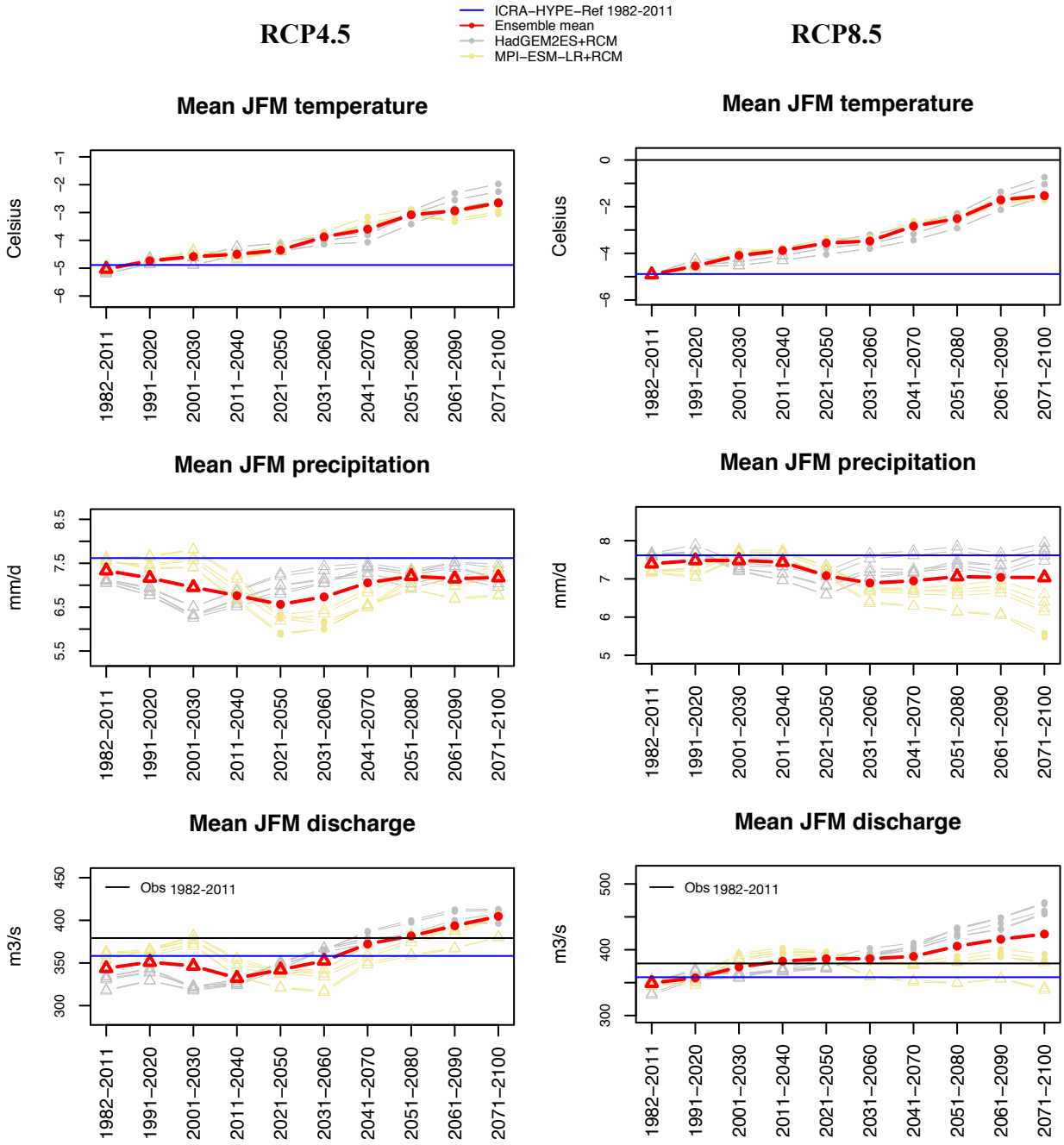

Fig. VII-13: Projected 30-year mean seasonal (JFM) temperature, precipitation and streamflow discharge for catchment vhm64 under RCP4.5 emission scenarios (left panel) and RCP8.5 emission scenarios (right panel). Time-windows where a statistically significant shift relative to the 1982-2011 reference period was detected by the Mann-Whitney test are marked with a solid circle and those where no shift was detected are marked with a triangle. Ensemble median of all scenarios (red).

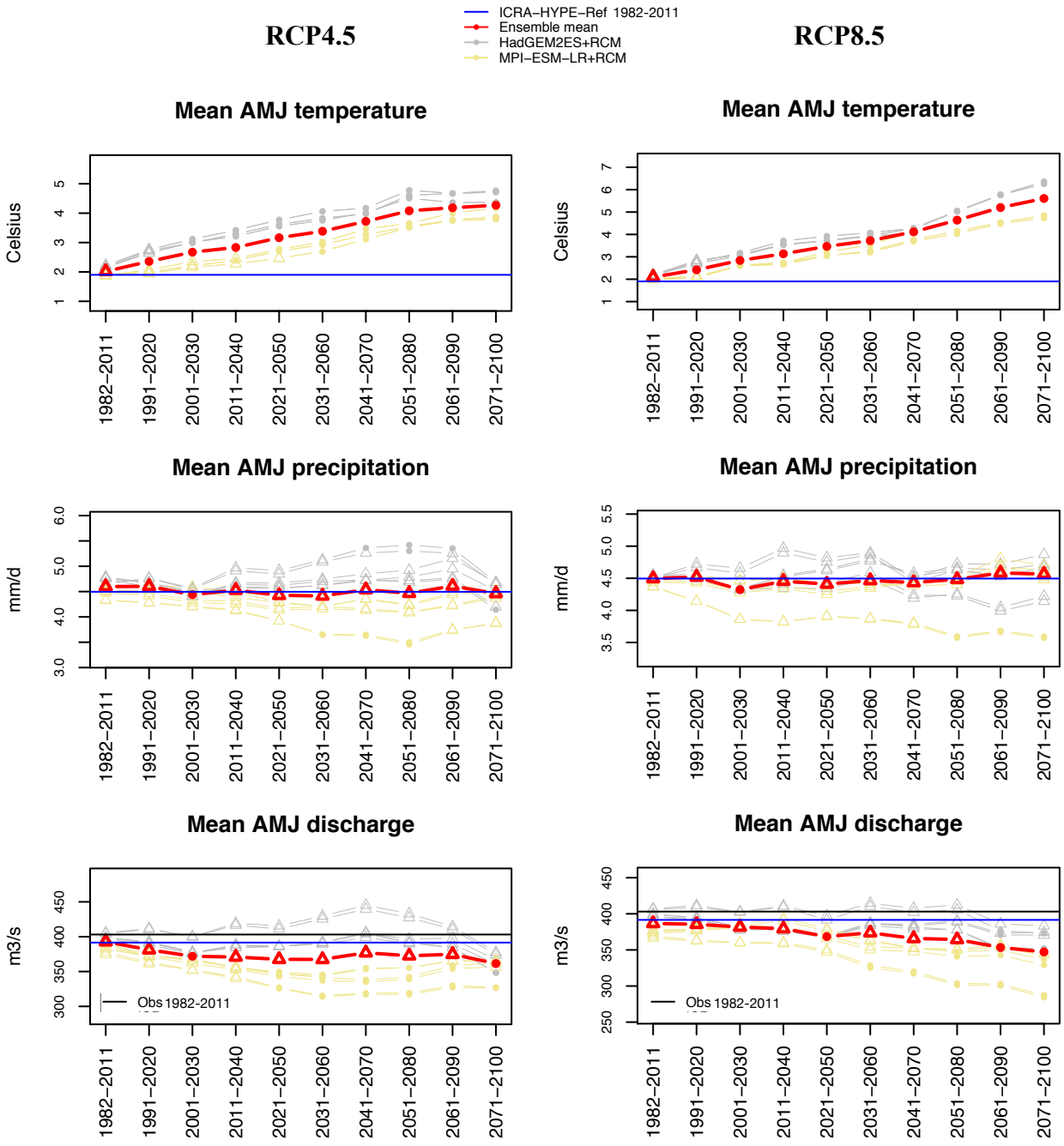

Fig. VII-14: Projected 30-year mean seasonal (AMJ) temperature, precipitation and streamflow discharge for catchment vhm64 under RCP4.5 emission scenarios (left panel) and RCP8.5 emission scenarios (right panel). Time-windows where a statistically significant shift relative to the 1982-2011 reference period was detected by the Mann-Whitney test are marked with a solid circle and those where no shift was detected are marked with a triangle. Ensemble median of all scenarios (red).

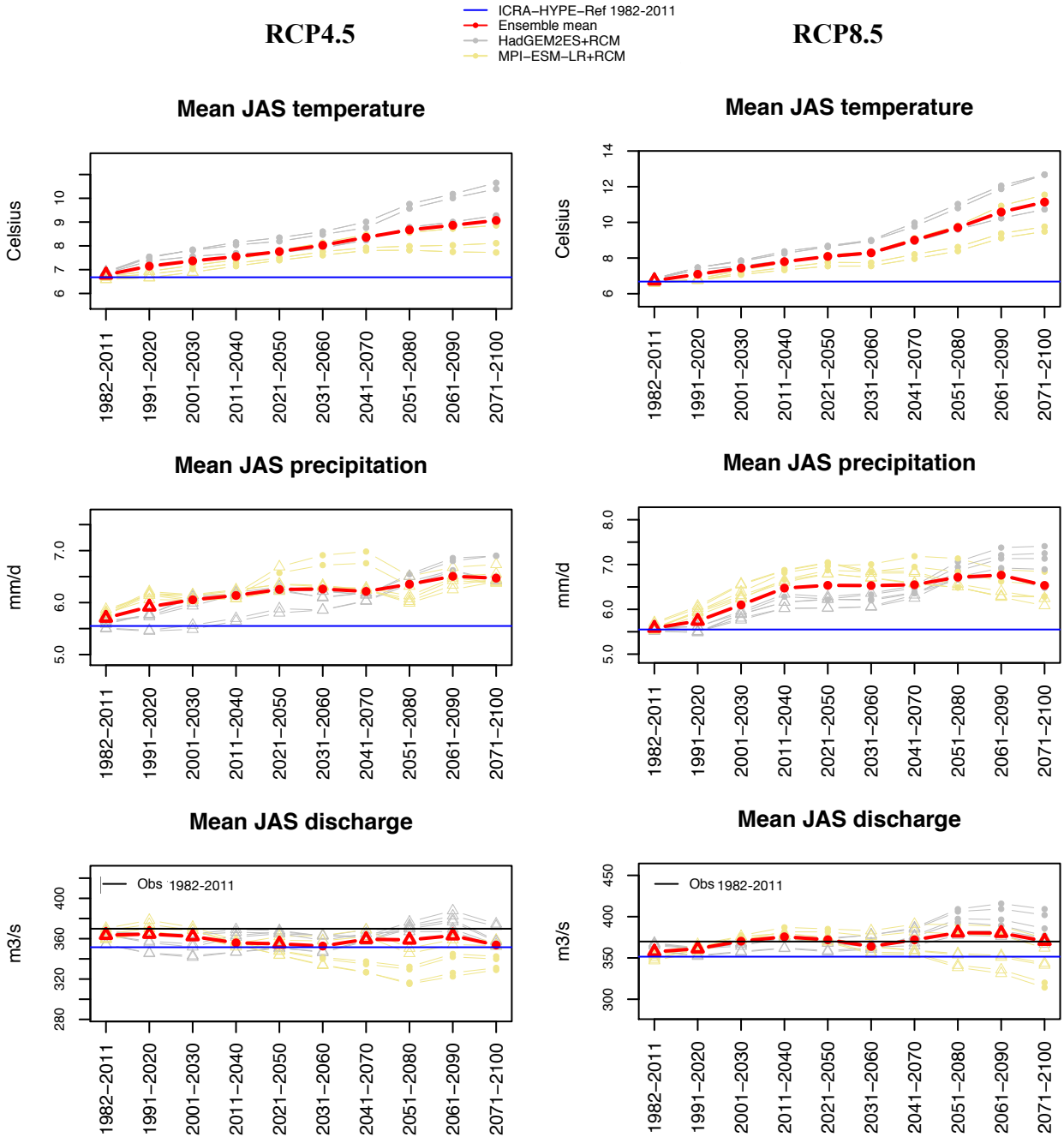

Fig. VII-15: Projected 30-year mean seasonal (JAS) temperature, precipitation and streamflow discharge for catchment vhm64 under RCP4.5 emission scenarios (left panel) and RCP8.5 emission scenarios (right panel). Time-windows where a statistically significant shift relative to the 1982-2011 reference period was detected by the Mann-Whitney test are marked with a solid circle and those where no shift was detected are marked with a triangle. Ensemble median of all scenarios (red).

Appendix 8

Projected number of AMF occurrences in each season within 30-year time-windows along the 21st century

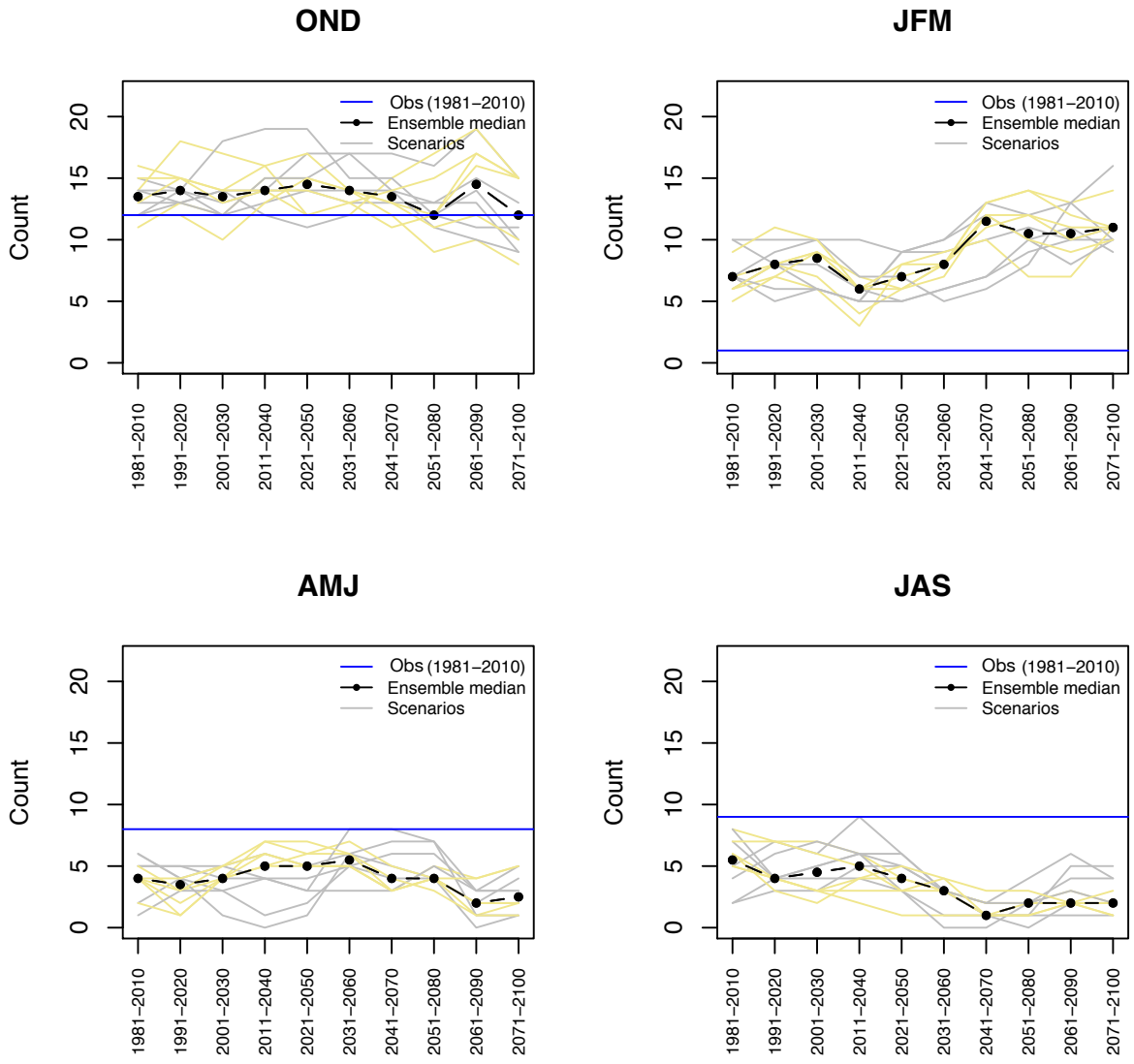

Fig. VIII-1: Catchment vhm148: Projected number of AMF occurrences in each season within 30-year time-windows under the RCP4.5 emission scenarios. Individual scenarios driven by HadGEM2ES GCM (grey lines) and by MPI-ESM-LR GCM (yellow lines). Ensemble median (black line and solid circles). Observed number of AMF in 1981-2010 (blue line).

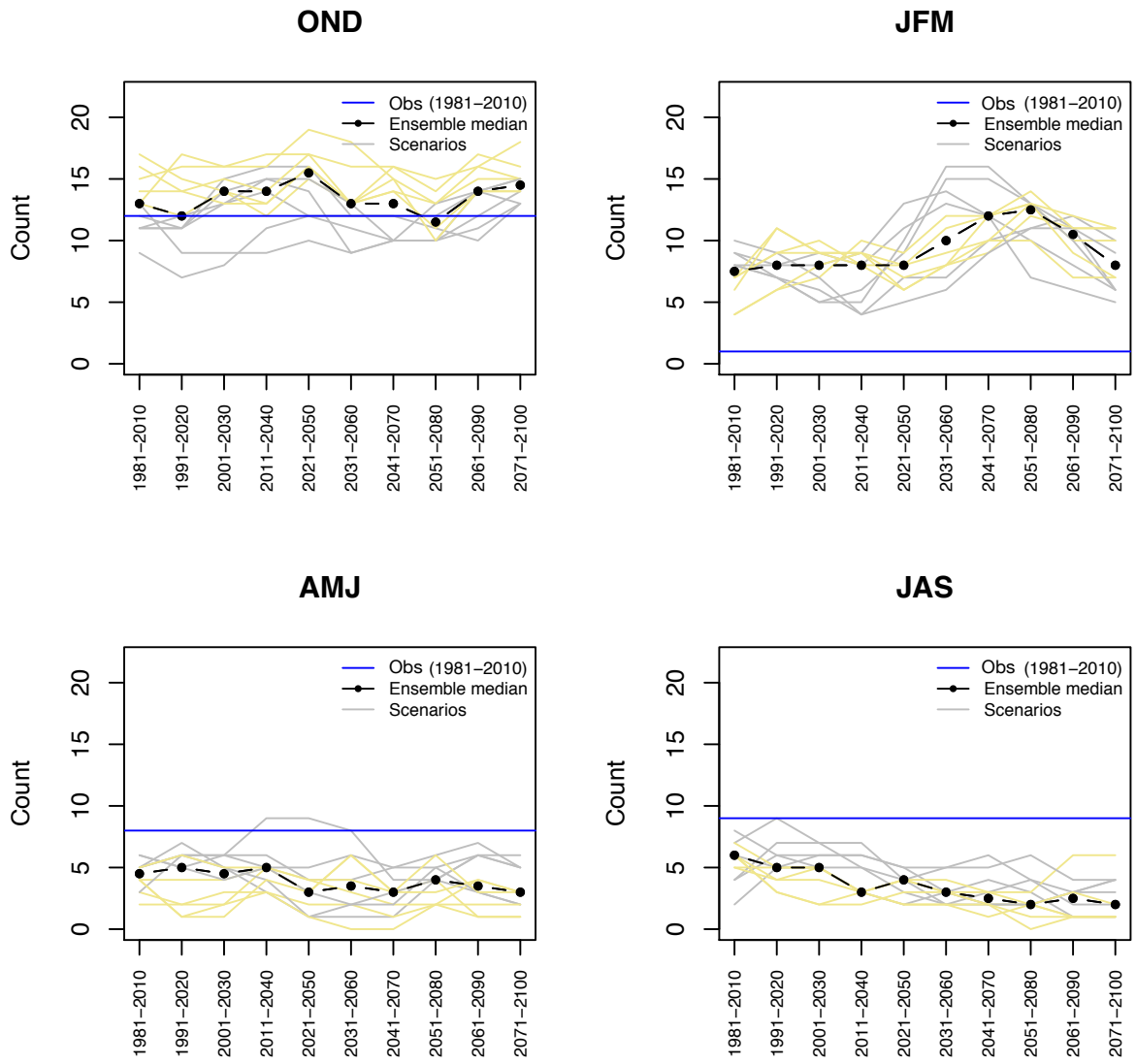

Fig. VIII-2: Catchment vhm148: Projected number of AMF occurrences in each season within 30-year time-windows under the RCP8.5 emission scenarios. Individual scenarios driven by HadGEM2ES GCM (grey lines) and by MPI-ESM-LR GCM (yellow lines). Ensemble median (black line and solid circles). Observed number of AMF in 1981-2010 (blue line).

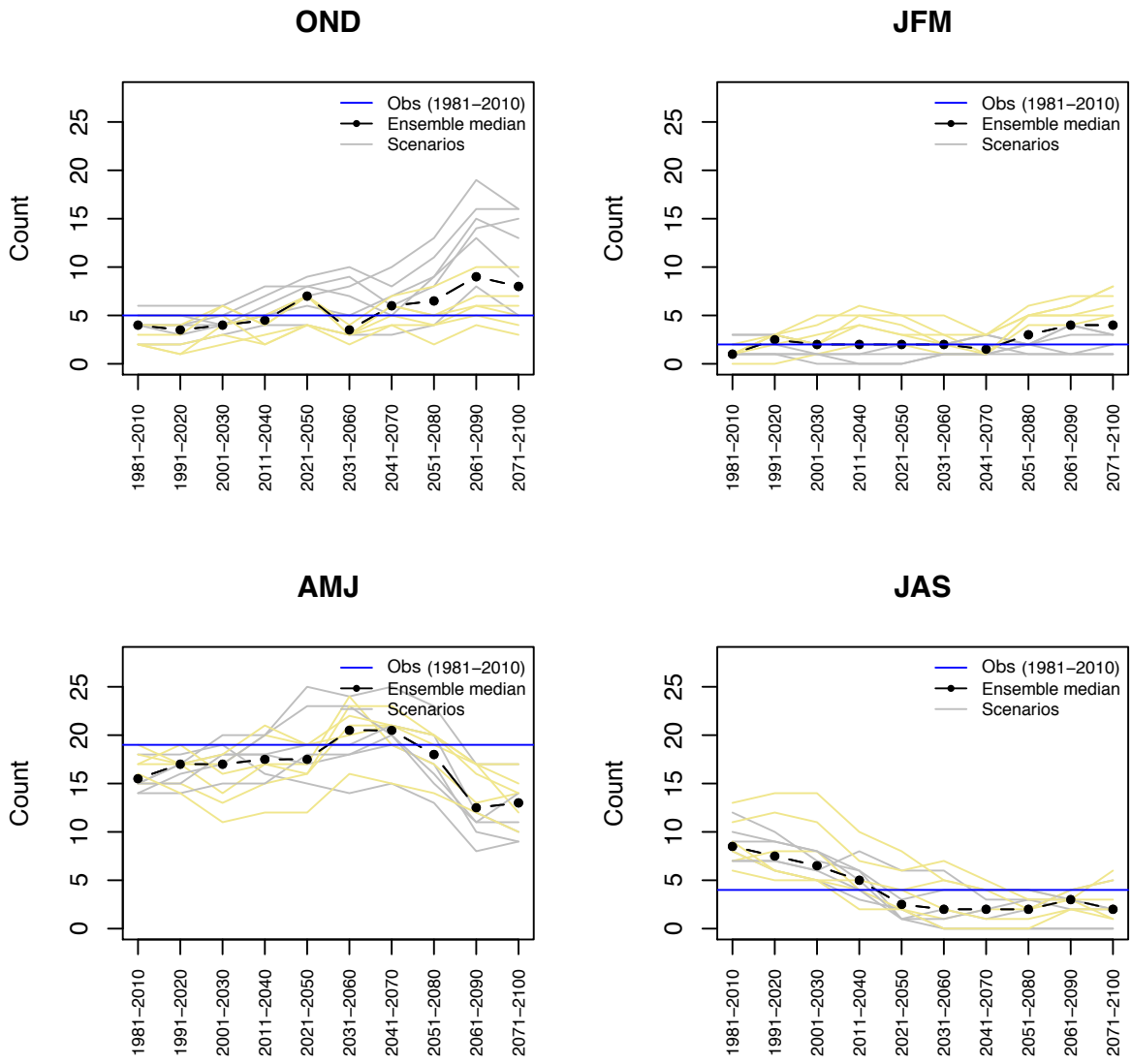

Fig. VIII-3: Catchment vhm51: Projected number of AMF occurrences in each season within 30-year time-windows under the RCP4.5 emission scenarios. Individual scenarios driven by HadGEM2ES GCM (grey lines) and by MPI-ESM-LR GCM (yellow lines). Ensemble median (black line and solid circles). Observed number of AMF in 1981-2010 (blue line).

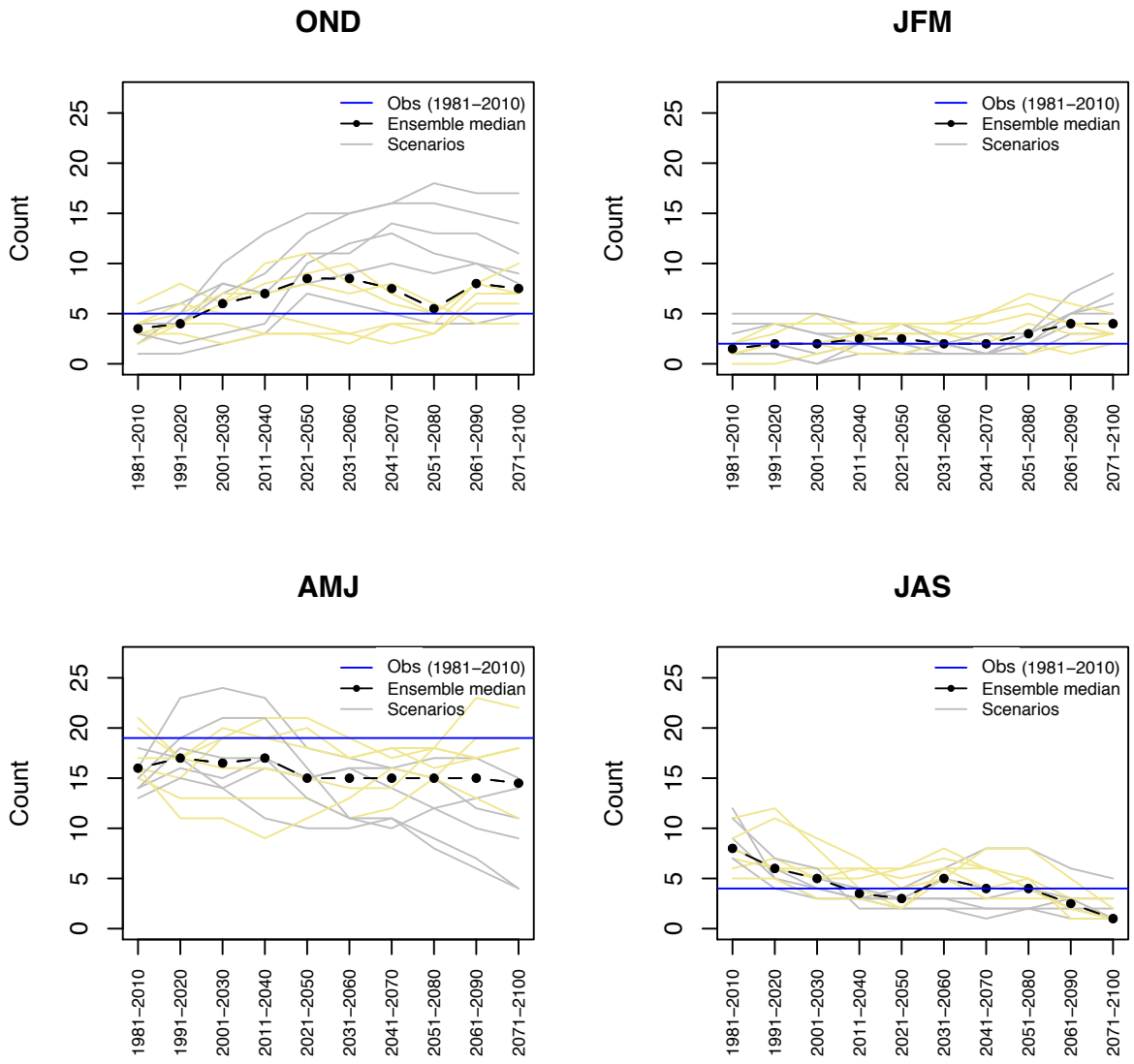

Fig. VIII-4: Catchment vhm51: Projected number of AMF occurrences in each season within 30-year time-windows under the RCP8.5 emission scenarios. Individual scenarios driven by HadGEM2ES GCM (grey lines) and by MPI-ESM-LR GCM (yellow lines). Ensemble median (black line and solid circles). Observed number of AMF in 1981-2010 (blue line).

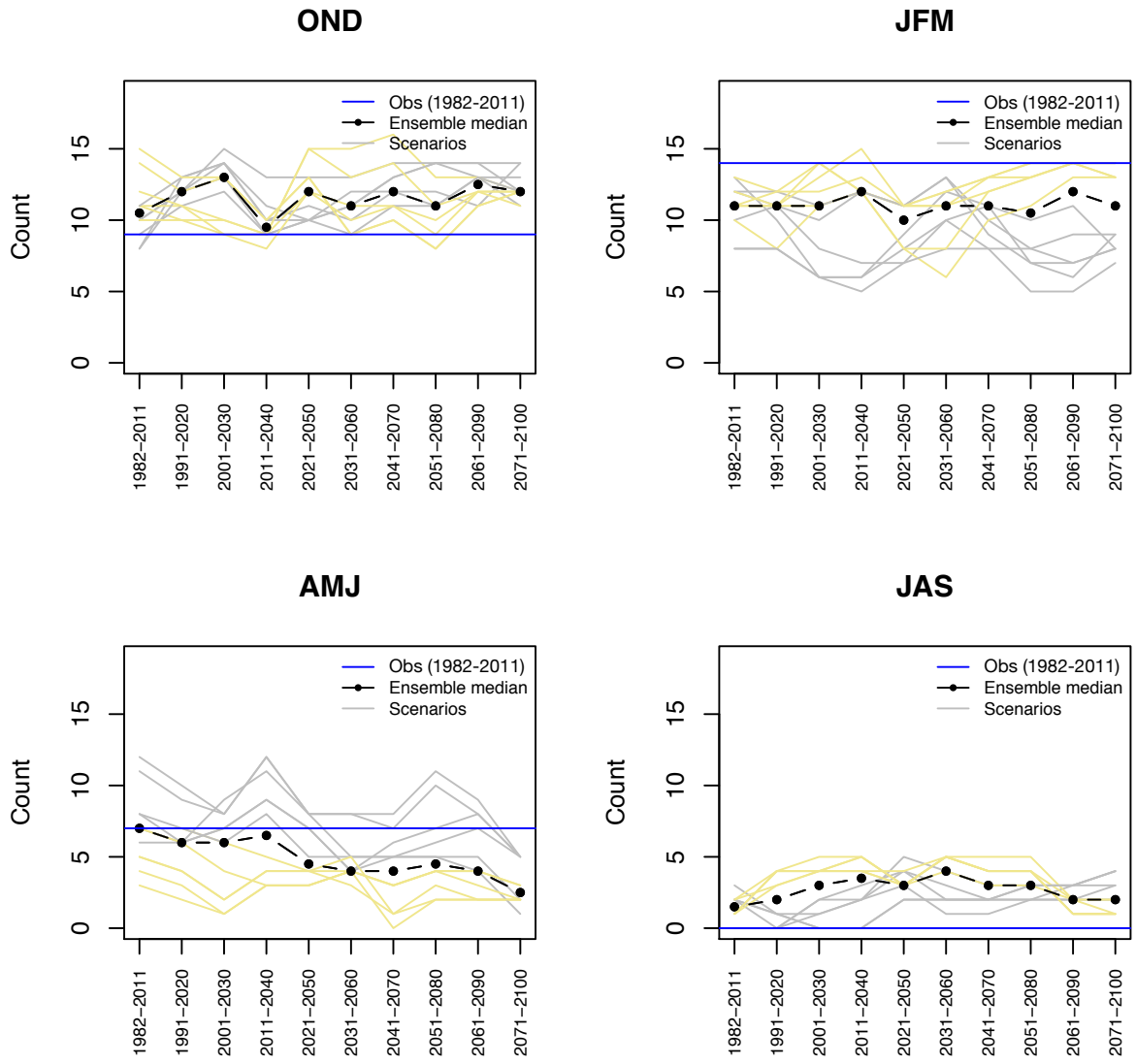

Fig. VIII-5: Catchment vhm64: Projected number of AMF occurrences in each season within 30-year time-windows under the RCP4.5 emission scenarios. Individual scenarios driven by HadGEM2ES GCM (grey lines) and by MPI-ESM-LR GCM (yellow lines). Ensemble median (black line and solid circles). Observed number of AMF in 1982-2011 (blue line).

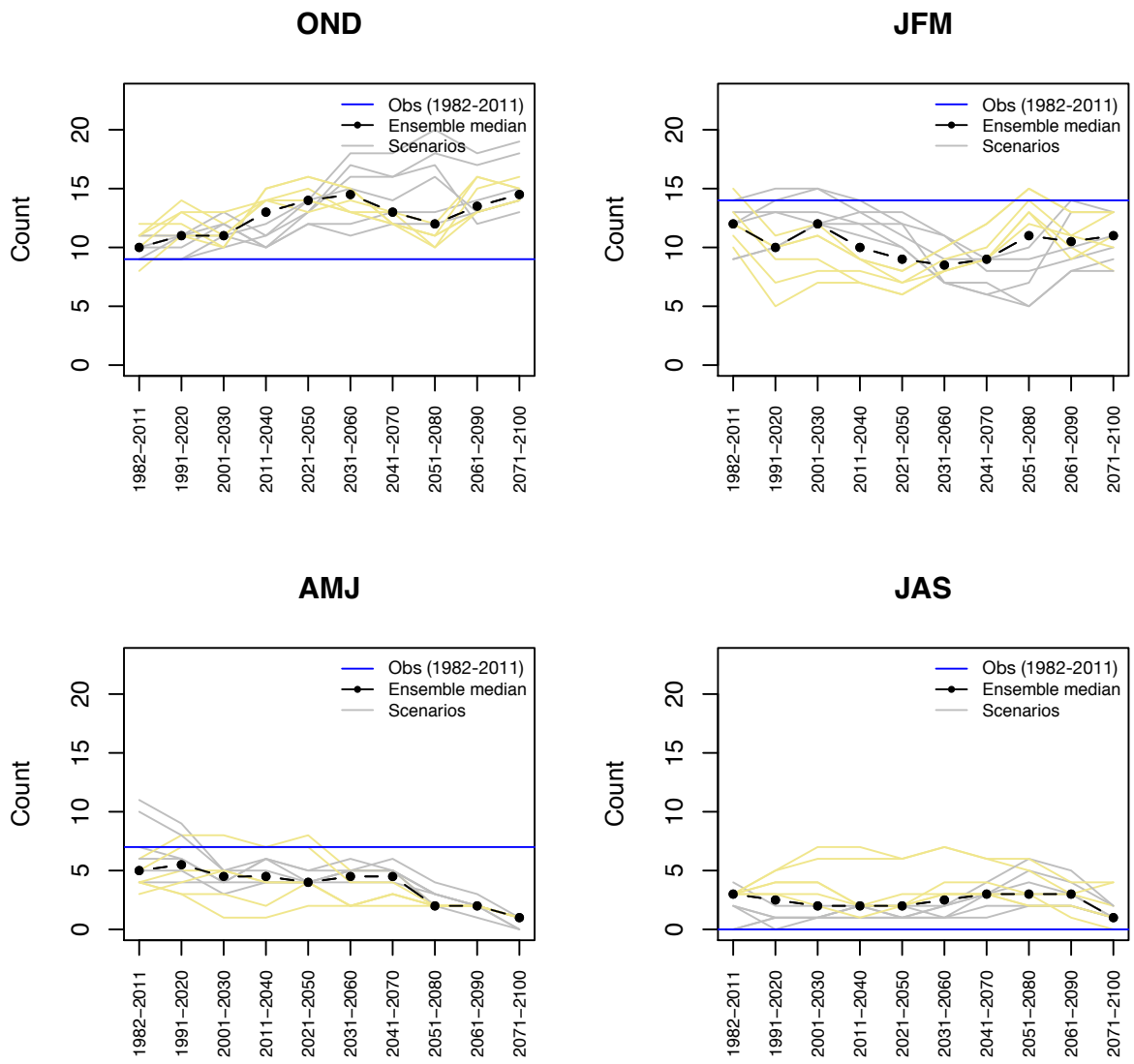

Fig. VIII-6: Catchment vhm64: Projected number of AMF occurrences in each season within 30-year time-windows under the RCP8.5 emission scenarios. Individual scenarios driven by HadGEM2ES GCM (grey lines) and by MPI-ESM-LR GCM (yellow lines). Ensemble median (black line and solid circles). Observed number of AMF in 1982-2011 (blue line).

Appendix 9

Projected AMF empirical cumulative distribution functions (CDFs), F(q)=Prob(Q≤q), for selected 30-year time-windows along the 21st century.

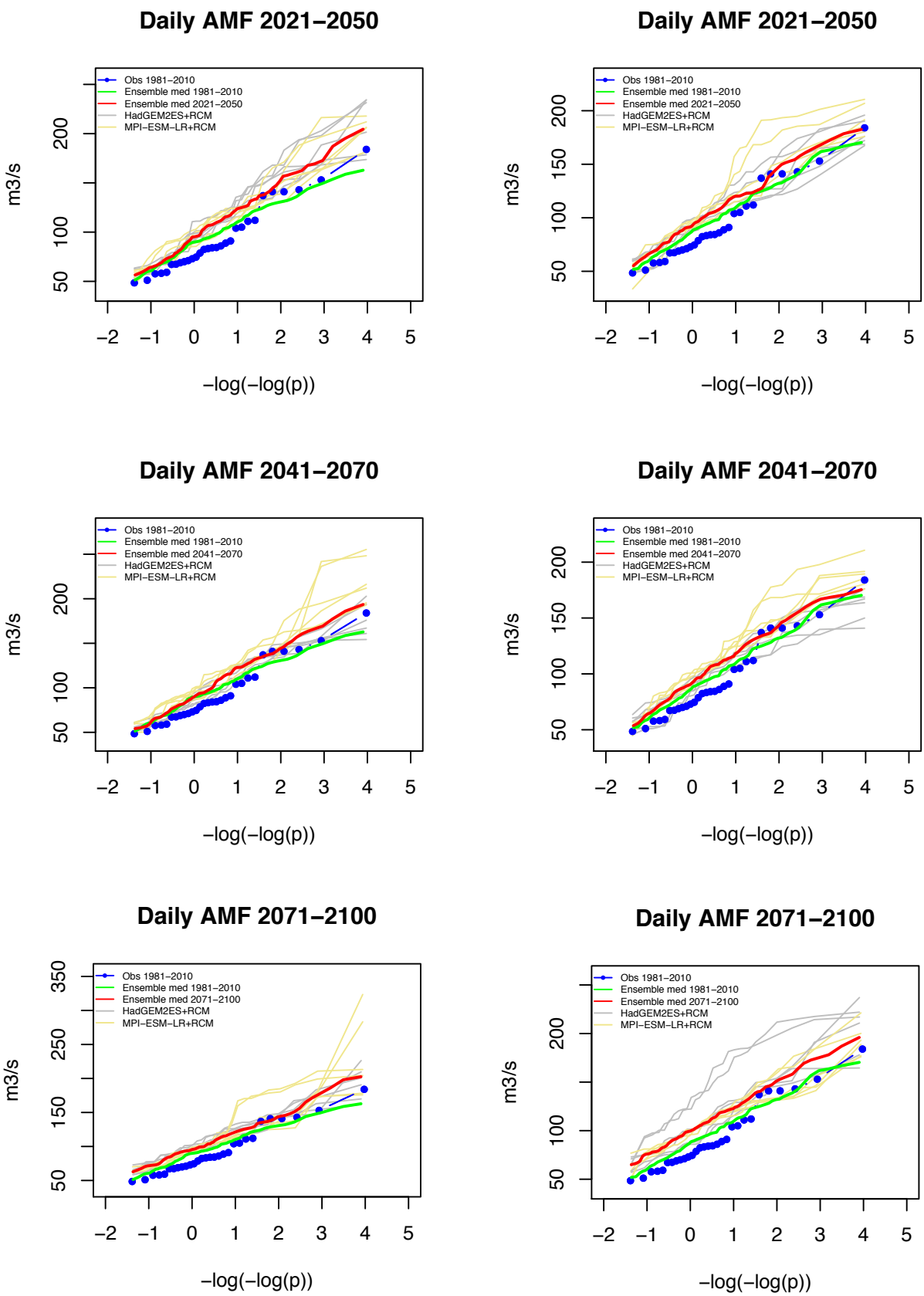

Fig. IX-1: Catchment vhm148: Projected AMF empirical CDFs, where Prob(Q≤q)=p, under RCP4.5 emission scenarios (left panel) and under RCP8.5 emission scenarios (right panel). Individual scenario CDFs (grey and yellow). Ensemble median CDF (red) and 1981-2010 ensemble median CDF (green). Observed 1981-2010 CDF (blue).

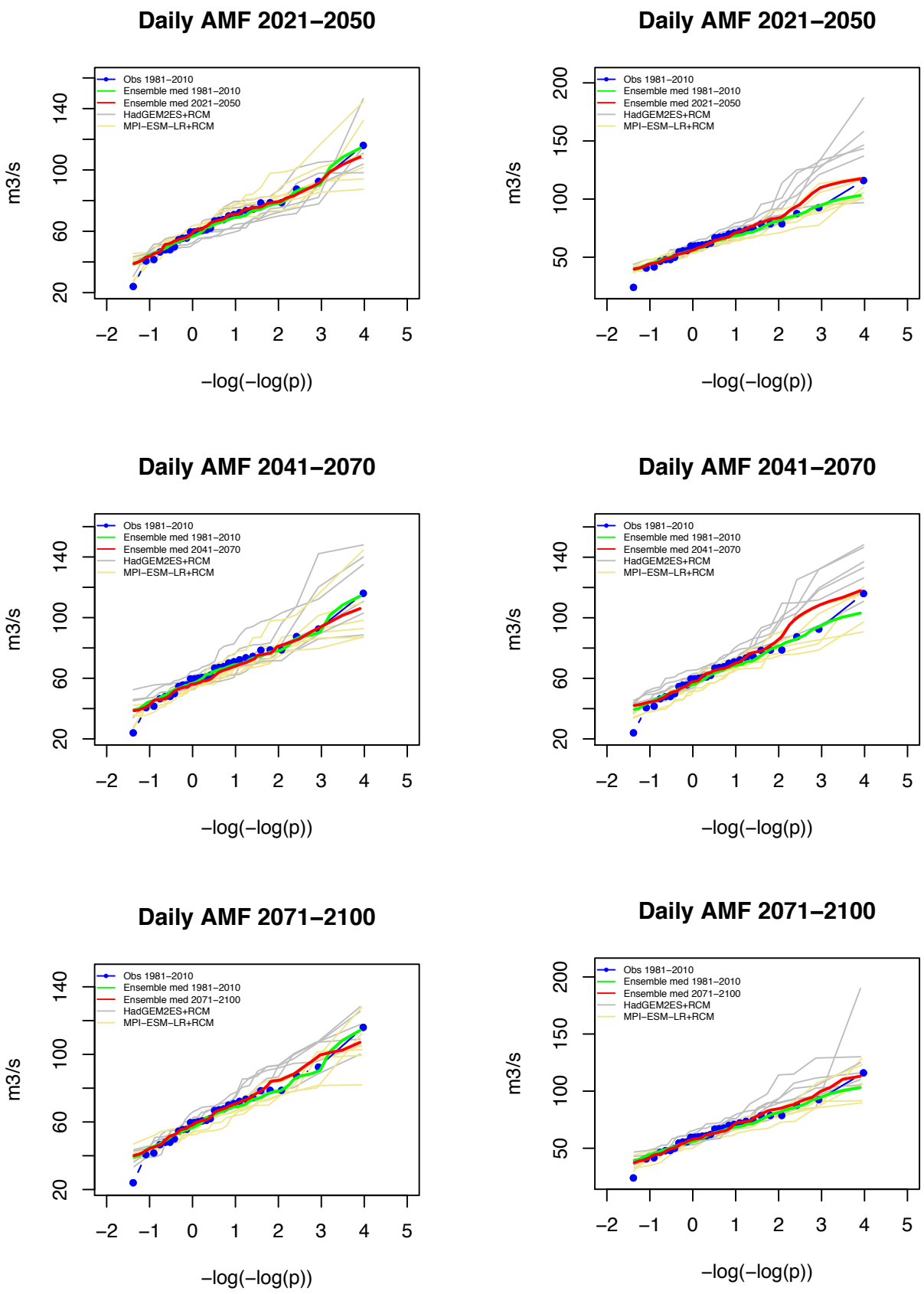

Fig. IX-2: Catchment vhm51: Projected AMF empirical CDFs, where Prob(Q≤q)=p, under RCP4.5 emission scenarios (left panel) and under RCP8.5 emission scenarios (right panel). Individual scenario CDFs (grey and yellow). Ensemble median CDF (red) and 1981-2010 ensemble median CDF (green). Observed 1981-2010 CDF (blue).

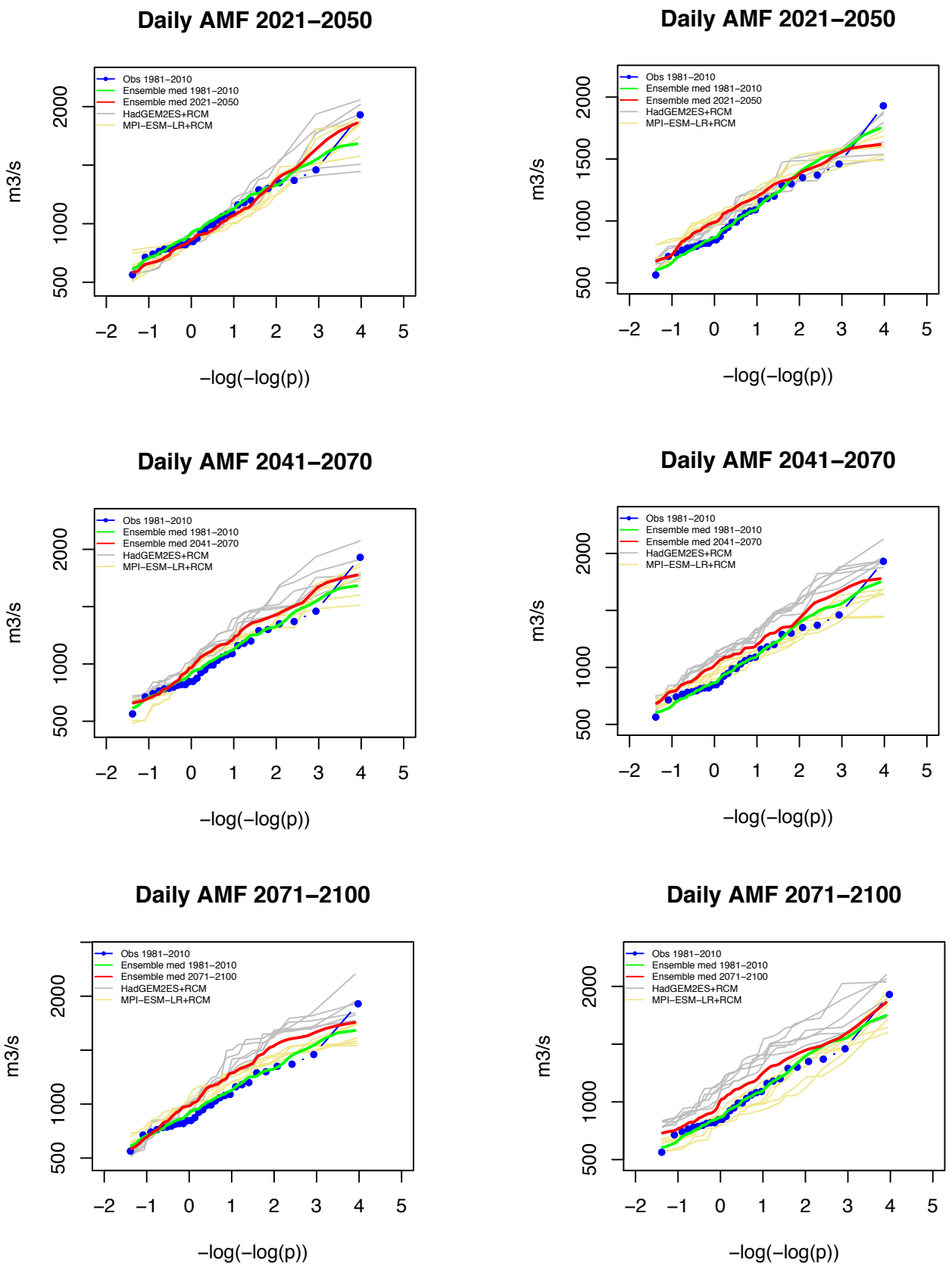

Fig. IX-3: Catchment vhm64: Projected AMF empirical CDFs, where Prob(Q≤q)=p, under RCP4.5 emission scenarios (left panel) and under RCP8.5 emission scenarios (right panel). Individual scenario CDFs (grey and yellow). Ensemble median CDF (red) and 1982-2011 ensemble median CDF (green). Observed 1982-2011 CDF (blue).

Appendix 10

Projected changes in the magnitude of T-year floods along 30-year moving time-windows in the 21st century, under the RCP4.5 emission scenarios.

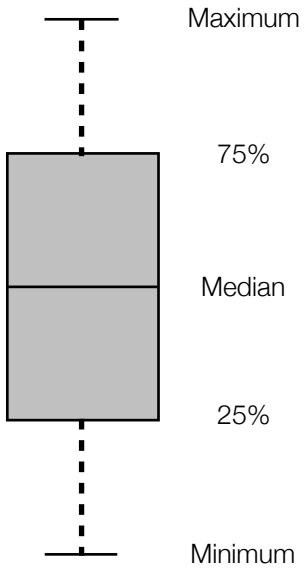

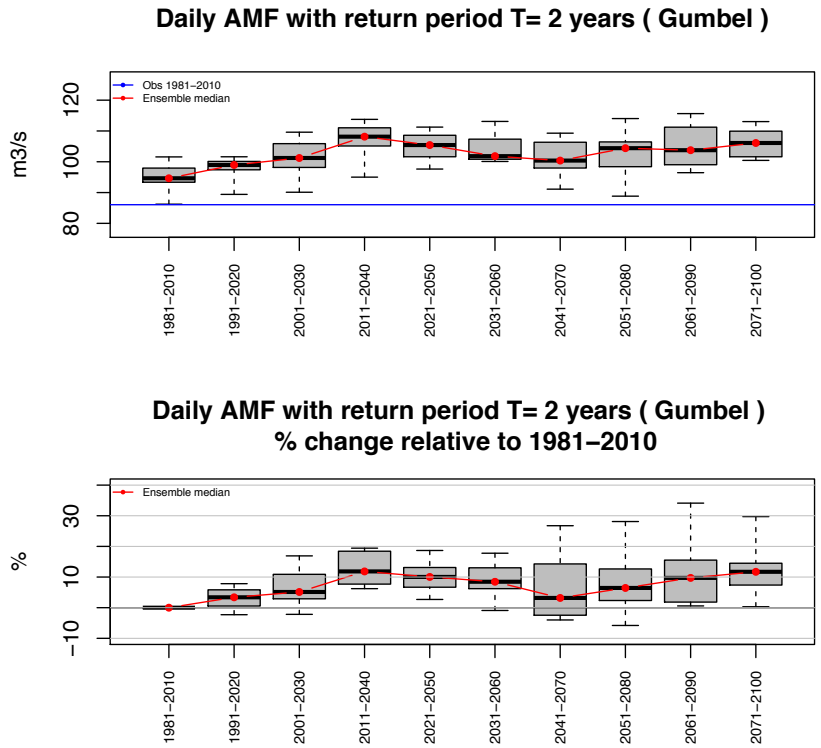

Fig. X-1: Catchment vhm148. Top: Box-plot of the projected 2-year flood under the RCP4.5 emission scenarios. Median 2-year flood (red). Observed 2-year flood in 1981-2010 (blue). Bottom: Box-plot of the percent change in 2-year flood relative to 1981-2010. Median change (red).

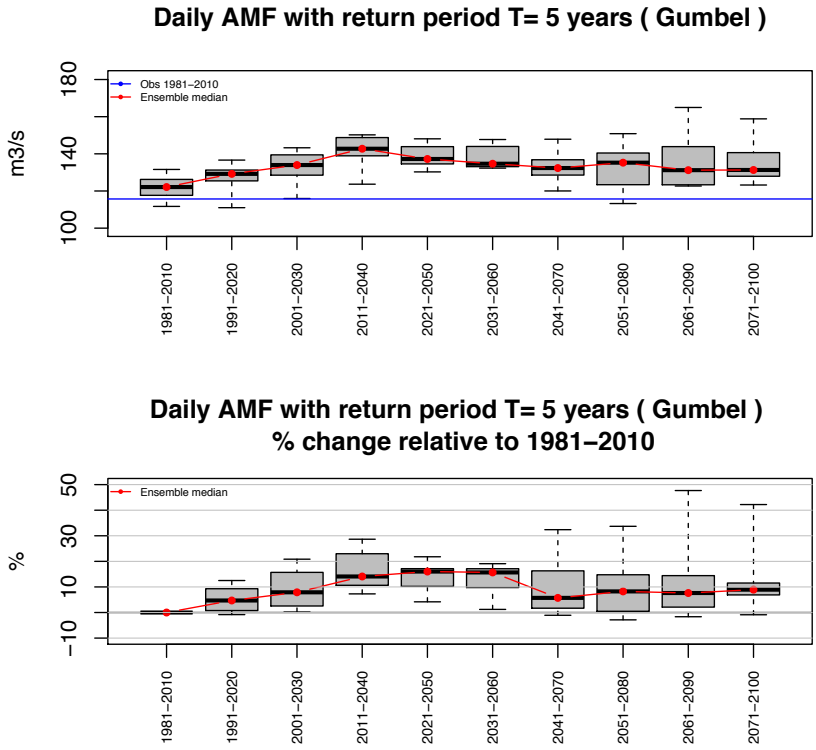

Fig. X-2: Catchment vhm148: projected changes in 5-year flood under the RCP4.5 emission scenarios (see caption Fig X-1).

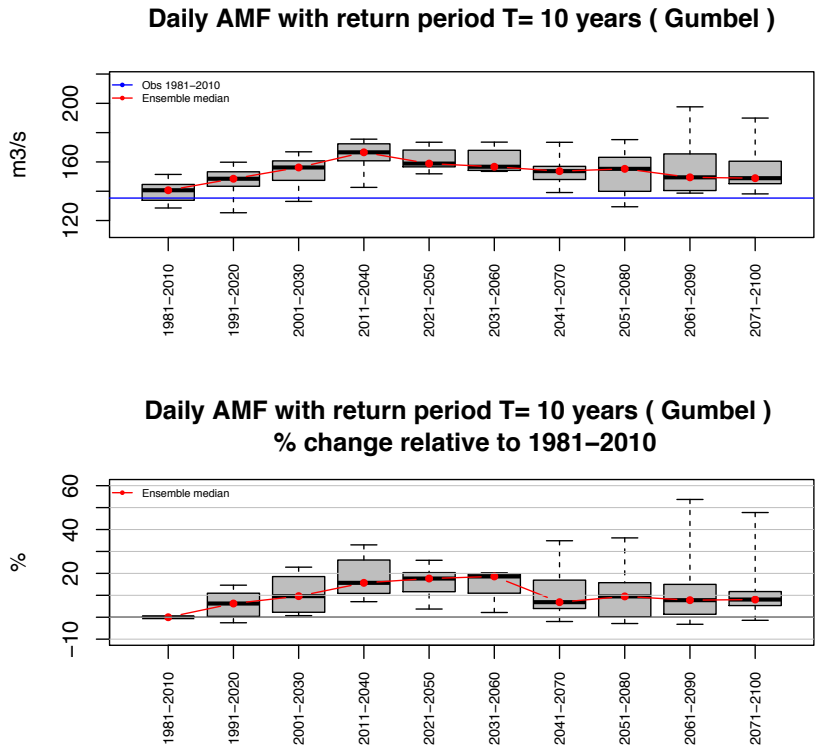

Fig. X-3: Catchment vhm148: projected changes in 10-year flood under the RCP4.5 emission scenarios (see caption Fig X-1).

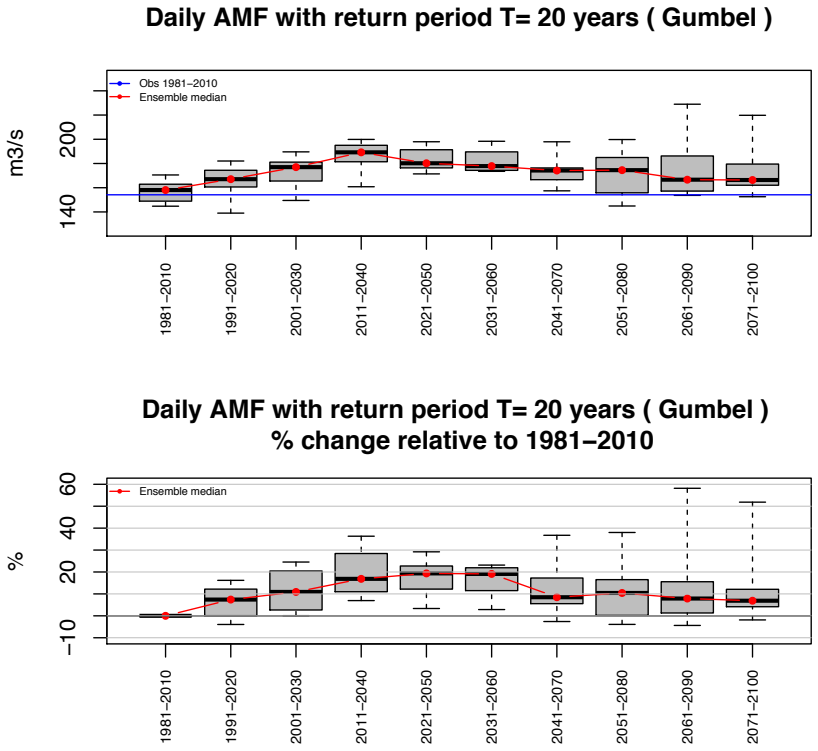

Fig. X-4: Catchment vhm148: projected changes in 20-year flood under the RCP4.5 emission scenarios (see caption Fig X-1).

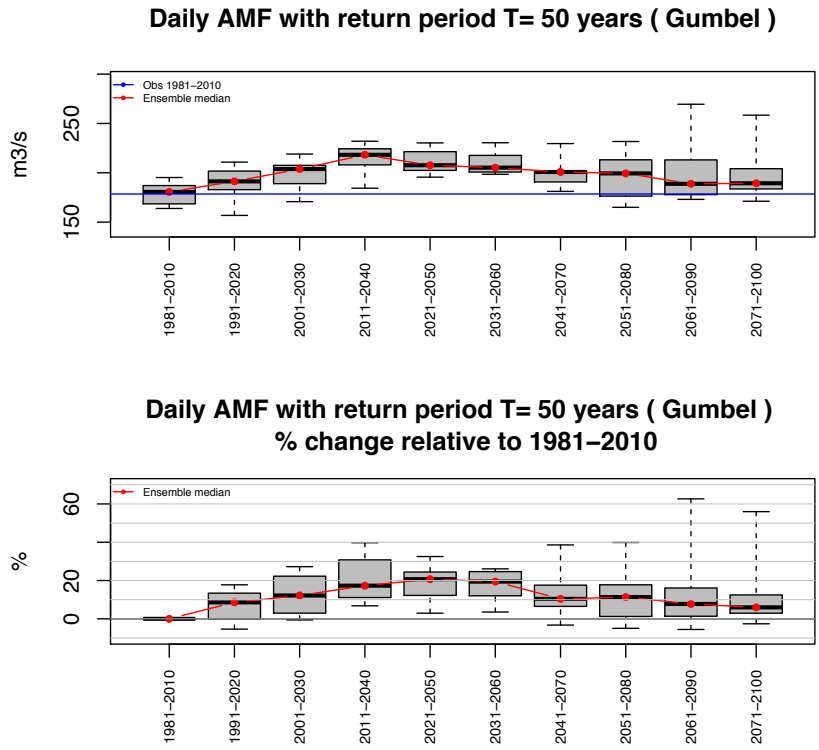

Fig. X-5: Catchment vhm148: projected changes in 50-year flood under the RCP4.5 emission scenarios (see caption Fig X-1).

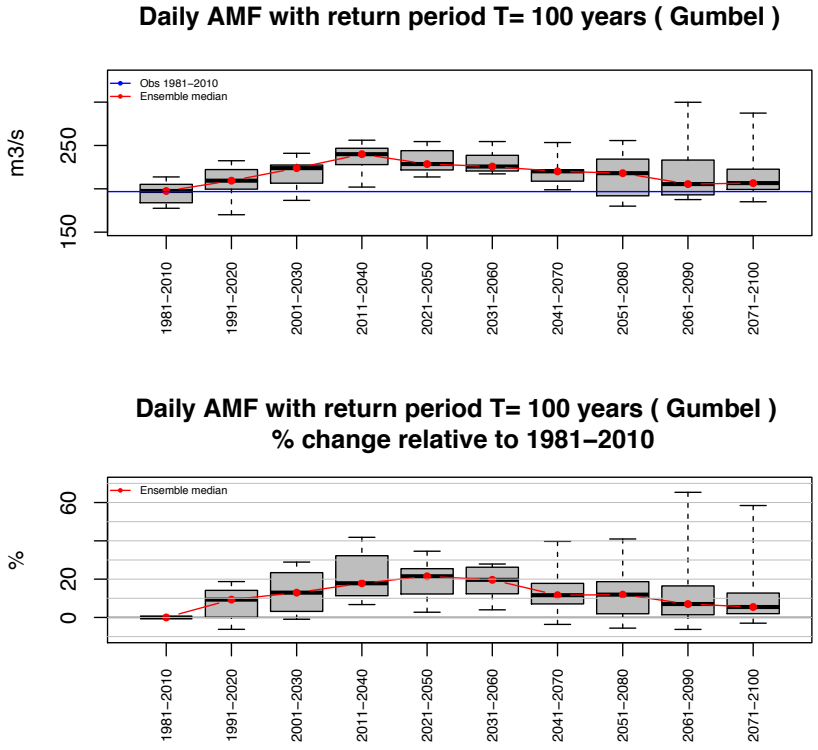

Fig. X-6: Catchment vhm148: projected changes in 100-year flood under the RCP4.5 emission scenarios (see caption Fig X-1).

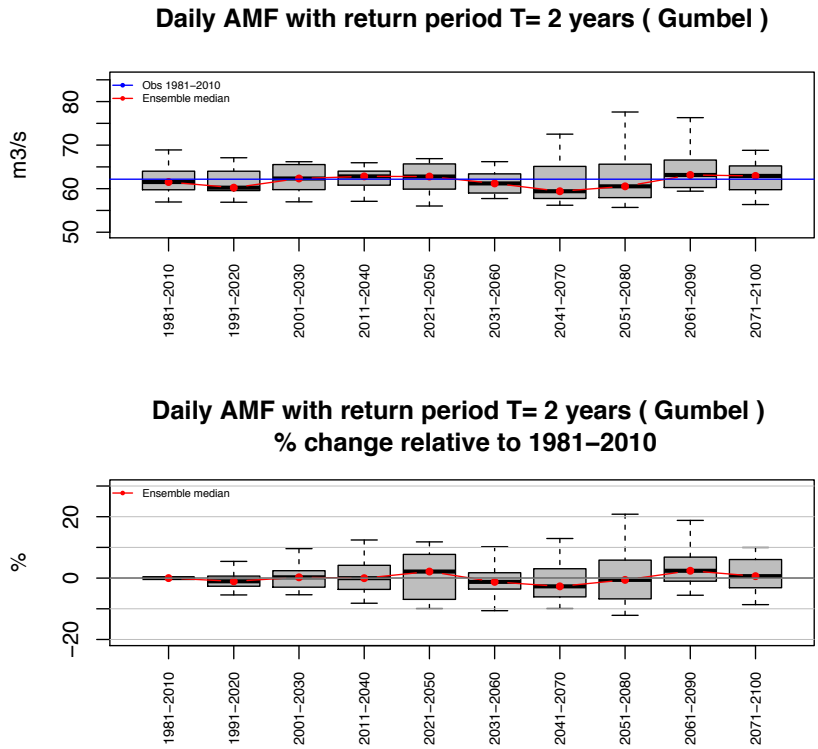

Fig. X-7: Catchment vhm51: projected changes in 2-year flood under the RCP4.5 emission scenarios (see caption Fig X-1).

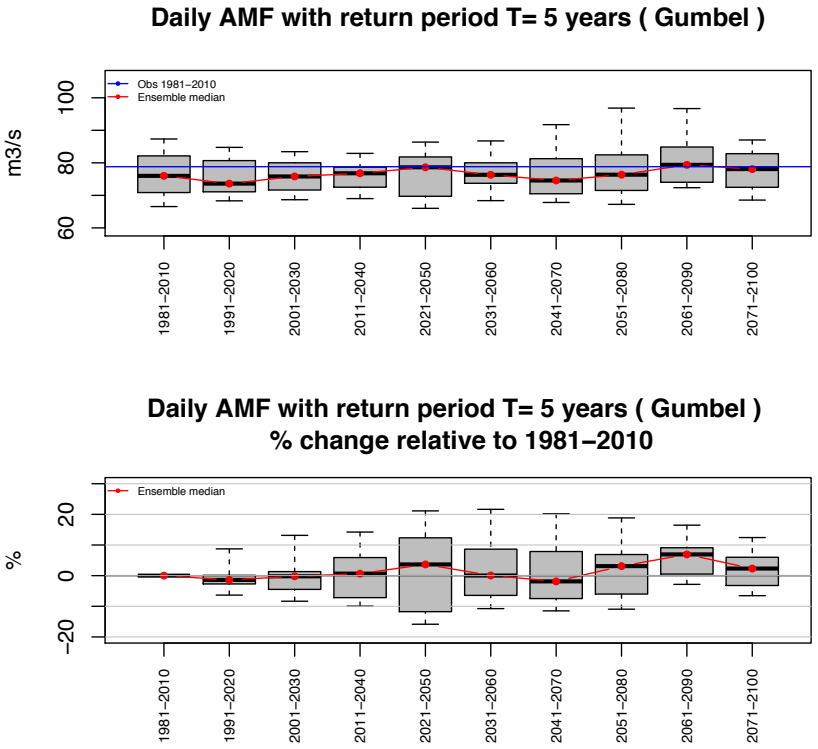

Fig. X-8: Catchment vhm51: projected changes in 5-year flood under the RCP4.5 emission scenarios (see caption Fig X-1).

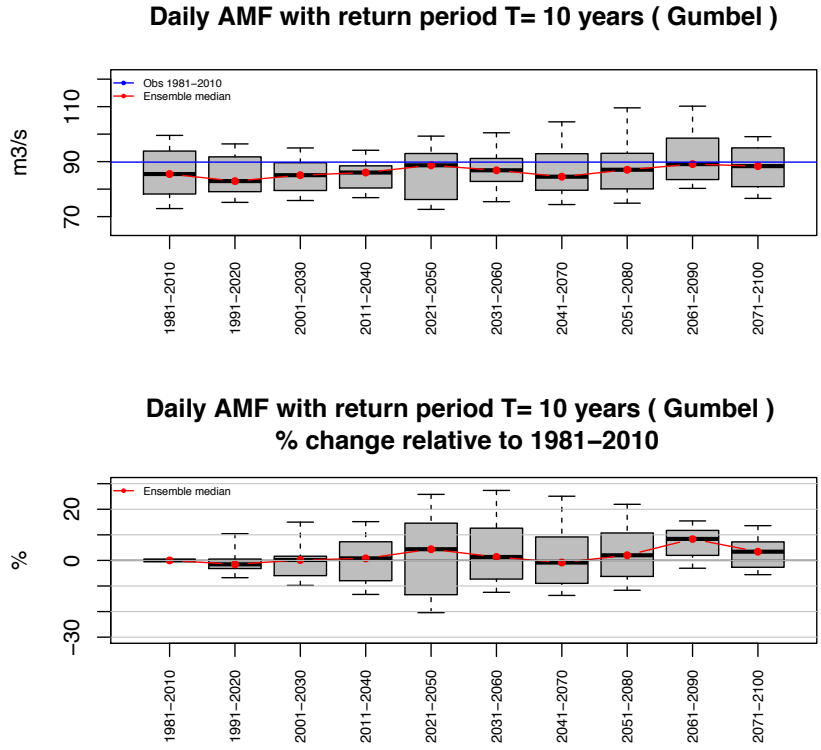

Fig. X-9: Catchment vhm51: projected changes in 10-year flood under the RCP4.5 emission scenarios (see caption Fig X-1).

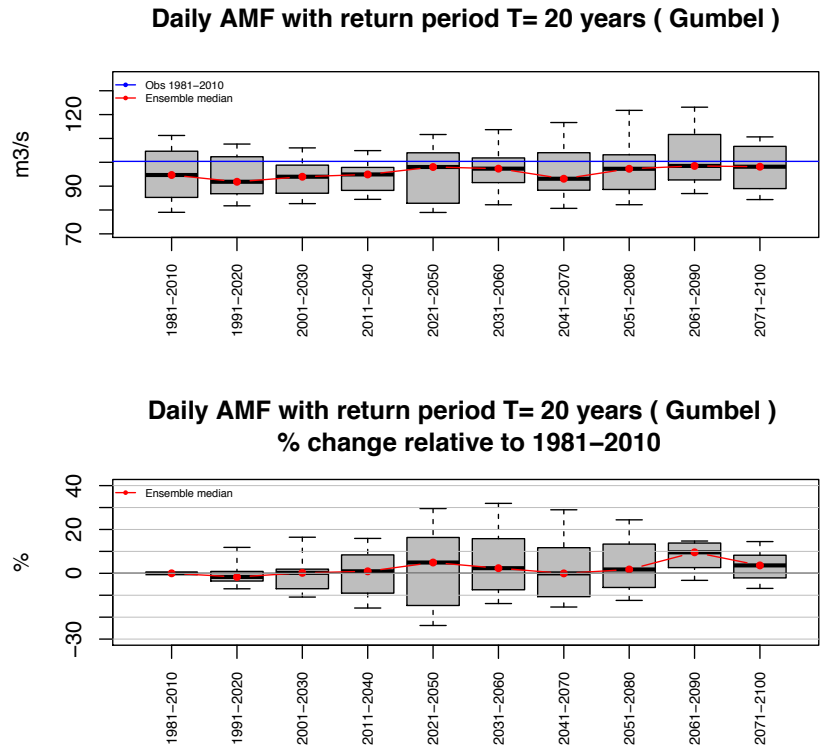

Fig. X-10: Catchment vhm51: projected changes in 20-year flood under the RCP4.5 emission scenarios (see caption Fig X-1).

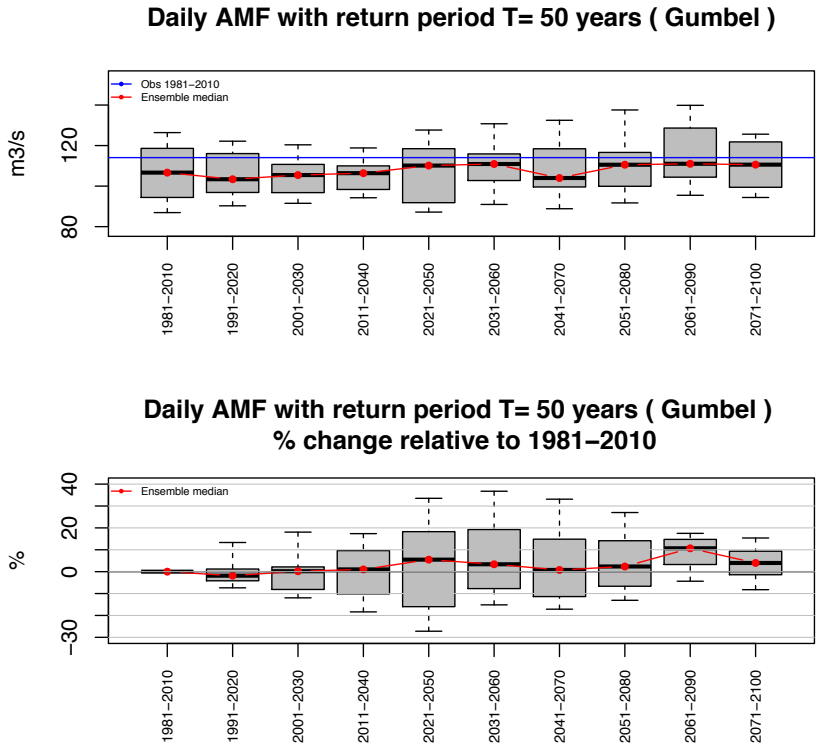

Fig. X-11: Catchment vhm51: projected changes in 50-year flood under the RCP4.5 emission scenarios (see caption Fig X-1).

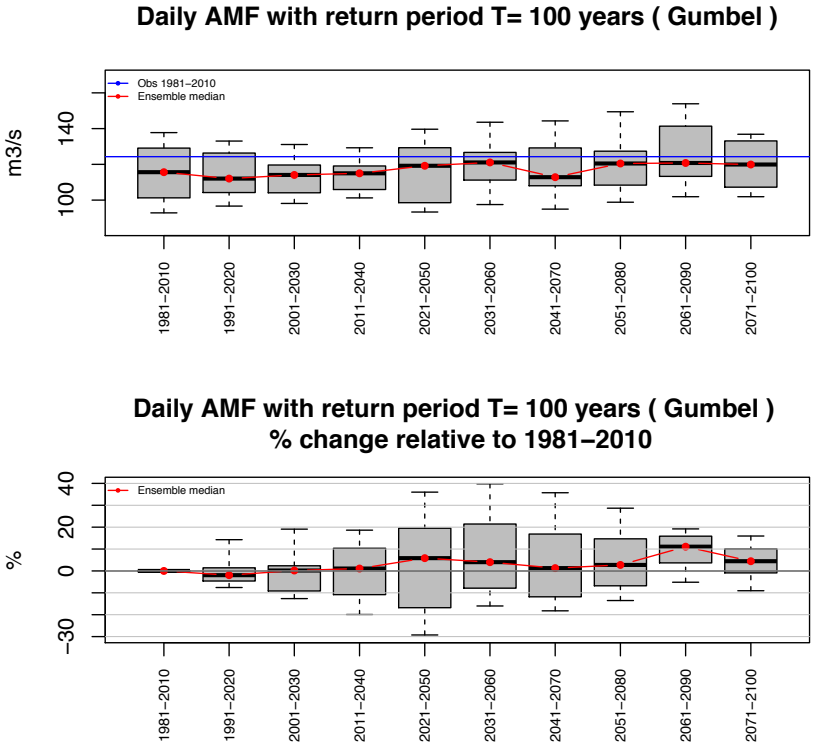

Fig. X-12: Catchment vhm51: projected changes in 100-year flood under the RCP4.5 emission scenarios (see caption Fig X-1).

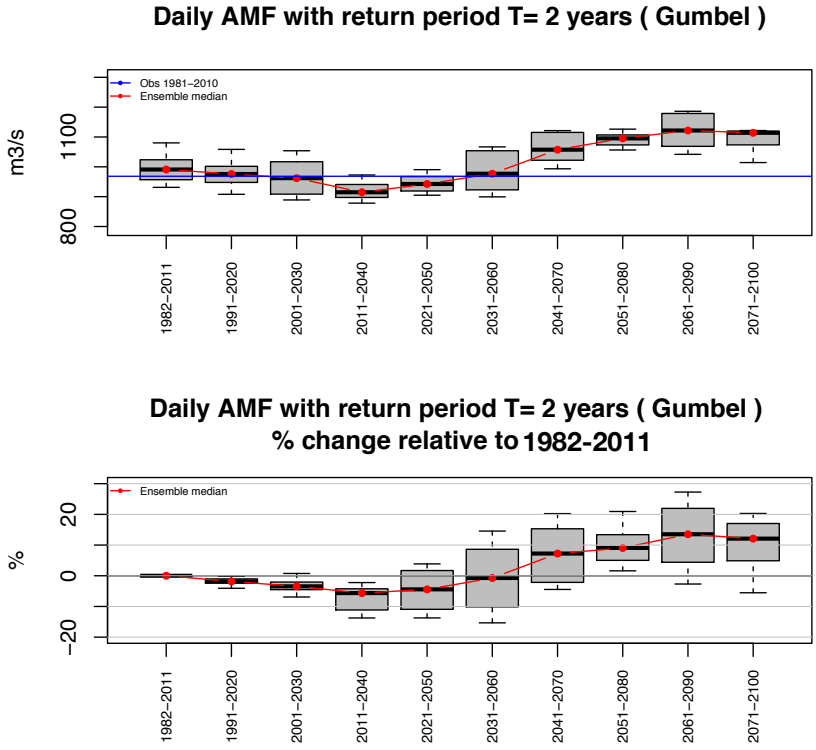

Fig. X-13: Catchment vhm64: projected changes in 2-year flood under the RCP4.5 emission scenarios (see caption Fig X-1). Observed 2-year flood in 1982-2011 (blue).

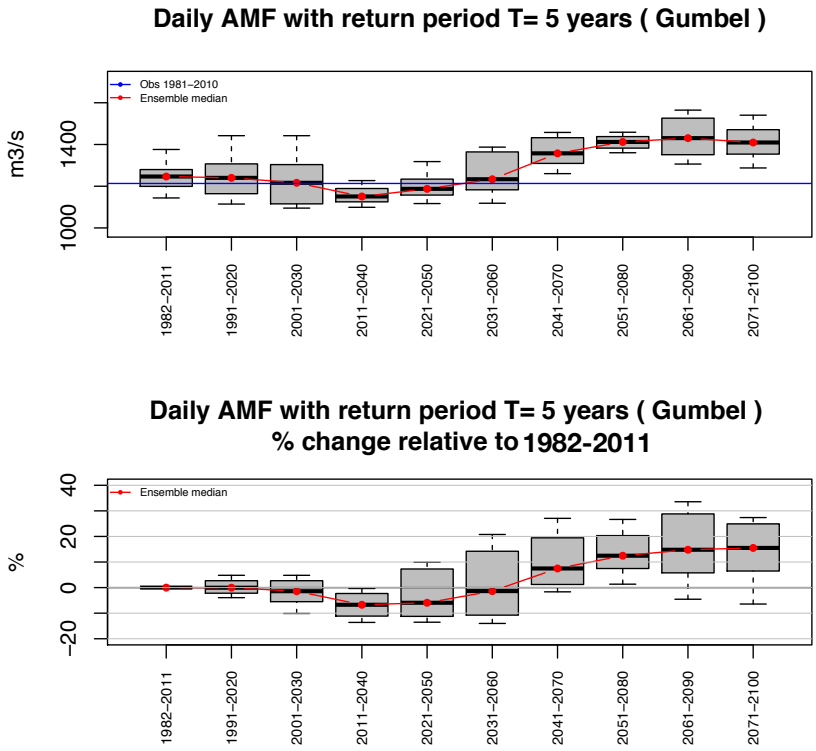

Fig. X-14: Catchment vhm64: projected changes in 5-year flood under the RCP4.5 emission scenarios (see caption Fig X-1). Observed 5-year flood in 1982-2011 (blue).

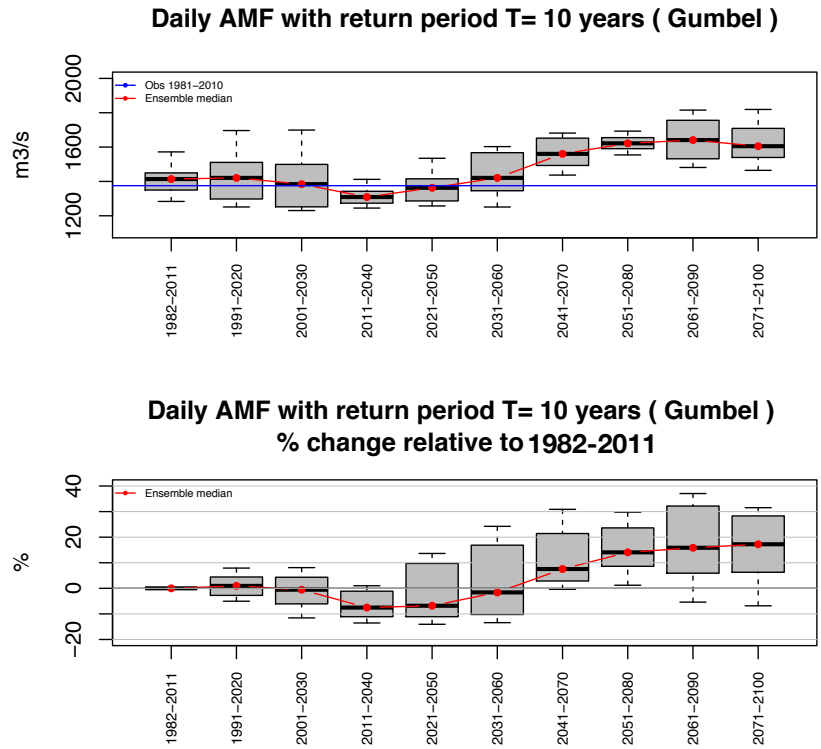

Fig. X-15: Catchment vhm64: projected changes in 10-year flood under the RCP4.5 emission scenarios (see caption Fig X-1). Observed 10-year flood in 1982-2011 (blue).

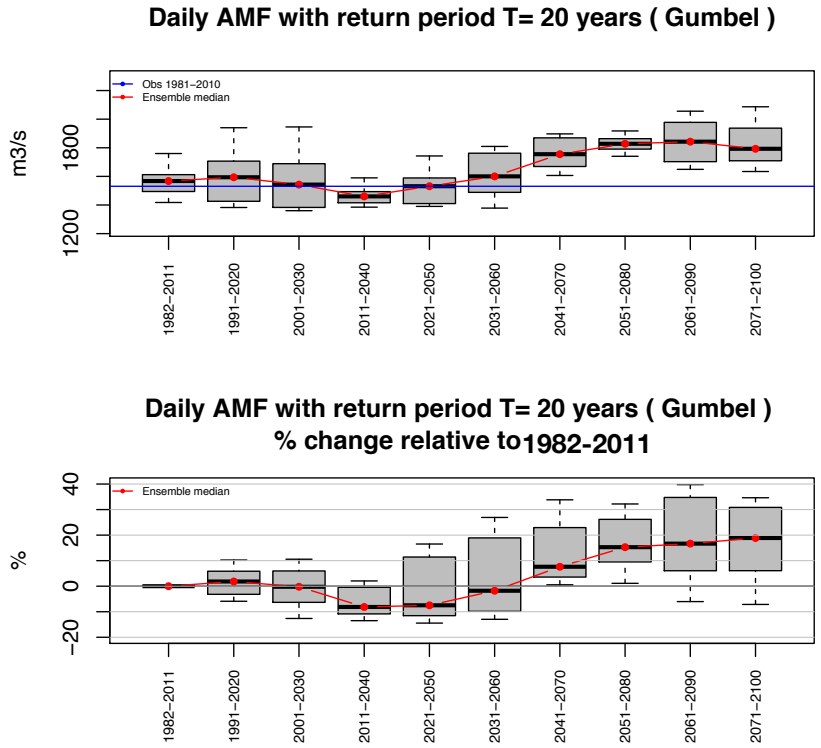

Fig. X-16: Catchment vhm64: projected changes in 20-year flood under the RCP4.5 emission scenarios (see caption Fig X-1). Observed 20-year flood in 1982-2011 (blue).

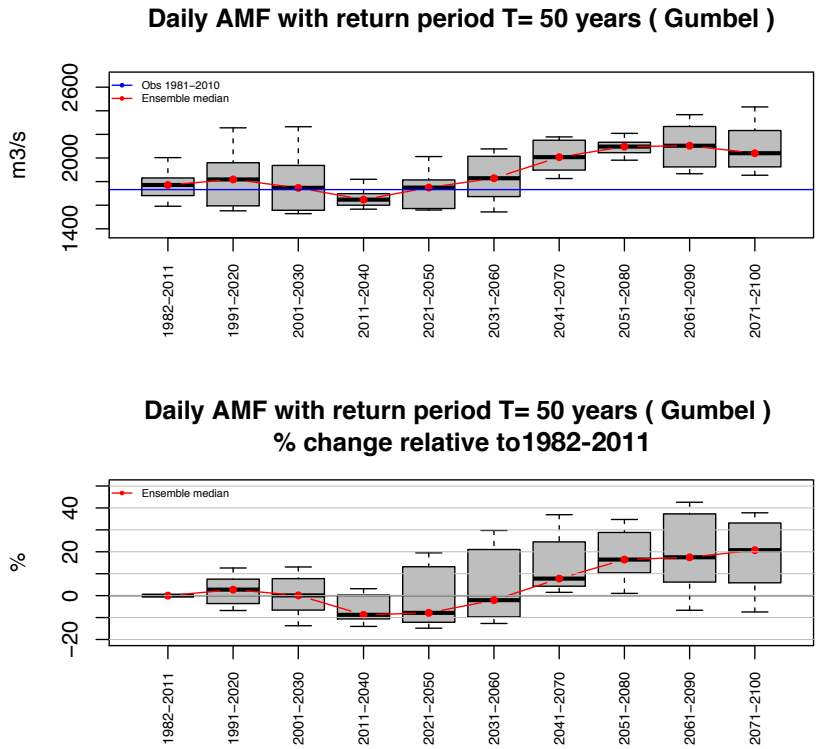

Fig. X-17: Catchment vhm64: projected changes in 50-year flood under the RCP4.5 emission scenarios (see caption Fig X-1). Observed 50-year flood in 1982-2011 (blue).

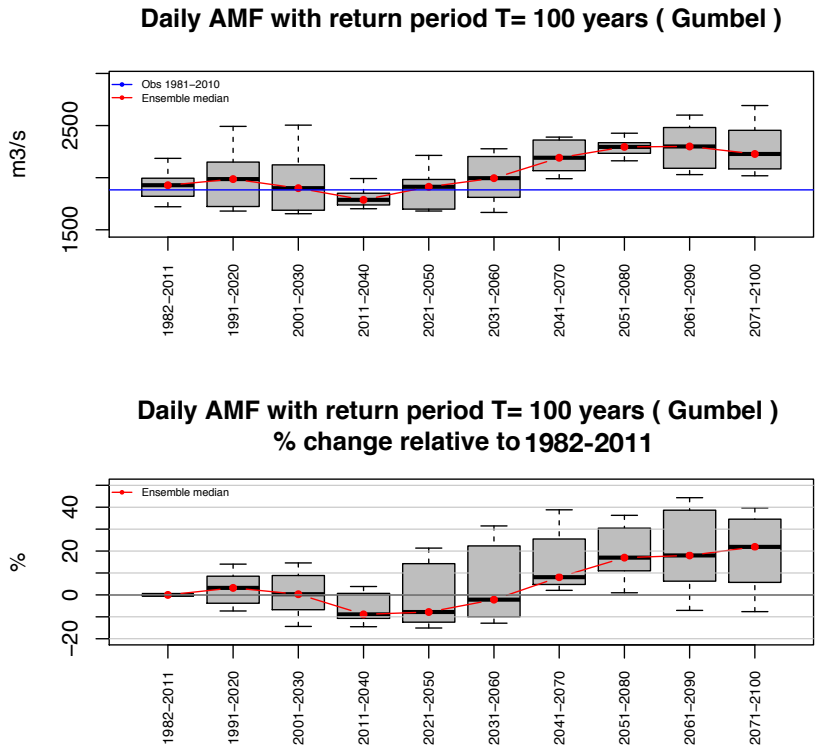

Fig. X-18: Catchment vhm64: projected changes in 100-year flood under the RCP4.5 emission scenarios (see caption Fig X-1). Observed 100-year flood in 1982-2011 (blue).

Appendix 11

Projected changes in the magnitude of T-year floods along 30-year moving time-windows in the 21st century, under the RCP8.5 emission scenarios.

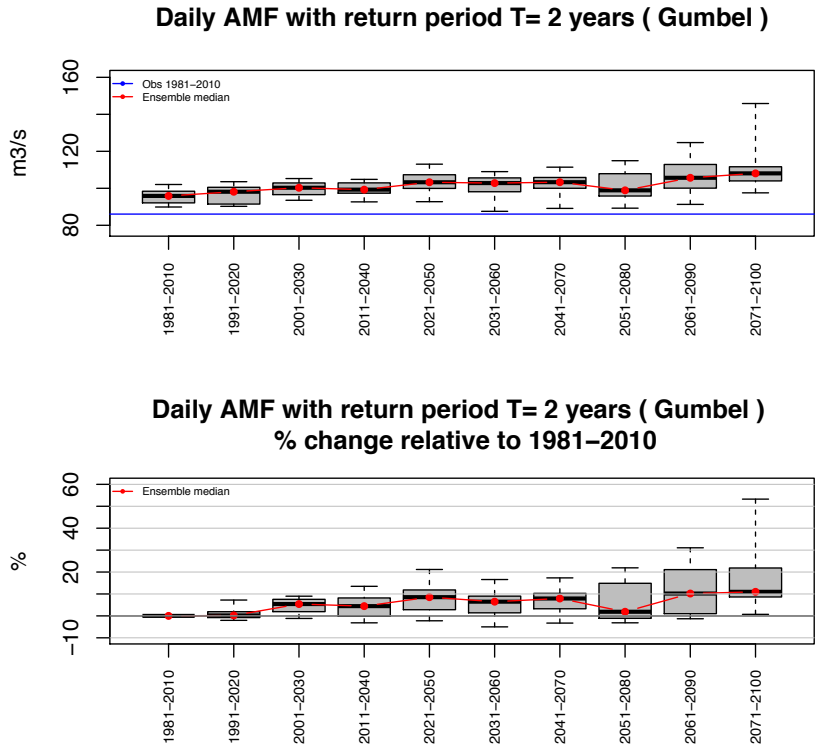

Fig. XI-1: Catchment vhm148. Top: Box-plot of the projected 2-year flood under the RCP8.5 emission scenarios. Median 2-year flood (red). Observed 2-year flood in 1981-2010 (blue). Bottom: Box-plot of the percent change in 2-year flood relative to 1981-2010. Median change (red).

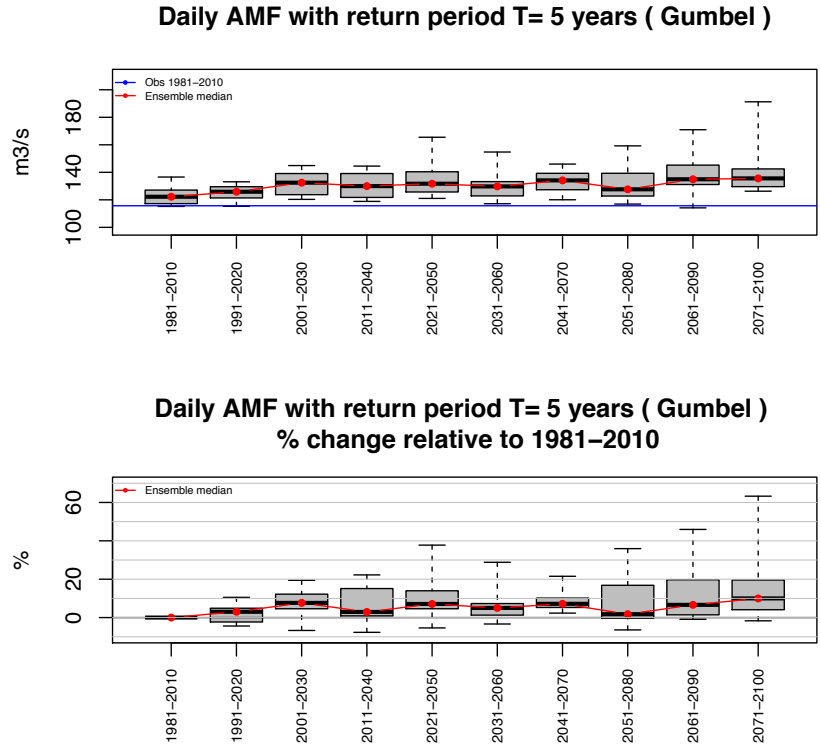

Fig. XI-2: Catchment vhm148: projected changes in 5-year flood under the RCP8.5 emission scenarios (see caption Fig XI-1).

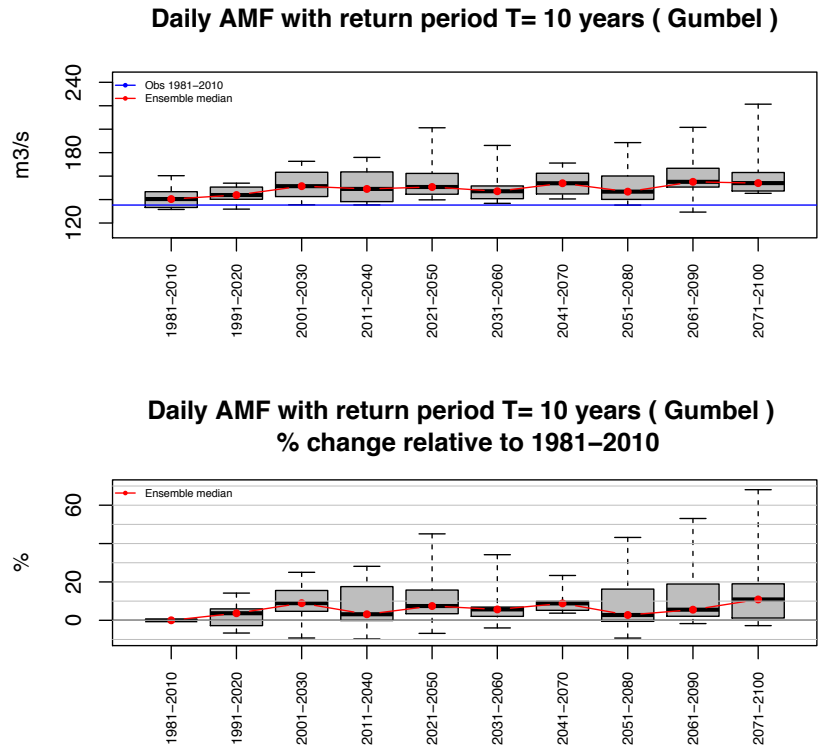

Fig. XI-3: Catchment vhm148: projected changes in 10-year flood under the RCP8.5 emission scenarios (see caption Fig XI-1).

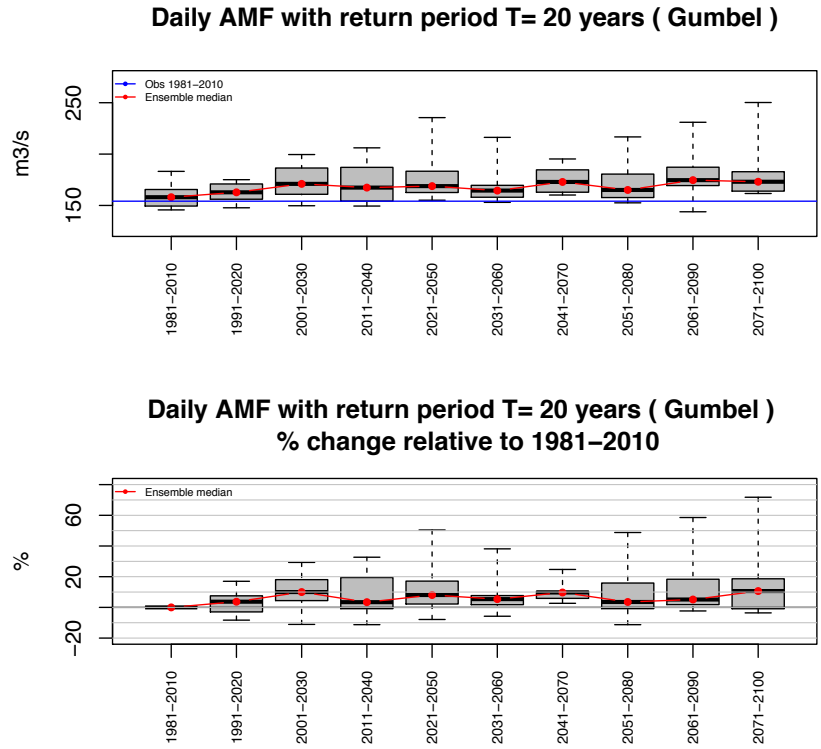

Fig. XI-4: Catchment vhm148: projected changes in 20-year flood under the RCP8.5 emission scenarios (see caption Fig XI-1).

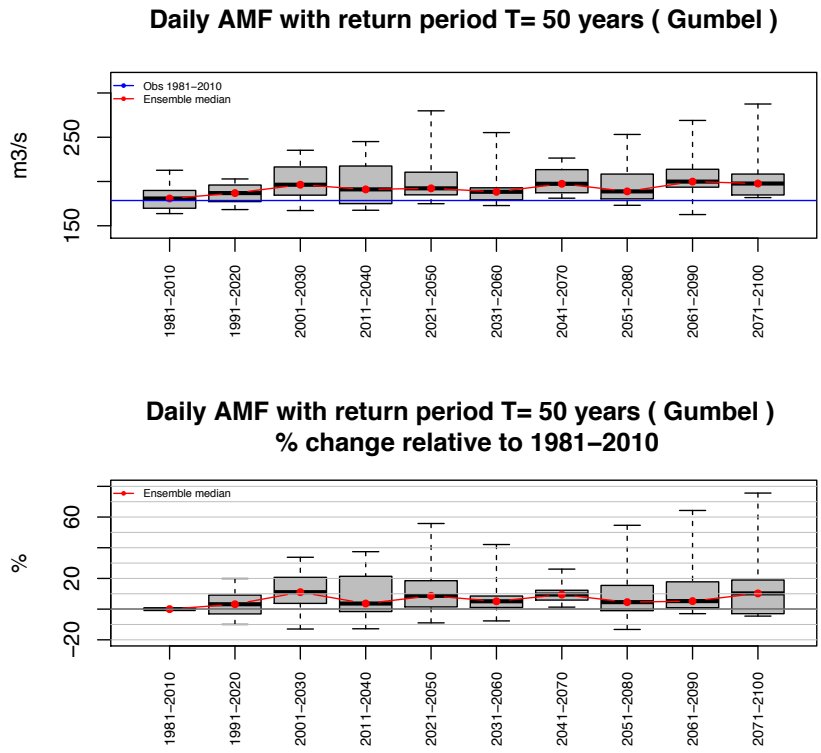

Fig. XI-5: Catchment vhm148: projected changes in 50-year flood under the RCP8.5 emission scenarios (see caption Fig XI-1).

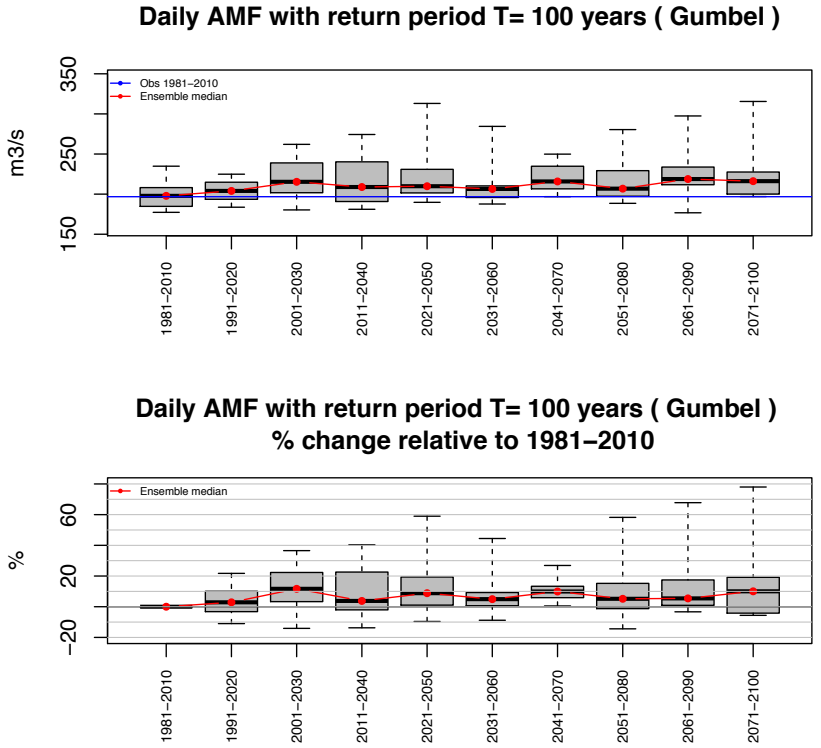

Fig. XI-6: Catchment vhm148: projected changes in 100-year flood under the RCP8.5 emission scenarios (see caption Fig XI-1).

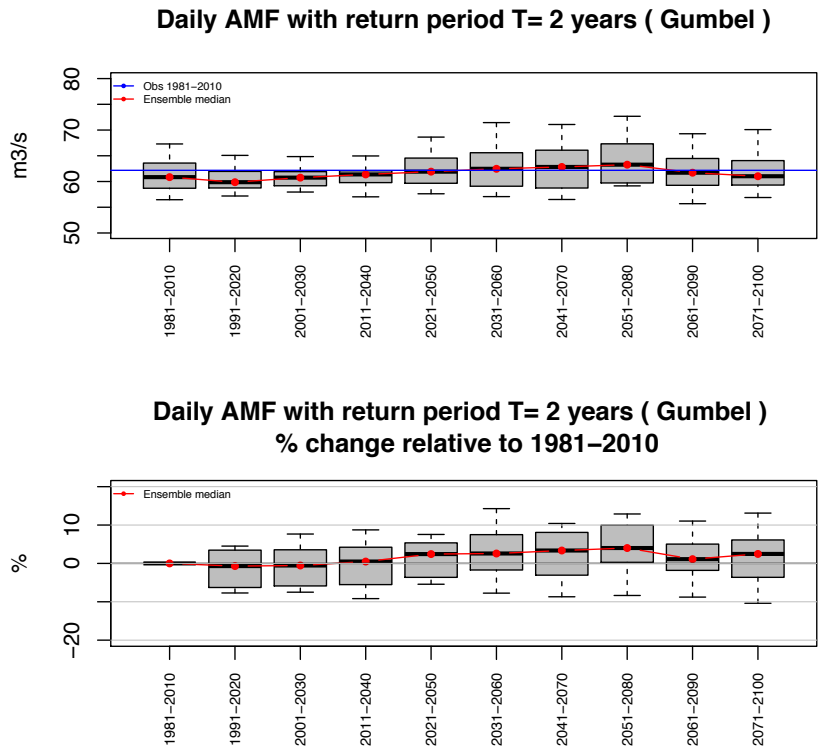

Fig. XI-7: Catchment vhm51: projected changes in 2-year flood under the RCP8.5 emission scenarios (see caption Fig XI-1).

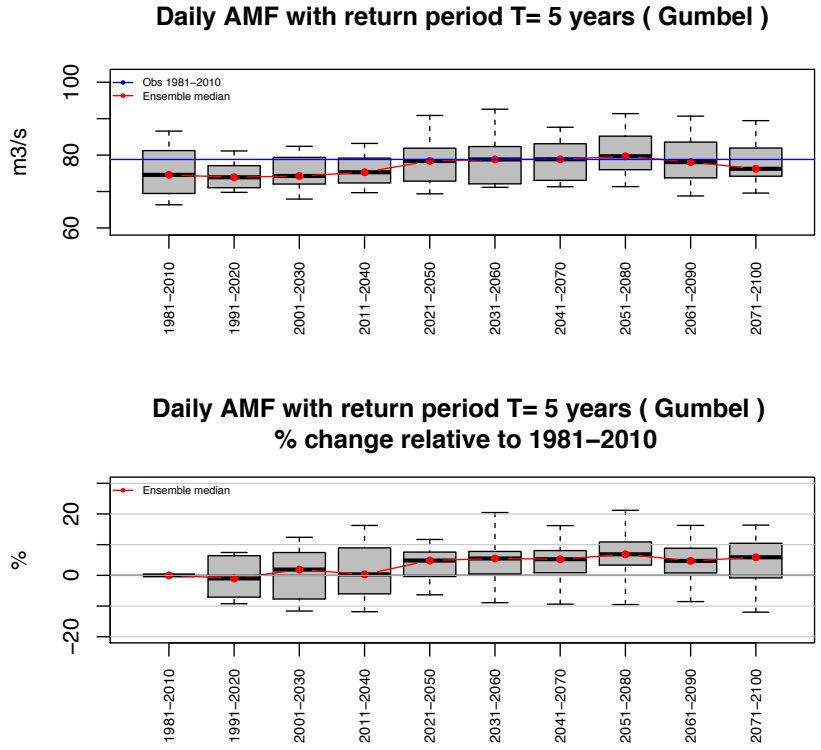

Fig. XI-8: Catchment vhm51: projected changes in 5-year flood under the RCP8.5 emission scenarios (see caption Fig XI-1).

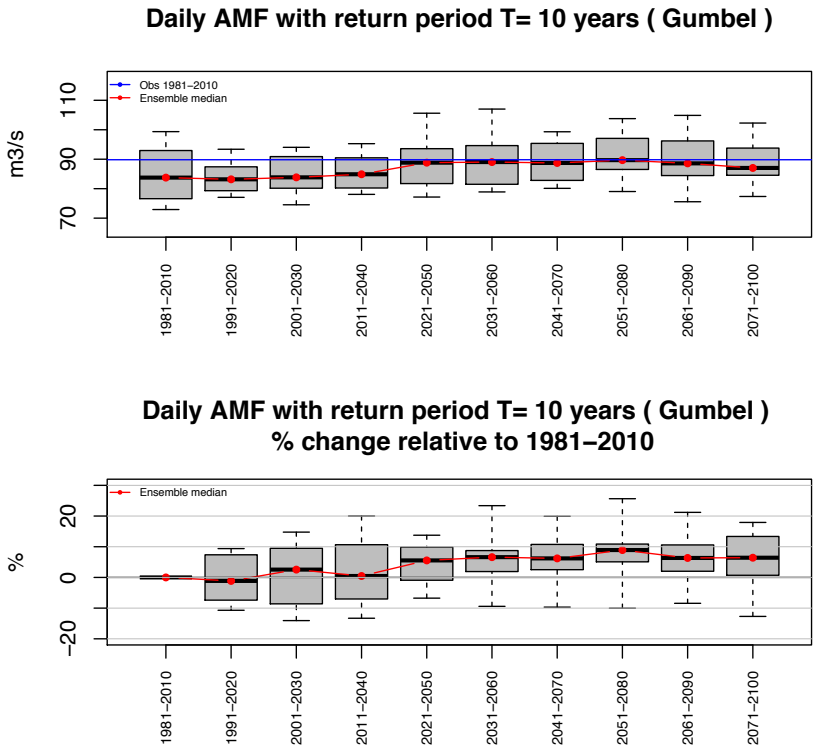

Fig. XI-9: Catchment vhm51: projected changes in 10-year flood under the RCP8.5 emission scenarios (see caption Fig XI-1).

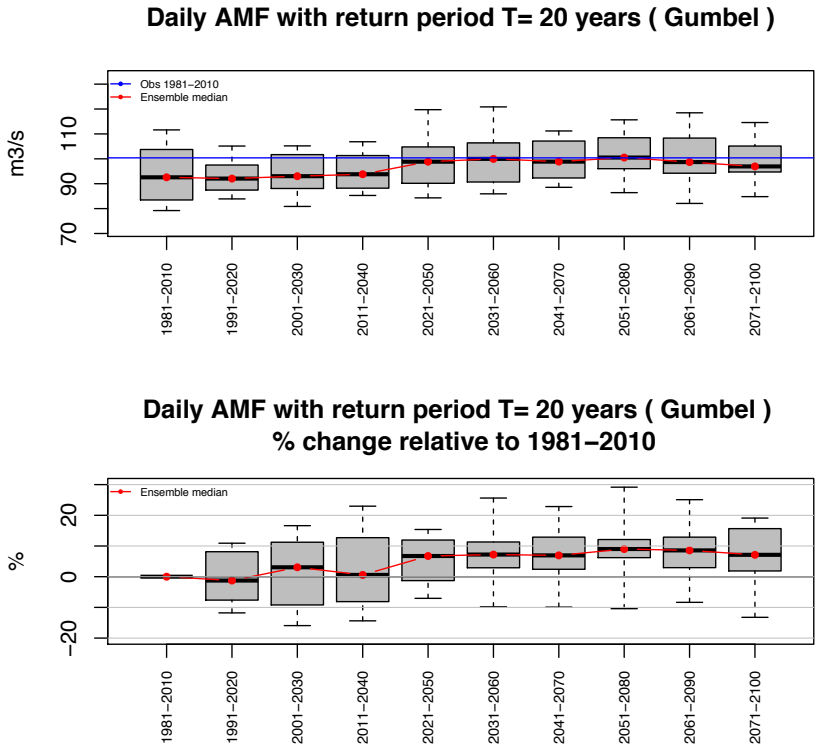

Fig. XI-10: Catchment vhm51: projected changes in 20-year flood under the RCP8.5 emission scenarios (see caption Fig XI-1).

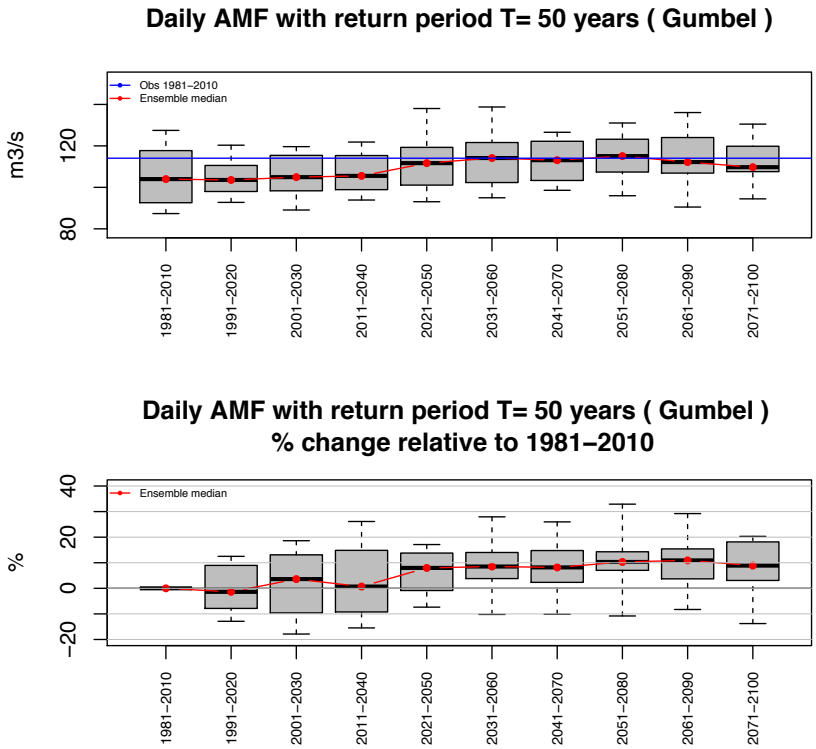

Fig. XI-11: Catchment vhm51: projected changes in 50-year flood under the RCP8.5 emission scenarios (see caption Fig XI-1).

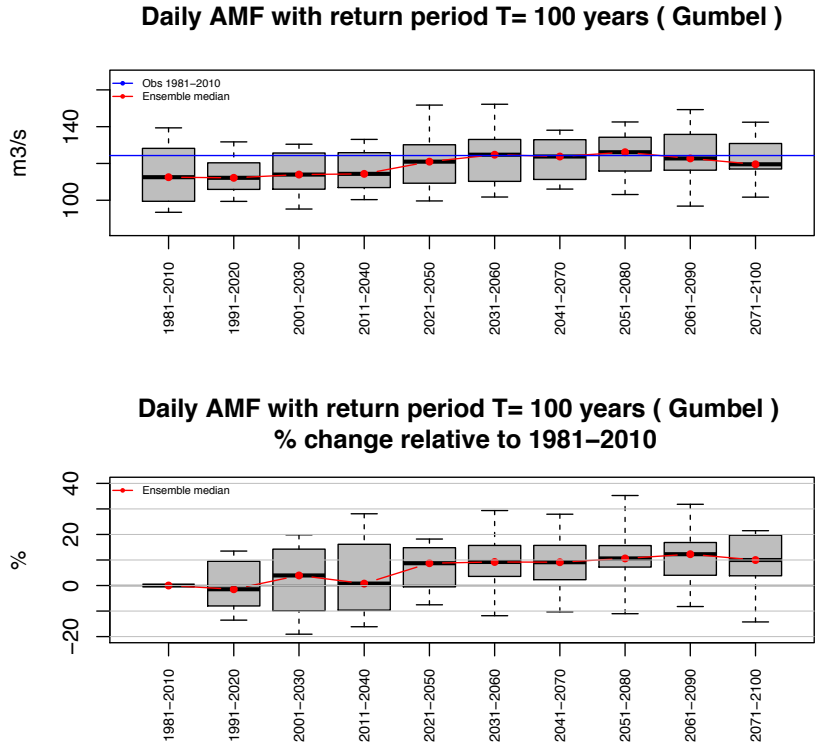

Fig. XI-12: Catchment vhm51: projected changes in 100-year flood under the RCP8.5 emission scenarios (see caption Fig XI-1).

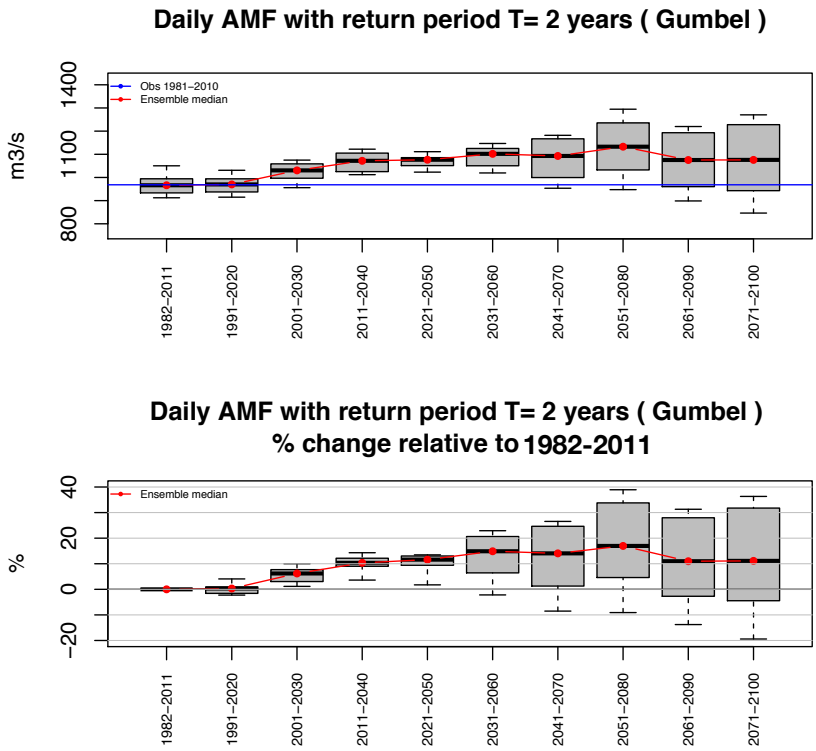

Fig. XI-13: Catchment vhm64: projected changes in 2-year flood under the RCP8.5 emission scenarios (see caption Fig XI-1). Observed 2-year flood in 1982-2011 (blue).

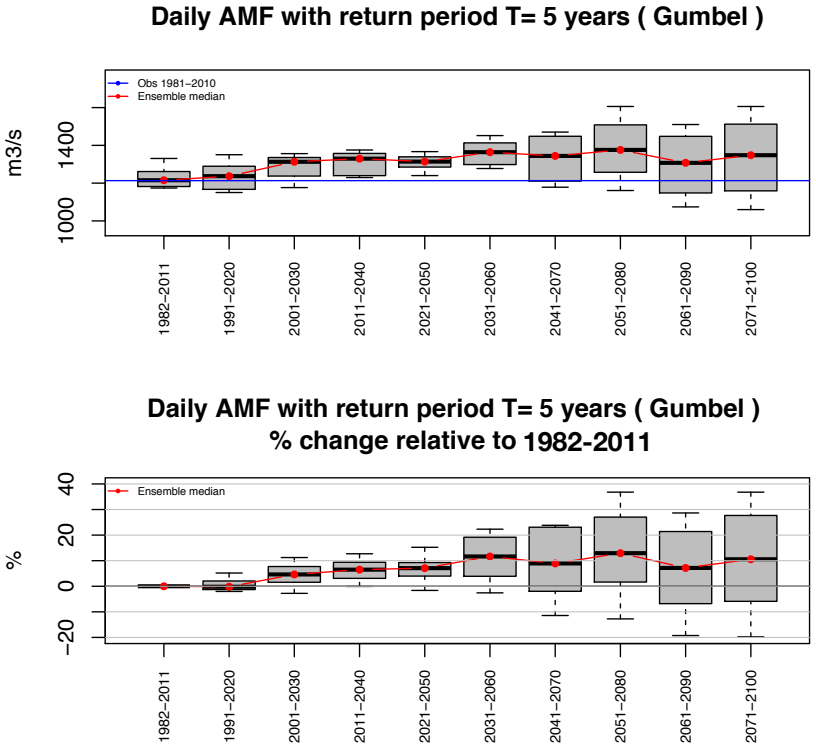

Fig. XI-14: Catchment vhm64: projected changes in 5-year flood under the RCP8.5 emission scenarios (see caption Fig XI-1). Observed 5-year flood in 1982-2011 (blue).

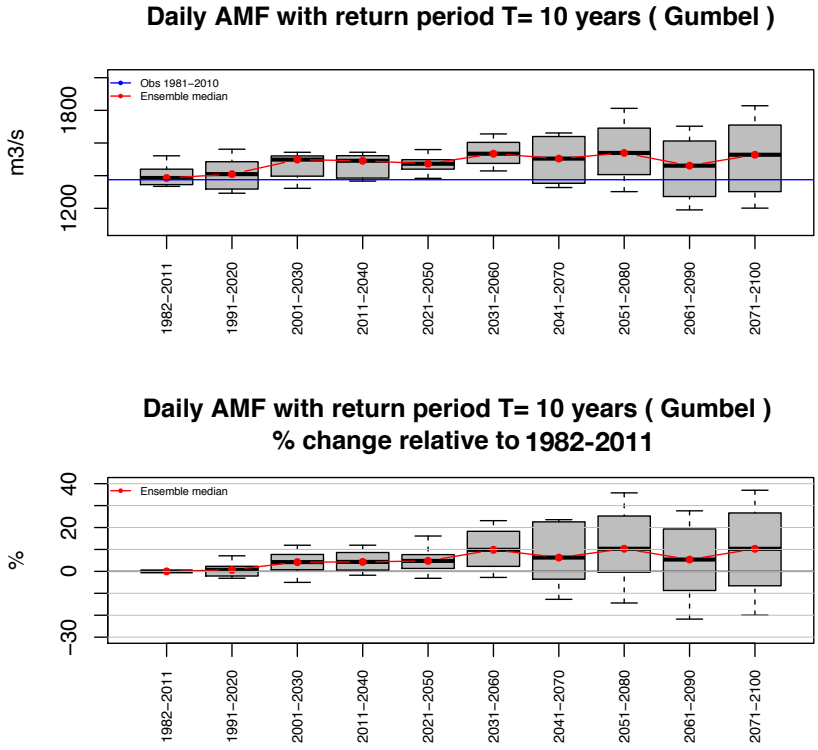

Fig. XI-15: Catchment vhm64: projected changes in 10-year flood under the RCP8.5 emission scenarios (see caption Fig XI-1). Observed 10-year flood in 1982-2011 (blue).

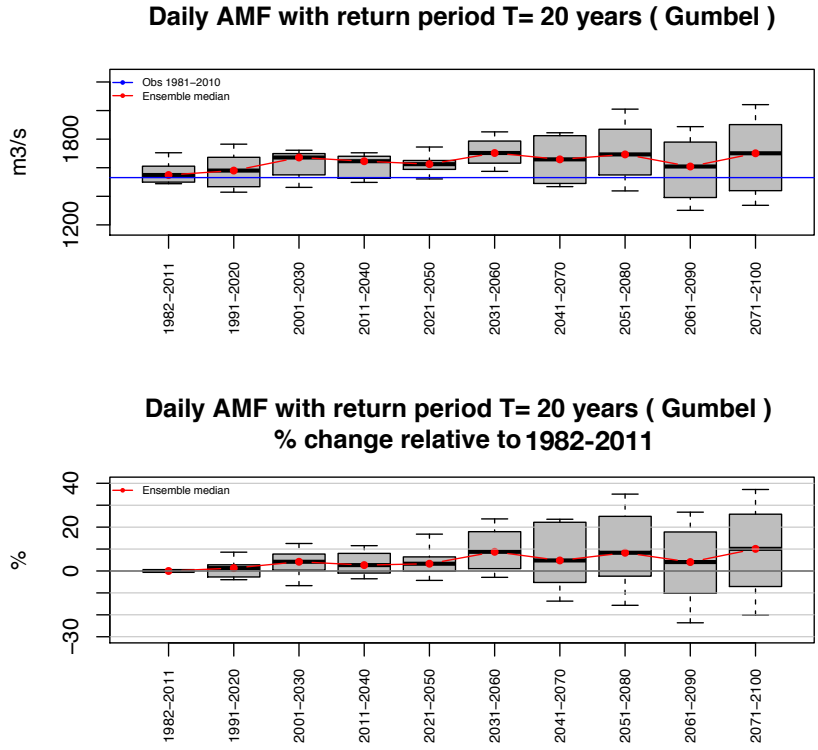

Fig. XI-16: Catchment vhm64: projected changes in 20-year flood under the RCP8.5 emission scenarios (see caption Fig XI-1). Observed 20-year flood in 1982-2011 (blue).

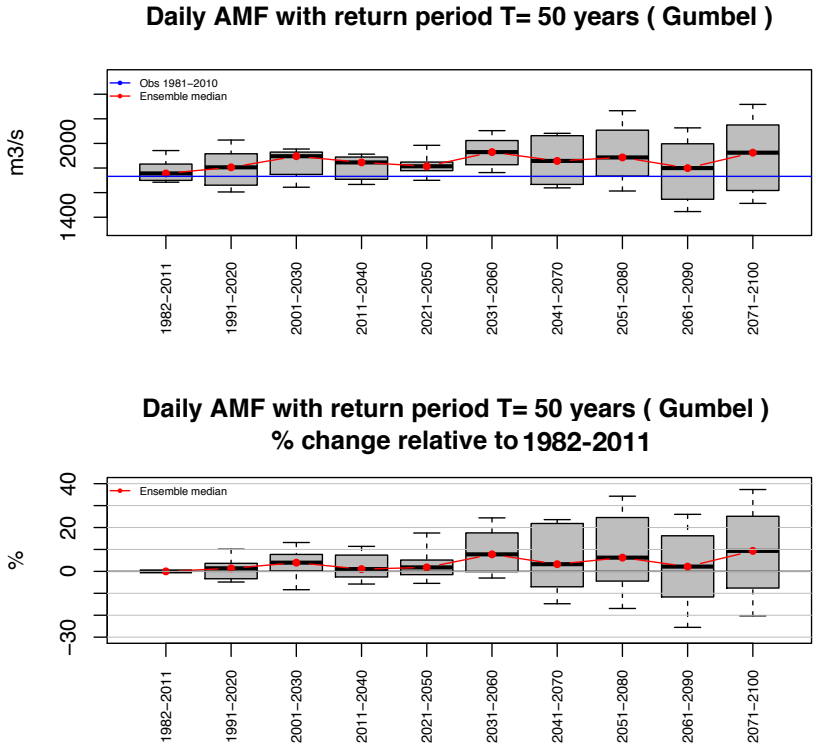

Fig. XI-17: Catchment vhm64: projected changes in 50-year flood under the RCP8.5 emission scenarios (see caption Fig XI-1). Observed 50-year flood in 1982-2011 (blue).

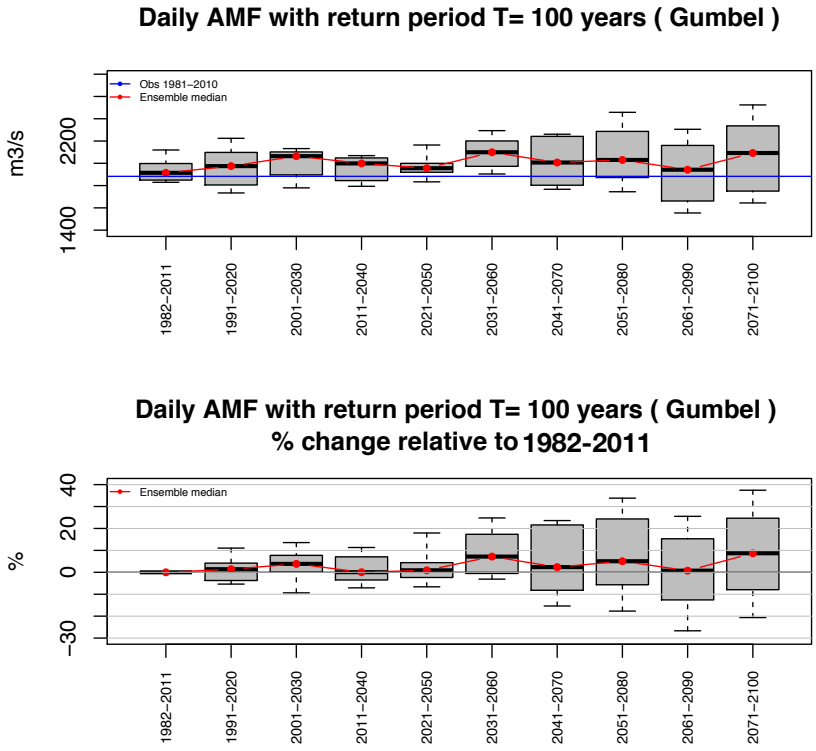

Fig. XI-18: Catchment vhm64: projected changes in 100-year flood under the RCP8.5 emission scenarios (see caption Fig XI-1). Observed 100-year flood in 1982-2011 (blue).

Appendix 12

Projected changes in the return period T of floods of a given magnitude, along 30-year moving time-windows in the 21st century, under the RCP4.5 emission scenarios.

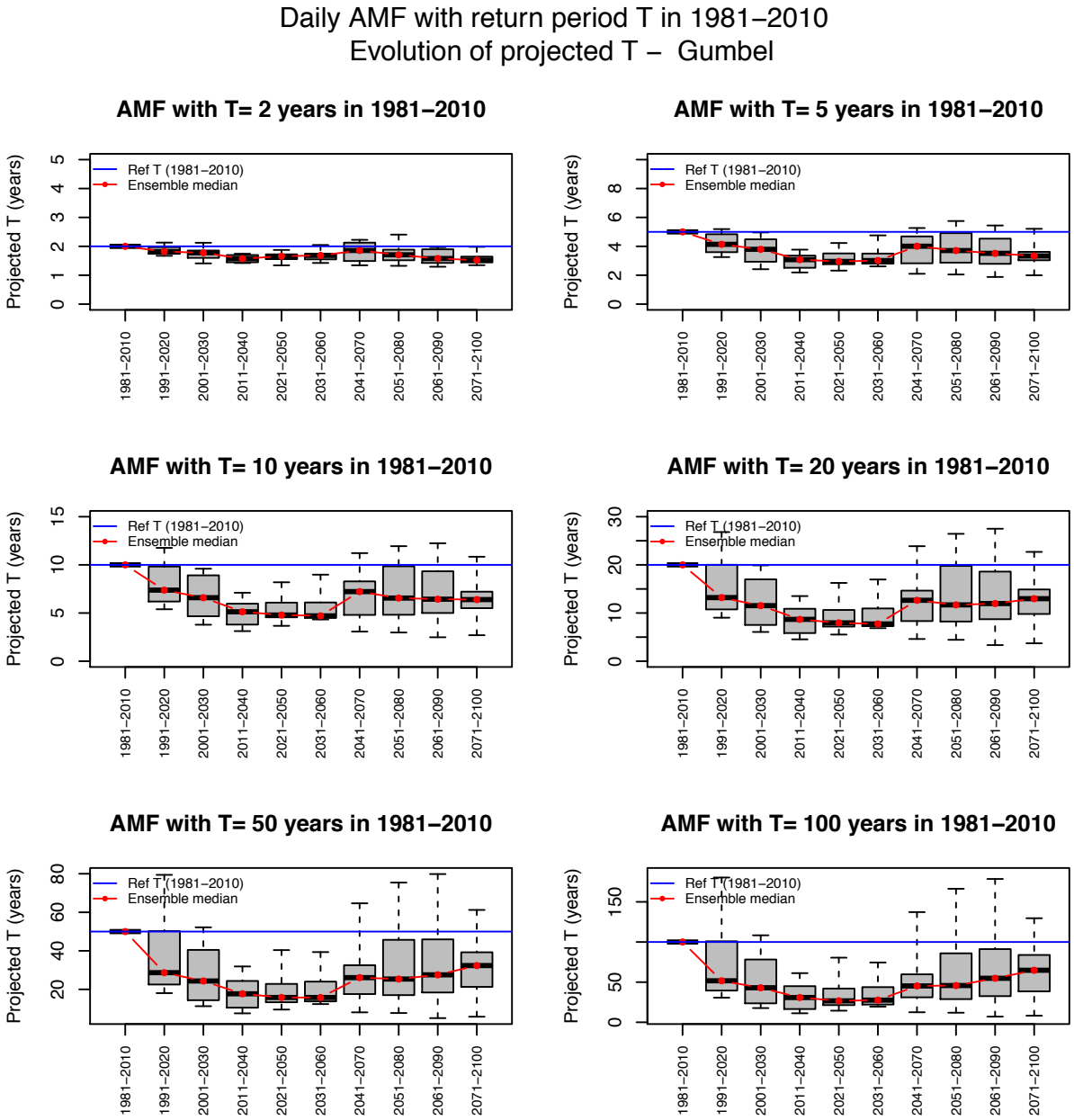

Fig. XII-1: Catchment vhm148. Box-plot of the projected change of return period T associated to a flood of a given magnitude (Q) under the RCP4.5 emission scenario. Median change (red), reference T in 1981-2010 (blue). The magnitudes Q correspond to a flood with return period T=2, 5, 10, 20, 50 and 100 years in 1981-2010, respectively.

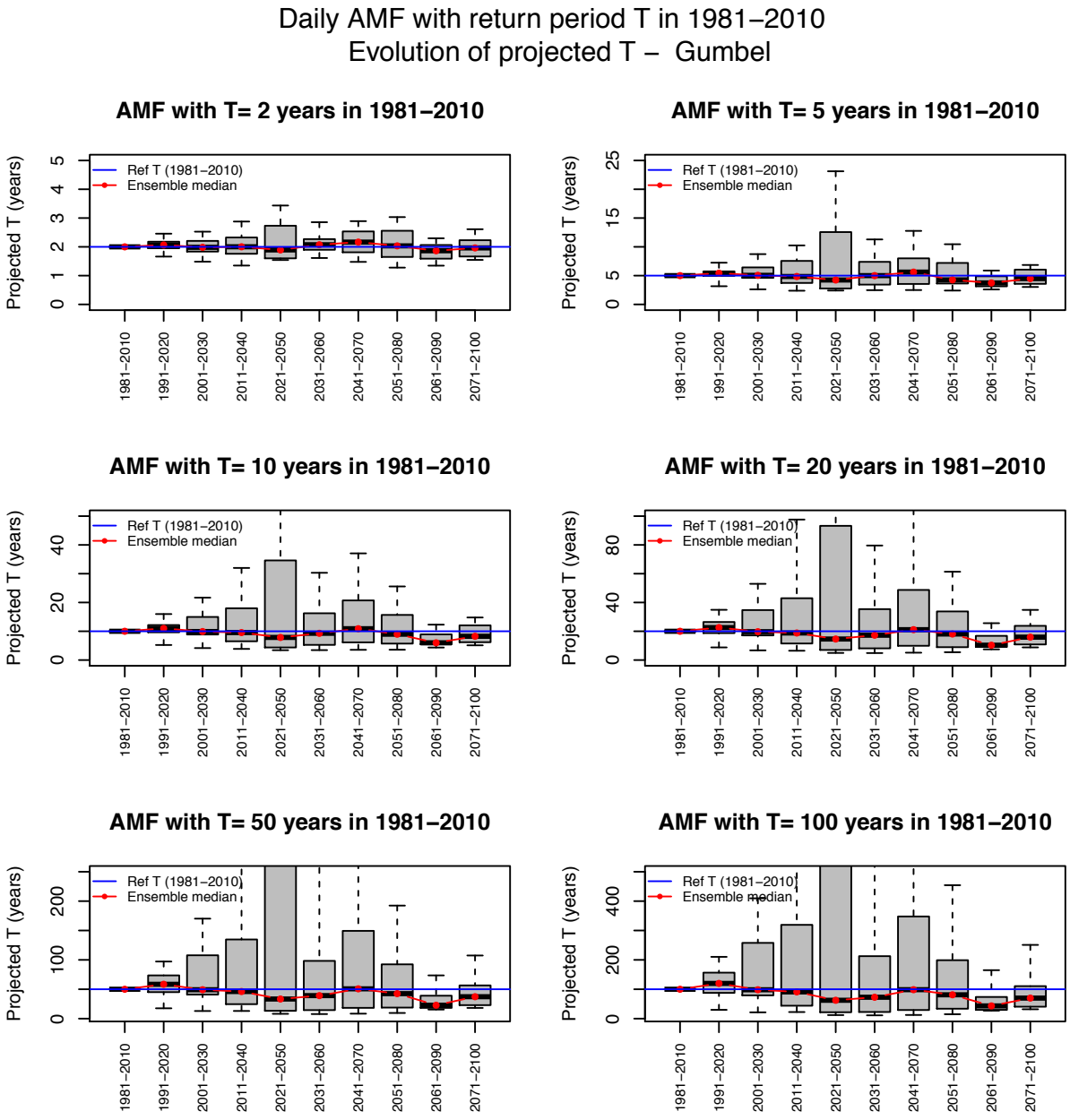

Fig. XII-2: Catchment vhm51. See caption Fig. XII-1.

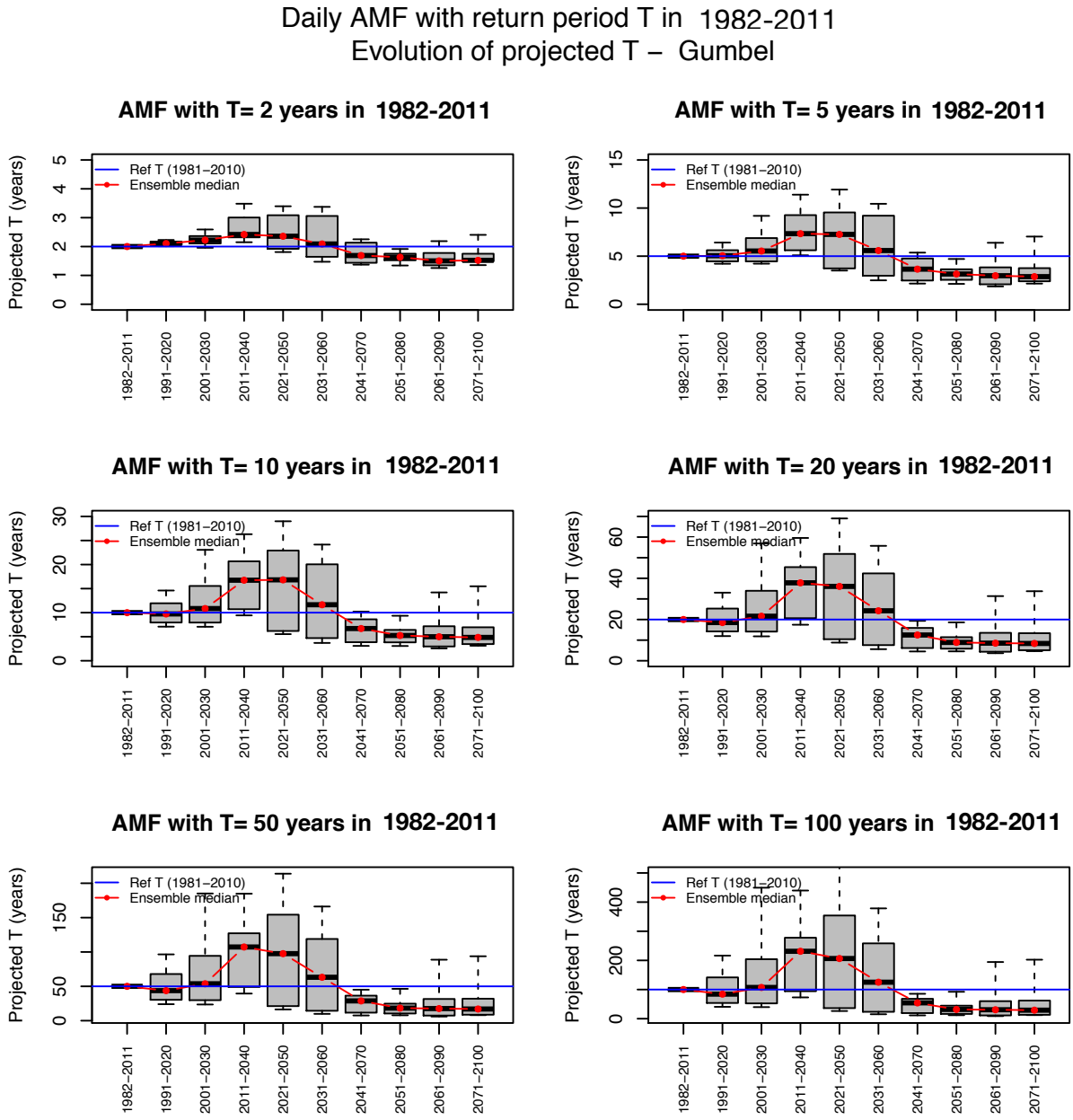

Fig. XII-3: Catchment vhm64. See caption Fig. XII-1. Reference T in 1982-2011 (blue).

Appendix 13

Projected changes in the return period T of floods of a given magnitude, along 30-year moving time-windows in the 21st century, under the RCP8.5 emission scenarios.

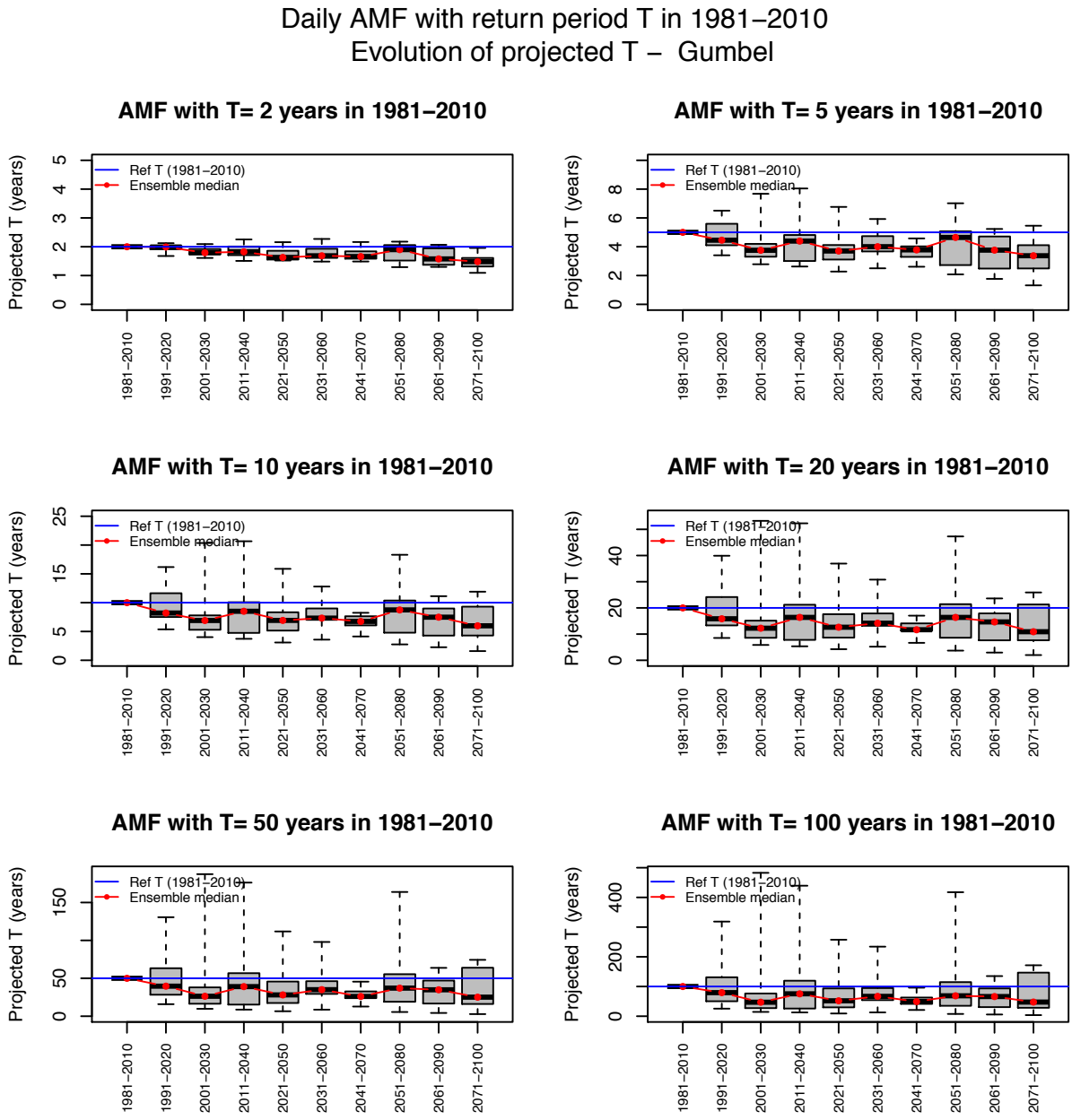

Fig. XIII-1: Catchment vhm148. Box-plot of the projected change of return period T associated to a flood of a given magnitude (Q) under the RCP8.5 emission scenario. Median change (red), reference T in 1981-2010 (blue). The magnitudes Q correspond to a flood with return period T=2, 5, 10, 20, 50 and 100 years in 1981-2010, respectively.

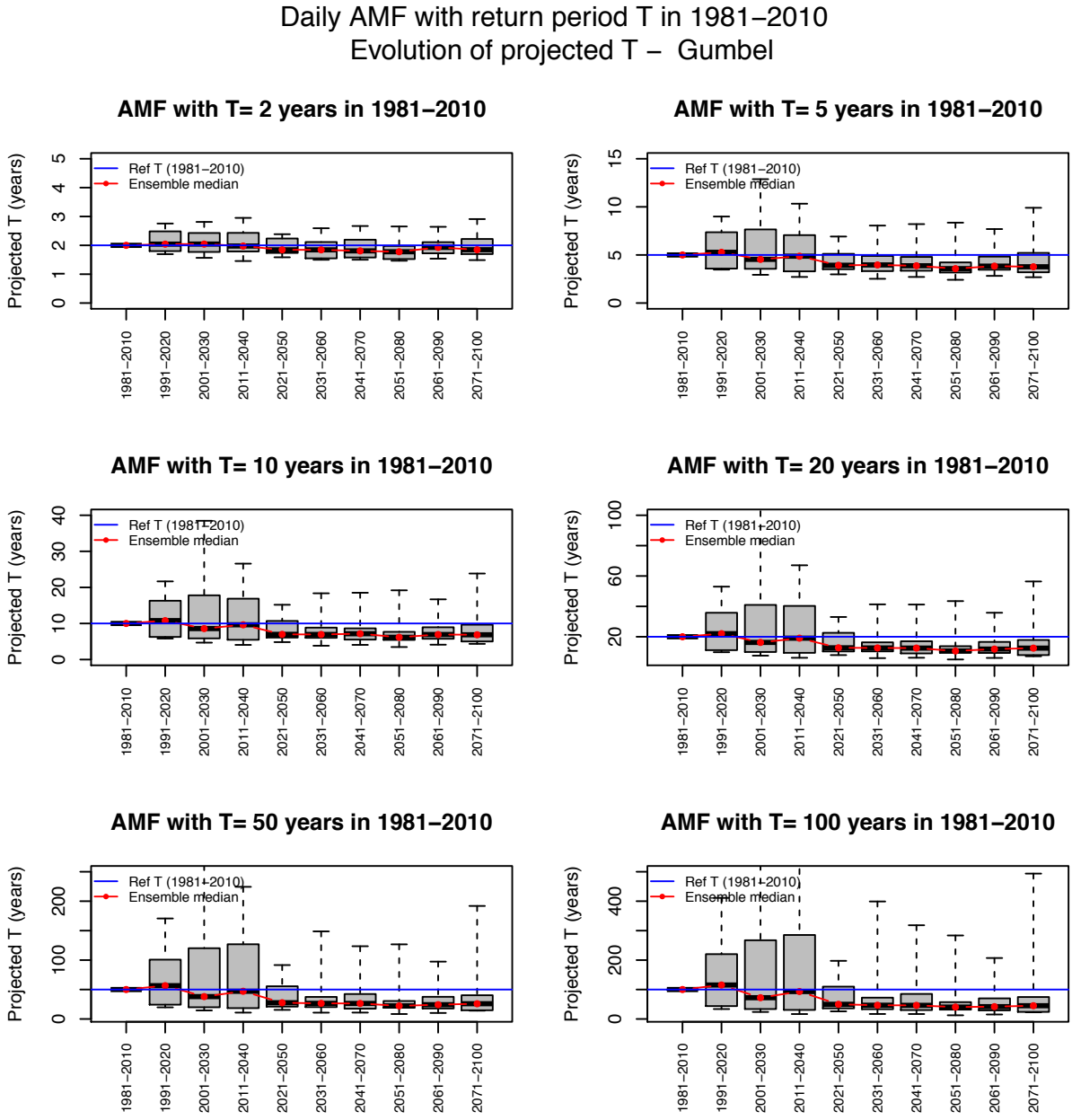

Fig. XIII-2: Catchment vhm51. See caption Fig. XIII-1.

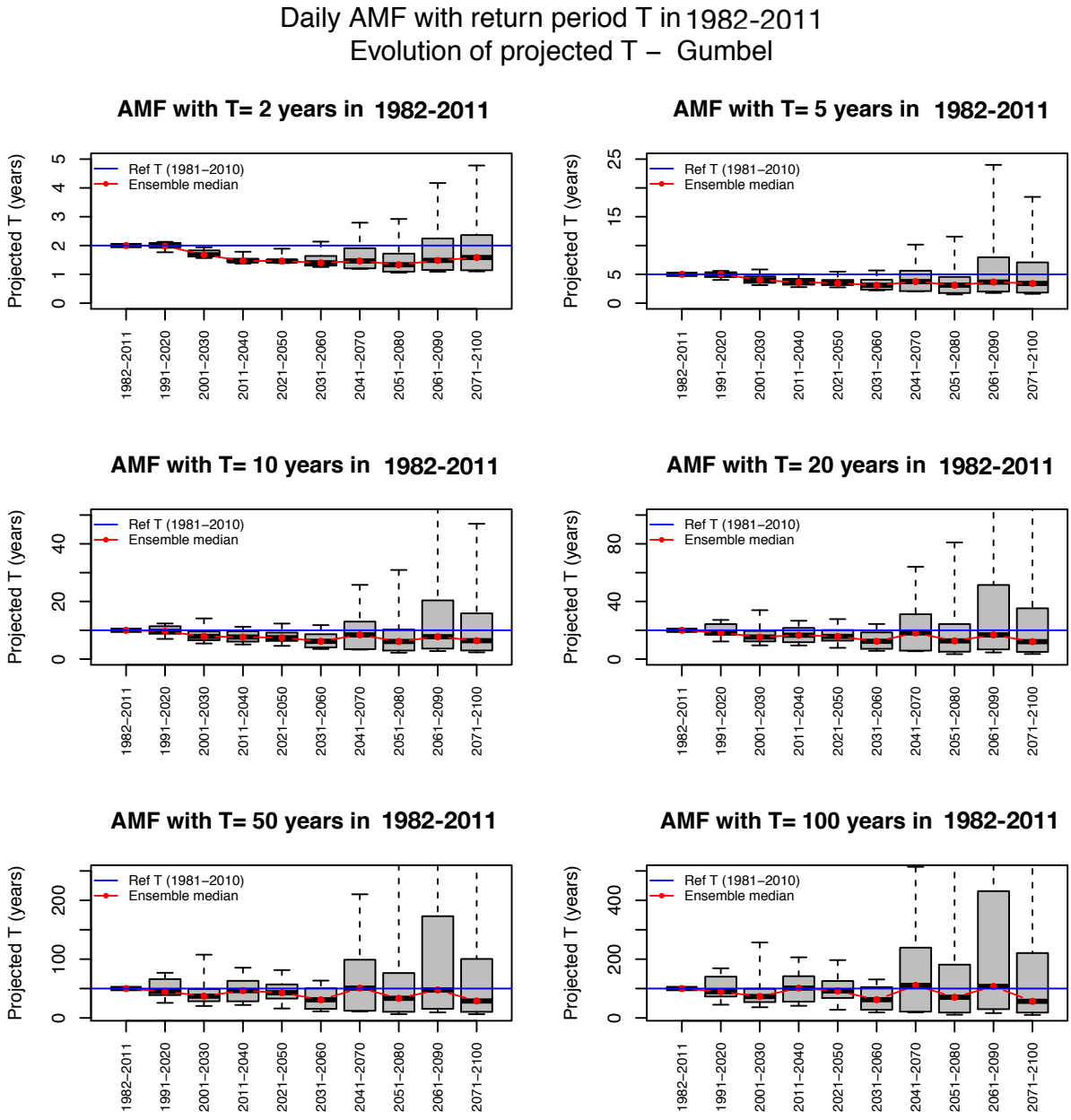

Fig. XIII-3: Catchment vhm64. See caption Fig. XIII-1. Reference T in 1982-2011 (blue).